GOVERNMENT OF INDIA
MINISTRY OF EARTH SCIENCES
INDIA METEOROLOGICAL DEPARTMENT

IMD Met. Monograph : ESSO/IMD/SYNOPTIC MET/01-2014/15



Northeast Monsoon of South Asia

M. Rajeevan, M. Mohapatra, C. K. Unnikrishnan, B. Geetha, S. Balachandran, O. P. Sreejith, Parthasarathi Mukhopadhyay, D. R. Pattanaik, Pulak Guhathakurta, Pankaj Kumar, K. Niranjan Kumar, Jyoti Bhate, P. Rohini, Monica Sharma, Raghu Ashrit, Ashim Mitra, Karuna Sagar

2022



India Meteorological Department
Ministry of Earth Sciences
Government of India

Northeast Monsoon of South Asia

M Rajeevan[1], M. Mohapatra[2], C. K. Unnikrishnan[3], B. Geetha[4], S. Balachandran[4], O. P. Sreejith[5], P. Mukhopadhyay[6], D. R. Pattanaik[2], Pulak Guhathakurta[5], Pankaj Kumar[9] , K. Niranjan Kumar[7], Jyoti Bhate[8], P. Rohini[5], Monica Sharma[2], Raghu Ashrit[7], Ashim Mitra[2], Karuna Sagar[10]

1. Ministry of Earth Sciences, NCESS, Thiruvananthapuram
2. India Meteorological Department, New Delhi
3. National Centre for Earth Science Studies, Trivandrum
4. India Meteorological Department, Chennai
5. Indian Institute of Tropical Meteorology, Pune
6. India Meteorological Department, Pune
7. National Centre for Medium Range Weather Forecasting, Noida
8. National Atmospheric Research Laboratory, Tirupati
9. Indian Institute of Science Education and Research (IISER), Bhopal
10. India Meteorological Department, Amravati



Copyright
© 2022 by India Meteorological Department
All Rights Reserved

Disclaimer and Limitations

IMD is not responsible for any errors and omissions. The geographical boundaries shown in the publication do not necessarily correspond to the political boundaries.

Published in India

By

India Meteorological Department, Lodi Road, New Delhi – 110 003 (India)
Phone: 91-11-24620701
Email:

Executive Summary

1	Document title	Northeast Monsoon of South Asia
2	Document type	Meteorological Monograph
3	Issue No.	
4	Issue date	
5	Security Classification	Unclassified
6	Control Status	Unclassified
7	No. of Pages	226
8	No. of Figures	140
9	No. of reference	135
10	Annexure	Nil
11	Distribution	Unrestricted
12	Language	English
13	Editors	
14	Originating Division/Group	National Climate Centre, Office of ADGM (R), India Meteorological Department, Pune
15	Reviewing and Approving Authority	Director General of Meteorology, India Meteorological Department
16	End users	Operational Forecasters, Modelers and Researchers, Government Officials etc.
17	Abstract	
18	Key Words	Southwest Monsoon, Indian Ocean Dipole, Multi-model Ensemble, Forecast Verification, Heavy rainfall, monsoon and agriculture

Contents

Foreword	**1**
Acknowledgements	**2**
Acronyms	**3-4**
Chapter-1: Introduction	**5-9**
Chapter-2: Climatological Features	**10-36**
Chapter-3: Mean Rainfall Distribution	**37-51**
Chapter-4: Synoptic Systems	**52-98**
Chapter-5: Onset and Withdrawal	**99-116**
Chapter-6: NE Monsoon Variability	**117-154**
Chapter-7: NE monsoon over Sri Lanka	**155-173**
Chapter-8: Numerical Weather Prediction Guidance	**174-190**
References	**191-202**
Bibliography	**203-218**

Foreword

Acknowledgements

The Meteorological Monograph on NE Monsoon of South Asia was prepared with the kind support of the Ministry of Earth Sciences (MoES) and India Meteorological Department (IMD). We thank Dr. M. Ravichandran, Secretary, MoES and Dr. Gopal Iyengar, Advisor for their kind support and encouragement to complete this monograph. We also would like to thank the Director, NCESS and Administration of NCESS for providing all the required facilities for completing this work.

We are also thankful to Dr. R. R. Kelkar, Dr. N. Jayanthi, Dr. Y. E. A. Raj, Dr. G. Srinivasan, Dr. E. N. Rajagopal, Dr. Arindam Chakraborty and Dr. Venkat Ratnam for their critical and elaborate comments on the earlier versions of the draft, which helped us to improve the quality of this Meteorological Monograph.

Acronym

AMO: Atlantic Multi-decadal Oscillation

AO: Arctic Oscillation

APCC: Asia-Pacific Economic Cooperation (APEC) Climate Center

CAP: Coastal Andhra Pradesh

CFS: Coupled Forecasting System

CS: Cyclonic Storms

CSI: Critical Success Index

CTCZ: Continental tropical convergence zone

CV: Coefficient of Variation

DCC: Deep convective clouds

FAR: False Alarm Rate

FIM: First Inter-Monsoon

GEFS: Global Ensemble Forecasting System

GFS: Global Forecasting System

IMD: India Meteorological Department

IOD: Indian Ocean Dipole

IPCC: Intergovernmental Panel on Climate Change-

ITCZ: Inter Tropical Convergence Zone

LOPAR: Low Pressure Area NAO: North Atlantic Oscillation

MJO: Madden Julian Oscillation

MME: Multi-Model Ensemble

MoES: Ministry of Earth Sciences

MSLP: Mean Sea Level Pressure (MSLP)

NCEP/NCAR: National Centres for Environmental Prediction/National Centre for Atmospheric Research

NCMRWF: National Centre for Medium Range Weather Forecasting

NCUM: NCMRWF Unified Model

NEM: North East Monsoon

NEMR: NE monsoon rainfall

NOAA: National Oceanographic and Atmospheric Administration

NWP: Numerical Weather Prediction

OLR: Outgoing Long Wave Radiation

PDO: Pacific Decadal Oscillation

POD: Probability of Detection

PSS: Pierce's Skill Score

PWC: Precipitable Water Content

SCS: Severe cyclonic storms

SEDI: Symmetric Extreme Dependency Index

SHET: Southern Hemispheric Equatorial Trough

SIM: Second Inter-Monsoon

SOI: Southern Oscillation Index

SPI: Southern Peninsular India

SST: Sea Surface Temperature

SWM: South West Monsoon

TEJ: Tropical Easterly Jet

UTC: Universal Coordinated Time

Chapter-1

Introduction

South Asia experiences two monsoons, Southwest monsoon or summer monsoon during June to September and the Northeast (NE) Monsoon or winter monsoon during October to December. While the boreal summer monsoon (June to Sept) is responsible for a major portion of annual rainfall over India, rainfall received during the NE monsoon season (Oct-Dec) is also important, especially for the south peninsula, Sri Lanka and Maldives. During the southwest monsoon season, the southeastern parts of India remain in the rain-shadow region and receive moderate rains.

NE monsoon is associated with the seasonal reversal of surface and lower tropospheric winds, which starts by October. During the southwest monsoon season, surface pressure gradient is directed from the Indian ocean to land with southwesterly monsoon winds in the lower troposphere. During the NE monsoon season, the pressure gradient reverses (from land to the Indian ocean) resulting in northeasterly trade winds, which is the basic state of the system. This change in surface pressure gradient and lower tropospheric winds is associated with the southward movement of the continental tropical convergence zone (CTCZ) and the subtropical anticyclone in the upper troposphere. Therefore, the NE monsoon is often described as the retreating phase of the southwest monsoon.

In a broader perspective, it is also associated with the northern hemispheric winter circulation dominated by a strong surface high pressure region over Siberia, a primary low over eastern equatorial Pacific region and secondary shallow lows over the north Indian ocean (Geetha, 2011, Raj 2012). A salient feature of the seasonal circulation during the winter monsoon is the low-level northeasterly flow over the Indian subcontinent and southeast Asia. There are similarities in circulation and rainfall patterns of southeastern peninsular India and other South / Southeast Asian regions and also the established roles of Siberian High, sub-tropical westerly jet stream and the

teleconnection influences of global parameters such as ENSO on the NE Monsoon rainfall (Geetha 2011). There is an asynhronicity in the establishment of northeasterlies over the Bay of Bengal and the South China Sea; the northeasterlies appear over the Bay of Bengal in late October, a month later than over the South China Sea (Sengupta and Nigam, 2019).

NE monsoon is relatively dry, stable and has less vertical extend compared to the southwest monsoon. The India Meteorological Department (IMD) refers to the October to December period as the northeast monsoon, which is a part of the northeast trades (Dhar et al., 1982, Dhar and Rakhecha, 1983). Dhar and Rakhecha (1983) studied monthly rainfall data for a 100-yr period (1877– 1976) to investigate the association between the northeast and southwest monsoons over Tamil Nadu, and concluded that summer rainfall is negatively correlated with NEM rainfall.

NE monsoon rainfall exhibits variability from diurnal to synoptic, intra-seasonal and inter-annual time scales. The inter-annual variability of the NE monsoon rainfall influences agricultural production and water resources over south peninsular India. The NEMR affects the productivity of rice and maize in the provinces of Tamil Nadu and Andhra Pradesh (Krishna Kumar et al., 2004). During the years when the NE monsoon is deficient it has been noted that there is a considerable decrease in agricultural production over the region. The NE monsoon rainfall is highly variable both spatially and temporally. The coefficient of variation (inter-annual) of the NEMR averaged over the five subdivisions is 25%, which is more than that of the southwest monsoon rainfall averaged over the country as a whole (10%). South peninsula is well known for large year to year variability. In 2015, the city of Chennai experienced deluge in 2015, which resulted significant loss of life and property. Four years later, in 2019, Chennai city experienced severe water shortage and crisis. During the NE monsoon season, south Asia also experiences many extreme weather events like heavy precipitation, strong

winds and floods. Some of these extreme events are associated with the passage of tropical cyclones forming over the Bay of Bengal.

In the literature, there is a controversy about using the term “Northeast” monsoon (IMD, 1973). As per the classifications given by the India Meteorological Department (IMD), the October-December period constitutes the “Post-monsoon season”. It is also known as “the Retreating Southwest Monsoon Season”, as the monsoon convergence zone shifts to lower latitudes during this season. Mr Blanford, who was the first Director General of the India Meteorological Department (IMD) in his Memoirs on “Rainfall of India” raised the question about the term “Northeast Monsoon Rains” (IMD, 1973). IMD discussed this aspect on many occasions and the IMD decided to retain the term. IMD recommends that “the term Northeast Monsoon should continue to be used for rainfall season over south peninsula during October to December”. Subbaramayya (1976) had examined meridional sea-level pressure profiles over India, the Atlantic and Pacific and of winter rainfall over India and Sri Lanka and suggested that that the so-called north-east monsoon over south-east India differs little, either in wind in weather, from the generality of the northern-hemisphere trade winds.

Compared to the southwest monsoon, adequate attention was not given to address various aspects of the NE monsoon. There are only a few research papers addressing NE monsoon over south Asia. After the classic work by Srinivasan and Ramamurthy (IMD 1973), a few papers have been published on different aspects of NE Monsoon. The review article by Raj (2012) in the Monsoon Monograph edited by Ajit Tyagi et al is an excellent documentation of various aspects of NE Monsoon season over India. The papers by Sreekala et al (2012) and Rajeevan et al (2012) also are good reviews on the variability of NE monsoon rainfall and its prediction aspects. Amudha (2016) using modern meteorological data analyzed the characteristics of Indian Northeast monsoon and cyclonic storms of the North Indian Ocean. The study revealed many interesting

aspects of the movement of clouds and other rainfall regimes associated with the NE monsoon.

These publications contain all relevant references of research papers on NE monsoon published till 2012. Since then, there is growing research interest on NE Monsoon with much more papers are getting published in the recent years (Satyanarayana et al., (2020), Raj and Amudha (2022), Raj and Geetha (2008), Balachandran et al., (2006), Nair et al., (2013), Dash et al., (2019), Naidu et al., (2012), Maharana et al., (2022), Prasanna et al., (2019), Mondal and Choudhari (2022), Suneetha et al., (2018), Prasanna et al., (2021), Geetha and Balachandran (2021), Saikranthi and Chiranjeevi (2022), Mishra and Nagaraju (2021), Geetha and Raj (2014), Amudha et al., (2016), Prasanna et al., (2020), Prakash and Gairola (2013), Kiran Kumar and Singh (2021), Pattanaik and Mohapatra (2017), Parvathi et al. (2017), Sengupta and Nigam (2019), Mishra and Bharadwaj (2019)). The paleoclimate aspects of NE monsoon are recently discussed in Achyuthan (2021) and the references therein.

In spite of the growing research interest, there is a lot of scope for an exhaustive compilation of research results based on recent data products and forecasting tools on different aspects of NE monsoon over south Asia. During the last one decade, our understanding on diurnal, intra-seasonal, seasonal variability, monsoon onset, synoptic weather systems during the NE monsoon season has improved substantially. At the same time, our capability to make more accurate forecasts also has improved by using the state-of-the-art dynamical models or Numerical Weather Prediction (NWP) models. The present monograph is designed accordingly to include more recent research results, which have resulted in better understanding of NE monsoon and its variability in all time scales and their prediction aspects. Such a compilation would be very useful for forecasters as reference material and also students, young researchers venturing into NE monsoon research.

In this monograph, the climatological features of NE monsoon are discussed using long term and updated climate data sets. Discussions on mean temperatures, sea level pressure, upper air circulation features, monthly and seasonal rainfall, heavy rainfall, extreme winds, characteristics of monsoon clouds, thunderstorm and lightning are included. The variability of NE monsoon from diurnal, synoptic, intra-seasonal and seasonal time scales is also discussed in detail with a few case studies. The details of synoptic systems affecting south peninsula and Sri Lanka during the season and forecasting aspects of these weather systems are also discussed. A brief summary of the verification of forecasts of NE monsoon rainfall over India using two different weather prediction systems is included as reference material for forecasters. A separate section of NE monsoon season over Sri Lanka is also provided to widen the scope of this book. The grey areas where more research is required are identified and discussed.

Chapter -2

Climatological Features

NE monsoon predominantly influences south peninsula, consisting of five meteorological sub-divisions (Coastal Andhra Pradesh, Rayalaseema, Tamil Nadu, South Interior Karnataka and Kerala) as shown in Fig. 2.1. In addition, NE monsoon contributes significant amount of rainfall over other south Asian countries like Sri Lanka and Maldives (Fig 2.2 a).

In Sri Lanka, the southwest monsoon season lasts during May to September. The period October to November is termed as second inter-monsoon season. The second Inter-monsoon period of October – November is the period with the most evenly balanced distribution of rainfall over Sri Lanka. Almost the entire island receives in excess of 400 mm of rain during this season, with the Southwestern slops receiving higher rainfall in the range 750mm to 1200 mm. NE monsoon is experienced during the period, December to February. During this period, the highest rainfall figures are recorded in the north, eastern slopes of the hill country and the eastern slopes of the Knuckles/Rangala range (http://www.meteo.gov.lk/index.php?option=com_content&view=article&id=94&Itemid=310&lang=en).

In India, the NE monsoon season (Oct-Dec) contributes about 11% of its annual rainfall over the country as a whole. South peninsula receives much more rainfall compared to northern parts of the country. Many districts over the south peninsula receive 30–60% of the annual rainfall during this season. This season is also termed the retreating monsoon season or the post-monsoon season in which the zone of maximum rainfall migrates to southern parts of India, Sri Lanka and the neighboring sea. With the withdrawal of the Southwest monsoon from the northern parts of India, the mean sea level pressure and upper tropospheric wind circulation patterns over India change rapidly from the summer monsoon type to winter type. By October, the Inter-tropical

Convergence Zone (ITCZ) or the monsoon convergence zone which is positioned over northern parts of India starts shifting southwards.

Fig.2.2 b shows the annual cycle of precipitation averaged over the longitudes 70^0-85^0, calculated using GPCP monthly rainfall data during the period 1979-2021. It clearly shows the northward movement of monsoon convergence and rainfall towards the northern parts starting from May and the retreat during October-December. NE monsoon season coincides with this retreating phase of the Inter Tropical Convergence Zone (ITCZ). There are also associated rapid changes in upper air circulation and sea level pressure patterns. During the October-December season, there is a clear evidence of rainfall maximum in the Southern Hemisphere (SH), coinciding with the presence of SH equatorial trough (SHET).

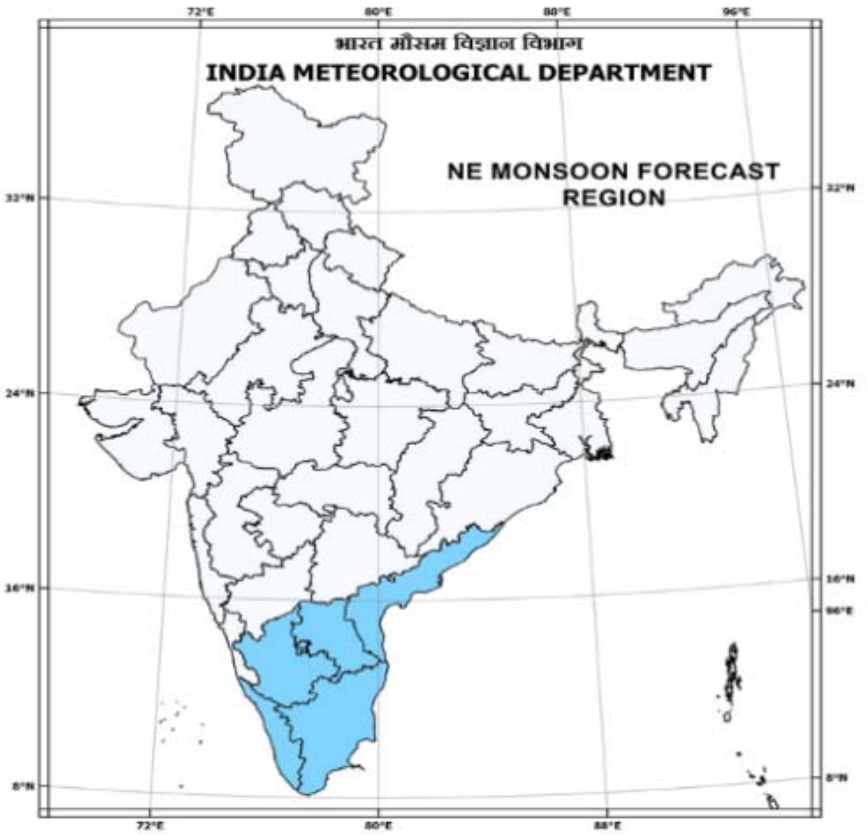

Fig. 2. 1 Five Sub-divisions over South Peninsula under the NE monsoon region

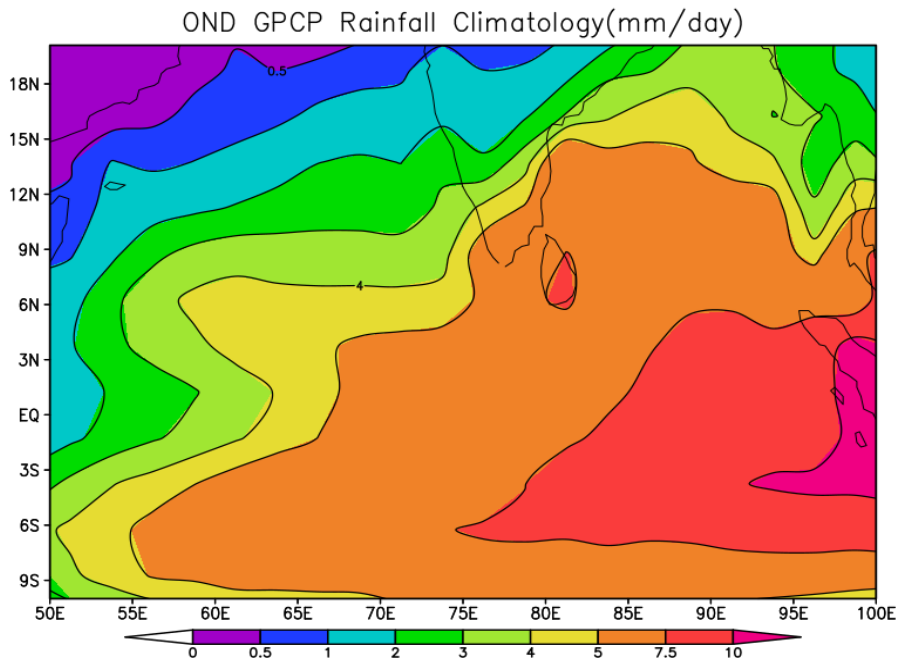

Fig. 2.2 a. NE monsoon rainfall (Oct-Dec) in mm/day over South Asia

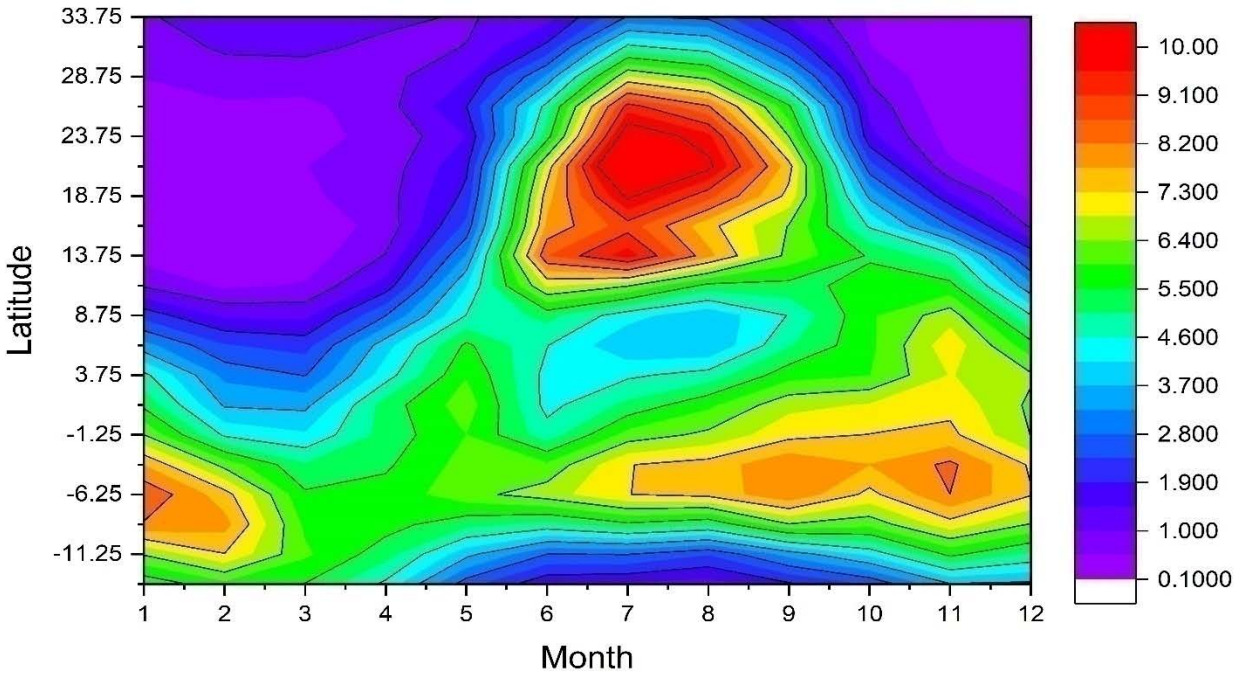

Fig 2.2 b. Hovmuller Diagram showing annual cycle of precipitation (mm/day) over the Indian region, averaged over the longitudes between 70^0E- 90^0E. This plot is prepared using GPCP monthly rainfall data (1979-2021).

In the next sections, climatological aspects of sea level pressure and upper air circulation features are discussed.

2.1 **Sea Level Pressure**

The mean sea level pressure chart for the month of July is shown in Fig 2.3. The pattern shows a heat low over the northwestern parts of India and adjoining Pakistan with a south-north pressure gradient. The pressure gradient between the equator and 10^0N is about 12 hPa. However, by September, the pressure gradient generally weakens and by October the pressure gradient completely reverses with higher pressure over the northern parts of India.

The surface sea level pressure charts for Oct to Dec are given in Fig.2.4, 2.5 and 2.6 respectively. By October, a low pressure area gets established over the Central and South Bay of Bengal and adjoining east coast, which shifts to south Bay in November and further southwards, close to the equator in December. This low pressure area is more marked over the southwest Bay in October and November. In the Arabian Sea, the low pressure area is not well marked during these months. However, an east-west oriented trough of low pressure is observed in nearly the corresponding latitudes as in the Bay of Bengal, at least in October and November. In October, the pressure gradient is generally weak, which gets strengthened by November. While the low pressure area gets shifted southwards, the high pressure area associated with the Siberian High also gets strengthened over the northern parts of the country. The surface pressure gradient (high in the north and low in the south) over the Bay of Bengal also strengthens. During November and December, the isobars are nearly parallel to the equator, suggesting stronger surface easterlies/northeasterlies over the Bay of Bengal.

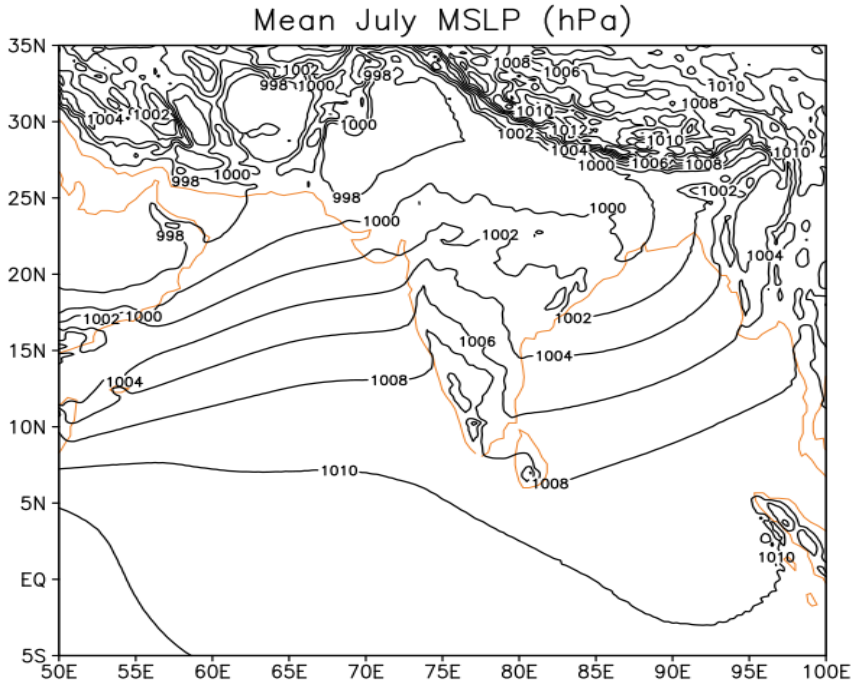

Fig 2.3. Mean Sea Level Pattern (hPa) during July (period: 1979-2021). Source: ERA5 reanalysis.

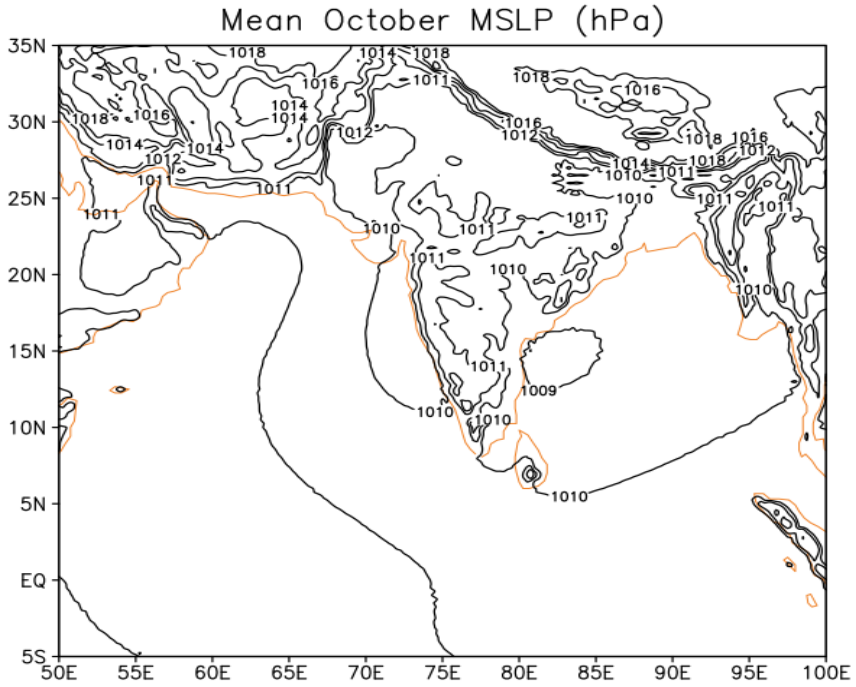

Fig 2. 4. Same as in Fig. 2.3 but for October.

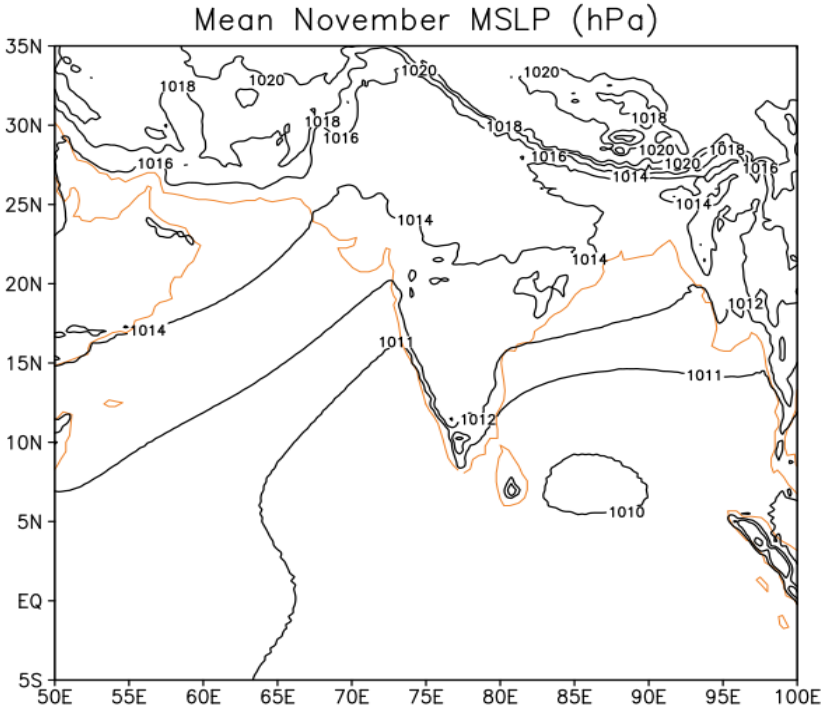

Fig 2.5. Same as Fig 2.3 but for November.

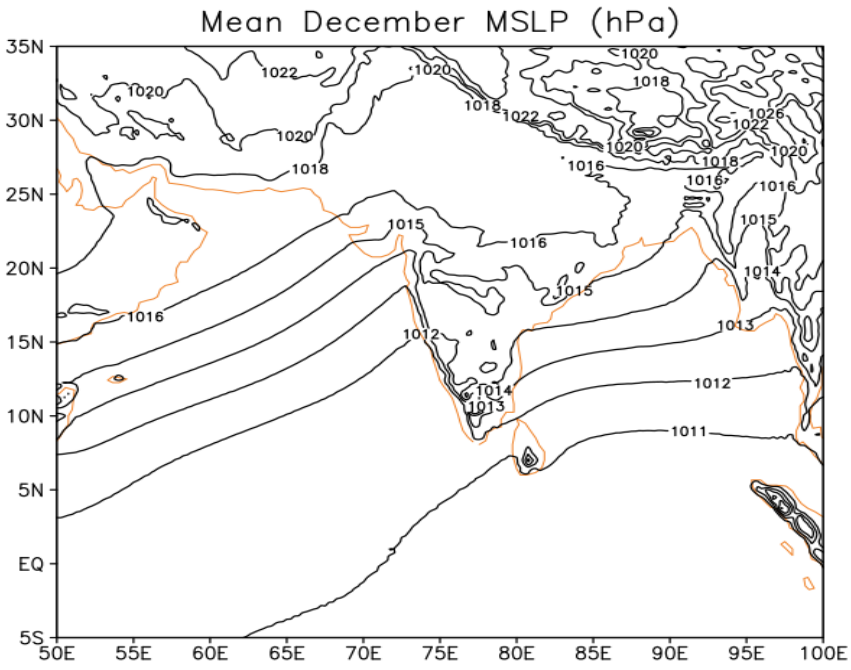

Fig. 2.6. Same as Fig 2.3 but for December.

2.2 **Upper Air Circulation Features**

The upper air circulation features from Oct to Dec are shown in Fig.2.7, 2.8 and 2,9 respectively. These maps show the mean wind pattern at 850, 700, 500 and 200 hPa levels. During October, an east-west trough is seen extending from the lower levels to 700 hPa from South Bay to the South Arabian Sea. This east-west trough is seen shifting southwards from October to December, consistent with the equatorward shifting of the ITCZ. By December, the east-west trough is seen close to 5^0 N. This east-west trough is the region with positive vorticity and convergence, thus causing abundant rainfall over this region. This shear zone in the lower troposphere contributes to the genesis of low-pressure systems over the Bay of Bengal and the Arabian Sea.

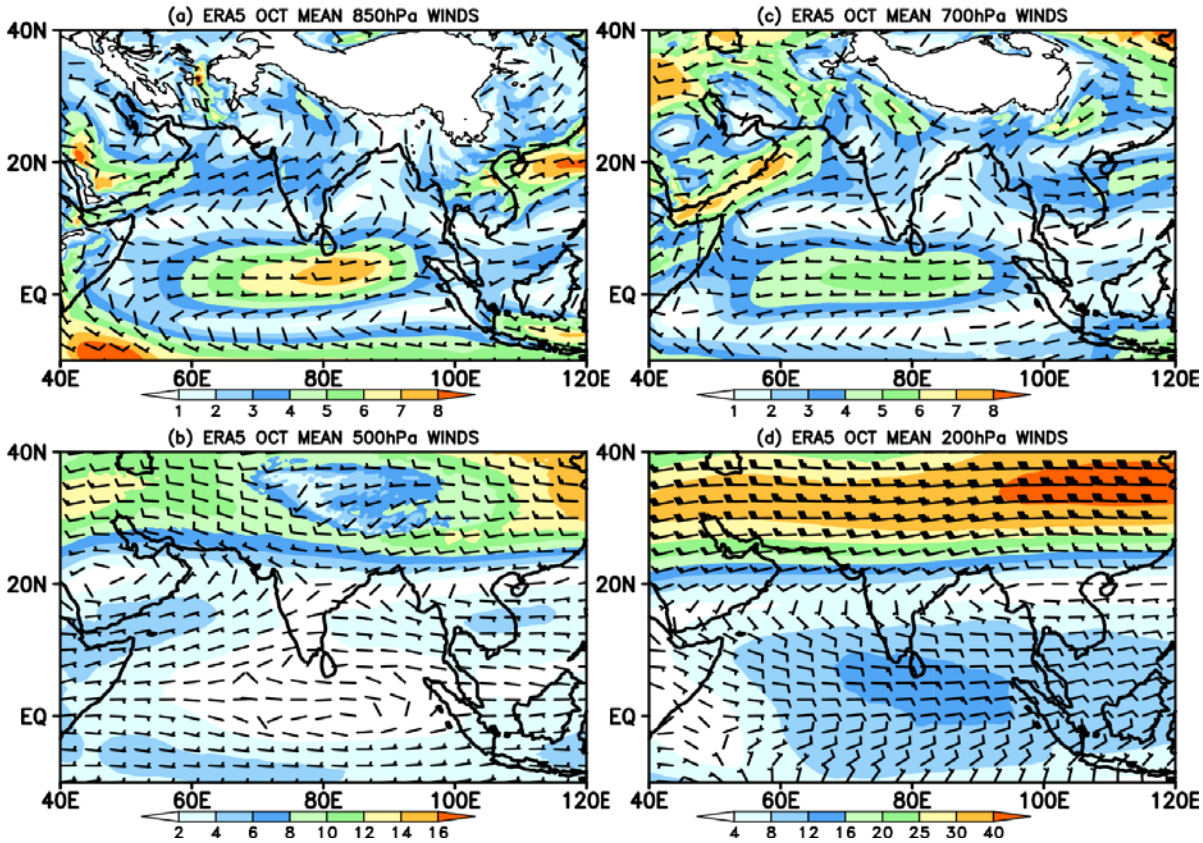

Fig 2.7. Mean wind flow pattern during October at a) 850 hPa b) 700 hPa c) 500 hPa and d) 200 hPa levels. Source: ERA5 reanalysis. The colour shading represents wind speed in m/s. The data period: 1979-2021.

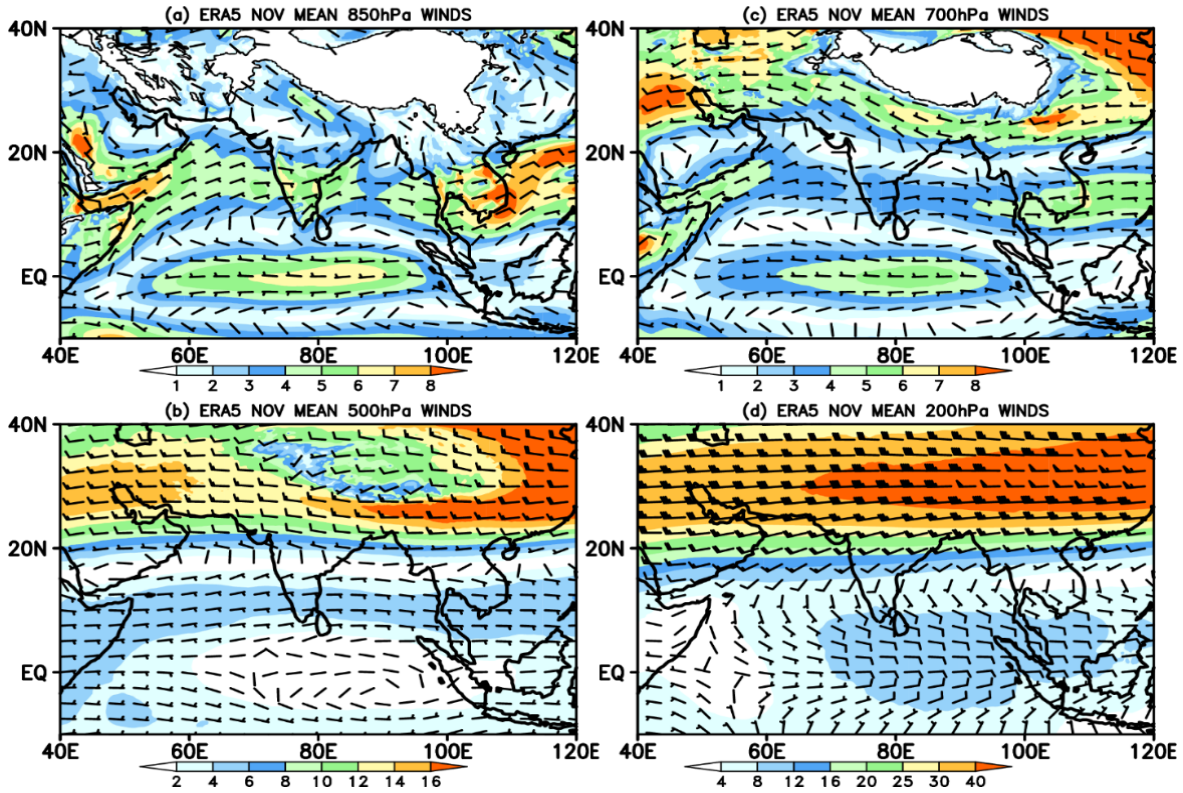

Fig 2.8. Same as Fig 2.7 but for November.

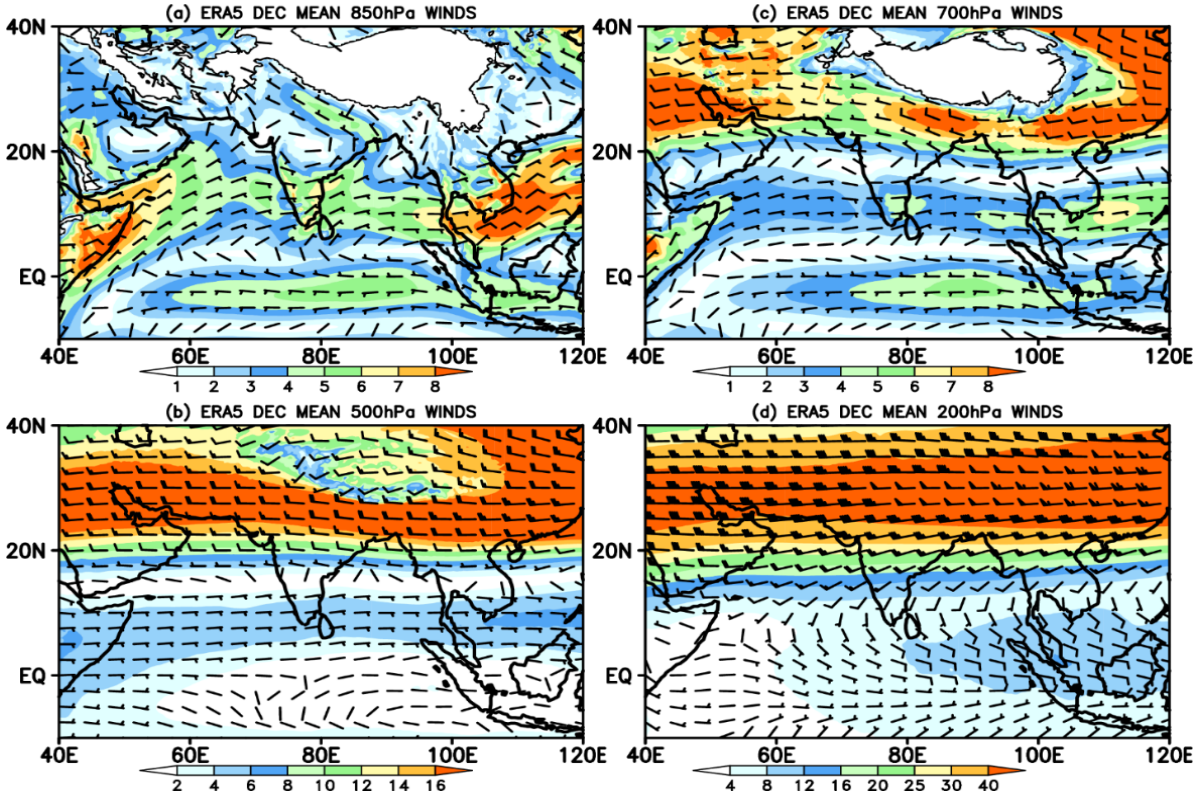

Fig 2.9. Same as Fig 2.7, but for December.

In the middle and upper troposphere (500 hPa and 200 hPa), easterlies prevail over the south Peninsula and adjoining seas. The sub-tropical ridge at these levels also shifts southwards from October to December. The sub-tropical ridge in the upper levels is an area of divergence and contributes to the intensification of low pressure systems over the region. The Tropical Easterly Jet (TEJ), which is one of the semi-permanent systems during the southwest monsoon totally disintegrates once the southwest monsoon is withdrawn from the country. From October to December, the sub-tropical westerlies over the northern parts of the country also get strengthened and start moving to lower latitudes. An upper tropospheric ridge gets established over the southern parts of India by October and November at the 200 hPa level.

2.3. **Mean Precipitable Water Content (PWC)**

Spatial distribution of mean precipitable water content provides useful information on moisture sources and sinks over the region during the NE monsoon season. Mean precipitable water content is calculated as the weighted average of moisture from surface to upper troposphere (normally up to 300 hPa). It provides information of moisture content in the whole atmospheric layer. Higher values suggest moisture sources.

The PWC is a measure of available moisture for precipitation in the atmosphere. It measures the maximum possible precipitation of water, which may precipitate out from a given atmospheric column, if nothing else (e.g., surface evaporation, moisture advection) happens over a given time span. Of course, this is rather an oversimplified picture, because it is hard to imagine that all PWC would condensate within a given column under any conceivable process. Nevertheless, it would be good enough to interpret PWC as an upper bound for a possible precipitation at a given moment with a given atmospheric column.

Fig 2.10 a, b and c show the spatial distribution of precipitable water content during October, November and December respectively. During October, the maximum

PWC is observed over the Southeast Bay of Bengal (east of Andamans) with values of 50 kg/m^2. The PWC reduces sharply westwards. Over the Bay of Bengal, PWAT values are more than 45 kg/m^2. Over south Peninsula, PWC varies between 40 to 45 kg/m^2. During November, the maximum zone of PWC slightly shifts southwards towards the equator. Over the south Peninsula, however, the PWC values are between 40 to 45 kg/m^2. During December, PWC maximum again shifts southwards and lies close to the equator. Over the south Peninsula, PWC values sharply reduce, ranging from 34 to 40 kg/m^2. During November and December, PWC decreases from south to north and isolines are almost parallel to the equator. Over the south Peninsula, PWC values are higher over the east coast as it reduces sharply towards interior parts.

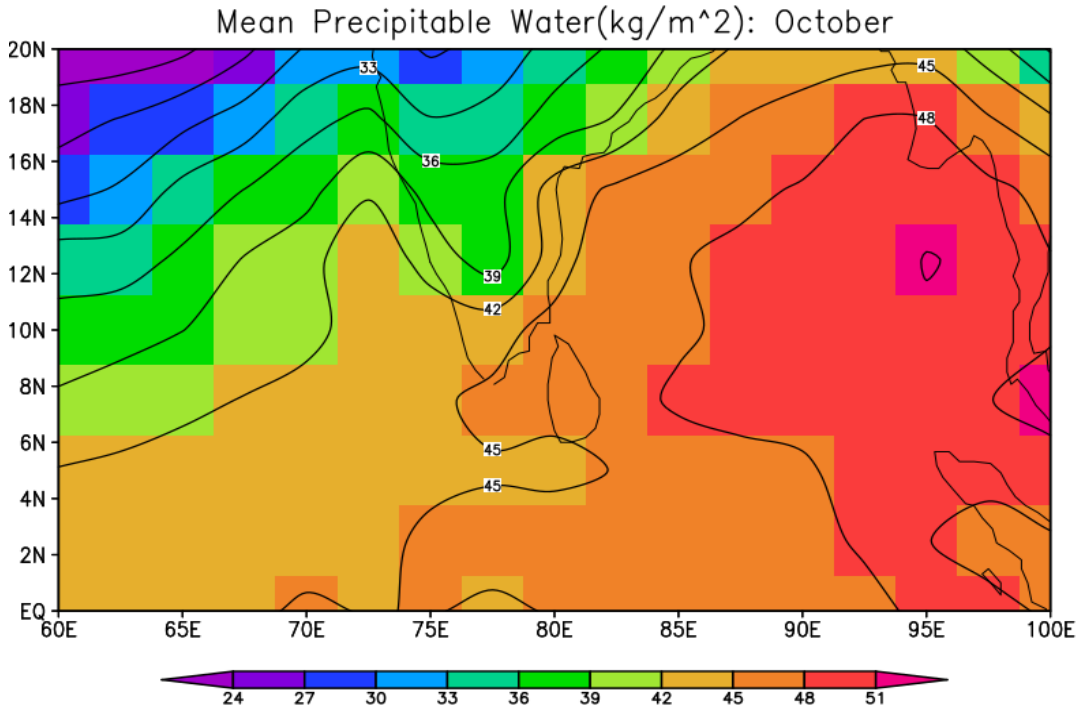

Fig. 2.10 a Mean precipitable water content (mm) during October (1979-2021). Data source: NCEP/NCAR reanalysis.

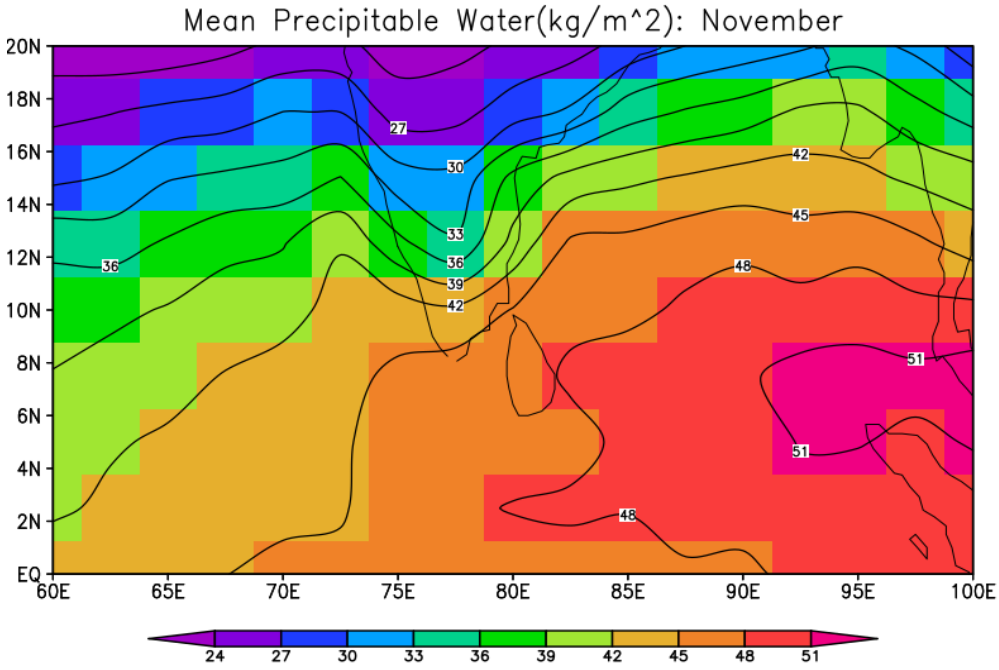

Fig. 2.10.b Same as Fig 2.10 a but for November.

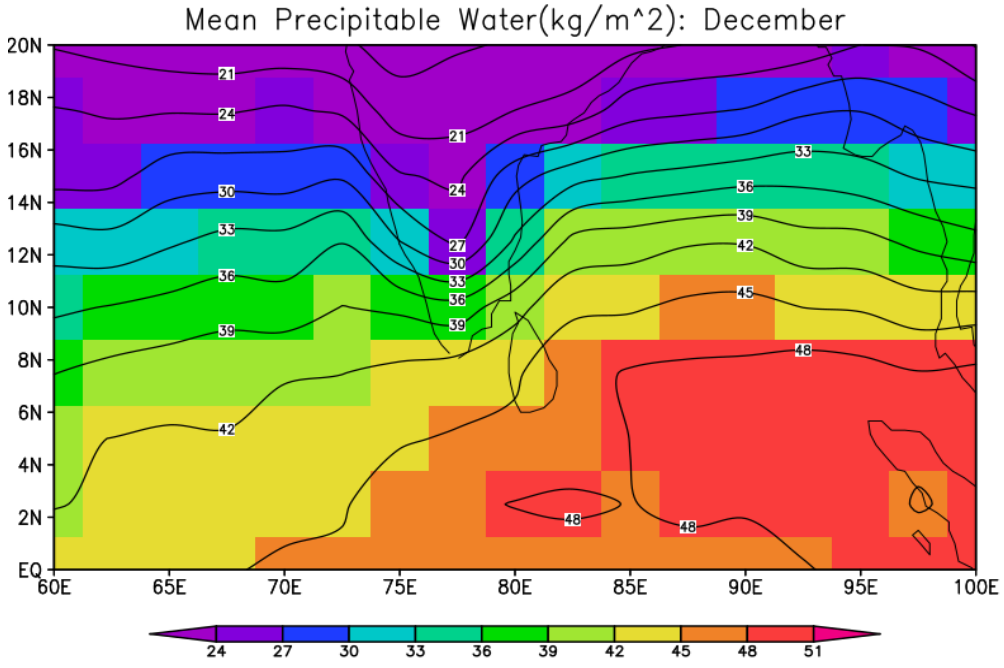

Fig. 2.10 c Same as Fig 2.10 a but for December.

These are monthly mean patterns, calculated using long term climatological data. However, on a typical day, PWC values can either increase or decrease, depending upon the prevailing synoptic conditions. For example, low pressure weather systems transport more moisture and PWC values can increase sharply in a day or two. To see the variation of moisture content in the atmospheric column, it is better to monitor the PWC changes in addition to low-level humidity. PWC can be easily calculated using radiosonde profiles of moisture.

2.4. Mean Air Temperatures

Seasonal (October-December) mean minimum, maximum and mean temperatures over South Peninsula are shown in Fig. 2.11 a, b and c respectively. This analysis was made using the IMD's 1 X 1 degree gridded daily temperature data (Srivastava et al., 2009). Seasonal mean minimum temperatures are the highest along the coasts and they decrease towards the interior parts. Over the east coast, seasonal mean minimum temperatures are of the order of 22-23^{0}C. Over the eastern parts of the south peninsula, the isotherms run parallel to the coast. Over the interior parts, minimum temperatures are below 20^{0}C. Seasonal maximum temperature over the south peninsula varies between 28^0 – 31^{0}C, except over the interior parts of Karnataka where maximum temperatures are below 28°C. Mean temperatures (Fig 2.11 c) over the coastal Andhra Pradesh are more than 26°C, while over the extreme south peninsula (Tamil Nadu and Kerala), the mean temperatures exceed 27^{0}C.

2.5. Sea Surface Temperatures (SST)

During the NE monsoon season, synoptic systems like tropical cyclones, lows and depressions and easterly waves, the presence of east-west trough contribute to rainfall over the South Peninsula. As these weather systems form over the Bay of Bengal and the Arabian Sea, oceanic conditions like Sea Surface Temperature (SST) play an important role. However, higher SSTs lead to more convection only if atmospheric

conditions also are favourable. Therefore, it is important to monitor closely the oceanic conditions like SST and Ocean heat content regularly during the NE monsoon season.

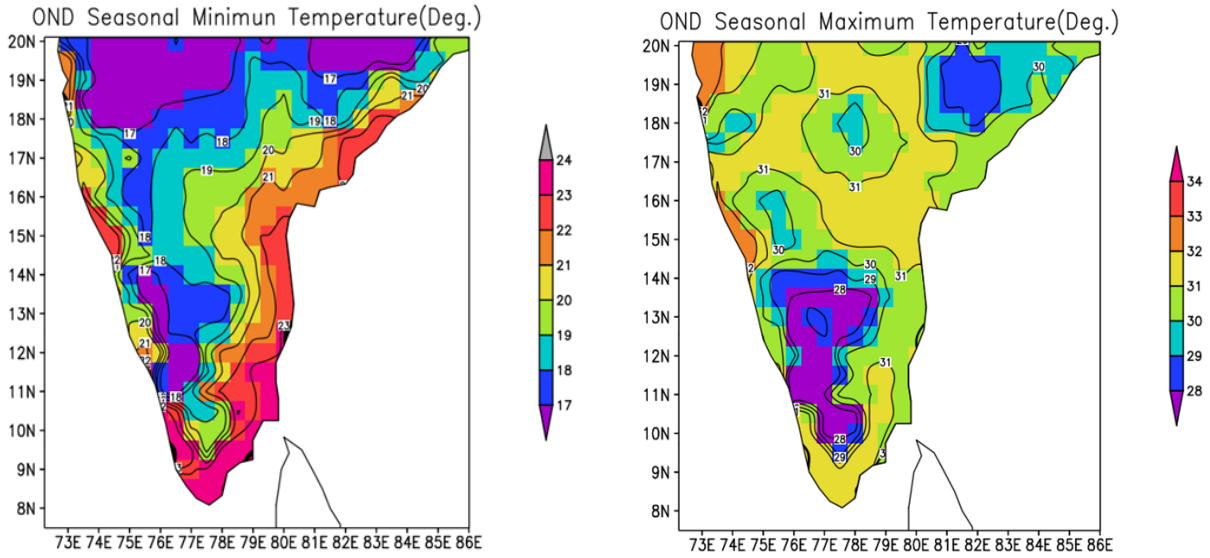

Fig. 2.11 a Mean Minimum Temperatures (^{0}C) (b) Mean Maximum Temperatures during October to December (1972-2021) Source: IMD gridded temperature data.

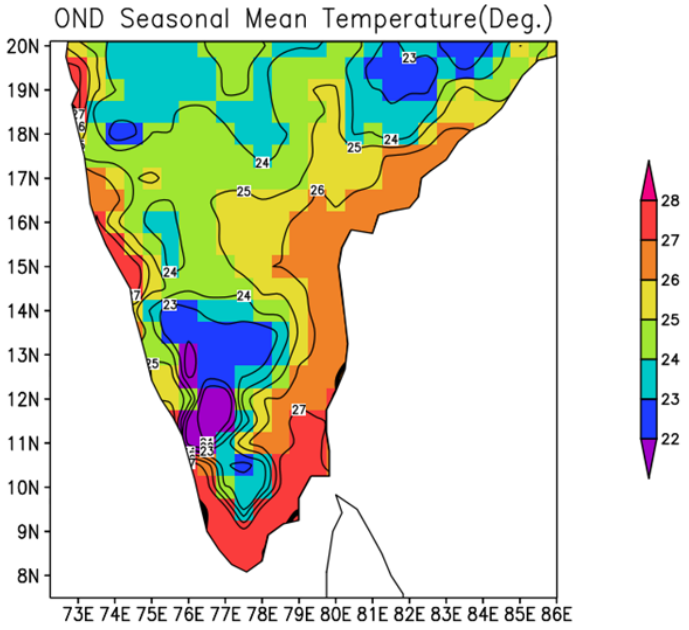

Fig. 2.11 c. Mean Temperatures during October to December (1972-2021) Source: IMD gridded data

Fig 2.12 a, b and c show the spatial distribution of SSTs during October, November and December respectively. During October, SSTs are of the order of 28.5^{0}C over the central Bay of Bengal. Over the eastern parts of the Arabian Sea, SSTs are of the order of 28.5^{0}C. But it sharply reduces westwards and over the western Arabian Sea, SSTs are below 27.5^{0}C. During November, the SST maximum slightly shifts southwards and is located near the east central Bay of Bengal with values exceeding 28.5^{0}C. Another SST maximum is observed over the east central Arabian sea off the Kerala and Karnataka coasts. By December, both the Bay of Bengal and the Arabian Sea cools off quickly. The 28.5^{0}C isotherm is now seen near the equator. SSTs over the west central Bay of Bengal are below 28.0^{0}C and sharply decreases towards the north Bay of Bengal.

The next section discusses the relationship between SST and convection during the NE monsoon season.

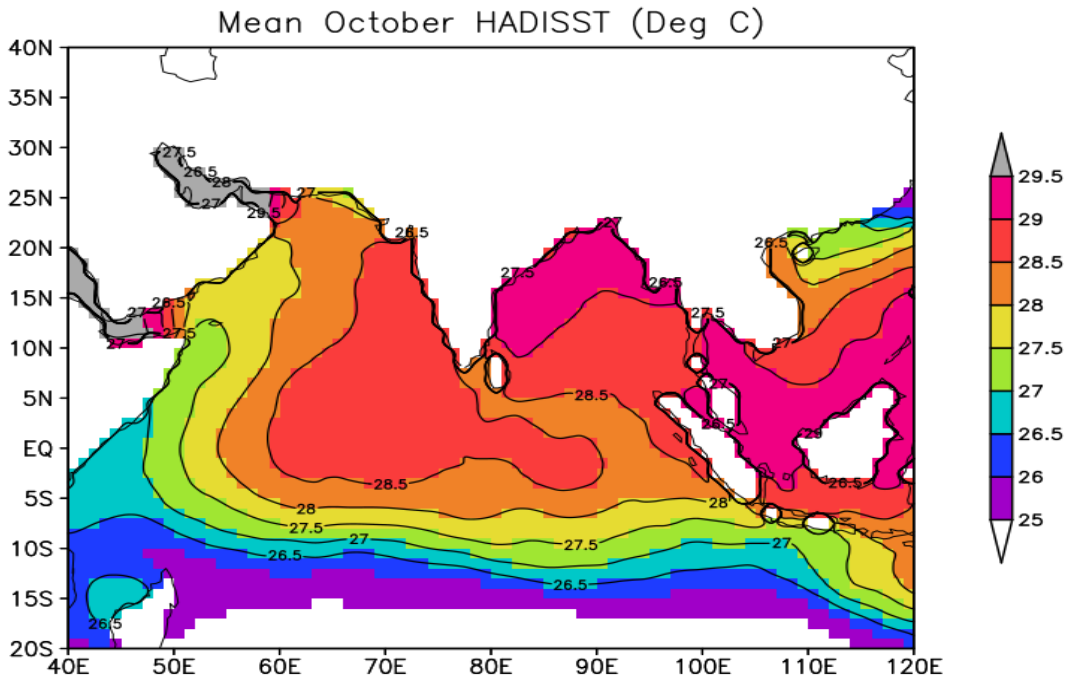

Fig.2.12 a Mean Sea Surface Temperature (SST) (degree C) during October, Period: 1972-2021. Source: HadISST, Met Office Hadley Centre.

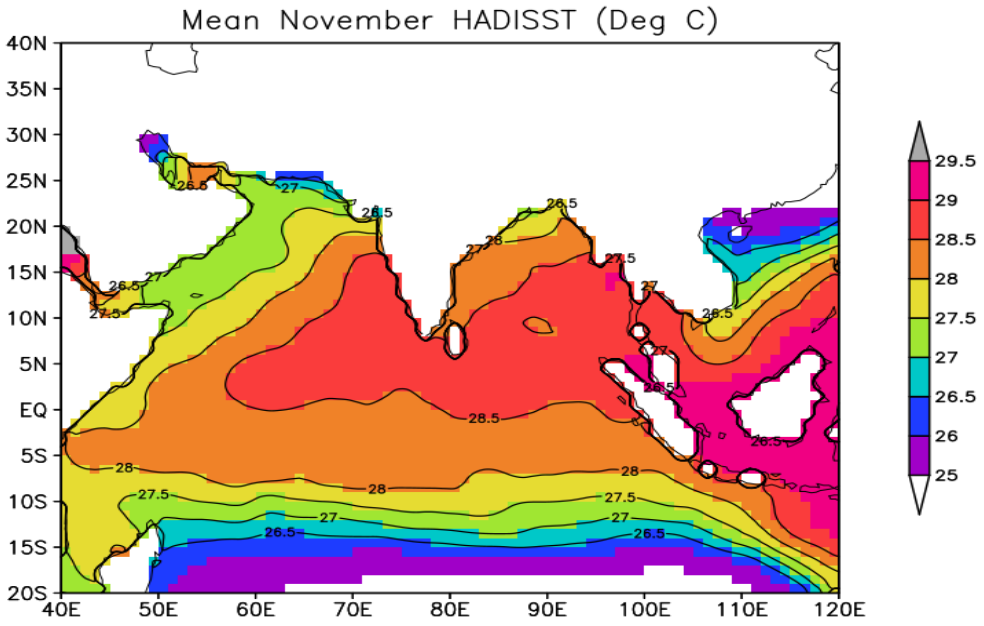

Fig.2.12 b Same as Fig 2.12 a but for November.

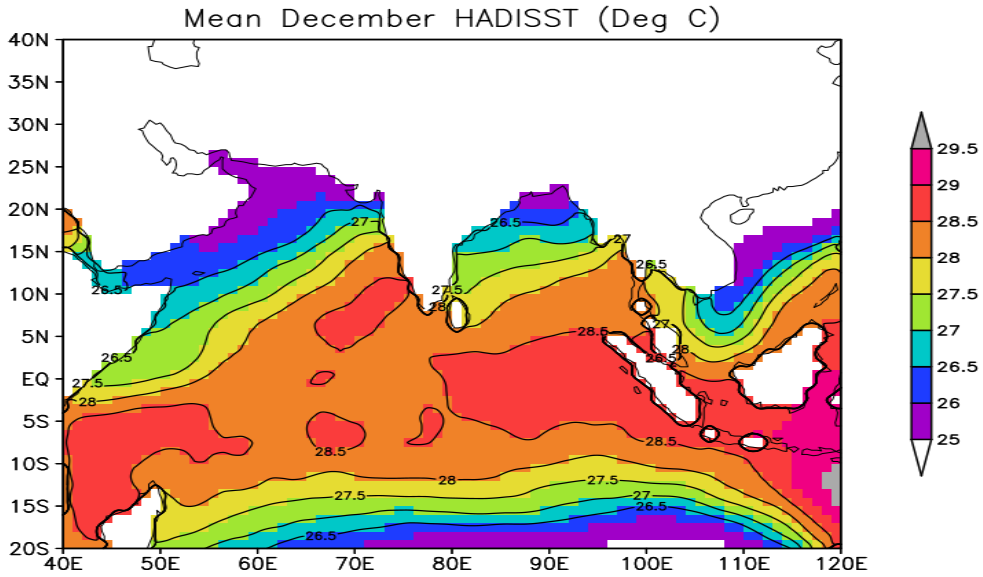

Fig.2.12 c Same as Fig 2.12 a, but for December.

2.6. Relationship between SST and Convection during the NE monsoon

There is a strong relationship between SST and atmospheric convection over the tropical ocean basins. Previous studies (Gadgil et al., 1984, Sabin et al., 2012) have shown that during the southwest monsoon season, convection over the Bay of Bengal is initiated when SSTs are between 27^0-28^0C. A similar analysis was made for the NE monsoon season (Oct-Dec) using long term data of SST and Outgoing Long Wave Radiation (OLR) data over the Indian Ocean. OLR is a proxy for atmospheric convection.

Fig 2.12 d shows the scatter plot between SST and OLR over the a) the Arabian Sea (0-20^0 N, 60-75^0 E) and b) the Bay of Bengal (0-20^0 N, 80-100^0 E). The data during 1982-2021 have been used for these plots. Over the Bay of Bengal, convection starts abruptly and increases sharply once the SST threshold crosses 28.0^0 C. At 28.5^0C, the OLR in the Bay of Bengal is 20 Wm^{-2} lower than in the Arabian Sea due to much deeper clouds over the Bay of Bengal. The mode with the highest probability for SST above the threshold of 28^0C over the Bay of Bengal has low OLR (about 210 Wm^{-2}) corresponding to deep convection whereas that for the Arabian sea it is around 250 Wm^{-2}.

It is interesting to note that even above the SST threshold of 28^0C, there are points with OLR values more than 240 Wm^{-2} suggesting severe convection is not present at these locations. It may be worthwhile to note that only SST threshold will not decide whether convection will occur or not. Initiation of convection also depends on atmospheric circulation, which should be conducive for low level convergence and ascending motion (Lau et al., 1997). This aspect is not further examined here and should be taken up as a separate study.

2.7. **Spatial distribution of cloud properties**

A further analysis was made on the spatial structure of some vital cloud properties during November over the region using the International Satellite Cloud Climatology Product (ISCCP) data (Rossow et al., 1991) for the period 1998-2019. Fig. 2.13 a, b and c show the spatial pattern of Deep convective clouds (DCC) (%), Cloud

Optical Thickness and Cloud Water Path (cm) respectively. Cloud optical thickness is the vertical optical thickness between the top and bottom of a cloud. The optical thickness of a cloud is the degree to which the cloud prevents light from passing through it. It depends directly on the cloud thickness, the liquid or ice water content and the size distribution of the water droplets or ice crystals.

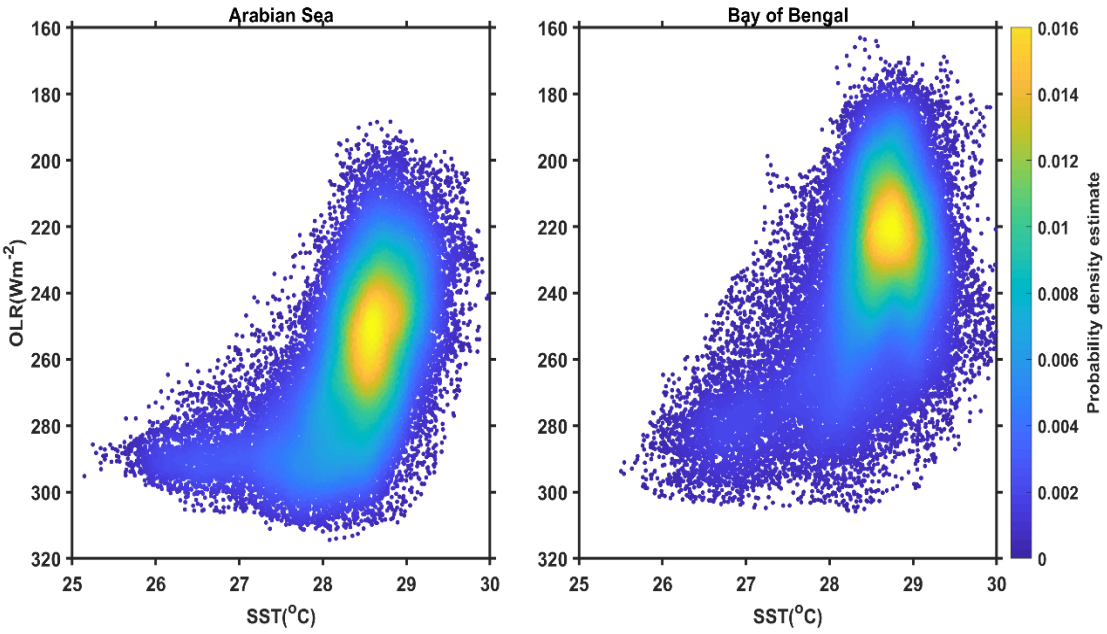

Fig 2.12 d. The scatter plot between SST and OLR over a) Arabian Sea (0-20^0 N, 60-75^0 E) and b) Bay of Bengal (0-20^0 N, 80-100^0 E). The data during 1982-2021 have been used for these plots.

Deep convective clouds are clouds with cloud top crossing above 400 hPa. The spatial distribution of DCC suggests maximum percent DCC over the east equatorial Indian Ocean (12-14%) coinciding with warmer SSTs (Figs 2.13 a, b and c). Over the southwest Bay of Bengal and off the Tamil Nadu coast, DCC is around 8%. Comparatively, DCC distribution over the Arabian sea is much smaller, suggesting the Bay of Bengal has much deeper convective clouds.

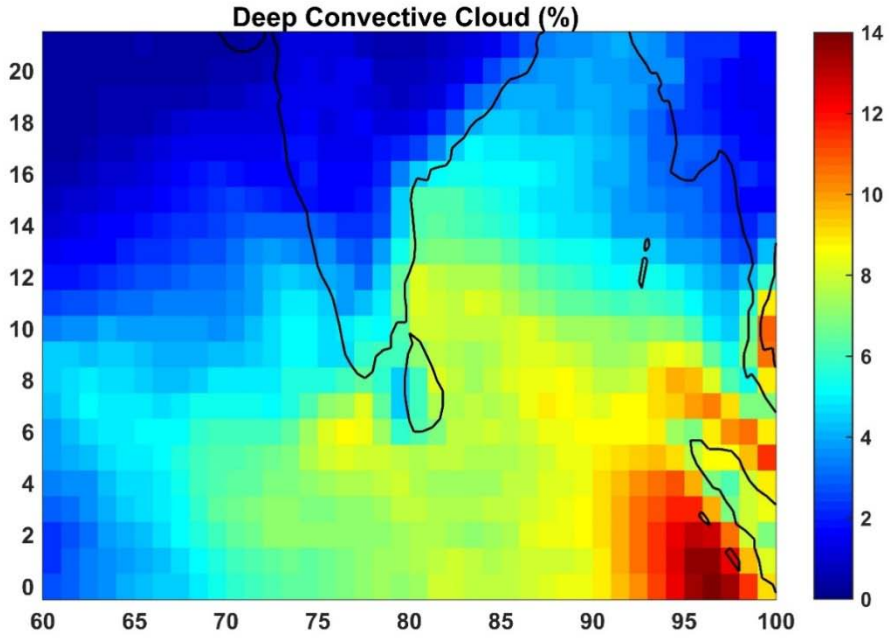

Fig. 2.13 a Spatial distribution of Deep Convective Clouds during the NE monsoon season (October- December) based on the ISCCP data. Period: 1998-2019.

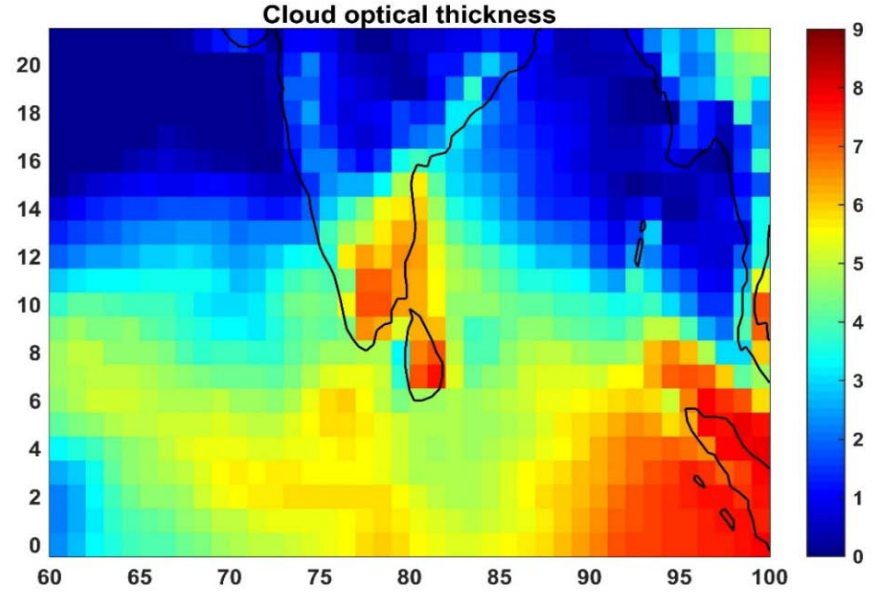

Fig.2.13 b Spatial distribution of Cloud Optical thickness during the NE monsoon season (October- December) based on the ISCCP data. Period: 1998-2019.

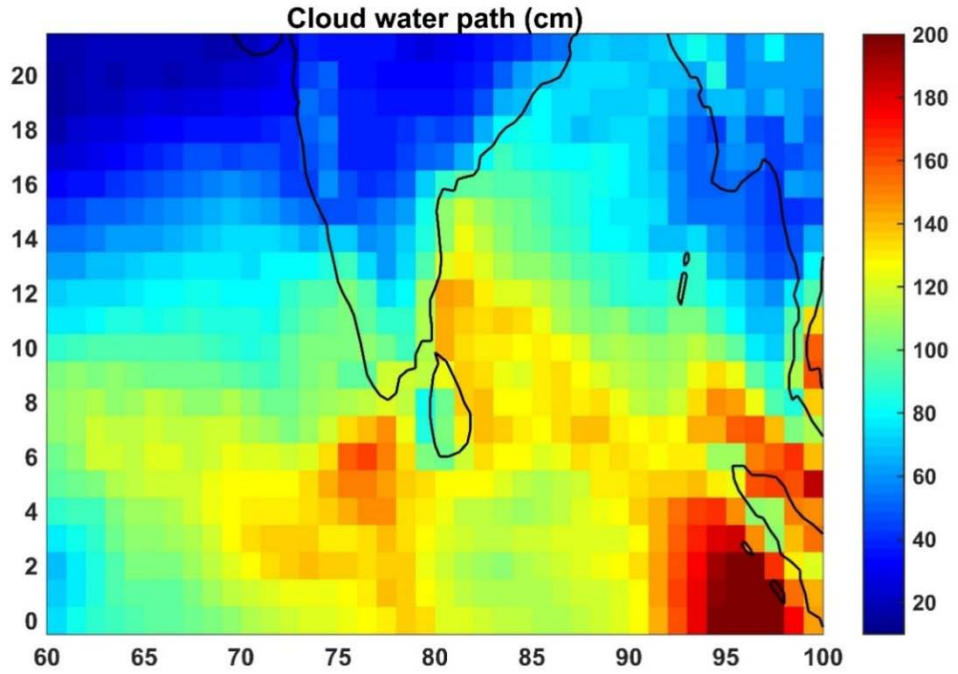

Fig.2.13 c Spatial distribution of Cloud water path (cm) during the NE monsoon season (October- December) based on the ISCCP data. Period: 1998-2019.

The spatial distribution of cloud optical thickness suggests maximum distribution over the east equatorial Indian Ocean coinciding with warmer SSTs and a large amount of deep convective clouds. Another maximum of cloud optical thickness is observed over the southeast Peninsula and adjoining Bay of Bengal. The spatial distribution of cloud liquid path (cm) shows that maximum is observed over the east equatorial Indian Ocean. Another maximum of cloud liquid path with values more than 120 cm is observed over the southwest Bay of Bengal off Tamil Nadu Coast. Therefore, the eastern parts of south peninsula and adjoining Bay of Bengal have deeper convective clouds with larger optical depth and cloud liquid water path. The spatial distribution shown here is based on long term climatology. On a day-to day basis, there could be significant variations in the distributions of cloud properties and they should be monitored using INSAT and similar satellite data products.

Characteristics of raindrop size distribution (DSD) are studied by Rao et al. (2009) during the southwest (SW) and northeast (NE) monsoon seasons using 4 1/2 years of Droplet Size Distribution (DSD) measurements made at Gadanki (13.5°N, 79.2°E) by an impact-type disdrometer. The observed DSD is found to be distinctly different in the NE monsoon from that of the SW monsoon. The stratified DSD (based on rain rate) shows more small drops and fewer bigger drops in the NE monsoon compared to the SW monsoon, particularly in the low rain rate regimes.

2.8. Thunderstorms/ Lightning

During the NE monsoon season, the south Peninsula experiences large scale thunderstorm activity. A good review of thunderstorm activity over India using station data is given in a recent paper by Omvir Singh and Bharadwaj (2017). A detailed study on lightning activity over the Indian region was published by Ranalkar and Chaudhari (2009) using the TRMM Lightning flash data. The average number of thunderstorm days during October, November and December are given in Fig 2.14 a, b and c respectively. These plots are taken from the IMD Climate Hazards and Vulnerability Atlas of India (2022) (https://imdpune.gov.in/hazardatlas/index.html). The data from 1981-2010 have been used to prepare these spatial maps.

During October, some districts in coastal Andhra Pradesh, Tamil Nadu and Kerala experience more than 4 thunderstorm days. Over south interior Karnataka and Rayalaseema, average number of thunderstorm days is between 2 and 3. During November, thunderstorm activity is reduced in Coastal Andhra Pradesh. However, Tamil Nadu and Kerala still experience thunderstorms with average number varying between 3 and 7 days. Over the coastal Andhra Pradesh, south interior Karnataka and Rayalaseema, thunderstorm activity is slightly reduced. By December, thunderstorm activity is further reduced. During December, maximum thunderstorm days are observed over Kerala and southern parts of Tamil Nadu.

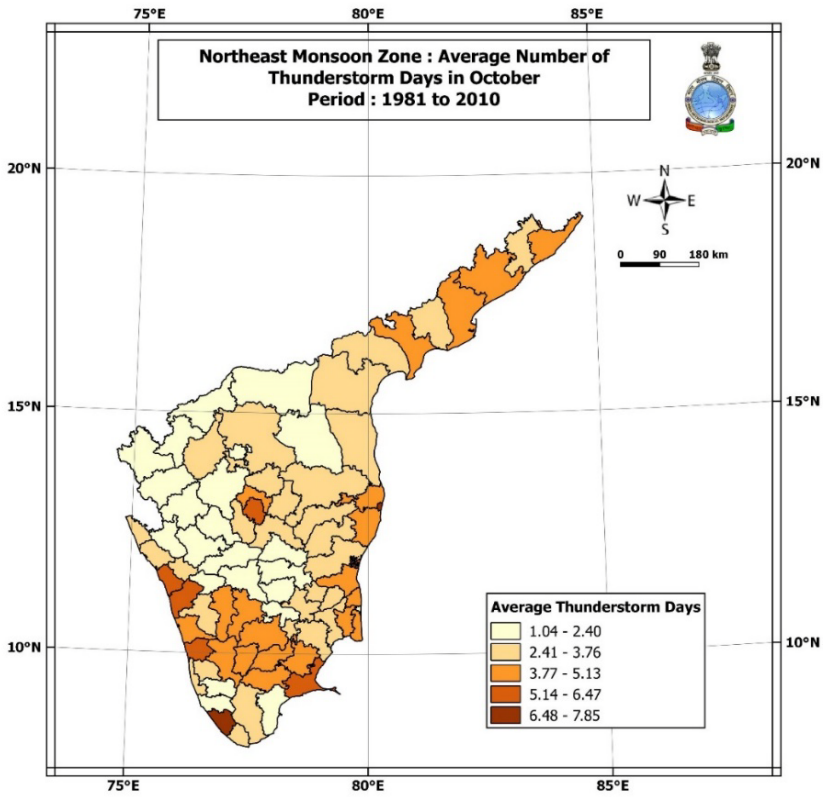

Fig 2.14 a. Average number of Thunderstorm Days during October, 1981-2010. (Source: IMD Climate Hazards and Vulnerability Atlas of India, 2022).

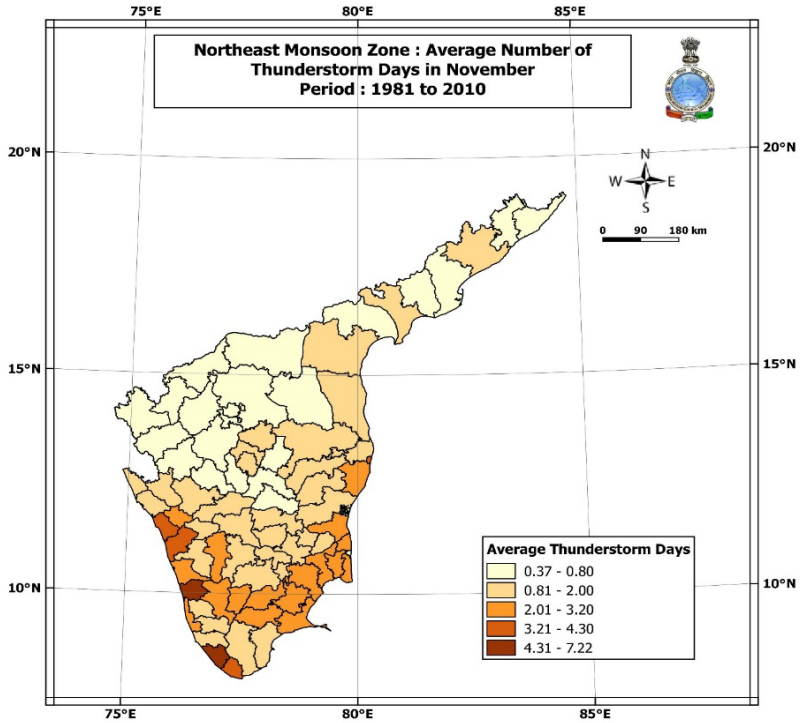

Fig 2.14 b. Same as Fig 2.14 a, but for November.

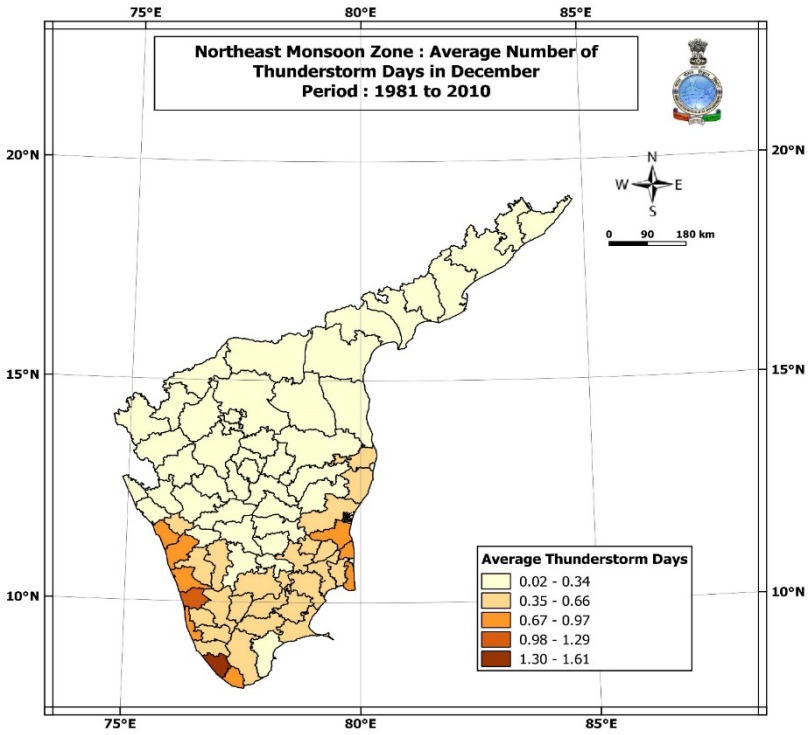

Fig 2.14 c Same as Fig 2.14 a, but for December.

Fig 2.15 a, b and c show the spatial pattern of the average number of lightning flashes per sq km per day during October, November and December respectively. These plots are also taken from the IMD Climate Hazards and Vulnerability Atlas of India (2022). During October, maximum lightning activity is observed over the interior parts of Tamil Nadu and the northern parts of Kerala. During November, lightning flash activity is mostly confined to Kerala and adjoining south Tamil Nadu. During December, the lightning activity is mostly confined to Kerala. Thus, during the NE monsoon season, the state of Kerala witnesses maximum lightning activity. This could be related to proximity to the Arabian Sea, thus abundant moisture transport and orography along the west coast supporting deeper convective activity.

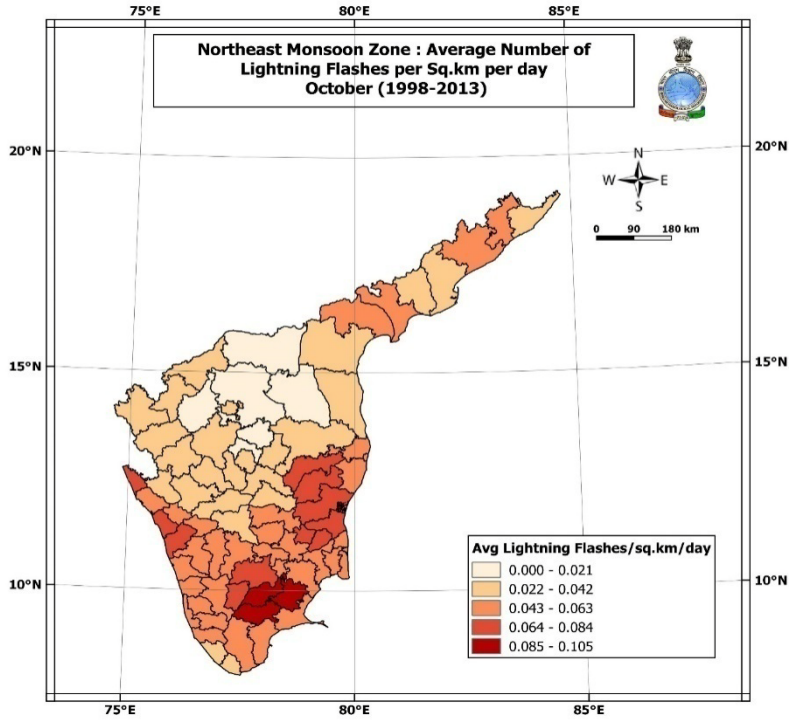

Fig 2.15 a. Average number of Lightning flashes per sq km per day during October. (Source: IMD Climate Hazards and Vulnerability Atlas of India, 2022).

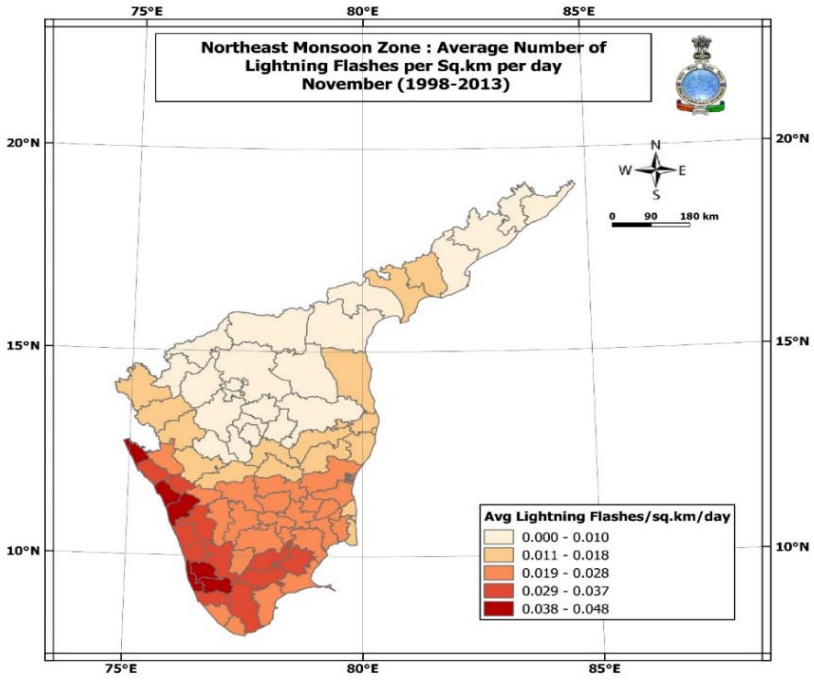

Fig 2.15 b Same as Fig 2.15 a, but for November.

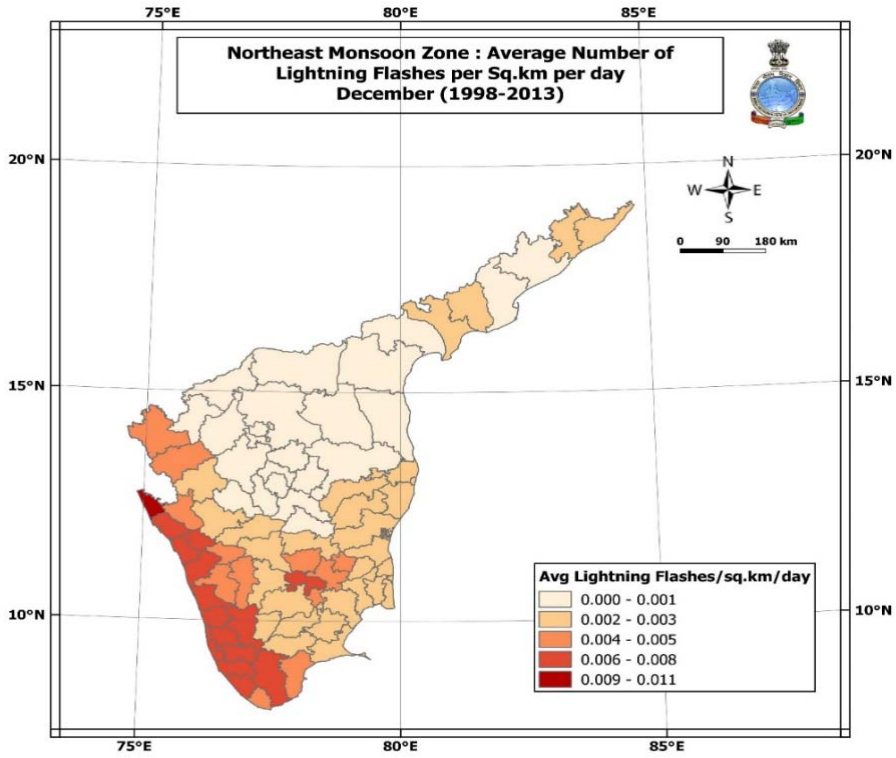

Fig 2.15 c. Same as Fig 2.15 a, but for December.

2.9. Extreme Wind Speed

For providing wind speed forecasts for specific purposes to users, it is important to know the climatology of extreme wind speed during the NE Monsoon season. Fig 2.16 a, b and c shows the spatial distribution of Extreme surface wind speed (in m/sec) in October, November and December respectively. The surface wind speed is normally measured at a height of 10.0 m. These maps are also derived from the IMD Climate Hazards and Vulnerability Atlas of India, 2022.

During October, extreme surface wind speeds exceeding 18 m/sec are observed over the north coastal Andhra Pradesh and interior parts of Tamil Nadu. Over other parts of the south Peninsula, extreme surface wind speed varies between 12 and 18 m/sec. During November, east coast of Tamil Nadu and coastal Andhra Pradesh has maximum risks due to extreme surface wind speeds. This region experiences tropical weather systems like depressions and cyclonic storms every year. Over this region,

extreme surface wind speed varies between 22 and 57 m/sec. Thus, this region is very prone to extreme surface wind speed.

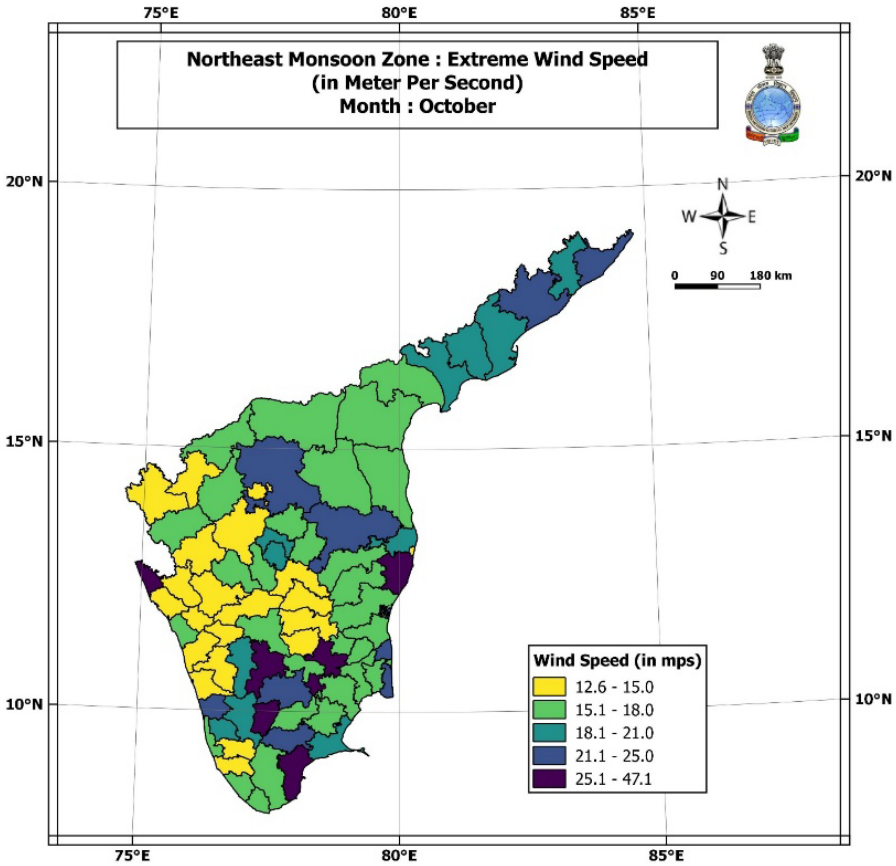

Fig. 2.16 a. Extreme Wind Speed (m/sec) during October (Source: IMD Climate Hazards and Vulnerability Atlas of India, 2022).

Extreme surface wind speed decreases sharply towards interior parts of south Peninsula. By December, northern parts of Tamil Nadu and adjoining parts of Rayalaseema experience the highest extreme wind speed. Over this region extreme surface wind speed varies between 41 and 59 m/sec. Over the southeast parts of Tamil Nadu, extreme surface wind speed varies between 31.0 and 41.0 m/sec. Over other parts of south Peninsula, extreme surface wind speed varies between 12.6 and 31.5 m/sec.

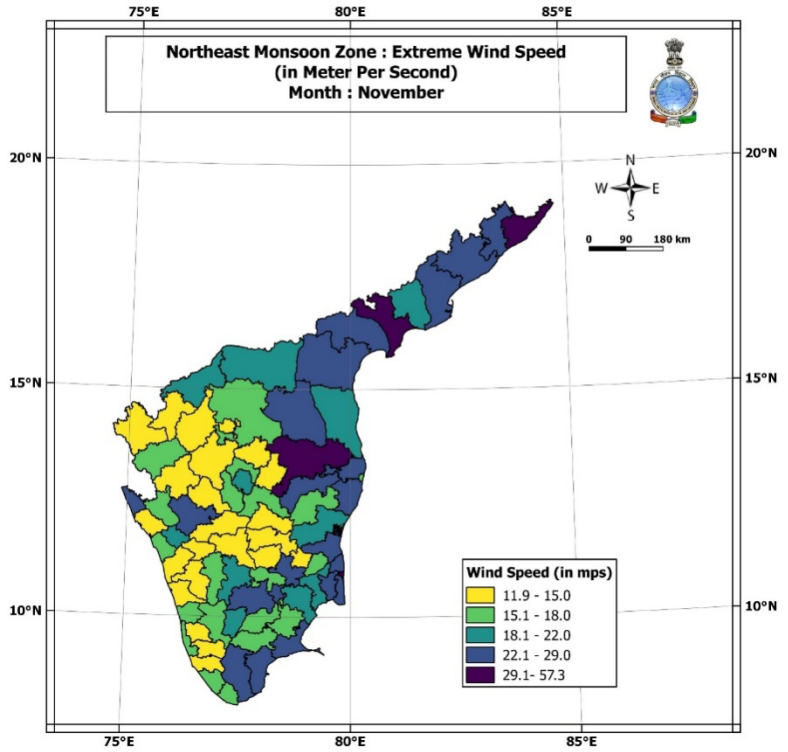

Fig. 2.16 b. Same as Fig 2.16 a, but for November.

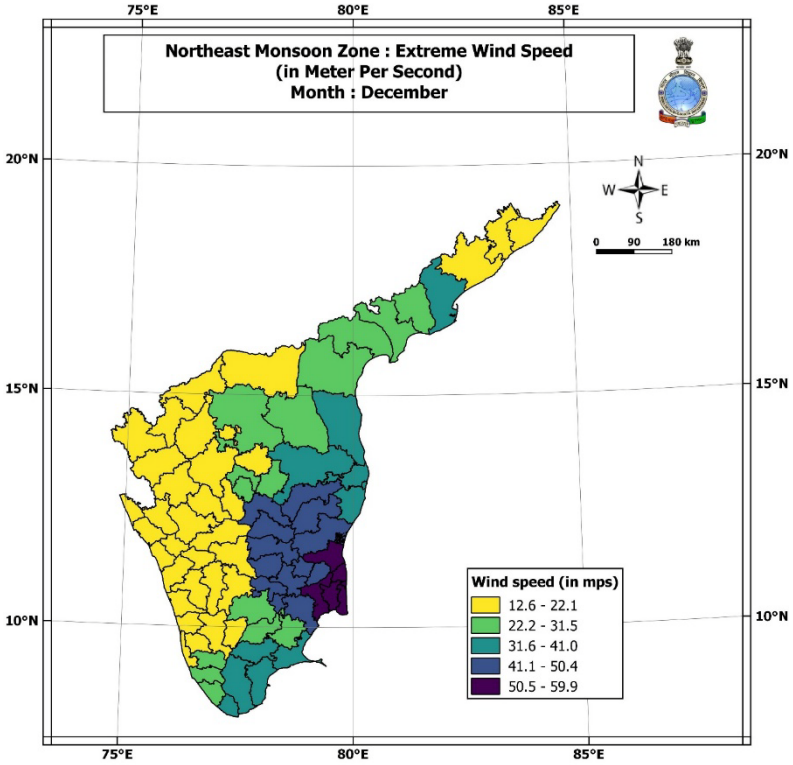

Fig. 2.16 c. Same as Fig 2.16 a, but for December.

Extreme surface wind speed observed over the eastern parts of south peninsula could be attributed to tropical cyclones making landfall over this region during the season. A detailed description of tropical cyclones including their tracks during the NE monsoon season is included in Chapter-4.

Chapter-3

Mean Rainfall Distribution

In this chapter, various features of mean rainfall during the NE monsoon are discussed.

3.1 Mean Rainfall over Met Sub-divisions

The mean monthly rainfall in the various meteorological sub-divisions in the south peninsula during the period October to December is given in Table-3.1. These mean values are calculated using the rainfall data of 1971-2020.

TABLE 3.1

Mean monthly, seasonal and annual rainfall (cm)

Based on the IMD sub-divisional data for the period 1971-2020

Subdivision name	OCT	NOV	DEC	Season's total	ANNUAL
COASTAL ANDHRA PRADESH & YANAM					
Rainfall(cm)	18	11	3	32	104
Rainfall as % of seasonal total	56	34	9		
Season's total as % of annual total				31	
RAYALSEEMA					
Rainfall(cm)	13	8	3	24	73
Rainfall as % of seasonal total	54	33	13		
Season's total as % of annual total				33	
TAMIL NADU, PUDUCHERRY & KARIAKAL					
Rainfall(cm)	17	18	9	44	92
Rainfall as % of seasonal total	39	41	20		
Season's total as % of annual total				48	

SOUTH INTERIOR KARNATAKA					
Rainfall(cm)	14	5	1	20	103
Rainfall as % of seasonal total	70	25	5		
Season's total as % of annual total				19	
KERALA & MAHE					
Rainfall(cm)	31	15	3	49	289
Rainfall as % of seasonal total	63	31	6		
Season's total as % of annual total				17	

Table 3.1 shows that for the South Peninsula as a whole, October is the rainiest month. However, in Tamil Nadu, November gets as much as rains in October. By December, the rainy season is practically confined over extreme south Peninsula including Tamil Nadu. The south peninsula receives rainfall, when the seasonal east-west convergence zone (ITCZ) and associated weather systems are present over the region. During December when the ITCZ moves further south, rainfall over the south peninsula sharply reduces. When the east-west trough is present, synoptic systems like lows and depressions form over this trough zone and move towards the south peninsula contributing to widespread rainfall activity.

Coastal Andhra Pradesh (CAP) gets rainfall during both the southwest and northeast monsoon seasons. During the NE Monsoon season, CAP receives about 32 cm of seasonal rainfall, with October contributing 56% of seasonal rainfall. About 34% of seasonal rainfall occurs during November. The NE monsoon season contributes about 31% of annual rainfall. Over Rayalaseema, the NE monsoon season contributes about 24 cm, which is 33% of the annual total. October is the rainiest month during the season and rainfall activity sharply reduces in November and December.

Tamil Nadu receives more rainfall during the NE monsoon season (October-December) compared to that during the Southwest monsoon season. There is a

considerable increase in rainfall activity from September to October and November. In December, rainfall activity is confined only to the coastal districts. The seasonal rainfall during the NE monsoon season is around 44 cm contributing to 48% of its annual rainfall. Over South-interior Karnataka (SIK) seasonal rainfall is around 20 cm, which is about 19% of the annual total. Over SIK, October contributes maximum rainfall during the season, while December hardly contributes to the seasonal total.

Over Kerala, the NE monsoon season contributes about 49 cm, which is about 17% of the annual total. During the NE monsoon season, Kerala receives maximum rainfall, even slightly more than Tamil Nadu. October contributes maximum rainfall over Kerala, which reduces in November and December.

3.2. Mean Spatial Distribution of Rainfall

Fig 3.1 a, b and c show the monthly rainfall climatology during the months of October, November and December. The mean values are calculated using the IMD gridded data (0.25 X 0.25 degree) from 1972-2021. During October, maximum rainfall exceeding 200 mm is observed over the coastal Andhra Pradesh, coastal Tamil Nadu and Kerala. Over central parts of Kerala, monthly rainfall exceeds 300 mm. However, rainfall reduces sharply towards the interior parts of south peninsula, where monthly rainfall is less than 150 mm. During November, monthly rainfall sharply increases over the northern parts of coastal Tamil Nadu and southern parts of coastal Andhra Pradesh, where monthly rainfall is more than 300 mm. Over Tamil Nadu, monthly rainfall sharply reduces towards the interior parts. Southern parts of Kerala experiences monthly rainfall exceeding 200 mm. Over the rest of Tamil Nadu and Kerala, rainfall is between 100 and 150 mm. Over the South interior Karnataka and Rayalaseema, monthly rainfall is less than 100 mm. During December, rainfall sharply reduces everywhere in the south peninsula. Maximum rainfall exceeding 200 mm is observed over coastal Tamil Nadu and reduces sharply towards interior parts. Over the rest of the south peninsula, monthly rainfall is less than 75 mm.

The spatial distribution of mean seasonal rainfall (October to December) is shown in Fig. 3.1 d. The spatial distribution suggests a rainfall maximum along the east coast of north Tamil Nadu and south coastal Andhra Pradesh with seasonal average exceeding 800 mm. Seasonal rainfall reduces sharply towards interior parts of South Peninsula. Another rainfall maximum is observed over Kerala. Over south peninsula, isohyets (lines of equal rainfall) run parallel to the east coast with maximum over the east coast and reducing towards the interior parts. During the NE monsoon season, the Kariakal-Vedarnyam belt receives the highest rainfall in the range 900-1000 mm with Vedarnyam receiving 103 cm. The decrease of rainfall south of Vedarnyam is probably due to sheltered nature of the coast (due to Sri Lanka land mass on the east). Tuticorin registers only 40-45 cm of normal rainfall.

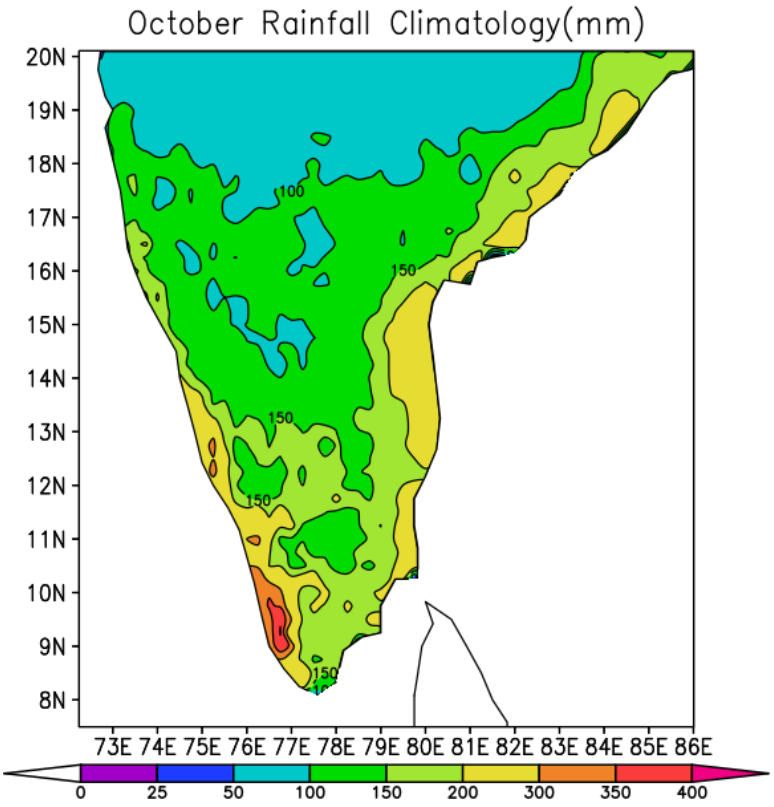

Fig. 3. 1 a IMD Observed Rainfall Climatology in mm during October (1972-2021). Source: IMD gridded data.

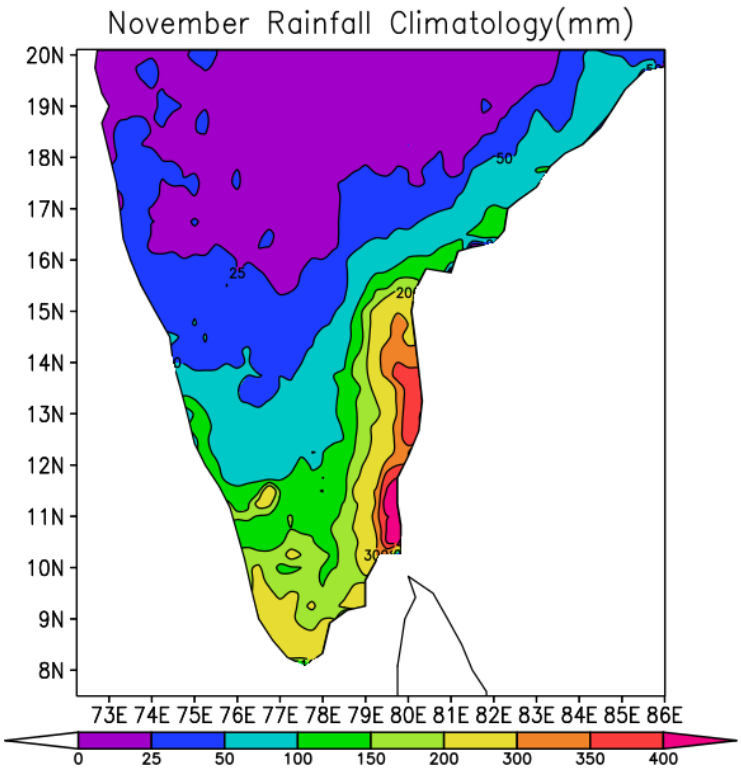

Fig. 3.1 b Same as 3.1 a, but for November.

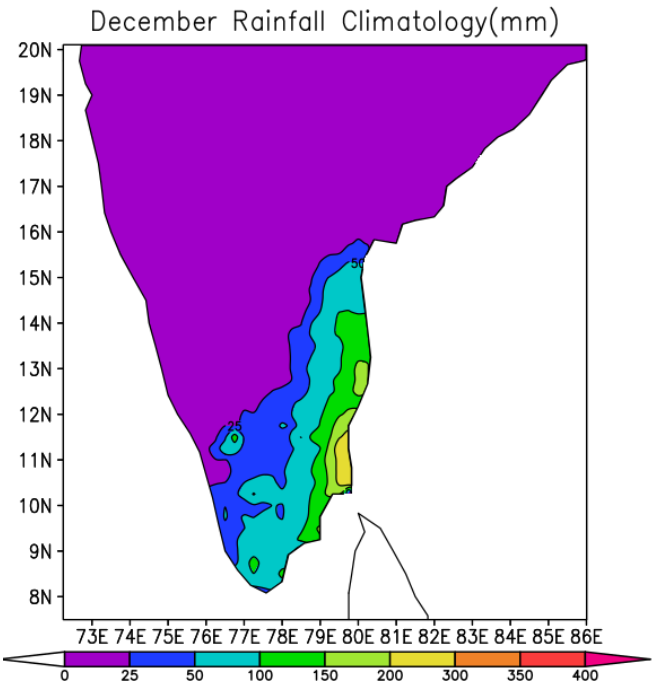

Fig. 3.1 c Same as Fig 3.1 a, but for December.

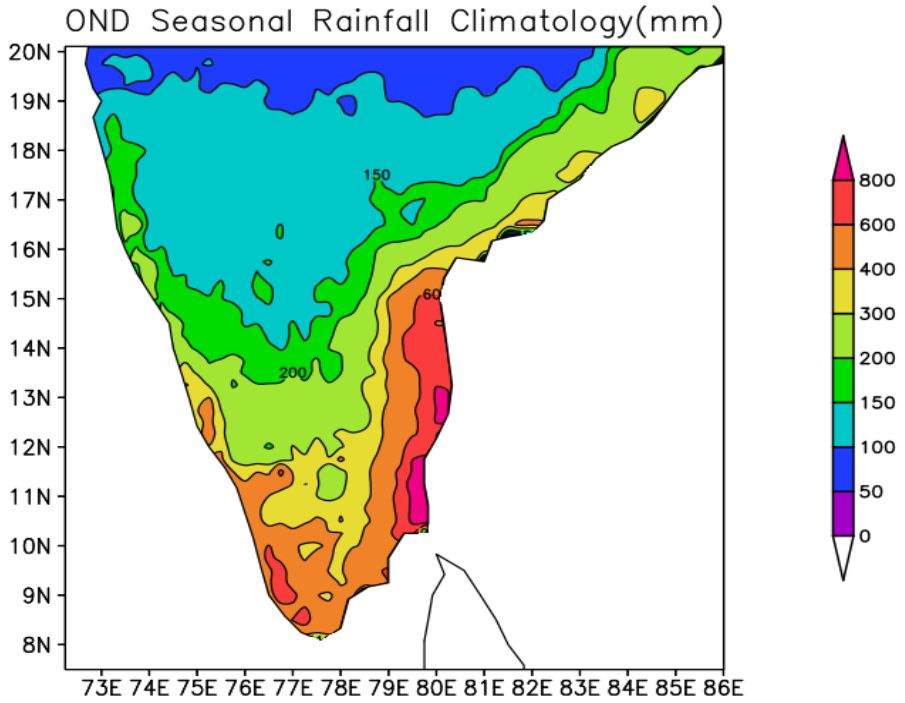

Fig 3.1 d. Seasonal Rainfall Climatology (in mm) during the northeast monsoon season (October- December), 1972-2021. Source: IMD gridded rainfall data.

Fig 3.2 shows the time variation of mean rainfall averaged over the south peninsula from 01 Sept to 31 Dec. The mean rainfall is calculated using the data of 1979-2021. The plot shows that October and December months contribute maximum rainfall over the region. From the first week of December, rainfall activity over the region is sharply reduced. This is due to the fact that by first week of December, the ITCZ shifts towards much south and rainfall activity is mostly confined south of 10^0N.

The Coefficient of Variation (CV) of seasonal (October to December) monsoon rainfall over the southern peninsula is given in Fig. 3.3. The CV of NE monsoon seasonal rainfall is generally higher compared to southwest monsoon season. CV varies from 30 to 50% over the south peninsula with the east coast experiencing smaller CVs compared to interior.

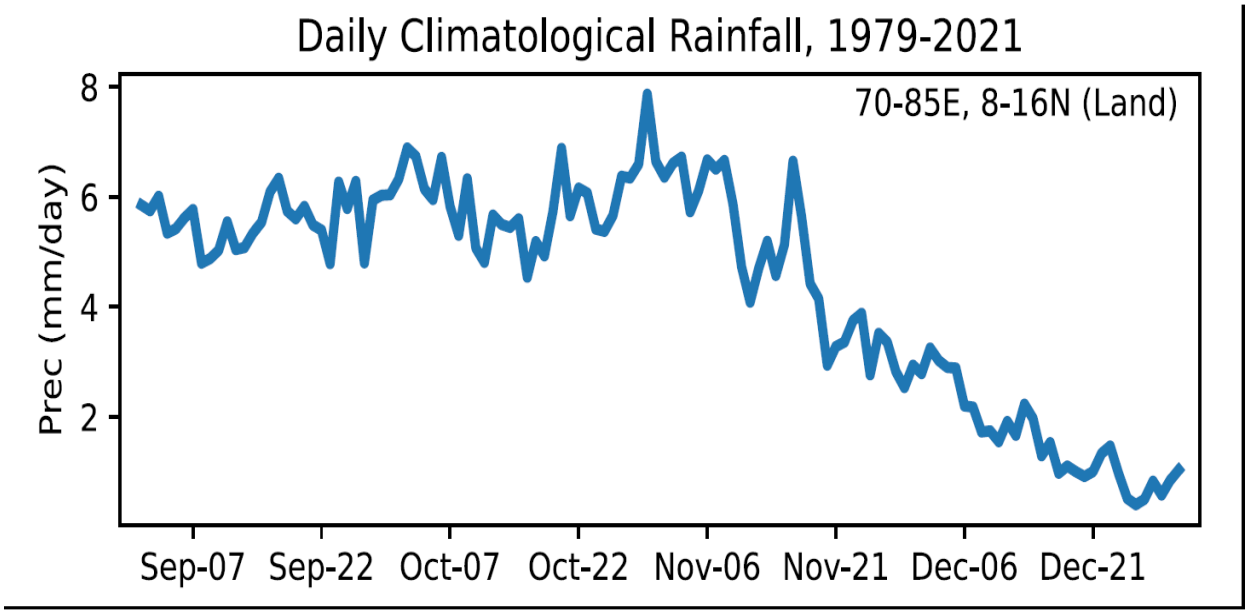

Fig 3.2. Daily climatological rainfall (in mm/day) over NE India from 1 Sept to 31 Dec averaged over the period 1979-2021. The averaging was done over the area 70-85^0 E, 8-16^0 N.

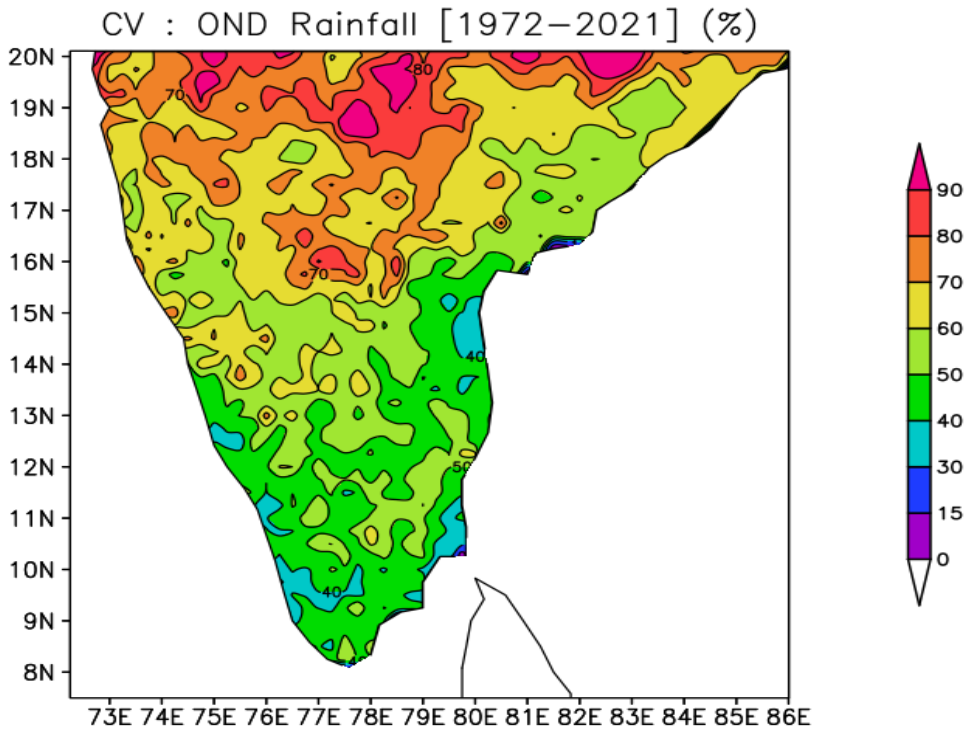

Fig 3.3. Coefficient of variation of seasonal Rainfall (in %) during the northeast monsoon season (October- December), 1972-2021. Source: IMD gridded rainfall data.

During the NE monsoon season, a rainy day is assumed to be a day with rainfall of 2.5 mm or more. Fig. 3.4 shows the spatial distribution of the mean number of rainy days during the NE monsoon season. Over the north Tamil Nadu coast and parts of Kerala and south Karnataka, mean rainy days are more than 30 during the season. Over the remaining parts of Tamil Nadu, coastal Andhra Pradesh and remaining parts of Kerala, number of rainy days varies between 20 and 30 days. Statistical trend analysis suggests (Fig 3.5), the mean number of rainy days over the interior parts of south Peninsula is increasing. It is important to note that this pertains to long term climatology. In a particular year, there could be an increase or decrease in the number of rainy days over a particular station.

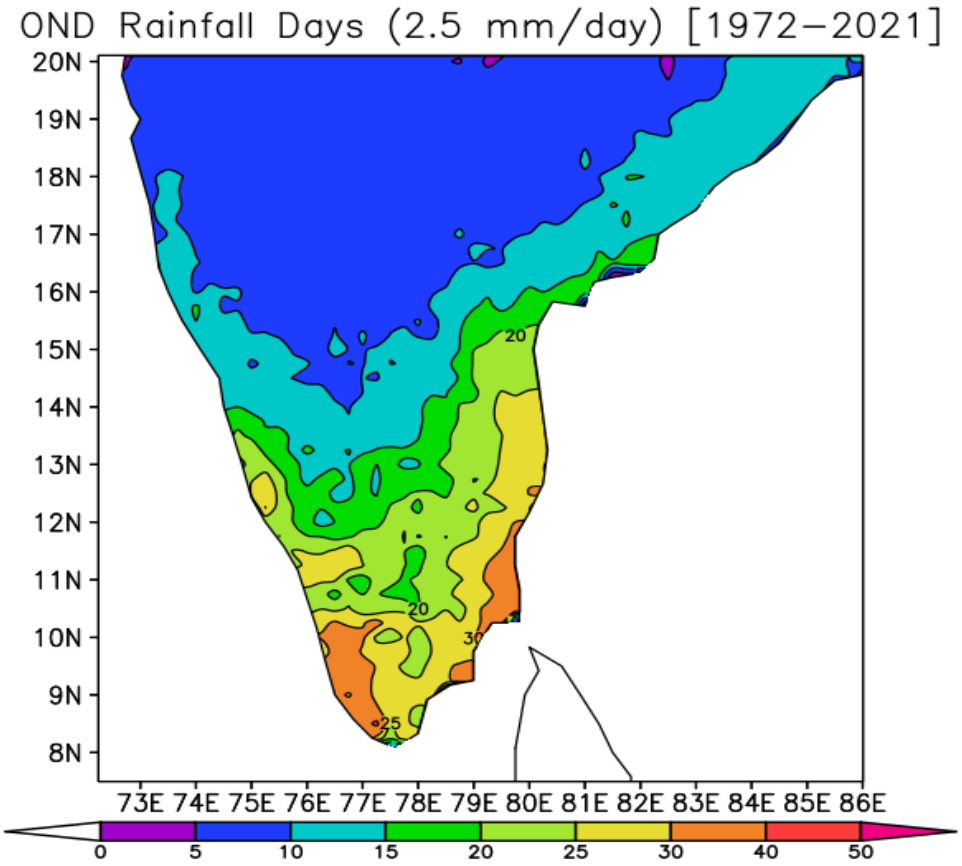

Fig. 3.4 Number of rainy days (> 2.5mm) during October to December (1972-2021). Source: IMD gridded Data

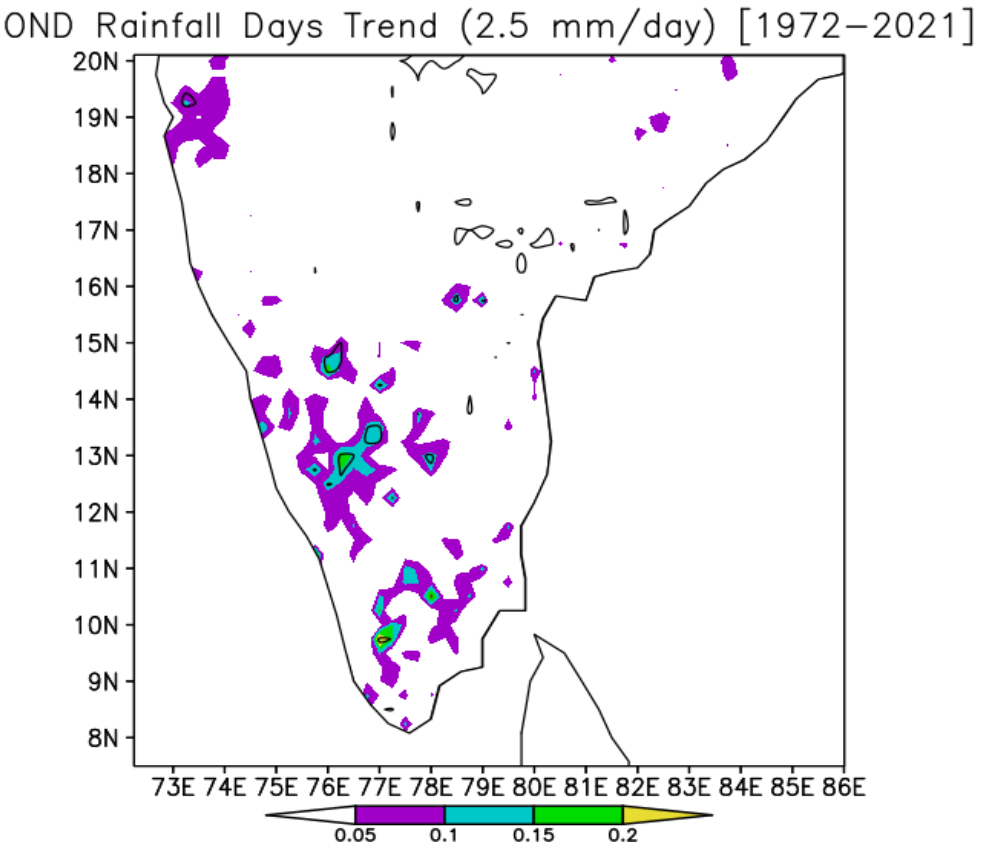

Fig. 3.5. Trend in rainfall days during October to December (1972-2021).

3.3. Heavy Rainfall events during the NE monsoon season

It is important to know the spatial pattern of climatology of heavy rainfall over the region. This will provide information on the climatological probability of heavy rainfall occurrence over the region during the season. The spatial pattern of heavy rainfall events was prepared using the IMD 0.25 X 0.25 degree daily rainfall data (Pai et al. (1972-2020). It may be noted that the IMD's definition of heavy, very heavy and extreme heavy rainfall is based on rainfall station data. Since the analysis given below is based on the IMD's gridded data and somewhat smoothed data, IMD's definition cannot be strictly used for defining heavy, very heavy and extreme rainfall. However, even with the gridded data, we could get a reliable understanding of the spatial distribution of such heavy rainfall events.

Fig 3.6 shows the spatial pattern of the number of days with heavy rainfall between 65 mm-124 mm. It suggests the maximum number of days with heavy rainfall is confined to the east coast of Tamil Nadu and the south coastal Andhra Pradesh, where on average we can expect more than 2 days of heavy rainfall. Another area of maximum heavy rainfall days is observed over south Kerala. Number of days with heavy rainfall sharply reduces towards the interior parts of the south Peninsula.

Fig 3.7 shows the spatial distribution of frequency (number of days) of rainfall with 125 mm or more during the NE monsoon season. It suggests maximum frequency is found over the coastal parts of north Tamil Nadu and Andhra Pradesh. It suggests that these very heavy rainfall spells are associated with the landfall of tropical cyclones/depressions and lows along the east coast. On an average, we can expect about one day of such an event over this region during the NE monsoon season.

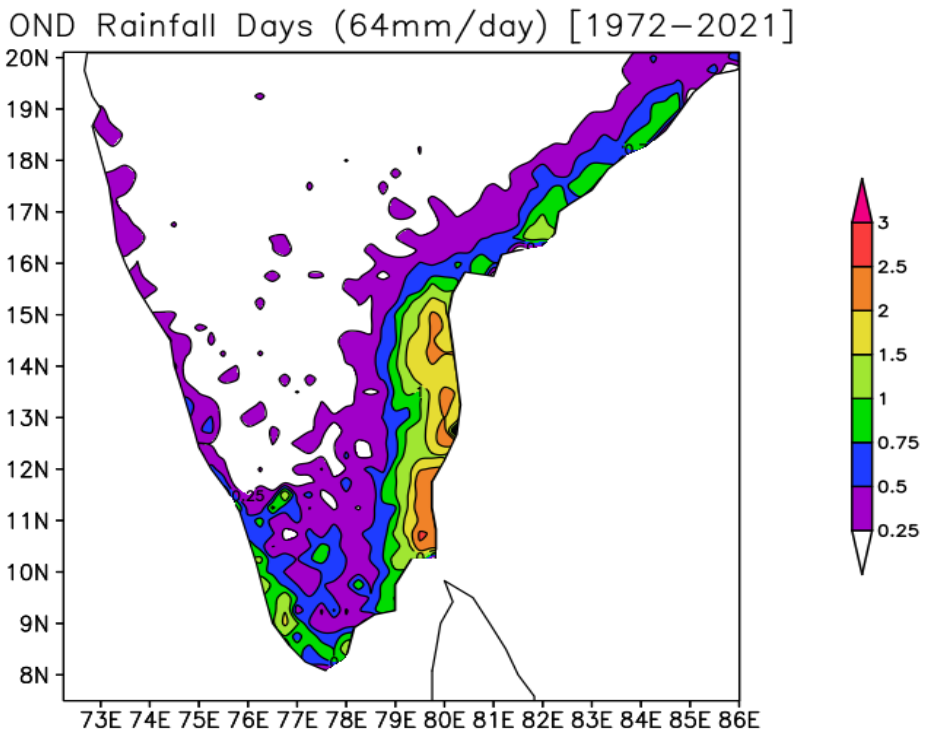

Fig. 3.6 Mean number of days during October-December with 65 mm-124mm. Period of the data 1972-2021.

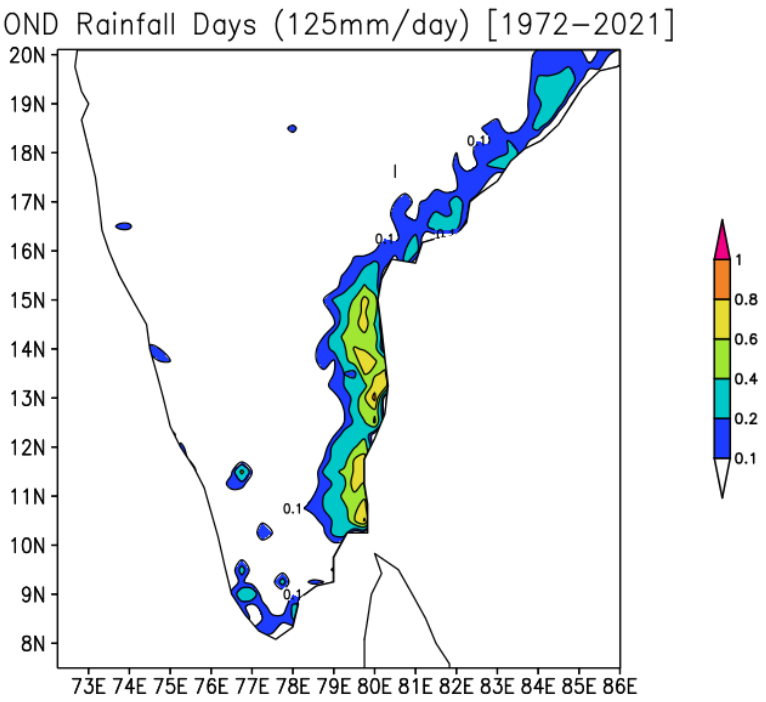

Fig. 3.7. Mean in rainfall days with more than 125 mm/day (Period: 1972-2021).

3.5. Maximum Probable frequency of heavy rainfall

Fig 3.8 shows the maximum probable frequency of heavy rainfall (between 65 and 124 mm) during October to December calculated using data from 1951-2019. This map was taken from the IMD Climate Hazards and Vulnerability Atlas of India, 2022. A maximum probability of more than 7 days can be expected over the east-coast of Tamil Nadu and Southern parts of Kerala and Tamil Nadu. Over the interior parts of the south Peninsula, the maximum probability lies between 3-4 days.

Fig 3.9 shows the maximum probable frequency of heavy, very heavy and extreme heavy rainfall (number of days) during the NE monsoon season (Oct-Dec). Over the east coast of north Tamil Nadu, South Coastal Andhra Pradesh and southern most districts of Tamil Nadu and Kerala, the maximum probable frequency is more than 15 days. Over other parts of coastal Pradesh, Tamil Nadu and south Kerala, the maximum probable frequency is between 10-14. Over interior parts of the south Peninsula, this number varies between 5-10 days.

Fig 3.10 shows the maximum probable frequency of very heavy and extreme heavy rainfall (number of days) during the season. Over the eastern coast of north Tamil Nadu, south coastal Andhra Pradesh and southern most parts of Tamil Nadu and Kerala, the maximum probable frequency of very heavy and extreme rainfall is between 5 and 11 days. Over the interior parts of the south Peninsula, this number varies between 1 and 4.

Thus, the eastern coast of north Tamil Nadu and south coastal Andhra Pradesh is the region, with maximum probable frequency of heavy rainfall days during the NE monsoon season. Southern parts of Tamil Nadu and Kerala also have similar maximum probable frequency.

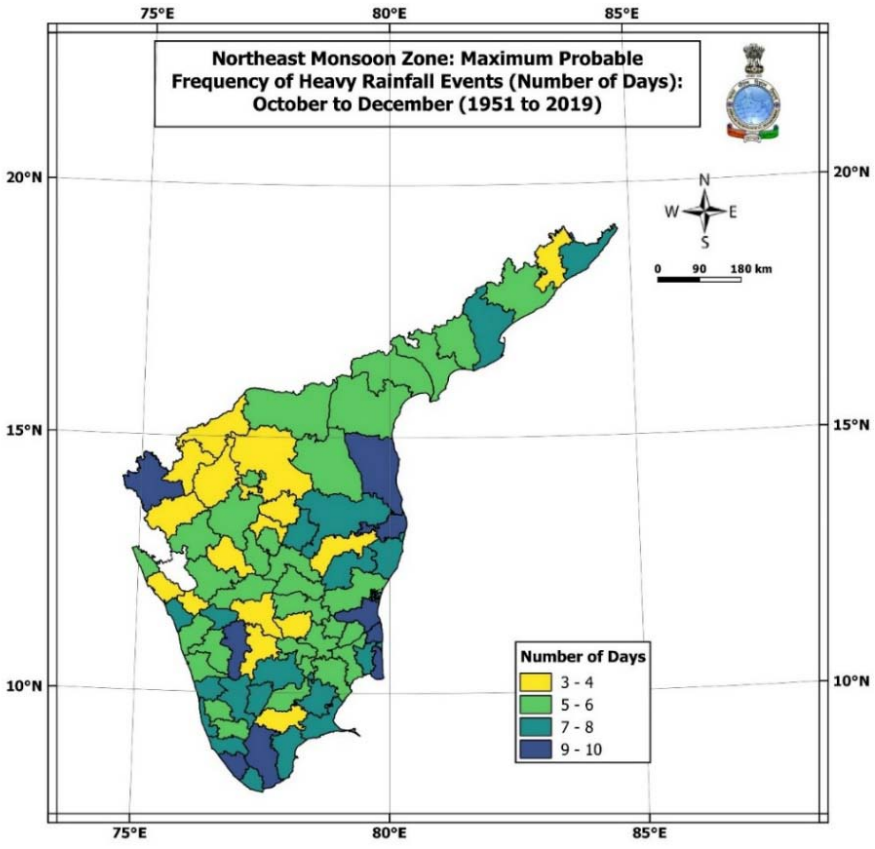

Fig. 3.8. Maximum Probable frequency of heavy rainfall events (Number of days): October-December, 1951-2019. (Source: IMD Climate Hazards and Vulnerability Atlas of India, 2022).

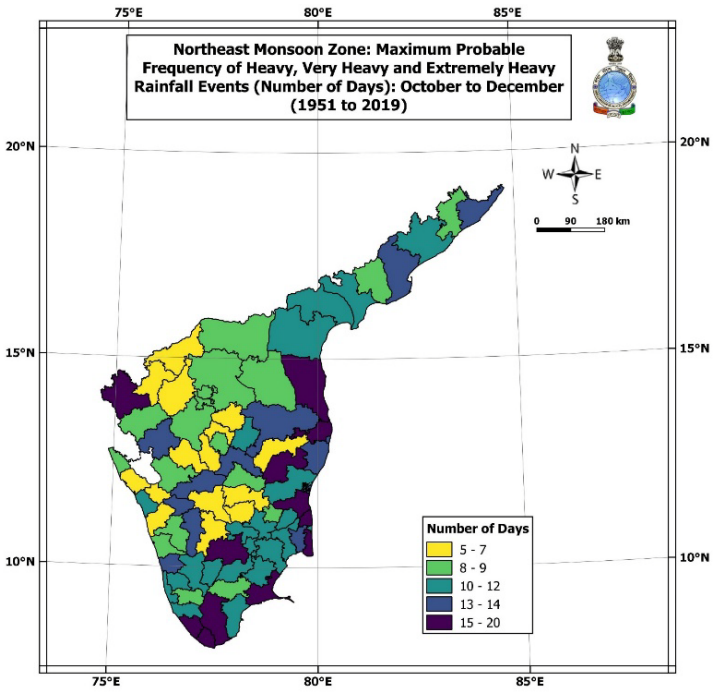

Fig. 3.9. Maximum Probable frequency of heavy, very heavy and extremely heavy rainfall events (Number of days): October-December, 1951-2019. (Source: IMD Climate Hazards and Vulnerability Atlas of India, 2022).

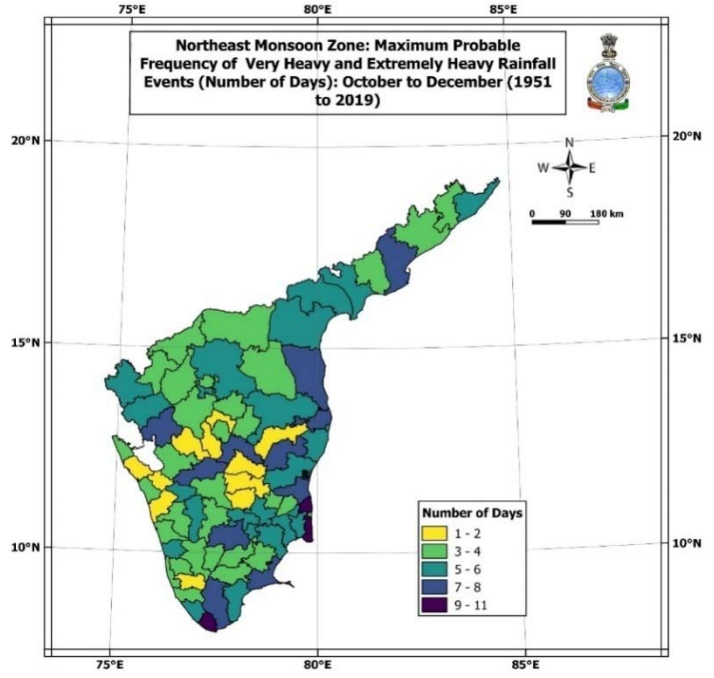

Fig. 3.10. Maximum Probable frequency of very heavy and extremely heavy rainfall events (Number of days): October-December, 1951-2019. (Source: IMD Climate Hazards and Vulnerability Atlas of India, 2022).

The city of Chennai experienced three phases of heavy rainfall that resulted in devastating floods during November and early December, 2015. Chakraborty (2015) examined synoptic aspects of this flood event in detail. The study revealed that propagating convective systems from the west Pacific Ocean intensified further over the warm Indian Ocean before moving north towards the Indian land region. This northward propagation was guided by two highs of mid-troposphere to the east and west of the Indian region. While the high to the east was typical of an El Nino year, that the west was associated with global phase shift of upper tropospheric Rossby wave. The study revealed that similar highs to the west were present during other years of heavy rainfall along the east coast of Peninsular India.

Fig 3.11 shows Spatial variation of correlation coefficient between monthly mean rainfall over the Indian landmass and area averaged 500 hPa geopotential height over 30-60^{0}E, 20-45^{0}N (Middle-east) in November for the period 1948-2014. It suggests that a high GPH over the Middle East is positively correlated with high amount of rainfall over central and south India land regions. The highest positive correlation is found along the east coast of the Indian peninsula over Tamil Nadu and Andhra Pradesh. The study concluded that an anomalous mid-tropospheric high to the west of the Indian region can induce anomalous northerly to the north that does not allows propagating systems to mover further north and west. This results in dry conditions in the northwest Indian region and wet conditions to the southeast Indian peninsula. It suggests that an anomalous high over Middle east in November can help increase the northeast monsoon rainfall over the south peninsula.

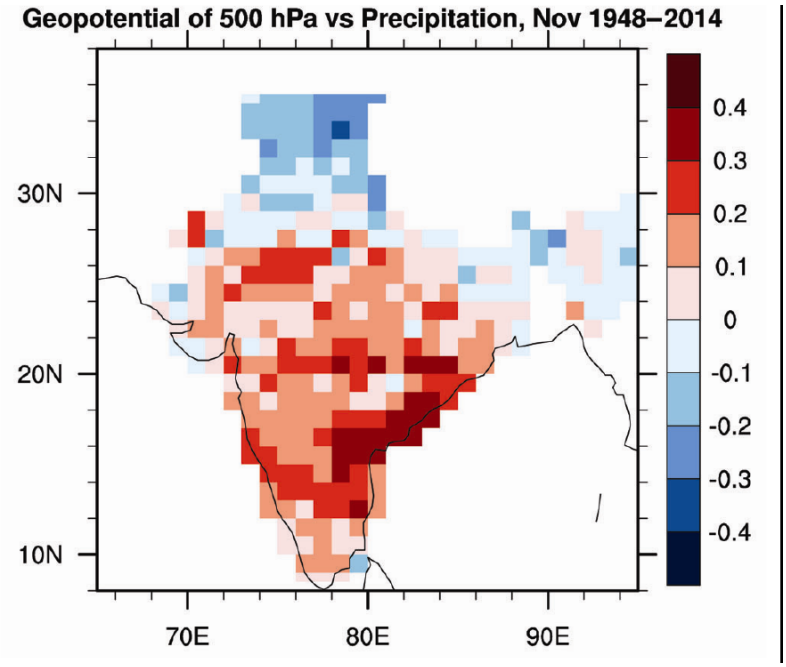

Fig 3.11 Spatial variation of correlation coefficient between monthly mean rainfall over the Indian landmass and area averaged 500 hPa geopotential height over 30-60^{0}E, 20-45^{0}N in November for the period 1948-2014 (After Chakraborty, 2016).

Nageswara Rao et al., (2019) made an extensive analysis of NE monsoon rainfall using IMD gridded data set. Their analysis revealed that the seasonal rainfall has increased over Tamil Nadu, Rayalaseema, as well as South Peninsula because of an increase in the number of high-intensity rainfall events in the recent period with respect to the earlier period (1901–1958), while it has decreased over the other sub-divisions. The percentage contribution of moderate rainfall events to the seasonal rainfall is more compared to the other events.

The study by Koteswara Rao et al (2020) revealed there will be an increase in precipitation in near future (about 5%). The future climate projections also indicate that both the intensity and frequency of precipitation extremes in most parts of the South peninsular India may increase under the warming scenarios during the northeast monsoon season.

Chapter-4

Synoptic Systems

In the previous chapters, the salient aspects of climatological features of atmospheric circulation and onset process have been discussed. With the onset of NE monsoon, the east-west seasonal trough (ITCZ) slowly shifts southwards. During the season, the mean position of the east-west trough extends from the south Arabian sea to south Bay of Bengal across the south Peninsula. This seasonal trough, an area of large scale convergence, can help formation of low level circulations and low pressure systems, which lead to large scale convection and rainfall over the region.

The main synoptic systems affecting rainfall over the south Peninsula are a) Low pressure areas b) Depressions, cyclonic storms and above c) troughs in easterlies or easterly waves and d) upper air troughs or cyclonic circulations, confined to lower levels. The troughs in easterlies could be observed at sea level or in lower atmosphere. The upper air trough could be generally oriented in an east-west direction.

A summary of different synoptic systems affecting the south peninsula during the NE monsoon season during the period 2000-2019 is given in Table-4.1. These details were obtained from the post-monsoon seasonal reports published by the IMD in ***Mausam***.

Table 4.1

Number of Synoptic systems affecting South Peninsula during the NE monsoon season (Oct-Dec)

Year	Low Pressure areas	Depressions and above	Upper air trough/cyclonic circulation	Trough in Easterlies/ Easterly Wave
2000	2	4	20	3
2001	4	3	8	8
2002	1	4	2	14

2003	4	4	7	11
2004	4	4	3	17
2005	7	5	4	2
2006	2	1	10	18
2007	3	3	20	6
2008	2	5	12	9
2009	3	2	10	10
2010	3	5	10	5
2011	0	5	9	9
2012	2	4	8	13
2013	1	6	8	7
2014	1	2	8	13
2015	6	4	14	7
2016	0	5	12	11
2017	3	5	29	3
2018	2	4	37	8
2019	2	6	22	5
2020	3	3	19	4
2021	4	2	28	7
Mean	2.7	3.9	13.6	8.6
Standard Deviation	1.7	1.3	9.1	4.4

In this table, low pressure areas, depressions and cyclonic storms forming over the south Arabian Sea and South Bay of Bengal are considered. The upper air troughs and cyclonic circulations are counted only those forming near the South peninsula contributing rainfall activity over the region.

On an average, around 3 low pressure systems form during the NE monsoon season, which do not intensify into depressions or above. During the season, four depressions/cyclonic storms can be expected to affect the south peninsula. On an average, 13 upper air cyclonic circulations/troughs and 10 troughs in easterlies/easterly waves also form affecting the south peninsula during the season. While there is little year to year variation in cyclonic storms (Depressions and above), there is, however, large year to year variation in the frequency of tropical easterly waves and upper air systems. It may be interesting to understand the contribution of each of these weather systems on the seasonal rainfall distribution over the region.

A preliminary analysis was made to understand the variability of the frequency of these synoptic systems and its linkage to global forcings like El Nino-Southern Oscillation (ENSO), Pacific Decadal Oscillation (PDO), North Atlantic Oscillation (NAO), Indian Ocean Dipole (IOD) etc. The time series of the global indices were taken from the website https://psl.noaa.gov/gcos_wgsp/Timeseries. The data of the period 2000-2021 (22 years) have been used to calculate the correlation coefficients and the results are given in Table 4.2. The seasonal mean of Oct-Dec period was considered for the analysis.

Table 4.2

Correlations between Global Circulation Indices and frequency of Synoptic systems

Global Index	Lows	Dep/CS	Troughs / Circulations	Easterly Waves
Nino 3.4	0.134	-0.216	-0.180	**0.489**
SOI	-0.109	0.249	0.290	**-0.504**
NAO	-0.084	-0.079	0.172	0.030
AO	-0.036	0.165	0.125	0.008
AMO	-0.036	0.165	0.125	0.008
PDO	-0.181	-0.013	-0.146	0.336
IOD	-0.183	-0.041	**0.386**	0.170

Note: Nino3.4: ENSO Index, SOI: Southern Oscillation Index, NAO: North Atlantic Oscillation. AO: Arctic Oscillation, AMO: Atlantic Multi-decadal Oscillation, PDO: Pacific Decadal Oscillation, IOD: Indian Ocean Dipole.

It is interesting to note that the frequency of easterly waves over the Bay of Bengal during the NE monsoon season has a statistically significant correlation with Nino 3.4 and SOI. This indicates, during the El Nino years, frequency of easterly waves is enhanced, which might lead to more seasonal rainfall over the south peninsula. The relationship between the ENSO and seasonal rainfall is discussed in detail later in the chapter on the NE monsoon variability. The seasonal rainfall is positively correlated with the Nino 3.4 index. It is also interesting to note that Pacific Decadal Oscillation (PDO) plays a positive role in enhancing the frequency of easterly waves. The positive phase of the Indian Ocean Dipole (IOD) leads to more troughs and upper air circulations over south peninsula which also contribute to the seasonal rainfall.

A brief description of various synoptic systems forming during the NE monsoon season is given below with an example, just for illustration. It may be noted that the characteristics of these synoptic systems may show large variability.

4.1 Trough of low over the Southwest Bay of Bengal (30 Oct-05 Nov 2018)

An example of a trough of low pressure that formed over the Southwest Bay of Bengal is discussed below.

A low-level cyclonic circulation was prevailing over the southwest BOB and adjoining Sri Lanka during 27-31 Oct and trough of low at mean sea level extending from this circulation from southwest – west central BOB off TN / south CAP / Sri Lanka coast during 30 Oct – 05 Nov. Fig 4.1 shows the different aspects of the trough of low which formed over the Southwest Bay, including satellite images and rainfall associated with the system. The average rainfall is taken from the IMD/NCMRWF merged satellite (GPM)-raingauge dataset. The streamline pattern and mean sea level pressure chart are taken from the archives of IMD. These plot shows a north-south trough over the

southwest Bay of Bengal and adjoining Tamil Nadu coast. This trough is observed on the sea level also. The presence of this trough had caused extensive rainfall off the coasts of Tamil Nadu and Sri Lanka (Fig 4.1 c).

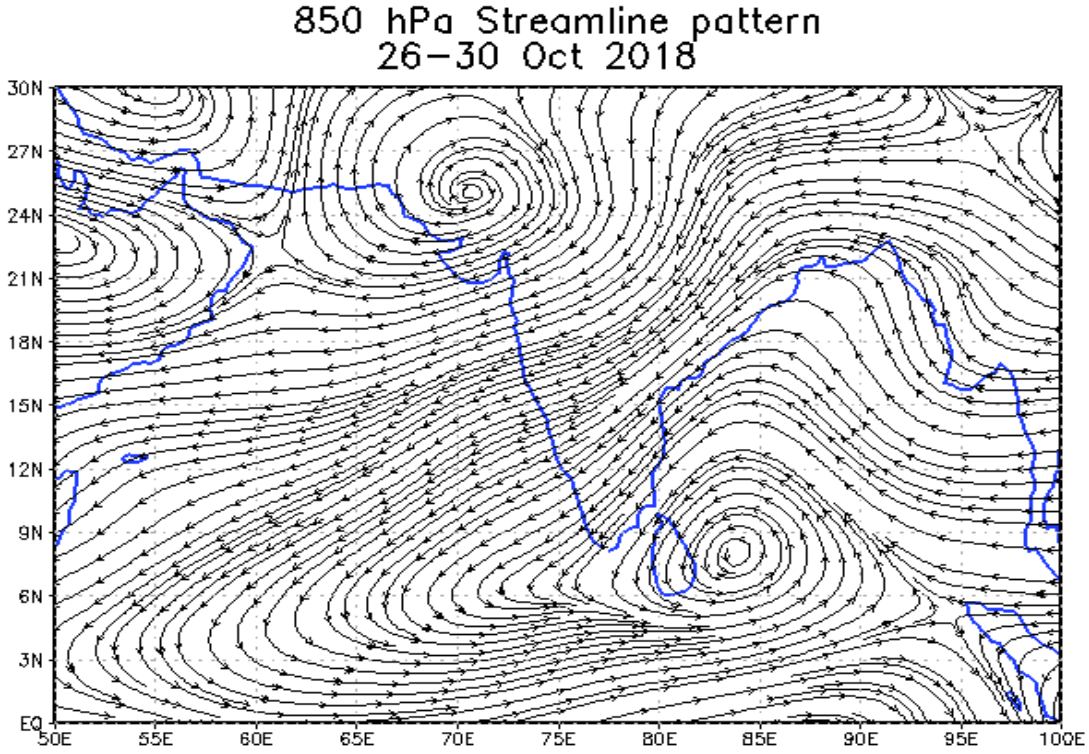

(a)

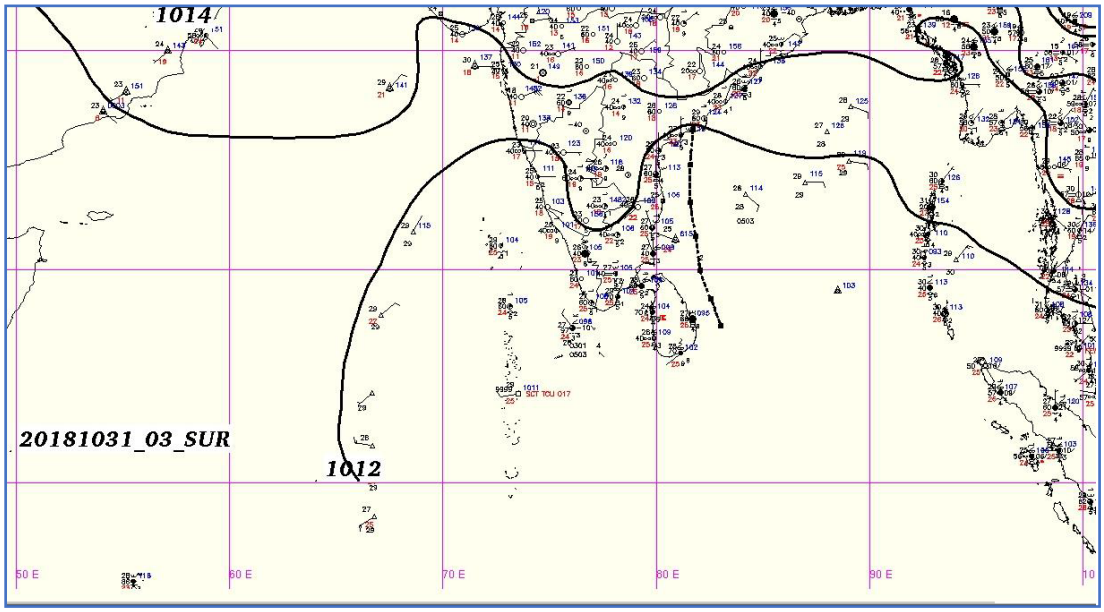

(b)

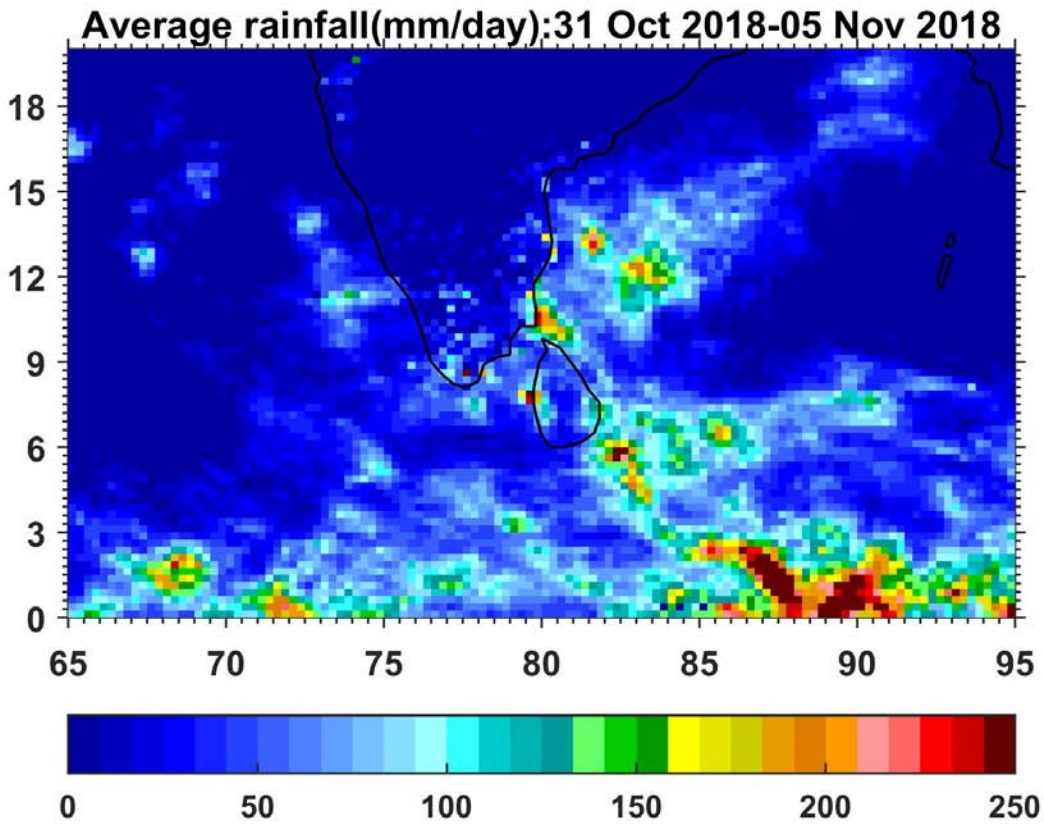

(C)

Fig 4.1. a) 850 hPa streamline analysis during 26-30 Oct, 2018 b) Isobaric analysis on 31 Oct, 2018 and c) average rainfall (mm/day) during 31 Oct to 05 Nov, 2018.

4.2. Upper air east-west trough

During the NE Monsoon season, occurrence of an east-west trough across the south peninsula is very common. This could be associated with the presence of ITCZ over the region. One good example of the east-west trough is shown in Fig 4.2 a-c. During 14-16 Nov 2021, an east-west trough was present passing across the south peninsula. The east-west trough provides large scale convergence and associated rainfall activity over the region, as seen in the vertical velocity (omega) shown in Fig.4.2 b. Associated with this east-west trough large scale rainfall activity was observed over the south Peninsula and the Arabian sea.

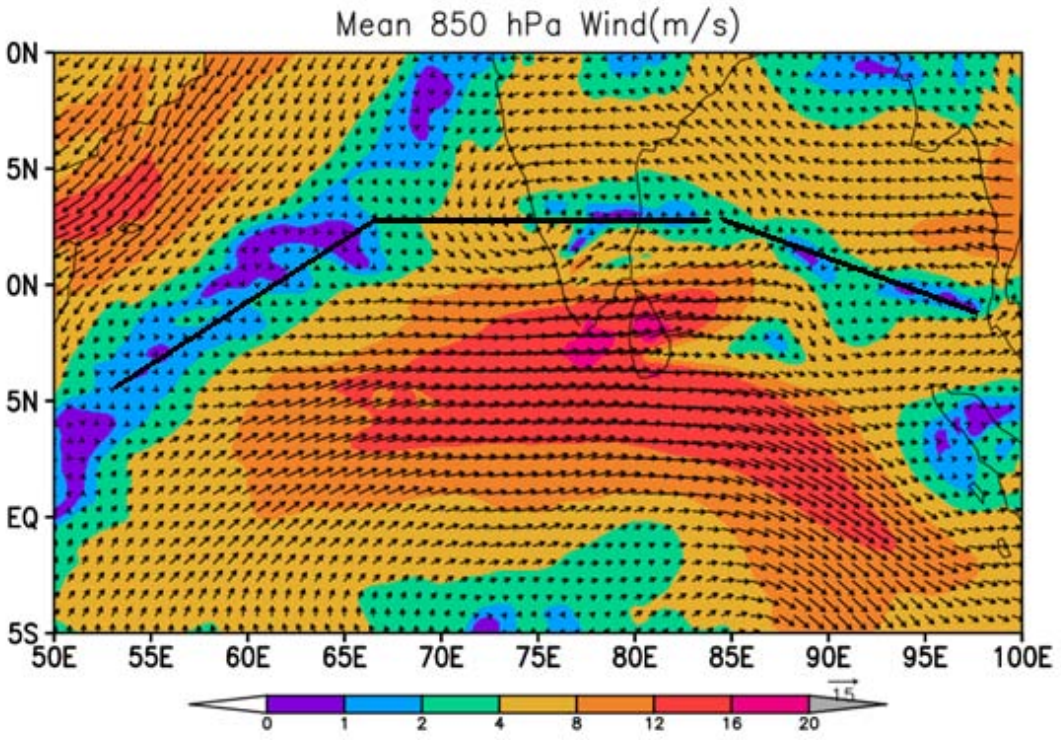
Mean 850 hPa Wind(m/s)
0N
5N
0N
5N
EQ
5S
50E
55E
60E
65E
70E
75E
80E
85E
90E
95E
100E
0
1
2
4
8
12
16
20

(a)

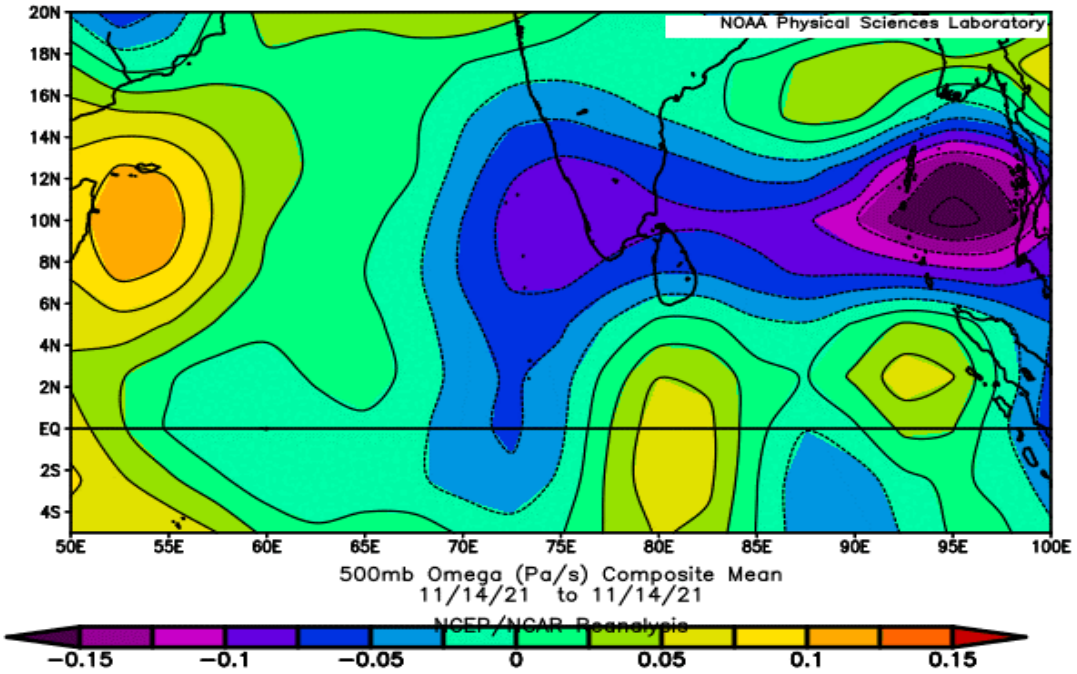
NOAA Physical Sciences Laboratory
20N
18N
16N
14N
12N
10N
8N
6N
4N
2N
EQ
2S
4S
50E
55E
60E
65E
70E
75E
80E
85E
90E
95E
100E
500mb Omega (Pa/s) Composite Mean
11/14/21 to 11/14/21
NCEP/NCAR Reanalysis
−0.15
−0.1
−0.05
0
0.05
0.1
0.15

(b)

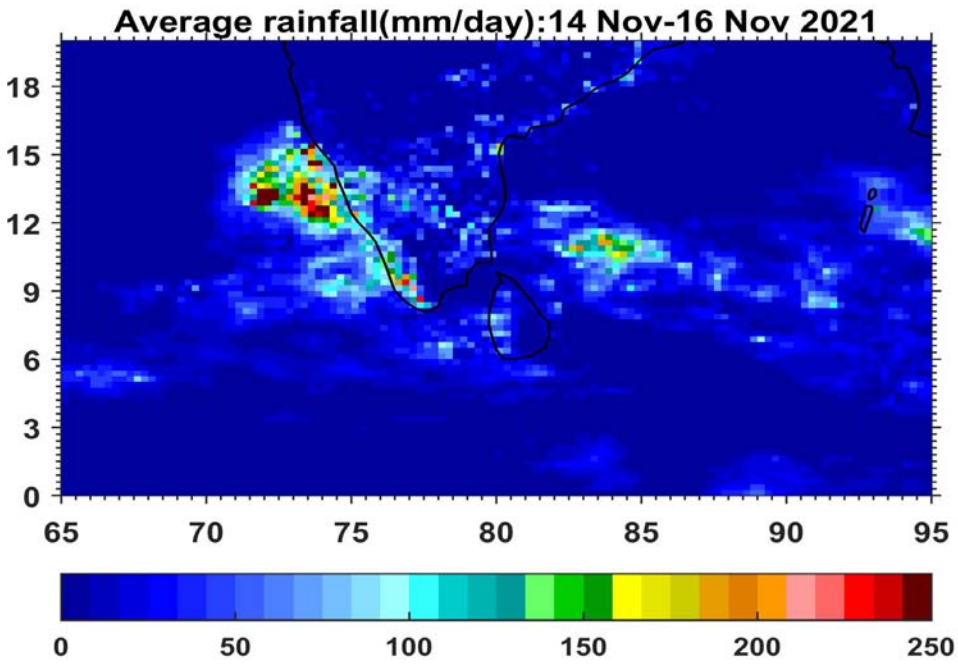

(c)

Fig. 4.2 a) 850 hPa winds on 14 Nov showing the east-west trough (shown as black line) and b) vertical velocity (omega) (Pa/s) at 500 hPa on 14th Nov and c) the cumulative rainfall during 14-16 Nov 2021.

4.2 **Low Pressure Area (LOPAR): 27 Oct-04 Nov 2021**

A low pressure formed over the central parts of south Bay of Bengal and associated cyclonic circulation extending up to 5.8 km above mean sea level on 27th Oct 2021. It lay over the southwest Bay of Bengal off Sri Lanka coast and associated cyclonic circulation extended up to 3.1 km above mean sea level on 28th; over southwest Bay of Bengal off Sri Lanka and Tamil Nadu coast and associated cyclonic circulation extended up to 3.1 km on 29th, 30th and 31st. It lay over the Comorin area and adjoining north Sri Lanka coast extending up to 3.1 km on 01st Nov; over the Comorin area and neighborhood on 02nd and over Lakshadweep area and neighborhood extending up to 4.1 km above mean sea level on 03rd and extending up to 4.5 km on 04th Nov 2021.

Various dynamical and thermodynamical features of the LOPAR are shown in Fig 4.3. The Low pressure area was observed off Sri Lanka Coast with an east-west trough of low pressure from the east Arabian sea to the east Bay of Bengal across the low pressure system. At 925 hPa level, the east-west trough is easily seen. The OLR spatial pattern suggests large scale convection of deep clouds with low OLR (less than 200 Wm^{-2}) over the south peninsula and adjoining Bay of Bengal. The Chennai DWR image as well as the Satellite image are also shown below, which suggests large scale clouding over the region. The cumulative rainfall from 01-04 Nov is shown in Fig 4.3 c. The spatial pattern suggests heavy rainfall exceeding 200 mm/day off the Tamil Nadu coast. Formation of a low pressure area with associated vertical extension over the seasonal east-west trough of low pressure is a regular synoptic system contributing to seasonal rainfall over the south Peninsula. The present day NWP models have capability in predicting the formation of these low pressure systems over the Bay of Bengal, at least 2-3 days in advance. Therefore, early warnings for adverse weather due to the low pressure systems are feasible.

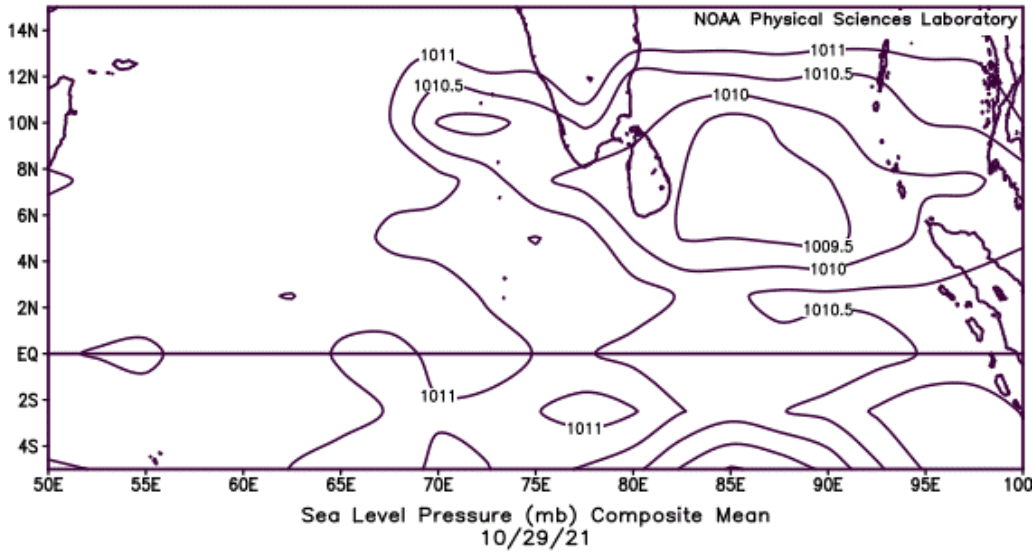

(a)

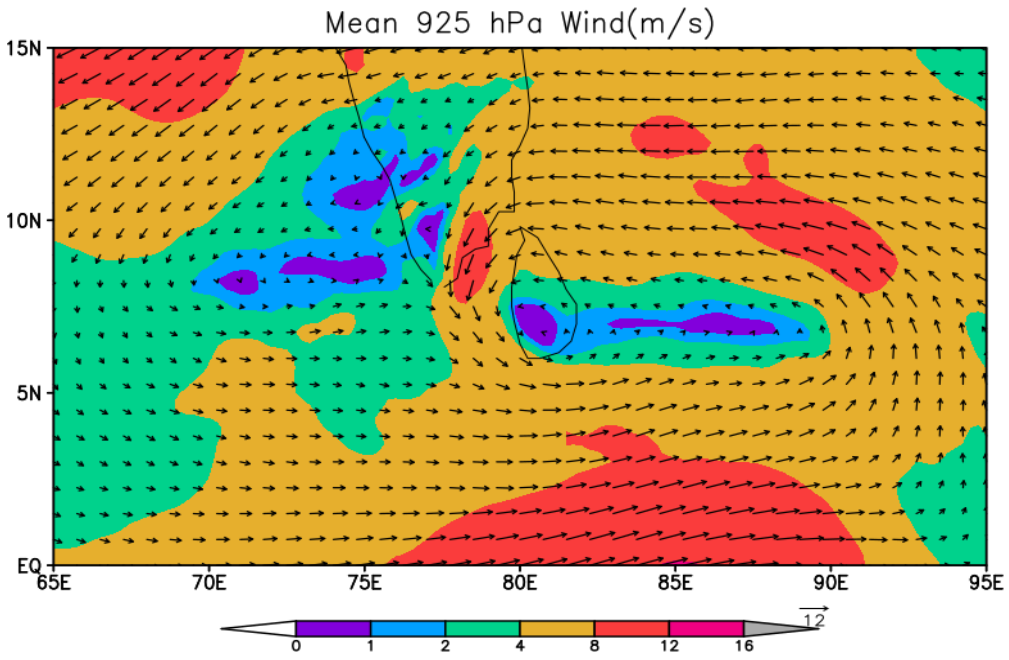

(b)

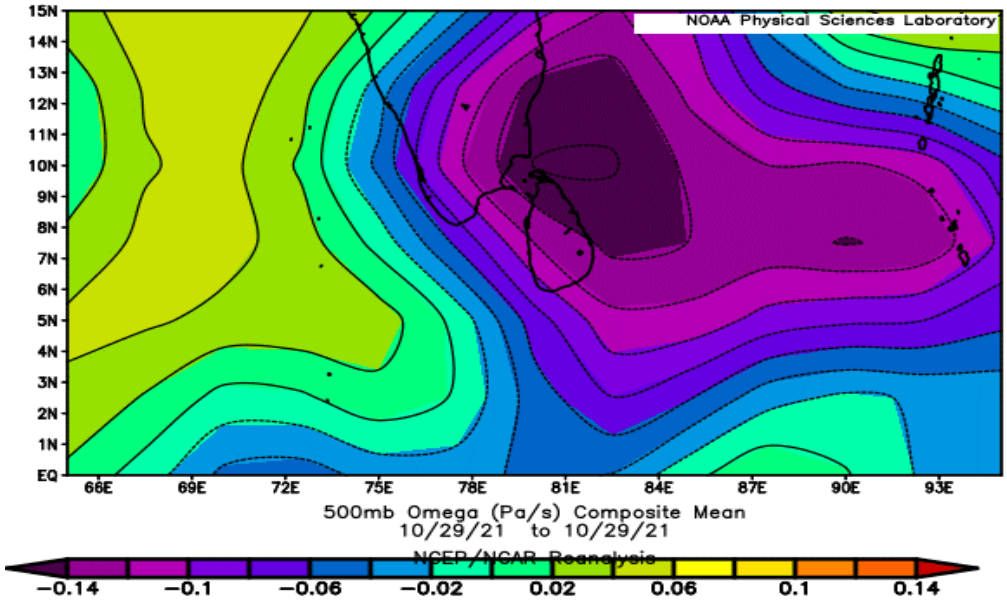

(c)

Fig 4.3. Various dynamic and thermodynamic features of the LOPAR a) Mean Sea Level Pressure b) 925 hPa winds c) vertical velocity (omega) at 500 hPa on 29 Oct 2021

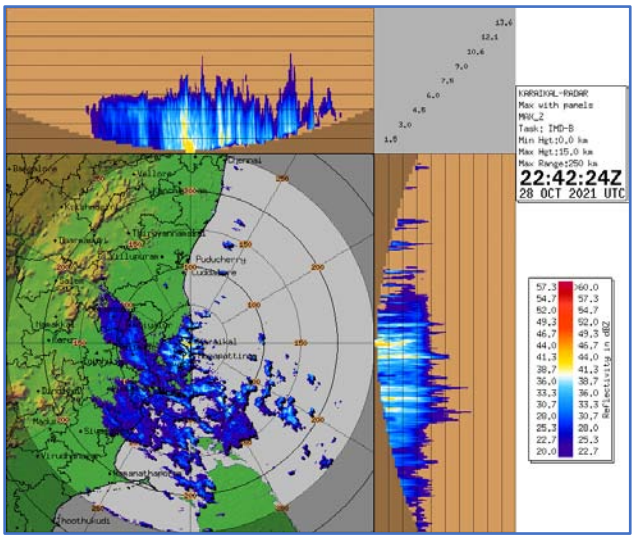

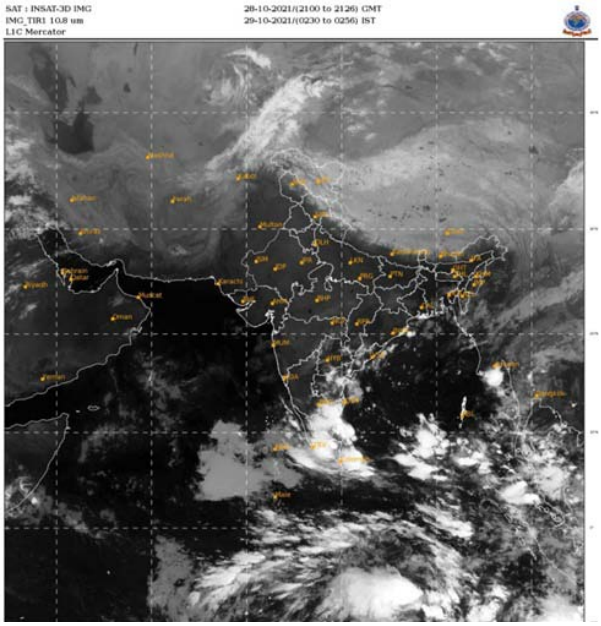

(d) **(e)**

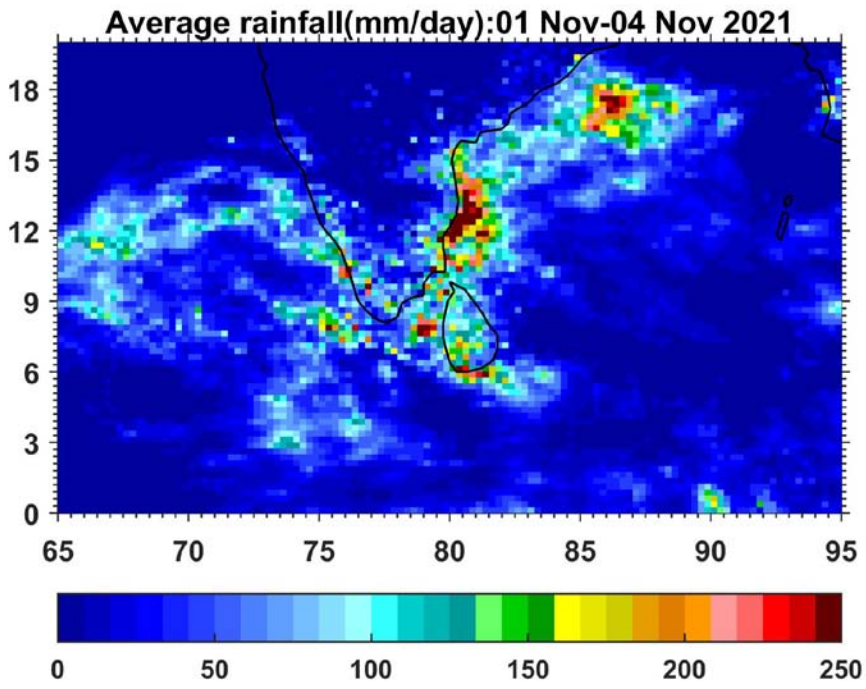

(f)

Fig. 4.3. d) DWR image on 28th Oct e) Satellite Image on 29th Oct and f) Cumulative Rainfall during 01-04 Nov 2021.

4. 3. Cyclonic Storms

In this section, the details of activity of cyclonic storms are discussed using the long term tropical cyclone track data. Fig 4.4 shows the frequency of Cyclonic Storms (Depressions and above) forming over each 2.5 x 2.5 degree boxes during the period 1961-2020. In each box, top figure shows the frequency of all systems together (Depressions+Cyclonic Storm + Severe Cyclonic Storm), middle one is the frequency of CS+SCS and bottom one is the frequency of SCS alone. These statistics are derived from the IMD Cyclone atlas (http://www.imdchennai.gov.in/). Frequency of cyclonic storms is maximum over the west central Bay of Bengal (10^0-17.5^0N, 80^0-90^0E). Therefore, during the NE monsoon season, north Tamil Nadu and Coastal Andhra Pradesh are most vulnerable to cyclonic storms.

The tracks of cyclonic storms (depressions and above) during the months October to December months are shown in Fig 4.5, 4.6 and 4.7 respectively. In October, north Tamil Nadu, Coastal Andhra Pradesh, Odisha and West Bengal experience the landfall of these storms. Some storms after moving northwestwards recurve towards northeast, due to the influence of sub-tropical high. Over south Peninsula, north Tamil Nadu and coastal Andhra Pradesh experience Tropical cyclonic storms.

In November, most of the storms forming over the Bay of Bengal move northwestwards and make landfall over Tamil Nadu and the coastal Andhra Pradesh. In November, a few storms recurve and make landfall over West Bengal and Bangladesh. In December, cyclonic storm activity is generally reduced. In December also, when storms form, they move northwestwards and make landfall over Tamil Nadu. A few storms recurve and make landfall over coastal Andhra Pradesh and Bangladesh. There are a few storms, which form over the Bay of Bengal, cross the south peninsula and emerge in the Arabian Sea, thus making longer lifetime. The systems forming over the Arabian Sea, either move westwards towards the Arabian sub-continent or towards Gujarat/Pakistan. The storms forming over the Arabian sea generally do not make

landfall over the south peninsula. They tend move northwestwards. A few storms however move north and affect the Gujarat coasts.

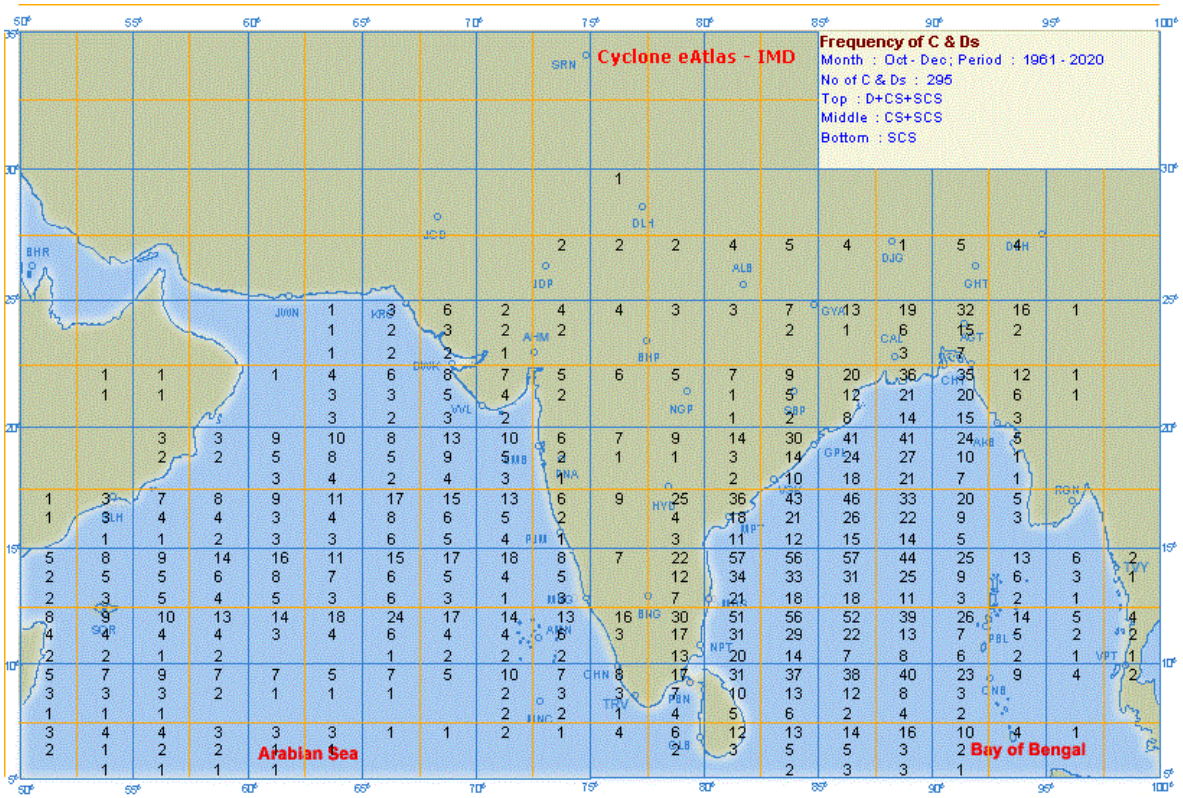

Fig 4.4. Frequency of all Cyclonic disturbances (Depressions and above) during the period 1961-2020. In each box top figure shows the frequency of Dep+CS+SCS, middle one CS+SCS and bottom one is the frequency of SCS. These statistics is derived from IMD Cyclone atlas.

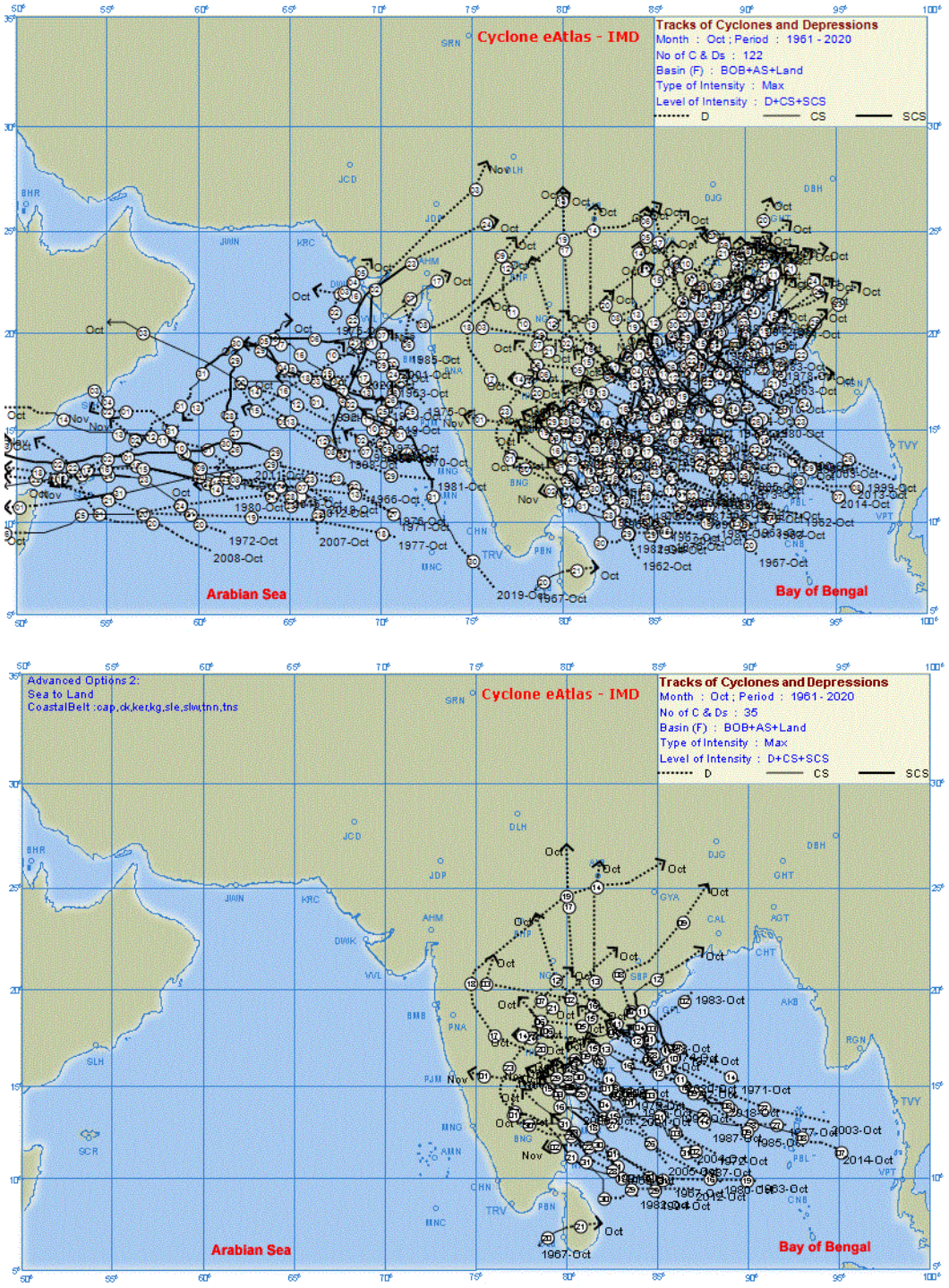

Fig 4.5. Tracks of cyclonic storms (Depressions and above) during October for the period 1961-2020 (Above) and tracks of cyclonic storms (depressions and above) during October, but which affected the south peninsular region. These tracks are derived from IMD Cyclone Atlas.

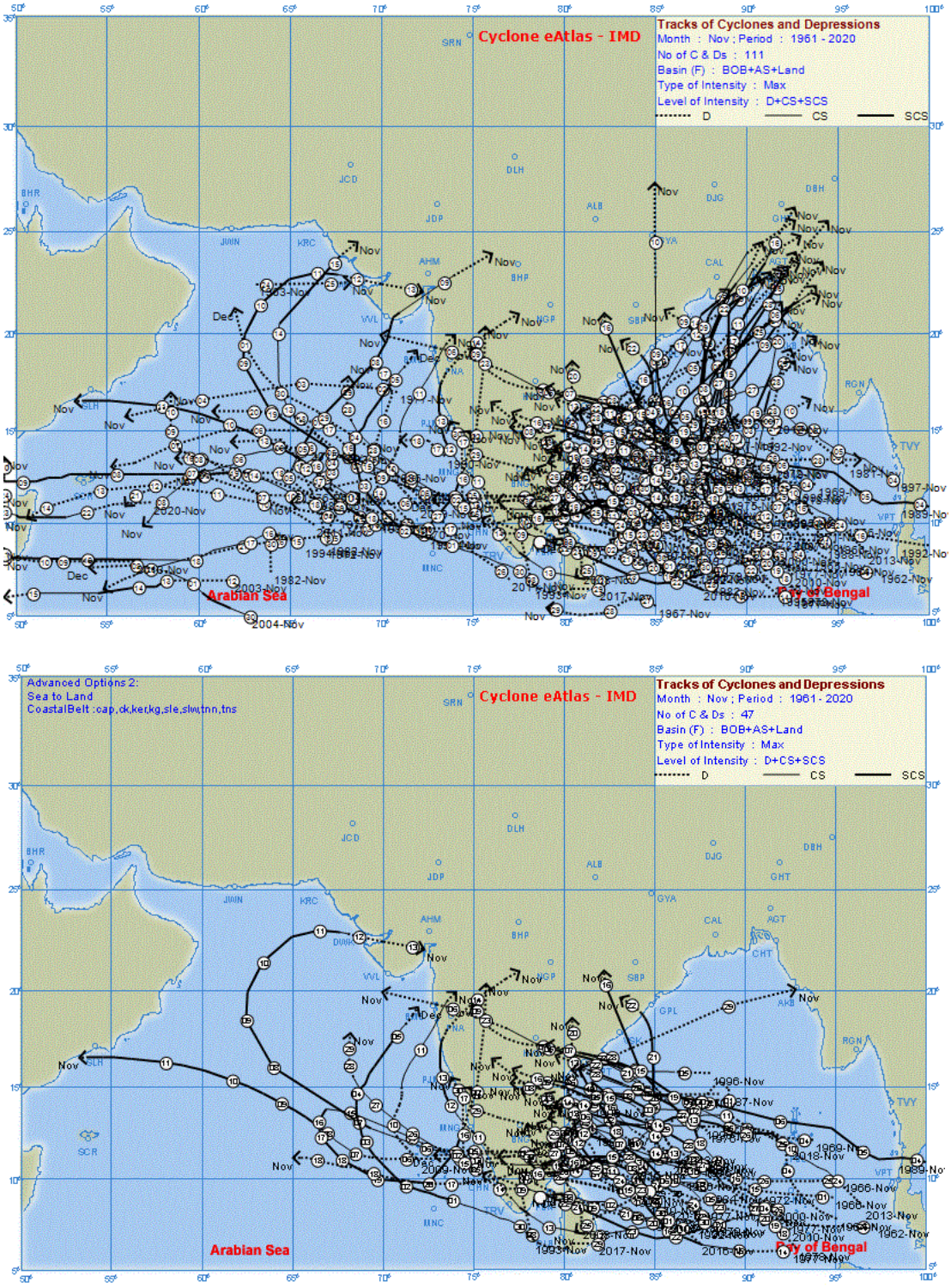

Fig 4.6. Same as Fig 4.5, but for November.

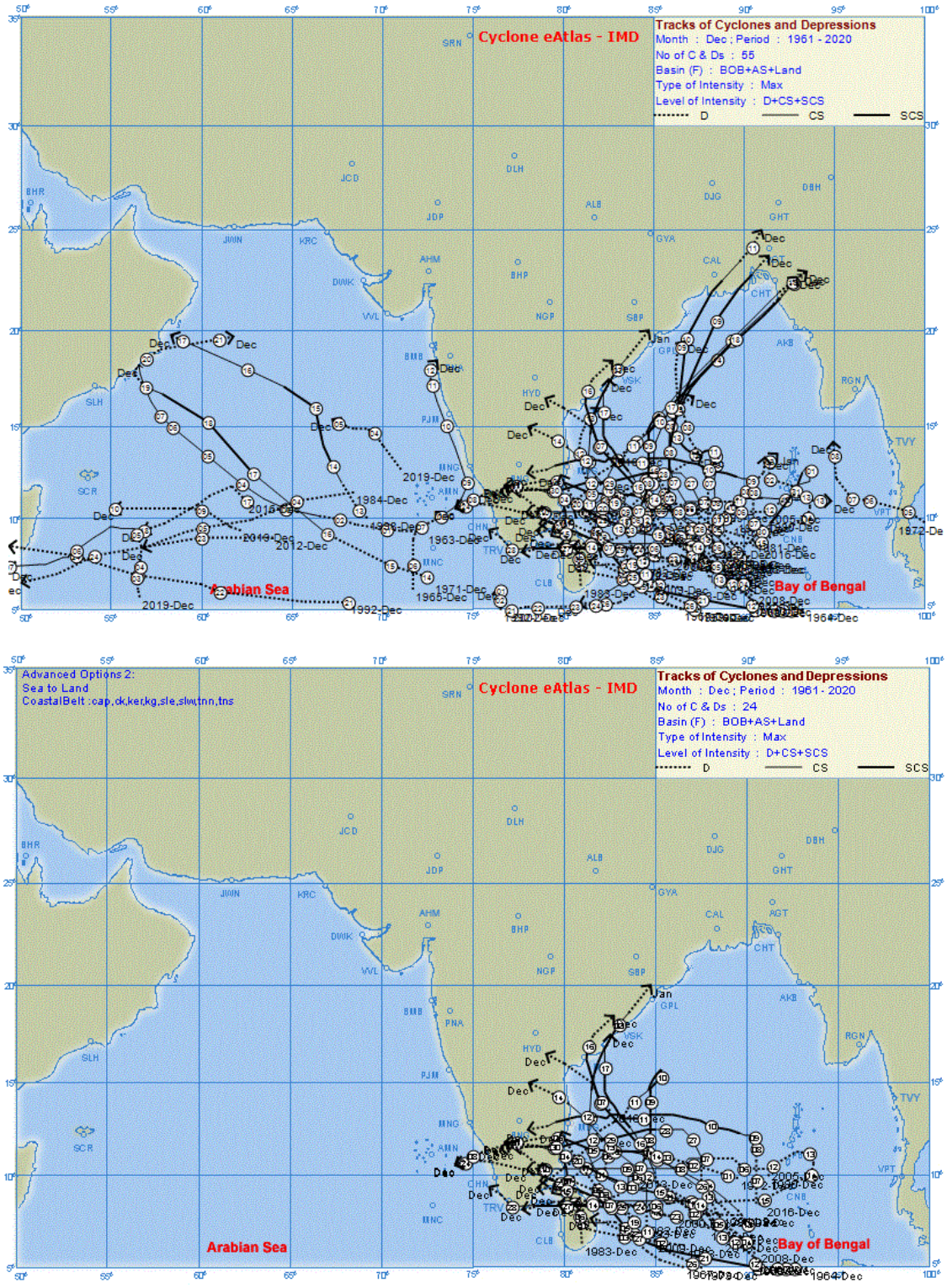

Fig 4.7. Same as Fig 4.5, but for December.

Figs 4.8 a, b and c show the return periods (year) of cyclonic storms (CS)/ Severe Cyclonic Storms (SCS) passing within 50 nm of the coastal districts during October, November and December respectively. The period 1961-2020 was considered for this analysis. The maps are derived from the IMD Climate Hazards and Vulnerability Atlas of India, 2022. The same maps for cyclonic storms (CS) and Severe cyclonic storms (SCS) separately are available in the IMD Climate Hazards and Vulnerability Atlas of India (2022). In October, the districts in coastal Andhra Pradesh and north Tamil Nadu have short return periods of 7.5 to 9.0 years. In November, a few coastal districts in south coastal Andhra Pradesh and north Tamil Nadu have much shorter return period of 3.7-5.0 days. Some more neighhouring districts have return periods of 5.1-10.0 years. In December coastal districts of Tamil Nadu show return periods of 7.5-9.0 years.

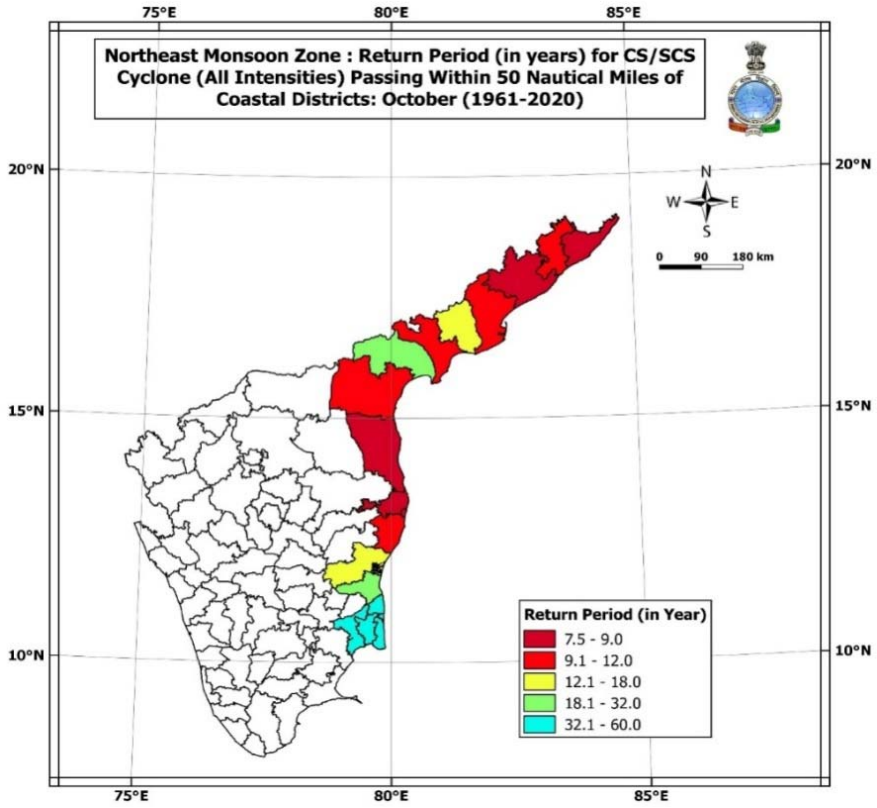

Fig 4.8 a: Return period (in years) for Cyclonic Storm (CS)/ Severe Cyclonic Storm passing within 50 nautical miles of coastal Districts during October for the period 1961-2020. (Source: IMD Climate Hazards and Vulnerability Atlas of India, 2022).

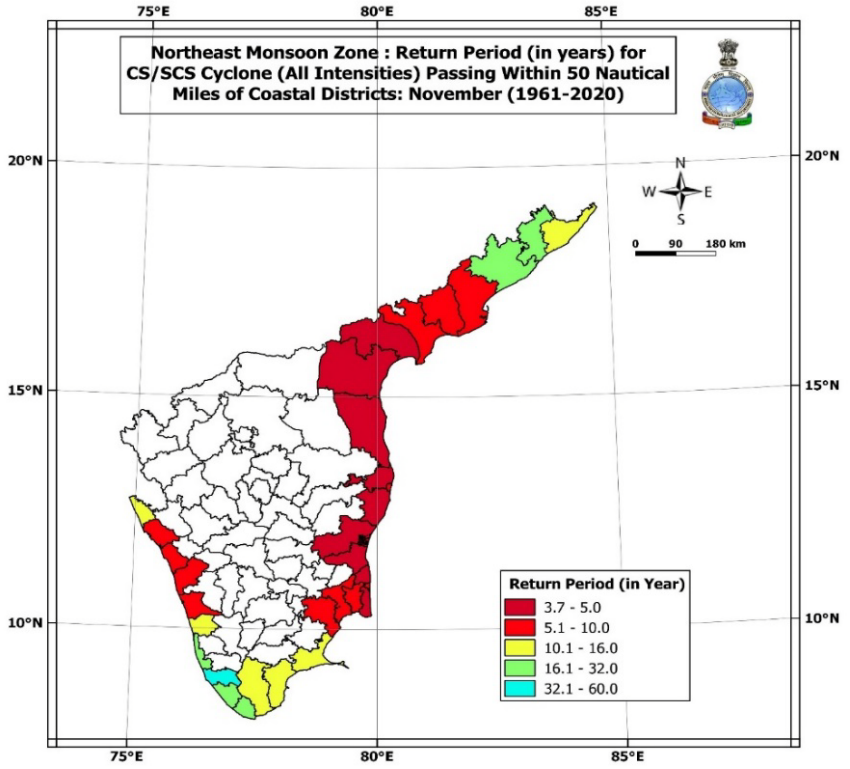

Fig 4.8 b: Same as Fig 4.5 a, but for November.

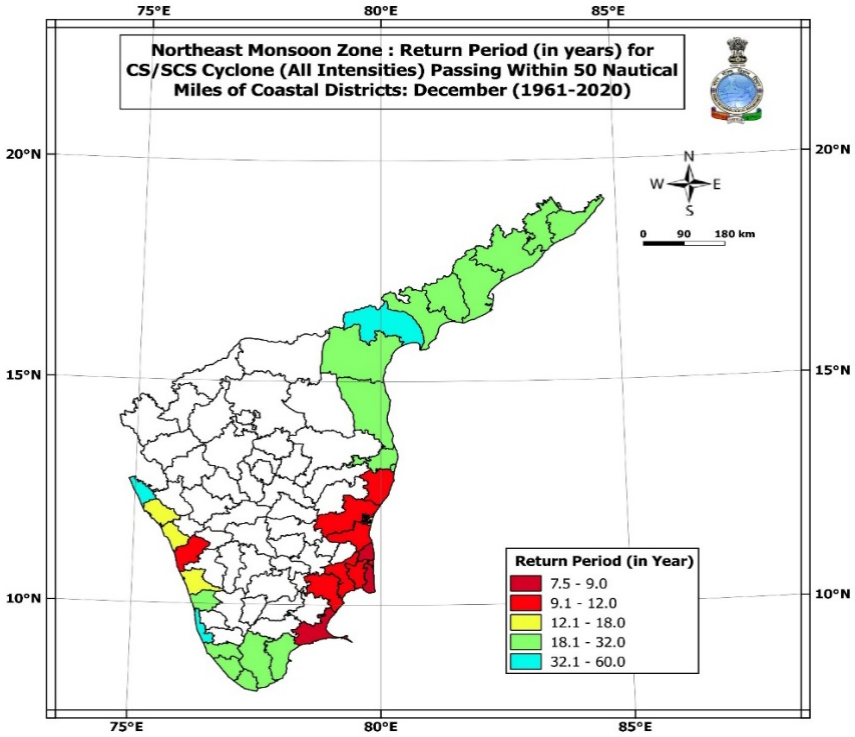

Fig 4.8 c: Same as Fig 4.5 a, but for December.

4.5. Track and intensity forecast errors of Tropical Cyclones

In this section, an analysis is presented on the Track and Intensity forecast errors of Tropical Cyclones over the North Indian Ocean during the NE monsoon (Oct-Dec) season. Data of the period 2012-2021 have been used to complete this analysis. Mohapatra et al. (2013) and Mohapatra et al. (2015) have carried out extensive analysis of tropical cyclone track forecast errors over the North Indian Ocean.

The comparative analysis of track and intensity forecast errors for the post monsoon season (October-December) during 2017-21 and 2012-16 are presented in Fig. 4.9 a and b respectively. The track forecast errors were 82 km, 107 km, 139 km & 272 km during the period 2017-21 for the 24, 48, 72 & 120 hours lead forecasts respectively. However, during the period 2012-2016, the corresponding errors were 88 km, 133 km, 185 km & 348 km. It indicates an improvement of 10% in track forecast errors for lead period up to 24 hours and 15-20% for lead period beyond that up to 120 hours (Fig. 4.9 a) during the recent years.

The intensity forecast errors were 8.1 knots, 11.7 knots, 14.2 knots & 15.8 knots during 2017-21 for 24, 48, 72 & 120 hours lead period respectively. The corresponding errors during the period 2012-2016 were 11.9 knots, 16.9 knots, 17.2 knots & 11.6 knots respectively. The intensity of a tropical cyclone is measured based on its maximum wind which is normally quoted in knots. This indicates an improvement of 30% in intensity forecast errors for lead period up to 48 hours and 15-25% for lead period of 60 to 84 hours (Fig. 4.9 b).

To carry out the analysis of landfall errors, only landfalling cyclones have been considered. There were 9 cyclones in each period making landfall over different places within the region during the NE monsoon season. The comparative analysis of landfall point forecast errors for the NE monsoon season during 2017-21 and 2012-16 are presented in Fig. 4.9 c. The landfall point forecast errors were 41.9 km, 59.3 km & 51.2 km during 2017-21 against 31.6 km, 85.3 km & 82.7 km during 2012-2016 for 24, 48 &

72 hours lead period respectively. The comparative analysis indicates that there is a significant improvement of 30-40% in landfall point forecast errors for lead period of 48-96 hours. However, there is no significant change in landfall point forecast errors up to a lead period of 36 hours during the two periods. It is needless to mention here that the diameter of the central region (eye) of the TC is about 10-100 km, and an average about 50 km. No significant change in the forecast errors up to 36 hours which vary from about 15-60 km can be attributed to the above fact. Further within 36 hours, the landfalling TCs are monitored with the help of the coastal hourly observations as well as Doppler weather radar observations, leading to lower detection error. It is very interesting to note that the landfall forecast errors during the recent epoch are much less than the previous epoch. This could be mainly attributed to the excellent modelling strategy used by the IMD; availability of global models with higher resolution with plenty of assimilated data. The global models used for predicting the track and the landfall point have the spatial resolution of about 12-25 km. Hence, there is scope to reduce the landfall point errors for higher lead periods like 48-120 hours with improvement in model resolution, data assimilation supported by augmented direct & remotely sensed observational system.

Cangialosi et al. (2020) have discussed the Hurricane forecast errors over the Atlantic Ocean since 1960s to 2019. It has been well documented that the National Hurricane Center (NHC) has made significant improvements in Atlantic basin tropical cyclone (TC) track forecasting during the past half century. In contrast, NHC's TC intensity forecast errors changed little from the 1970s to the early 2000s. Recently, however, there has been a notable decrease in TC intensity forecast error and an increase in intensity forecast skill. The advancement of NWP models, especially as supported in the past decade, creation of the consensus aids, development of rapid intensification guidance, and the ability of the NHC forecasters to add value to the TC guidance has greatly improved intensity forecast skill over the Atlantic Ocean.

The study by Cangialosi et al. (2020) revealed that the track forecast errors over the Atlantic Ocean during the period 2010-2019 are 83 km, 110 km, 185 km and 213 km respectively for 24 hr, 48hr, 72 hr and 120 hr forecasts. Similarly for Hurricane Intensity forecasts the errors are 8 knots, 12 knots, 14 knots and 15 knots respectively for 24 hr, 48hr, 72 hr and 120 hr forecasts during the same period. This suggests, the tropical cyclone forecast intensity errors over the North Indian Ocean are larger compared to the intensity forecasts errors for the Atlantic Ocean. Therefore, more efforts should be made to reduce track and intensity forecast errors of tropical cyclones over the North Indian Ocean.

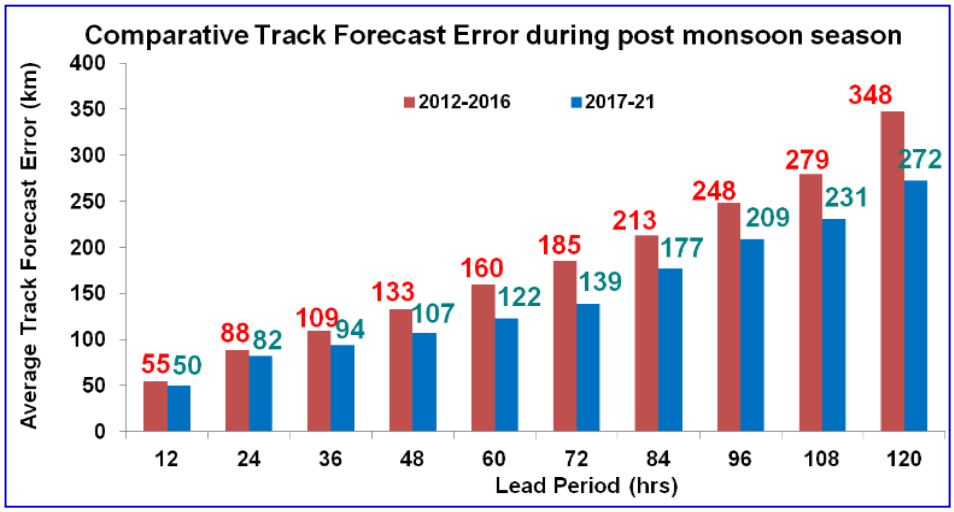

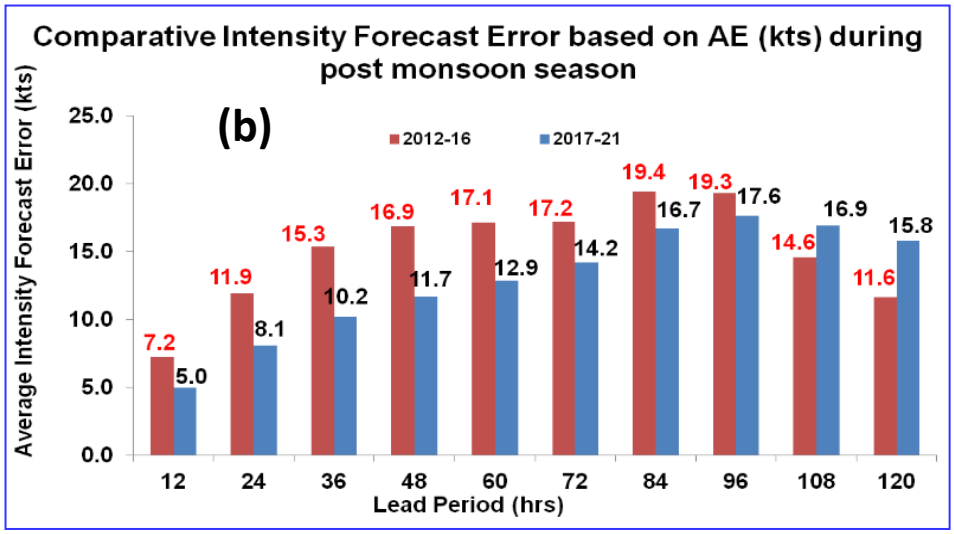

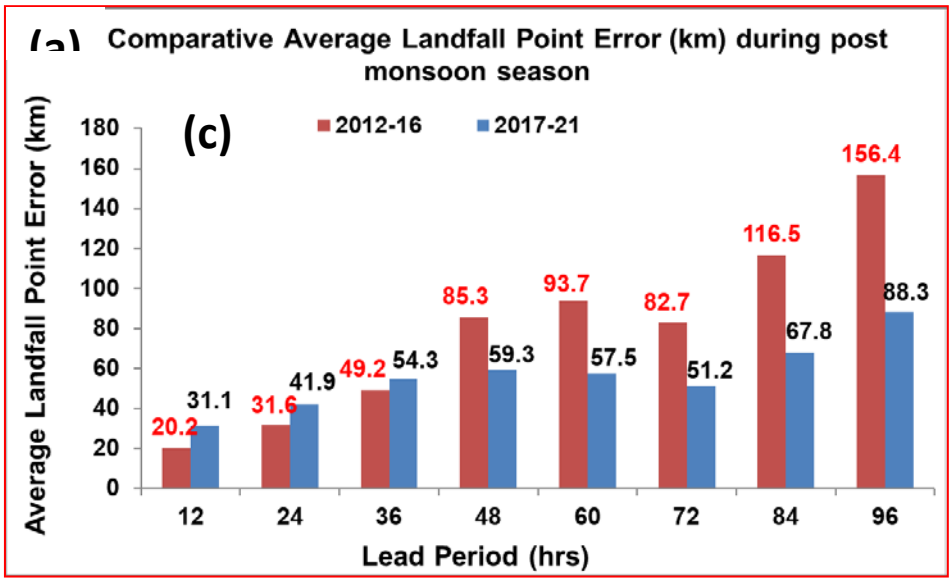

Fig. 4.9. Comparative operational (a) track and (b) intensity and (c) Landfall forecast in the post monsoon season during 2017-21 against 2012-16**.**

4.6. A case study of Tropical Cyclone Ockhi

In this section, the details of the tropical cyclone (TC-OCKHI) are discussed to bring out various forecasting issues and challenges related to the cyclone during the NE monsoon season. The TC- Ockhi was responsible for deaths of over 350 people from southern Tamil Nadu and Kerala, between 30 Nov and 3 Dec 2017. There were also some unidentified fishers from the north-eastern states of India who were lost at sea while working on-board fishing vessels. The full force of the storm was borne by fishermen at sea, unlike the previous cyclones over the Arabian sea (Manas Roshan 2019).

The TC OCKHI formed as a low pressure area over southwest Bay of Bengal (BOB) and adjoining areas of south Sri Lanka on 28th Nov /0300 UTC and became well marked on 29th /0000 UTC over the same region. The vertical wind shear of horizontal wind was moderate to high (15-30 knots) over the southwest Bay of Bengal and adjoining Sri Lanka coast. Under the favourable environmental conditions, it concentrated into a Depression (D) over southwest BOB off southeast Sri Lanka coast on 29th / 0300 UTC.

Moving westwards, it crossed Sri Lanka and emerged into Comorin area by 29th /1200 UTC. It intensified into a Deep Depression (DD) on 29th/2100 UTC. Moving northwestwards it intensified into a Cyclonic Storm (CS) on 30th / 0300 UTC over the Comorin area, into a Severe Cyclonic Storm (SCS) over Lakshadweep area on 01st December / 0000 UTC and further into a Very Severe Cyclonic Storm over southeast Arabian Sea (AS) to the west of Lakshadweep by 01st / 0900 UTC.

Generally, for the North Indian Ocean basin, TCs are considered to have undergone rapid intensification (RI)/ rapid weakening (RW) whenever 30 knots increase/decrease is noted in maximum sustained surface wind speed (MWS; Vmax) in 24 hrs. It is interesting to note that OCKHI underwent RI between 01st /0000 UTC to 02nd 0000 UTC and attained its peak intensity of 150-160 kmph gusting to 180 kmph on 2nd /0900 UTC with lowest central pressure of 976 hPa over the Arabian Sea. It then gradually recurved north-northeastwards, maintained its VSCS intensity till 04th / 1200 UTC and then weakened gradually. It crossed the south Gujarat coast as a well-marked low on 06th Dec/0000 UTC (IMD, 2018). More details of its genesis and tracks are available in Geetha and Balachandran (2020) and the IMD (2018) report on TC-Ockhi (https://rsmcnewdelhi.imd.gov.in/uploads/report/26/26_83ec45_ockhi%20pre.pdf).

The system caused extensive damages over extreme south Tamil Nadu and south Kerala during its developmental stages on 29-30 Nov. The system centre was about 60 km from Kanyakumari, the southern-most tip of peninsular India on 30th Nov/ 0300 UTC when it intensified from DD to CS stage (as per IMD's best track data). Even though the centre of the system did not cross the coast and move inland, Kanyakumari and Thiruvananthapuram (Kerala) bore the brunt of the fury of the eye-wall region of the TC during 29th night-30th Nov morning. The IMD's best track of TC-OCKHi is shown in Fig.4.10 and spatial pattern of mean sea level pressure on 29th Nov and 30th Nov is shown in Fig 4.11. These charts show the movement of TC-OCKHI and quick intensification by 30th Nov near the Comorin area.

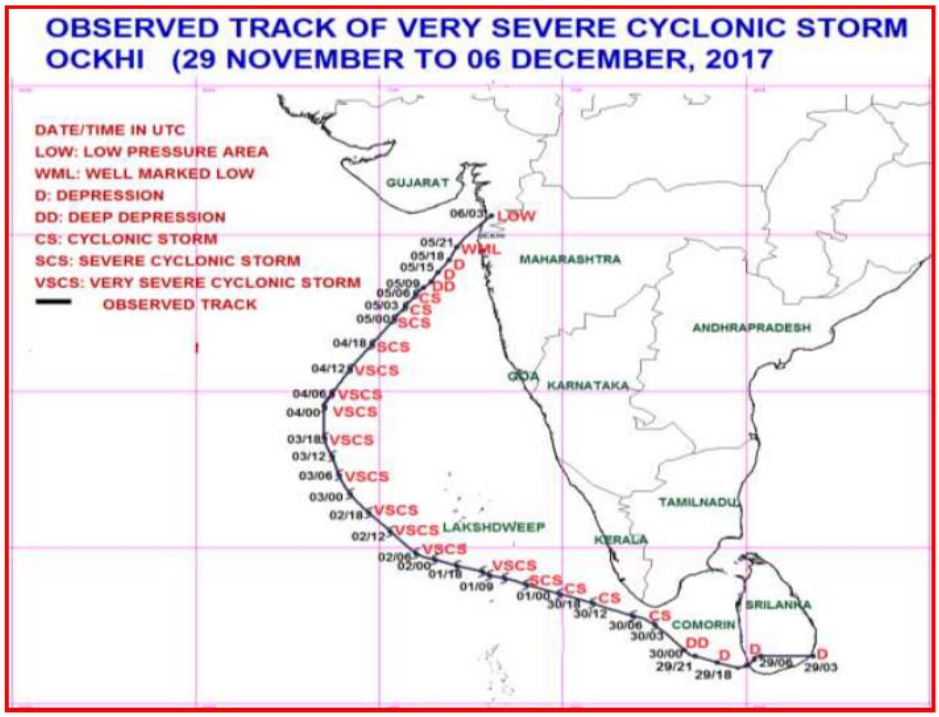

Fig 4.10. Observed track of very severe cyclonic storm OCKHI, 29 Nov to 06 Dec 2017. Source: India Meteorological Department (IMD).

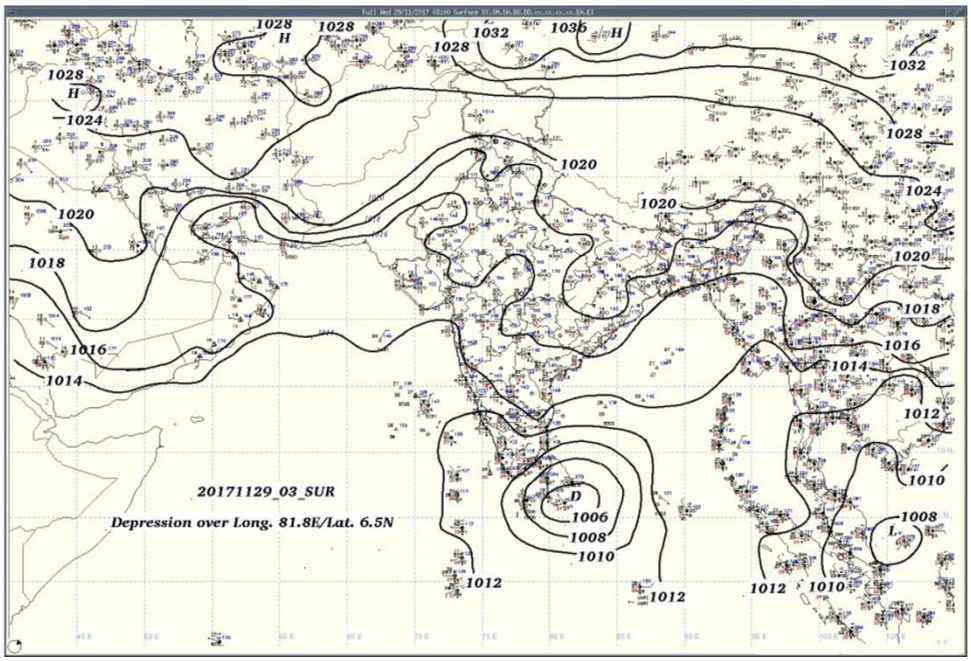

(a)

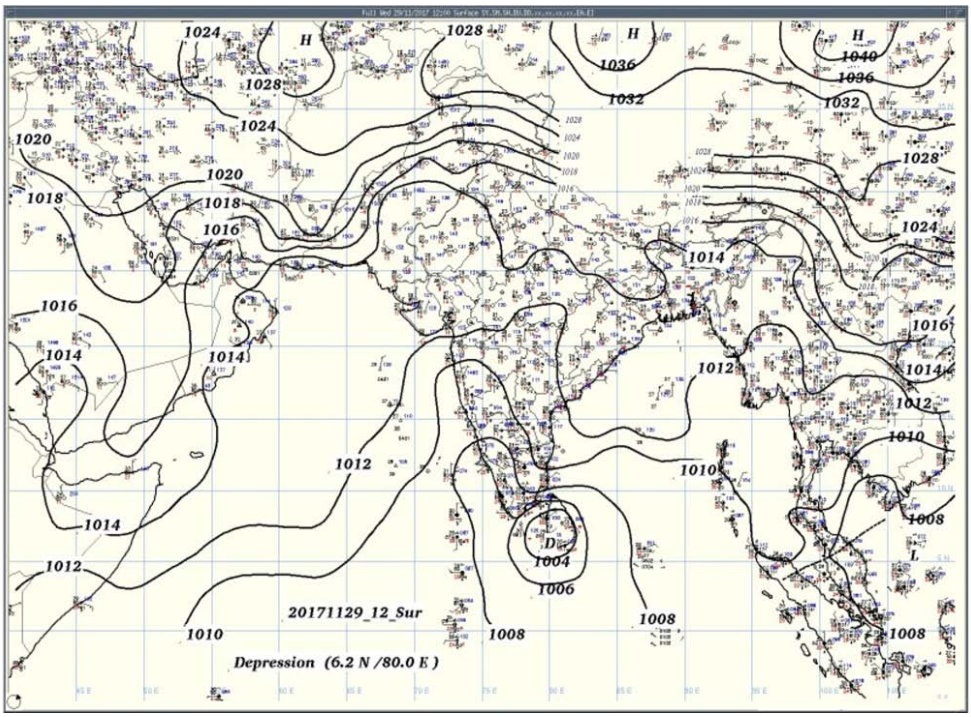

(b)

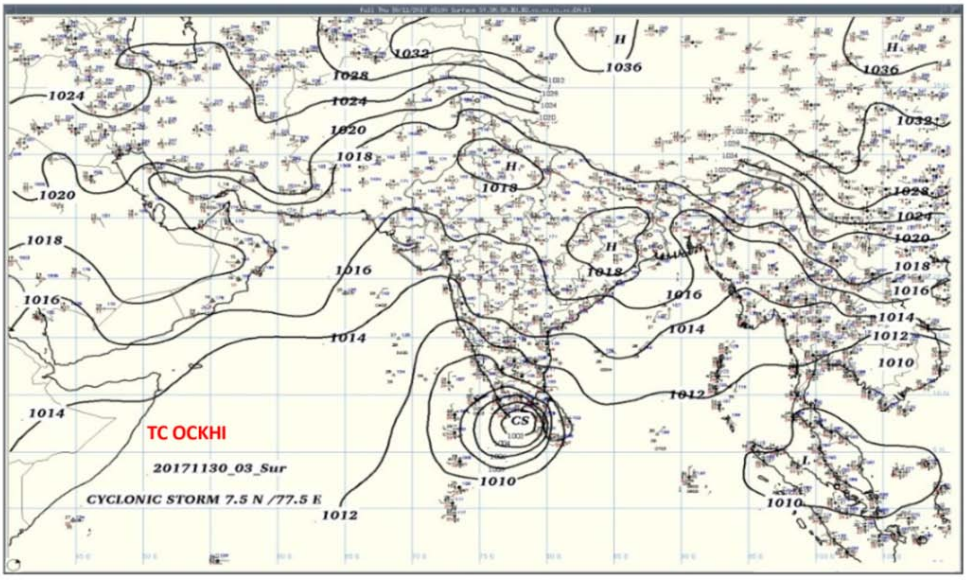

(C)

Fig. 4. 11 Mean Sea Level Pressure Chart on a) 29 Nov 2017, 03 UTC b) 29 Nov 2017 12 UTC and c) 30 Nov 2017 03 UTC. Source: India Meteorological Department.



Fig 4.12. 24 hour change in MSLP (on left) and MSLP departure from normal (right) on a) 29th Nov 2017 12 UTC and b) 30th Nov 2017 03 UTC. Source: IMD Meteorological Department.

Fig 4.12 above shows the Mean Sea Level Pressure (MSLP) changes in 24 hour and MSLP departures from normal on 29th and 30th Nov 2021. These charts show rapid fall of mean sea level pressure by 30th Nov and large-scale negative departure (of the order of 8 hPa) off the Kerala coast.

Fig. 4.13 shows low level convergence and 850 hPa vorticity patterns at 03 and 12 UTC on 29th Nov, when the system intensified into a cyclonic storm. The low-level convergence pattern shows a rapid increase in the low-level convergence over the region associated with the weather system. The INSAT satellite pictures of TC-Ockhi are shown in Fig 4.14. These images are provided by the Satellite Directorate of IMD, which shows the westward movement and then north-northeasterly recurvature towards the Gujarat coast.

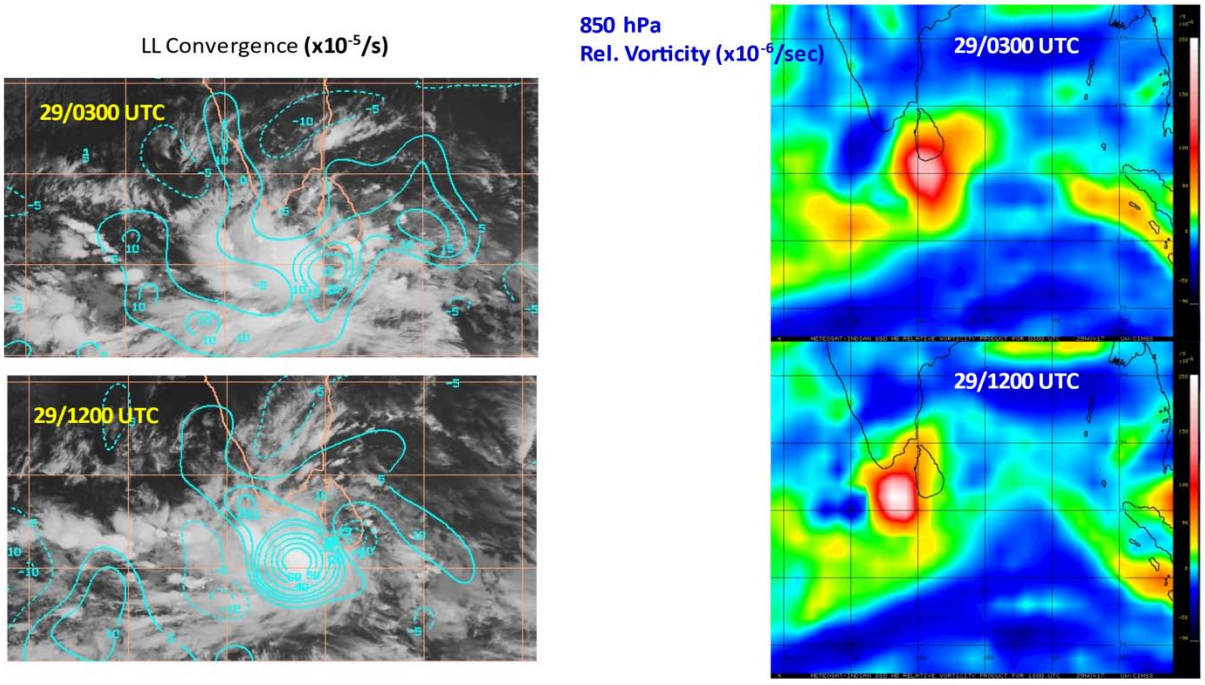

Fig 4.13. Low-level convergence (10^{-5}/s) (left) and 850 hPa vorticity (10^{-5}/s) (right) at 03 and 12 UTC on 29th Nov 2017. Source: IMD

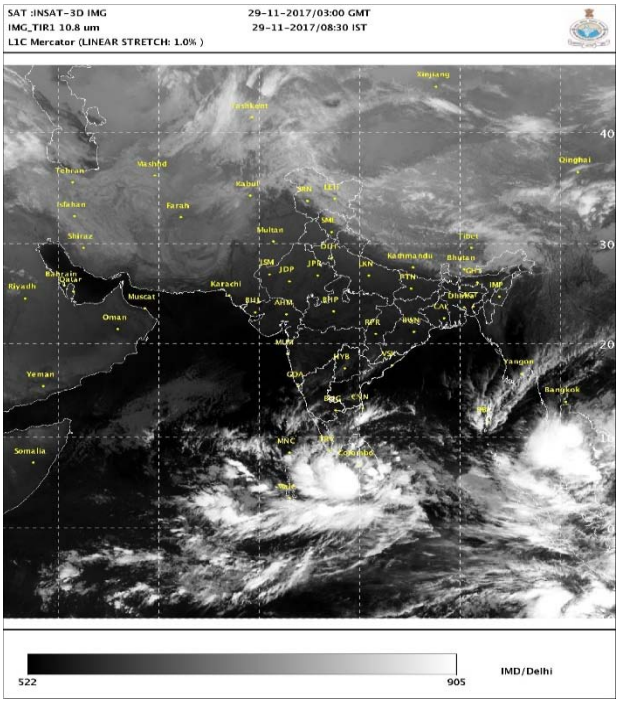

a) 29 Nov 0300 UTC

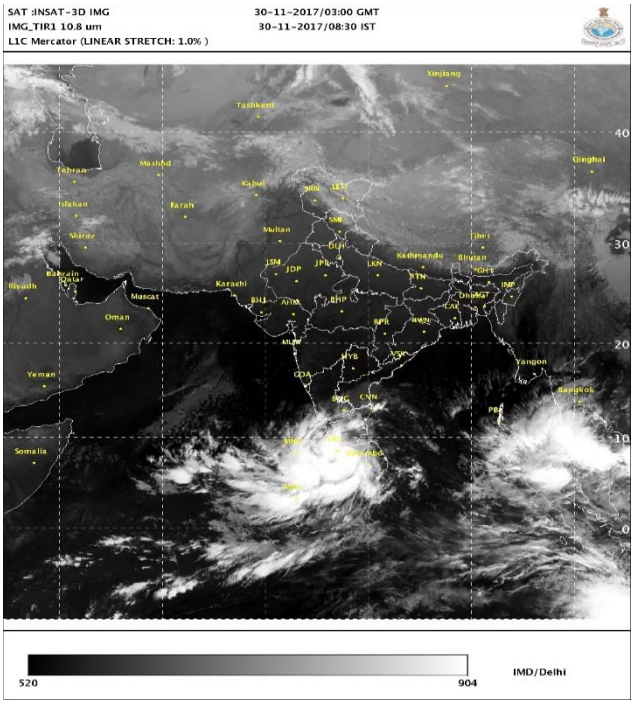

b) 30 Nov 0300 UTC

b)

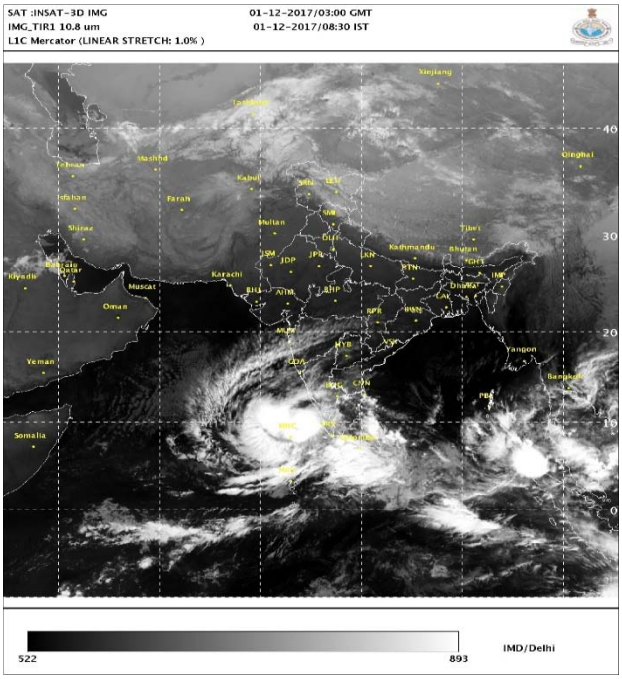

c) 01 Dec 0300 UTC

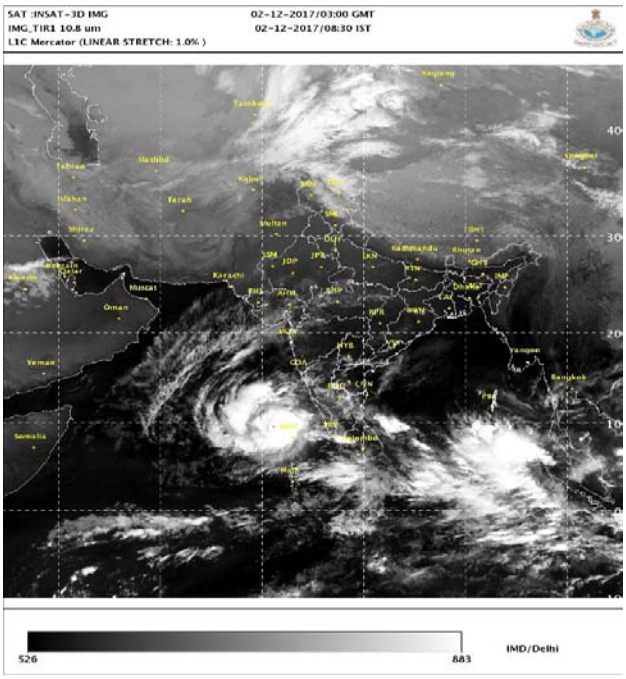

d) 02 Dec 0300 UTC

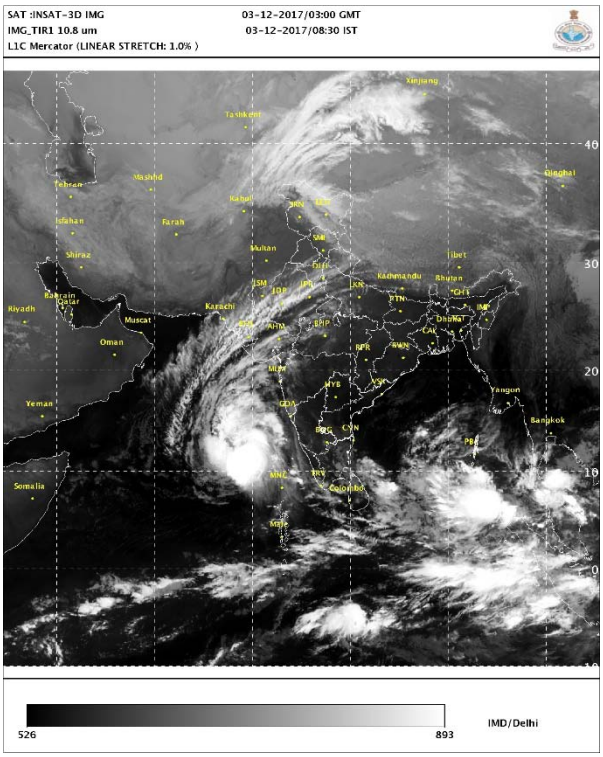

e) 03 Dec 0300 UTC

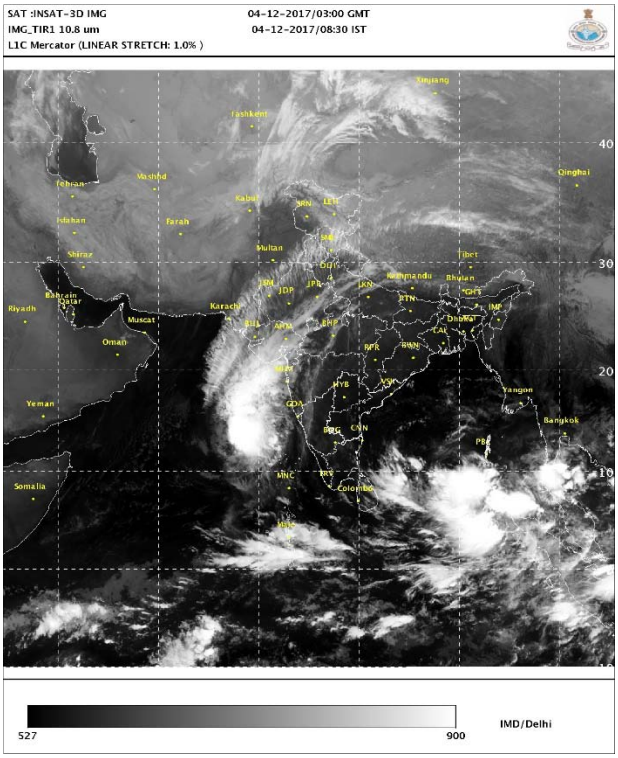

f) 04 Dec 0300 UTC

Fig 4.14. INSAT IR image at 0300 UTC showing TC-Ockhi during 29 Nov- 04 Dec 2017. Source: IMD Satellite Directorate.

Fig 4.15 shows the spatial distribution of 10 m wind (in knots) from 29 Nov to 4th Dec showing the intensification and weakening of surface winds associated with TC-Ockhi. These plots are prepared using the ERA5 reanalysis data with 0.25 degree resolution.

It caused heavy to very heavy rainfall over Lakshadweep on 01st and 2nd Dec. There was heavy rainfall over north coastal Maharashtra and adjoining south coastal Gujarat on 5th Dec. Thiruvananthapuram recorded 62 kmph wind in gustiness at 1300 IST of 30th Nov. Storm surge of height 1m over Lakshadweep Islands was observed on 30th Nov.

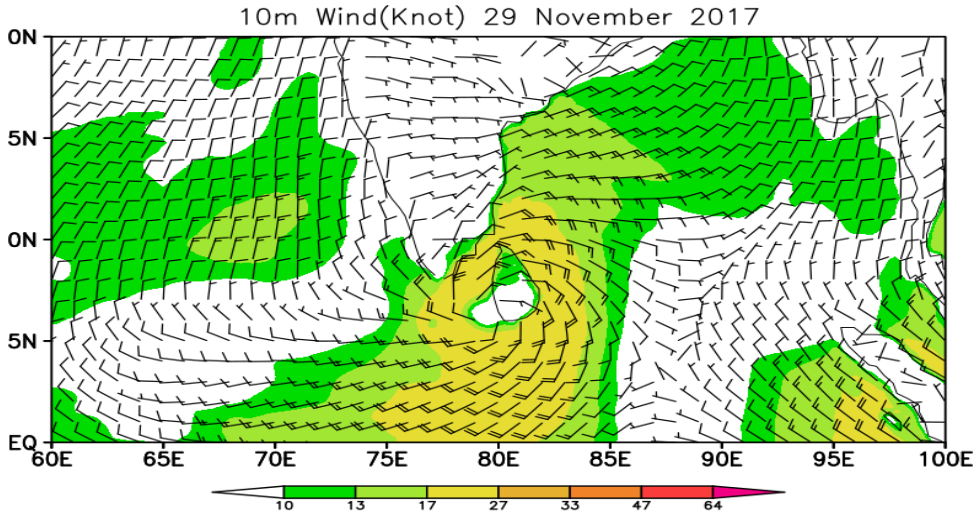
10m Wind(Knot) 29 November 2017
10N
5N
0N
5N
EQ
60E
65E
70E
75E
80E
85E
90E
95E
100E
10
13
17
27
33
47
64

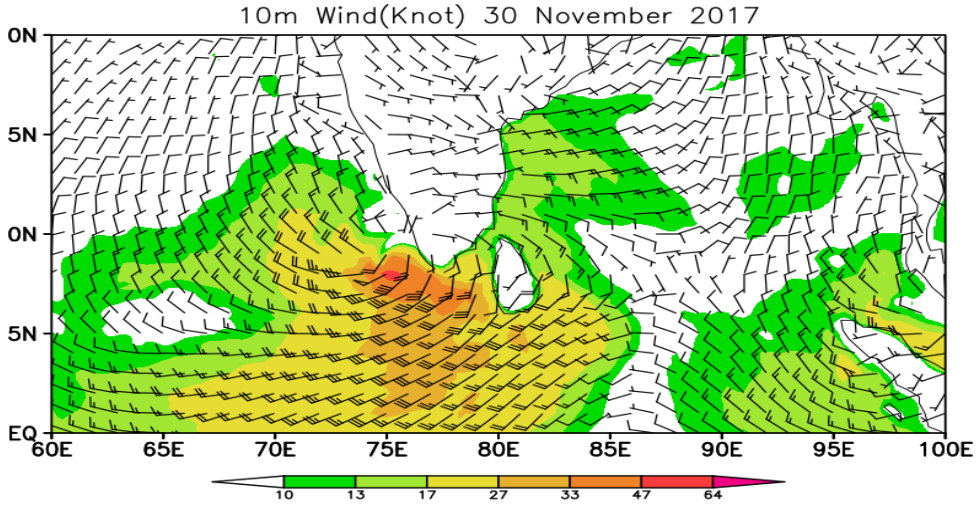
10m Wind(Knot) 30 November 2017
10N
5N
0N
5N
EQ
60E
65E
70E
75E
80E
85E
90E
95E
100E
10
13
17
27
33
47
64

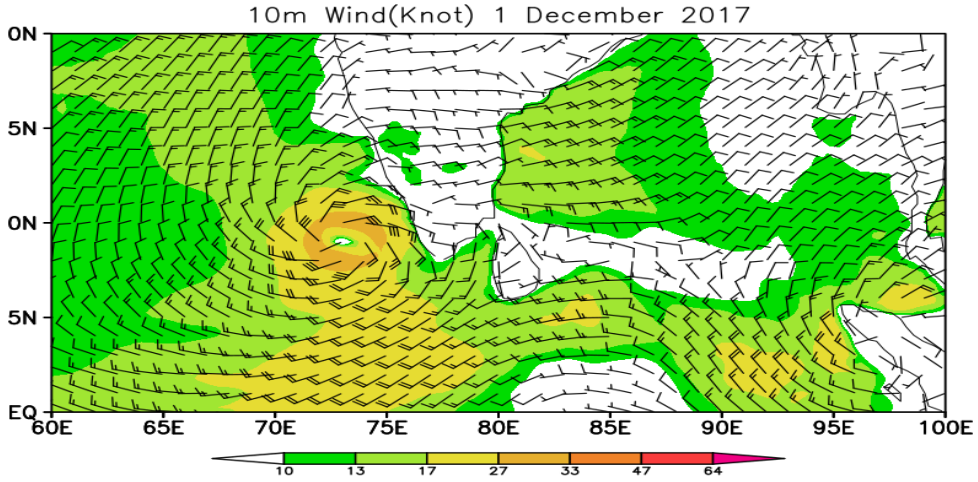
10m Wind(Knot) 1 December 2017
10N
5N
0N
5N
EQ
60E
65E
70E
75E
80E
85E
90E
95E
100E
10
13
17
27
33
47
64

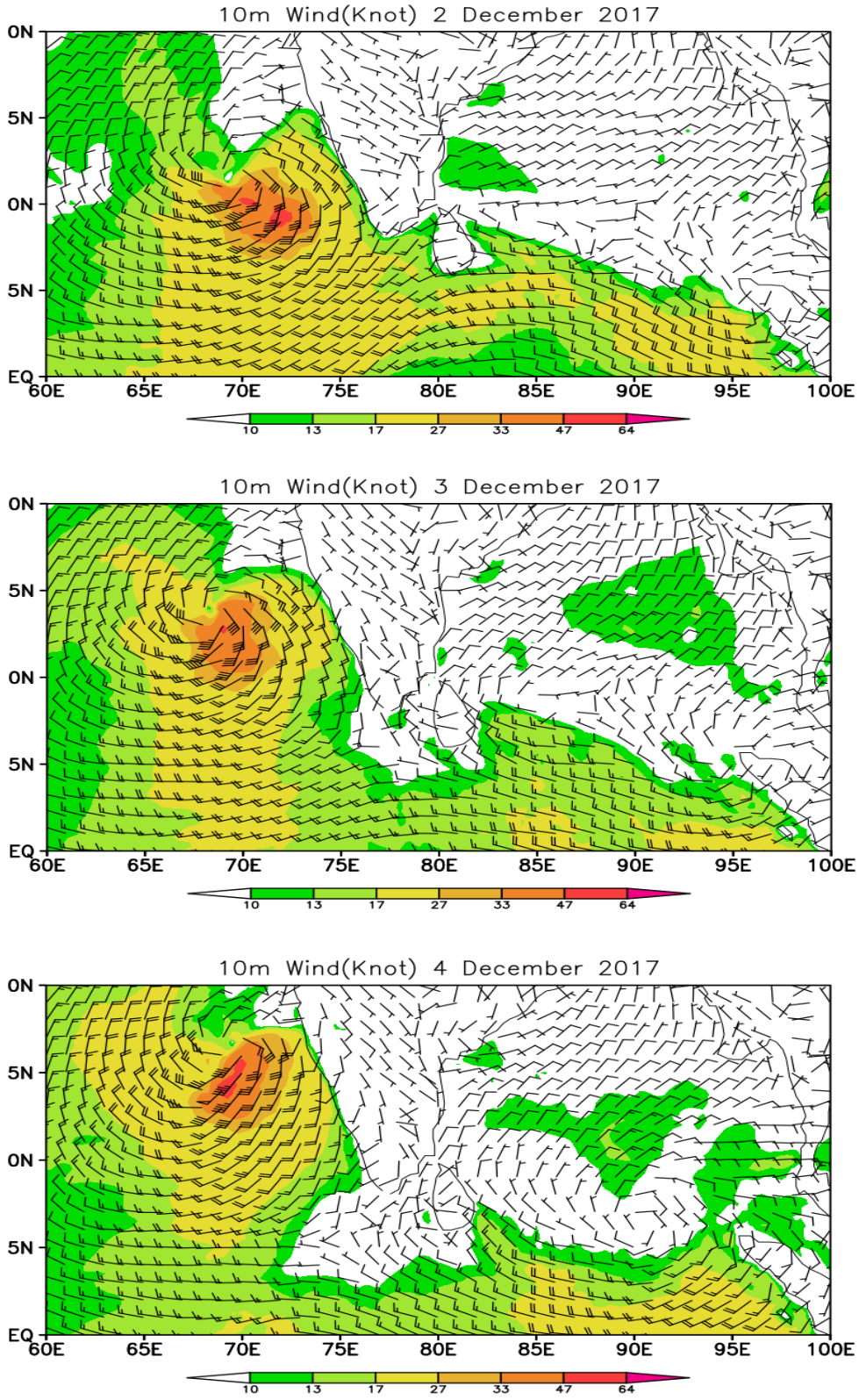

Fig 4.15. Spatial distribution of 10 m wind in knots from 29 Nov to 4 Dec 2017. Source: ERA reanalysis data

The salient features of TC-Ockhi are given below (IMD, 2018):

- This was the only fourth cyclonic storm developing over the Comorin Sea (south of Kerala and Tamil Nadu and west of Sri Lanka) during the past 120 years. Previously two cyclones (19-22 Nov and 17-19 Dec) in 1912 and another in 1925 (06-10 Nov) developed over the Comorin Area. All these cyclones affected south Kerala and south Tamil Nadu.
- TC-Ockhi was thus a rare cyclone with rapid intensification in genesis stage (from depression to cyclonic storm within 24 hours). The system intensified rapidly from 1800 UTC of 30th to 0000 UTC of 2nd Dec (increase in wind speed by 30 kts in 24 hours) (Fig 4.16).
- The total track length of the cyclone was 2538 km.
- The 12 hourly average translational speed of the cyclone was 15.0 kmph. However, it moved faster in the genesis stage (29/0830 IST to 30/0830 IST) with 12 hourly average translational speed of 19 kmph.
- The life period of cyclone was 6 days & 18 hours against long period average of 4.7 days for very severe cyclonic storm over north Indian Ocean.
- The peak maximum sustained surface wind speed (MSW) of the cyclone was 150-160 kmph gusting to 175 kmph (85 knots) during 0600 UTC of 2nd to 0000 UTC of 3rd December (Fig 4.17)
- The lowest estimated central pressure was 976 hPa (from 0300 UTC of 2nd to 0000 UTC of 3rd December) with a pressure drop of 34 hPa (Fig 4.17).
- The intensification/weakening of TC-Ockhi was largely governed by the Ocean heat content. However, the rapid weakening on 4th and 5th Dec was facilitated by dry and cold air intrusion and high vertical wind shear under the influence of a trough in midlatitude westerlies.

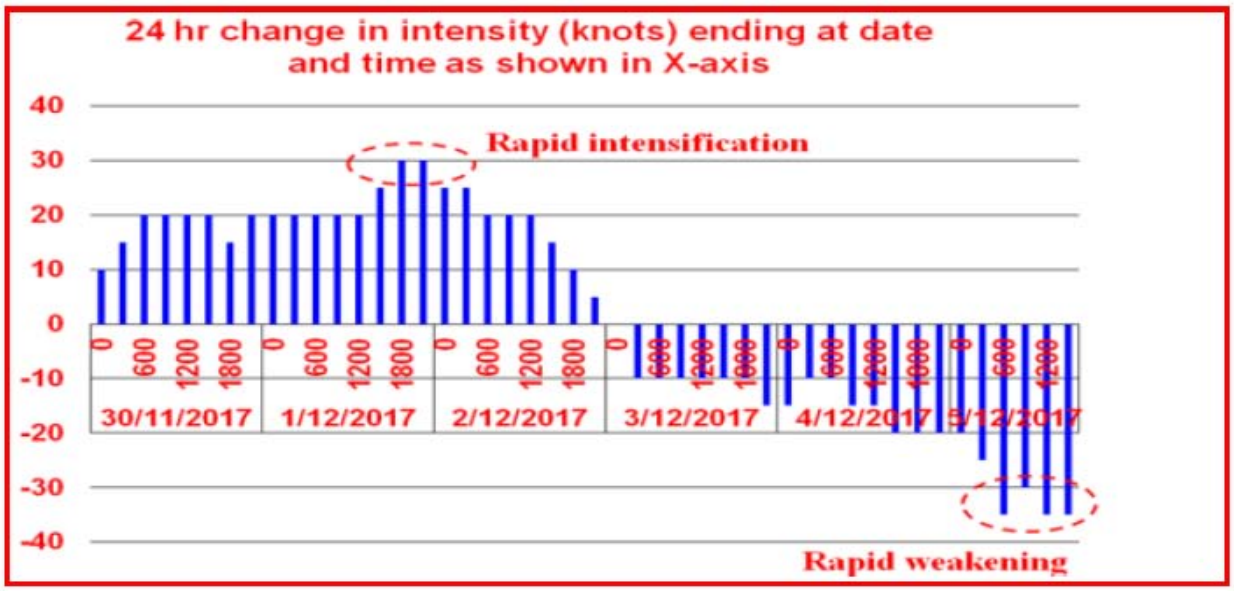

Fig 4.16. 24-hour change in intensity (knots) ending on different date and time. Rapid intensification and rapid weakening are indicated. Source: IMD 2018 report.

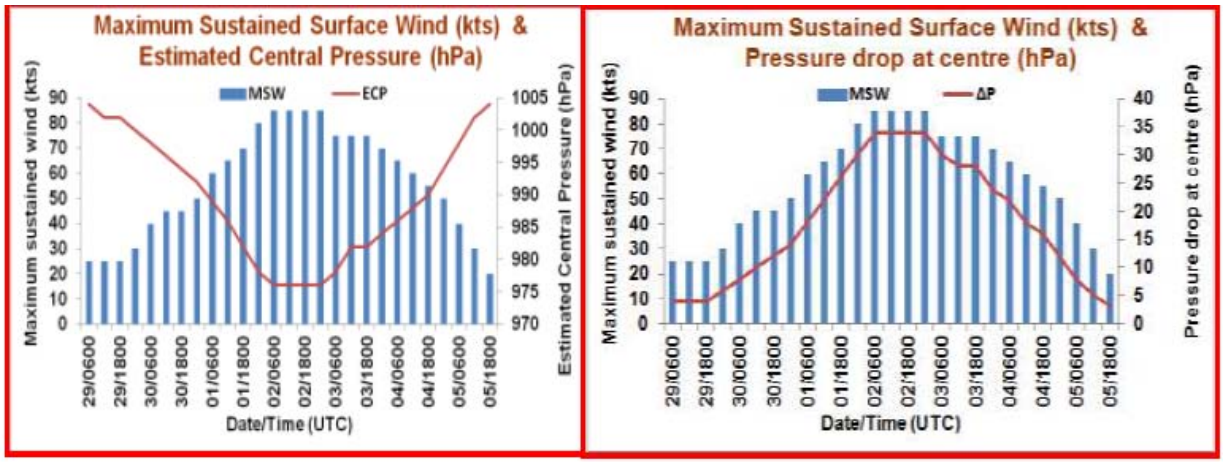

Fig. 4.17 a) Maximum sustained surface wind (kts) and estimated centre pressure (hPa) and b) Maximum sustained surface wind (kts) and pressure drop at centre (hPa). Source: IMD 2018 report.

Genesis and intensification of tropical cyclones are closely related to oceanic conditions like sea surface temperatures (SST) and ocean heat content. Fig 4.18 shows the spatial distribution of SST during 23-28 Nov, just prior to the formation of TC-Ockhi.

This plot clearly shows sea surface temperatures were more than 28.5^{0}C over the southwest Bay of Bengal (where the TC-Ockhi initially formed), which is much more than the SST threshold for formation of tropical cyclones. Over southeast Arabian sea, SSTs were even more than 29.0^{0}C. Many previous studies (for example, Jangir et al., 2021, Sanap et al., 2020) have documented the relationship between the ocean heat content and intensification of tropical cyclones. Fig 4.19 shows the Tropical cyclone heat potential (TCHP), which clearly suggests the presence of large ocean heat content over southwest Bay of Bengal (Comorin area) and southeast Arabian sea (over the observed track of TC-Ockhi), TCHP was more than 70 KJ/cm^2. This large amount of heat potential was mainly responsible for the rapid intensification of TC-Ockhi.

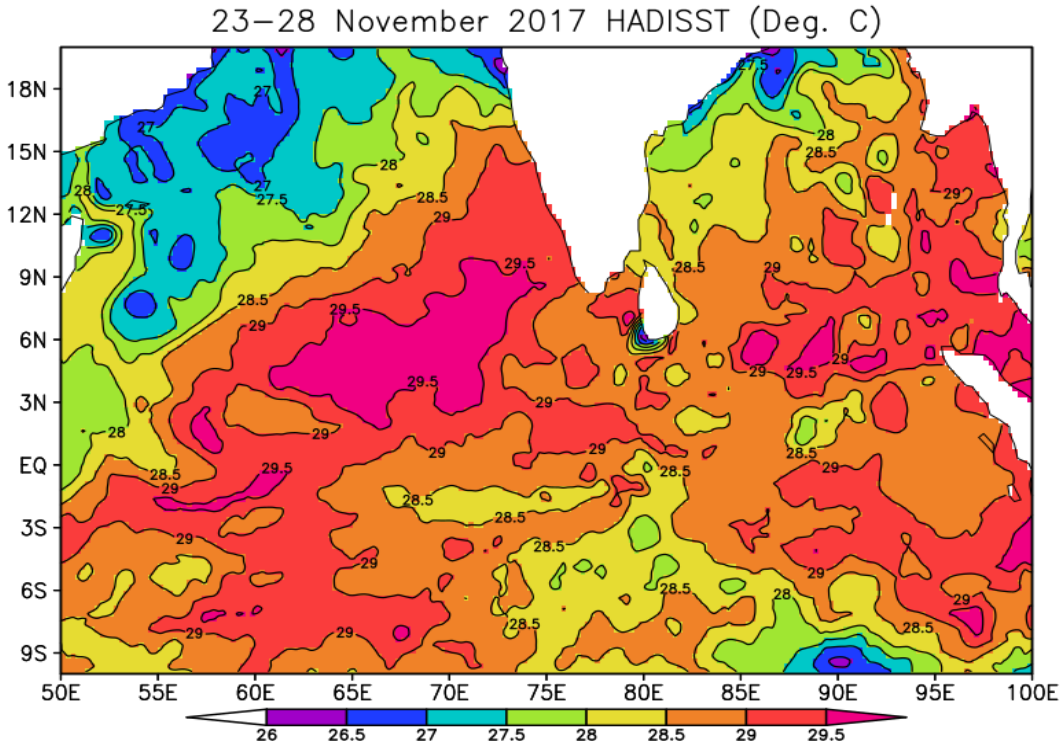

Fig 4.18. Spatial distribution of Sea Surface Temperatures (SST) in ^{0}C averaged during 23-28 November 2017, just before the TC-OCKHI formed over southwest Bay of Bengal. Source: UK Met office, HADISST.

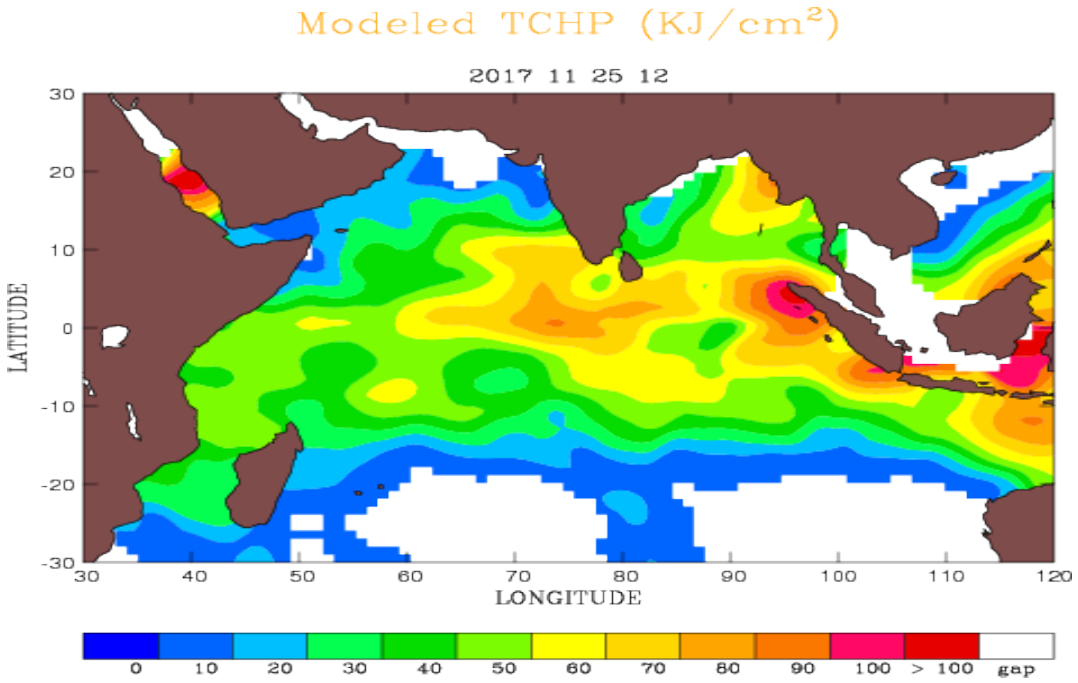

Fig. 4.19. Spatial distribution of Tropical Cyclone Heat Potential (TCHP) in KJ/Cm^2 on 25 November 2017, just prior to the formation of TC-OCKHI. Source: NRSC, ISRO.

Singh et al., (2020) studied the role of eastward moving Madden and Julian Oscillation (MJO) in the genesis of TC-Ockhi. Mohapatra and Adhikary (2011) also studied the role of MJO on tropical cyclone genesis over the Indian Ocean region. MJO is an eastward-moving wave in the tropical belt associated with enhanced convective activity in the regions from which it passes. Previous studies have shown that MJO in phase 4 is conducive for cyclogenesis in the south of Bay of Bengal by ensuing increased vorticity and anomalous cyclonic circulation on the westward side of MJO-induced convective activity. As the MJO propagated from phase 3 to phase 4 in November, 2017, it resulted in anomalous westerlies over the entire south Bay of Bengal (near the equator) in response to the shift in the convection over the maritime continent The anomalous westerlies along with anomalous easterlies over a narrow zone centred near 10°N, caused a strong shear zone and positive vorticity (Singh et al., 2020).

Jyothi et al., (2020) investigated the oceanic and atmospheric processes that have contributed to the Rapid Intensification (RI) and Rapid Weakening (RW) of Cyclone Ockhi using the HYbrid Coordinate Ocean Model (HYCOM) simulations and Global Forecast system (GFS) outputs. The environmental conditions prevailed before RI showed the presence of thick warm and fresh waters, ample supply of mid-tropospheric relative humidity, and moderate wind shear. The intrusion of dry air, strong vertical wind shear, and unfavourable oceanic conditions annihilated the storm intensity during the RW stage. Compared to the ocean temperatures, the vertical structure of salinity showed remarkable differences between the RI and RW locations resulting in contrasting upper-ocean stratification.

NWP Forecast Guidance for TC-Ockhi

India Meteorological Department (IMD) refers to many forecast products for preparing warnings for tropical cyclones over the north Indian Ocean. In this case of TC-Ockhi also, IMD had referred to many NWP products from IMD GFS, NCUM, ECMWF and JMA models. An analysis of inferences drawn from these models suggests that none of the models could provide an early forecast guidance for the genesis of TC-Ockhi as a Low/depression and its further intensification. The first model forecast guidance was available from the ECMWF model based on 28 Nov 0000 UTC in which the model indicated formation of a depression and its intensification into a severe cyclonic storm over the Arabian sea. The other models started indicating the formation of this system and its intensification from 29th Nov only. It is very important to note that none of the models correctly indicated the rapid intensification of TC-Ockhi during the course of its travel around the Comorin area.

However, the track forecasts by some of the models in predicting track of TC-Ockhi have been reasonably accurate as shown in Table-4.3 below. Numbers given in the bracket is number of verified forecasts. It can be seen that the Multi-Model Ensemble (MME) of IMD has the lowest errors compared to other models up to 48

hours lead time. Beyond 48 hours, ECMWF performed better than IMD-MME. The forecast errors of IMD-HWRF beyond 24 hours was far inferior compared to other models. The observed track of TC-Ockhi and IMD-MME predictions are given in Fig 4.20 and that of NCUM model are given in Fig 4.21. The models could indicate the recurvature and weakening of the TC-Ockhi very well.

In summary, the NWP models did not provide enough lead time for the IMD about its genesis over the Comorin area and its likely intensification into a cyclonic storm. IMD could get only 36 hours lead time to inform Kerala and Tamil Nadu government officials about its genesis and likely intensification. However, once the TC-Ockhi started moving, the forecast track errors were found reasonable and comparable with the climatological forecast errors. Despite considerable improvements in the prediction of genesis, intensity and track of cyclones in the north Indian Ocean in the recent decade, most of the models failed to capture the genesis of cyclone Ockhi in advance and its rapid intensification.

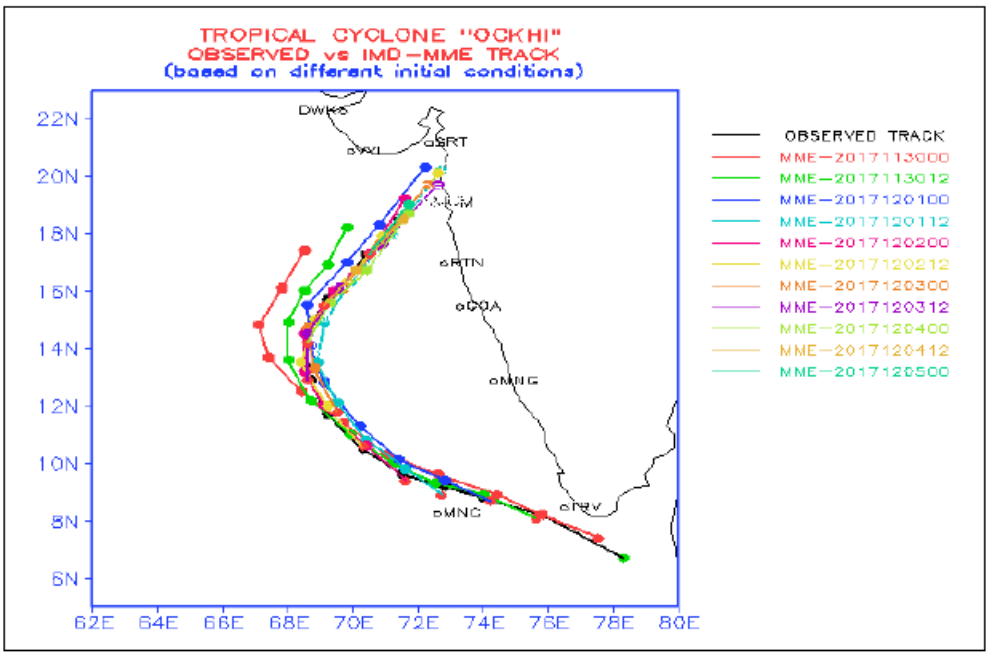

Fig 4.20. Observed and Predicted track of TC-Ockhi by the IMD-MME prediction system.

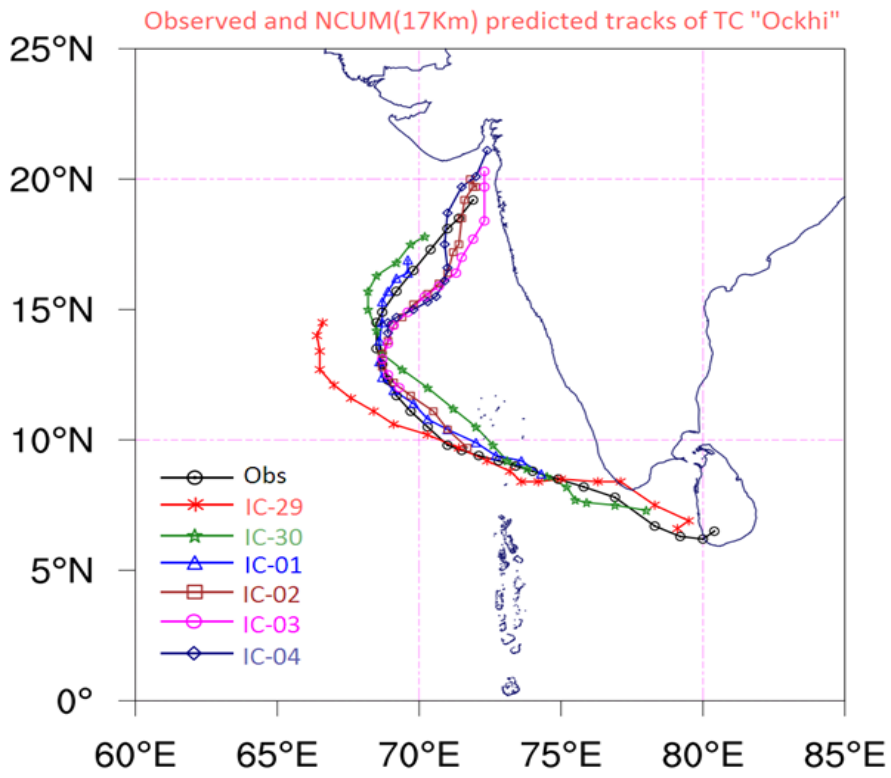

Fig 4.21. Observed and Predicted track of TC-Ockhi by the NCUM prediction system.

A detailed study is required to understand why the NWP models could not provide adequate lead time in predicting the genesis and the further intensification of TC-Ockhi. One of the reasons could be that its genesis was very close to the equator. The models might have had problems in predicting its genesis near the equator. It may be mentioned that the models referred by IMD for forecast guidance are atmospheric models and do not treat the oceanic conditions and ocean-atmosphere coupling explicitly. This leads to an inference that even for short to medium range forecasting of weather systems like Tropical Cyclones, a coupled modelling strategy may be required.

This may be considered as a special case in which the NWP models had problems in predicting its genesis and rapid intensification. Otherwise, the recent NWP models are known for their accurate prediction of tropical cyclones.

Table 4.3

TC-OCKHI Average Track Forecast Errors in km by different models

(Source: IMD report)

Lead time	12 hrs	24 hrs	36 hrs	48 hrs	60 hrs	72 hrs
IMD-GFS	51(11)	68(10)	98(9)	117(8)	123(7)	145(6)
IMD-WRF	59(11)	115(10)	166(9)	226(8)	271(7)	278(6)
JMA	70(11)	70(10)	85(9)	103(8)	148(7)	215(6)
NCEP-GFS	60(11)	65(10)	75(9)	110(8)	91(7)	104(6)
UKMO	42(11)	63(10)	76(9)	122(8)	146(7)	173(6)
ECMWF	58(11)	69(10)	64(9)	62(8)	86(7)	100(6)
IMD-HWRF	58(21)	99(20)	130(18)	180(16)	234(14)	251(12)
IMD/MME	29(11)	44(10)	58(9)	86(8)	100(7)	112(6)
NCUM	82(13)	122(12)	129(11)	121(10)	144(9)	180(8)
NEPS	90(7)	134(6)	178(6)	217(5)	211(5)	208(4)

4.7. Easterly Waves/Troughs in Easterlies

From the Table – 4.1, it is observed that easterly waves/trough in easterlies form a substantial portion of synoptic systems affecting south peninsula during the NE monsoon season. However, there are not adequate studies on easterly waves forming over the Indian Ocean.

Easterly wave is a wave within the broad easterly current and moves from east to west, generally more slowly than the current in which it is embedded. Although best described in terms of its wave like characteristics in the wind field, it also consists of a weak trough of low pressure. Easterly waves do not extend across the equatorial trough. To the west of the trough line in an easterly wave, there is generally found divergence, a shallow moist layer, and exceptionally fine weather. The moist layer rises rapidly near

the trough line; in and to the east of the trough line intense convergence, cloudiness and heavy rain showers prevail. Easterly waves occasionally intensify into tropical cyclones over the Bay of Bengal.

These waves are first identified in the Carribean (Dunn, 1940) and subsequently studied in detail over the African region using synoptic / satellite observations and numerical models. Considerable work on the passage of easterly waves over the African region, their structure, movement and roles in genesis of Atlantic hurricanes have been carried out and reports available in the literature (Burpee (1974), Jury et al., (1991), Berry and Thorncroft (2005) and Ross and Krishnamurti (2007)). Similar studies have also been undertaken for other oceanic regions such as Eastern and Western Pacific (Tai and Ogura,1987). For the Indian region, Saha et al., (1981) have analysed 24 hour sea level pressure change charts of July-August of three stations for the 10 year period of 1969-1978 and have identified passage of westward propagating disturbances as predecessors to formation of monsoon lows and depressions. Using cross-correlation and power spectral analysis, they have determined the period of the wave as about 5 days, speed of about 6 ms^{-1} and wavelength of 2300 km. There are not adequate studies on Easterly waves forming over the Indian Ocean. Balachandran et al., (1998) have reported some features of an inverted V-type easterly wave over the Indian seas during December 1995 and have determined the speed of the wave as 8.2 knots using satellite imageries.

Conceptually, northerly meridional winds, subsidence, divergence and fair weather are the general atmospheric characteristics ahead of an approaching easterly wave trough and southerly meridional winds, rising motion, convergence and active weather are the characteristics behind the wave trough. The southerly meridional winds approaching the wave trough encounter an upgradient motion (moving from a low in the south towards a high in the north) and hence slow down leading to velocity convergence. The northerly winds approaching the wave ridge face a downgradient

motion as a result of which the wind speeds increase leading to velocity divergence. Thus, the winds approaching the wave trough are sub-geostrophic and the winds approaching the wave ridge are super-geostrophic (Hess, 1959). The pictorial representation of an easterly wave, taken from Riehl (1968, Tropical Meteorology) is given in Fig 4.22.

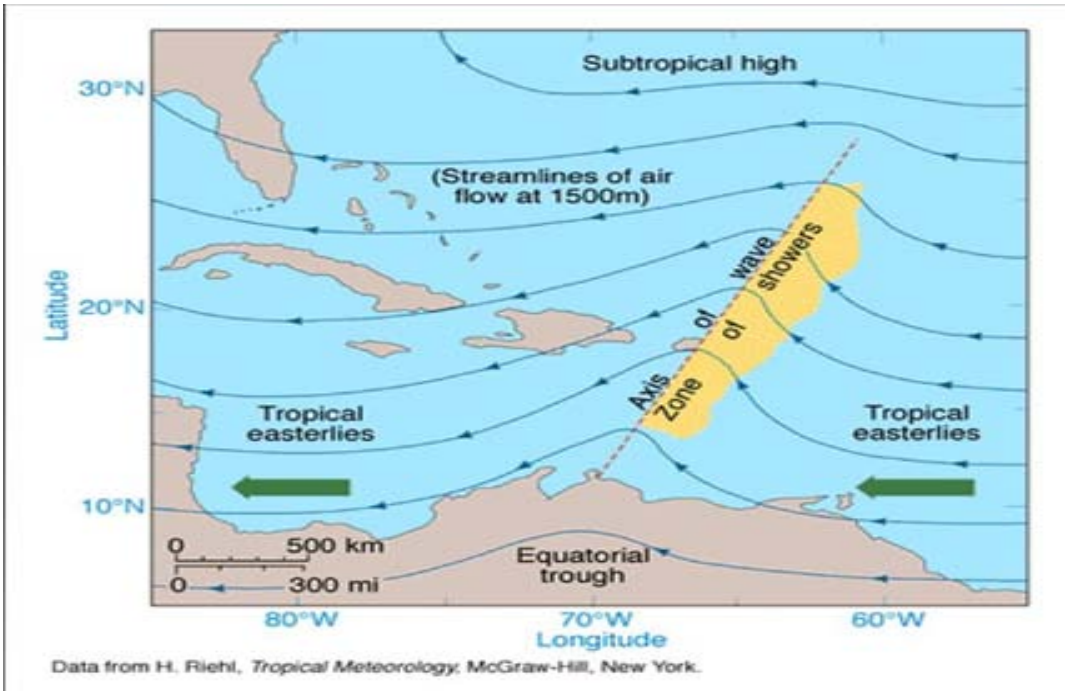

Fig.4.22. Pictorial Representation of an Easterly Wave observed over the north Atlantic. After Riehl (Tropical Meteorology).

There are a few studies on examining the role of Easterly Waves for enhancing rainfall over south Peninsula during the NE Monsoon season. Reba et al. (2022) examined the years 2015, 2016 and 2017 to understand the variability of synoptic conditions including the propagation of easterly waves (EWs). Further, it is also seen that many active rainfall spells during 2015 and 2017 over Tamil Nadu met-subdivision were associated with passage of EWs over the southern peninsula along east of 85^0E, whereas, the large deficient NE monsoon of 2016 witnessed no such active spell of

monsoon and the passage of EW was confined to the eastern part of Bay of Bengal and never entered into the Indian peninsula. Geetha and Balachandran (2014) studied the easterly wave characteristics during 2010 NE monsoon season by means of synergetic analysis using synoptic, statistical and numerical methods. The easterly waves during 2010 had time periods of about 4.5 days. The speed of movement, wavelength and amplitude of EWs were 7.28 ms^{-1}, 2800 m, and 6.7 ms^{-1} respectively. Sanap et al. (2018) examined the 2015 NE Monsoon season in respect of easterly wave activities. Their results indicated that EW activity over the Indian Ocean plays a seminal role in occurrence of heavy rainfall events during the positive phase of the ENSO (El-Niño), while it is found to be weak during negative (La-Niña) and neutral phase.

Here, we now discuss on a case study of formation of an easterly wave and its westward movement across south peninsula during 13-18 November, 2010. As shown in Fig 4.23, there was widespread rainfall activity over south peninsula and adjoining Bay of Bengal associated with the Easterly wave. It is interesting to note that a wave type structure is observed in precipitation pattern during this period. Fig 4.24 shows the vector winds at 700 hPa during the period 13-18 November, 2010 and vorticity at 700 hPa. Positive vorticity suggesting large scale ascending motion can be noticed on the eastern side of the trough line of the easterly wave. The easterly wave which formed over southeast Bay of Bengal moved westwards and crossed south peninsula by 17 November and emerged into the Arabian sea on 18th November. This weather system caused widespread rainfall activity over the region. The relevant satellite pictures of this easterly wave are shown in Fig. 4.25.

Fig 4.26 shows the Longitude-Time cross section of a) Meridional wind at 700 hPa b) Outgoing Longwave radiation c) Precipitable water content and d) Precipitation rate at 10^{0}N during the period 13-18 November 2010, showing different aspects of an easterly wave, which travelled from east to west during 10-20 November, 2010 and contributed to large scale rainfall activity over south peninsula. These plots very clearly

show the westward movement of easterly wave representing meridional winds at 700 hPa, OLR, precipitation rate and vertical velocity, omega. The zero-line separating southerlies and northerlies is shown in Fig 4.26. It is interesting to note that lower values of OLR, large precipitation rate and large ascending motion (negative omega) are observed east of the zero line. This suggests that in and to the east of the trough line intense convergence, cloudiness and heavy rain showers prevail.

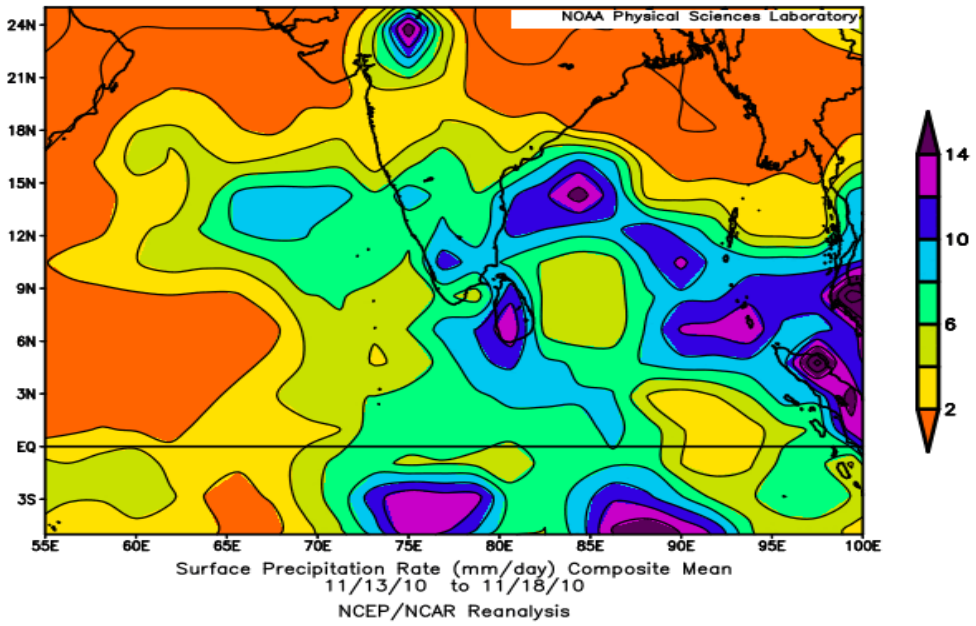

Fig 4.23. Precipitation rate (mm/day) averaged during 13-18 November 2010 associated with the Easterly Wave. Source: NCEP/NCAR reanalysis.

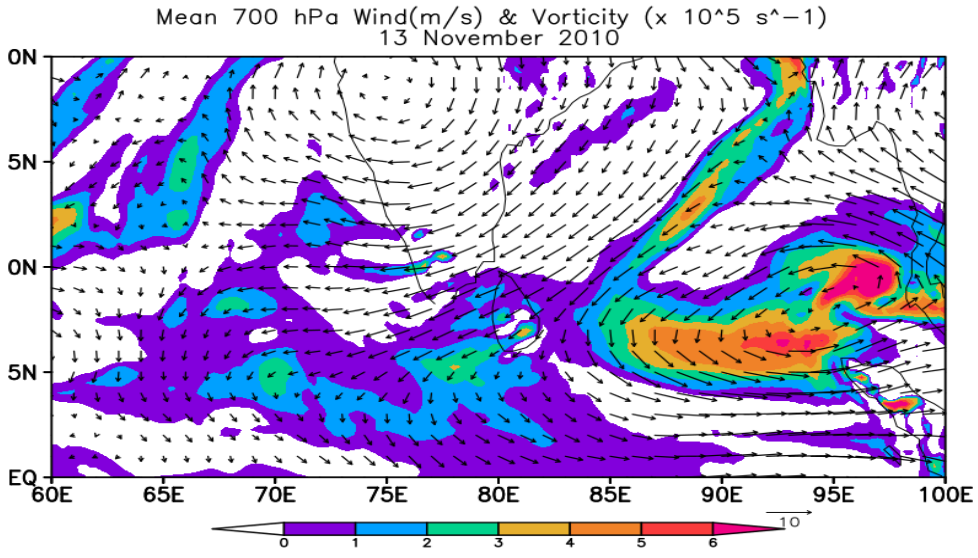

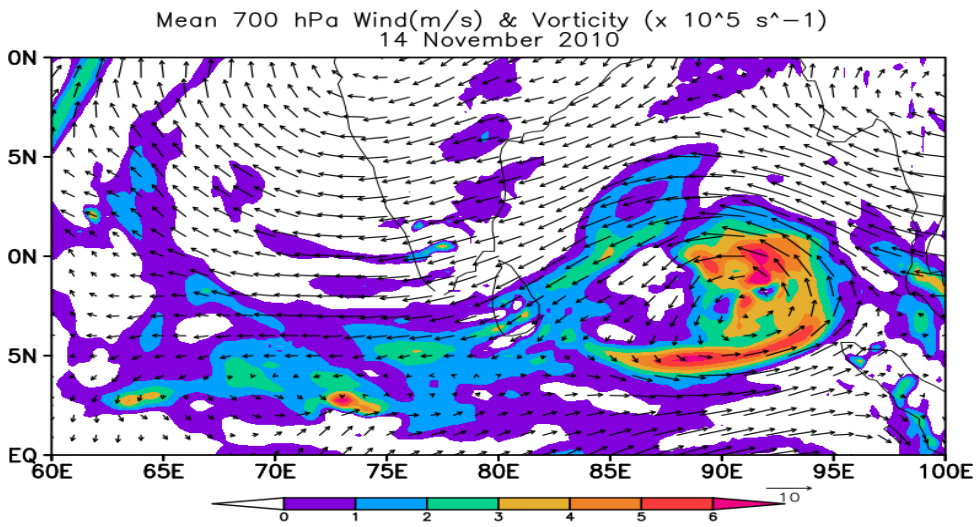
Mean 700 hPa Wind(m/s) & Vorticity (x 10^5 s^-1)
14 November 2010
10N
5N
0N
5N
EQ
60E
65E
70E
75E
80E
85E
90E
95E
100E
0
1
2
3
4
5
6
10

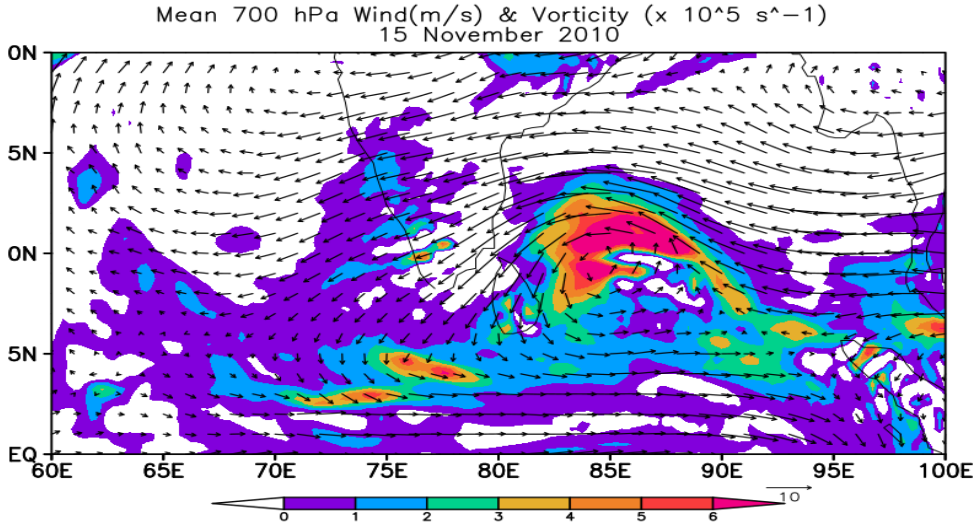
Mean 700 hPa Wind(m/s) & Vorticity (x 10^5 s^-1)
15 November 2010
10N
5N
0N
5N
EQ
60E
65E
70E
75E
80E
85E
90E
95E
100E
0
1
2
3
4
5
6
10

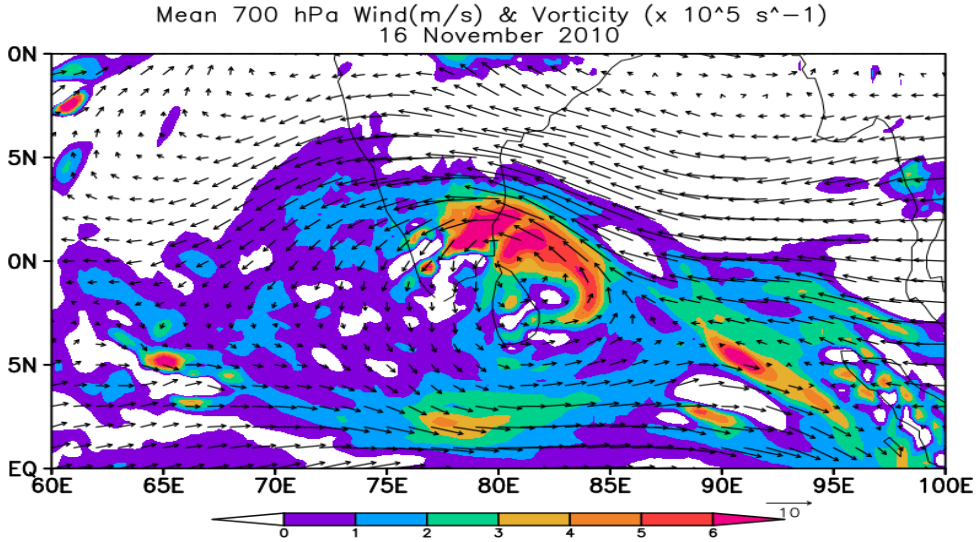
Mean 700 hPa Wind(m/s) & Vorticity (x 10^5 s^-1)
16 November 2010
10N
5N
0N
5N
EQ
60E
65E
70E
75E
80E
85E
90E
95E
100E
0
1
2
3
4
5
6
10

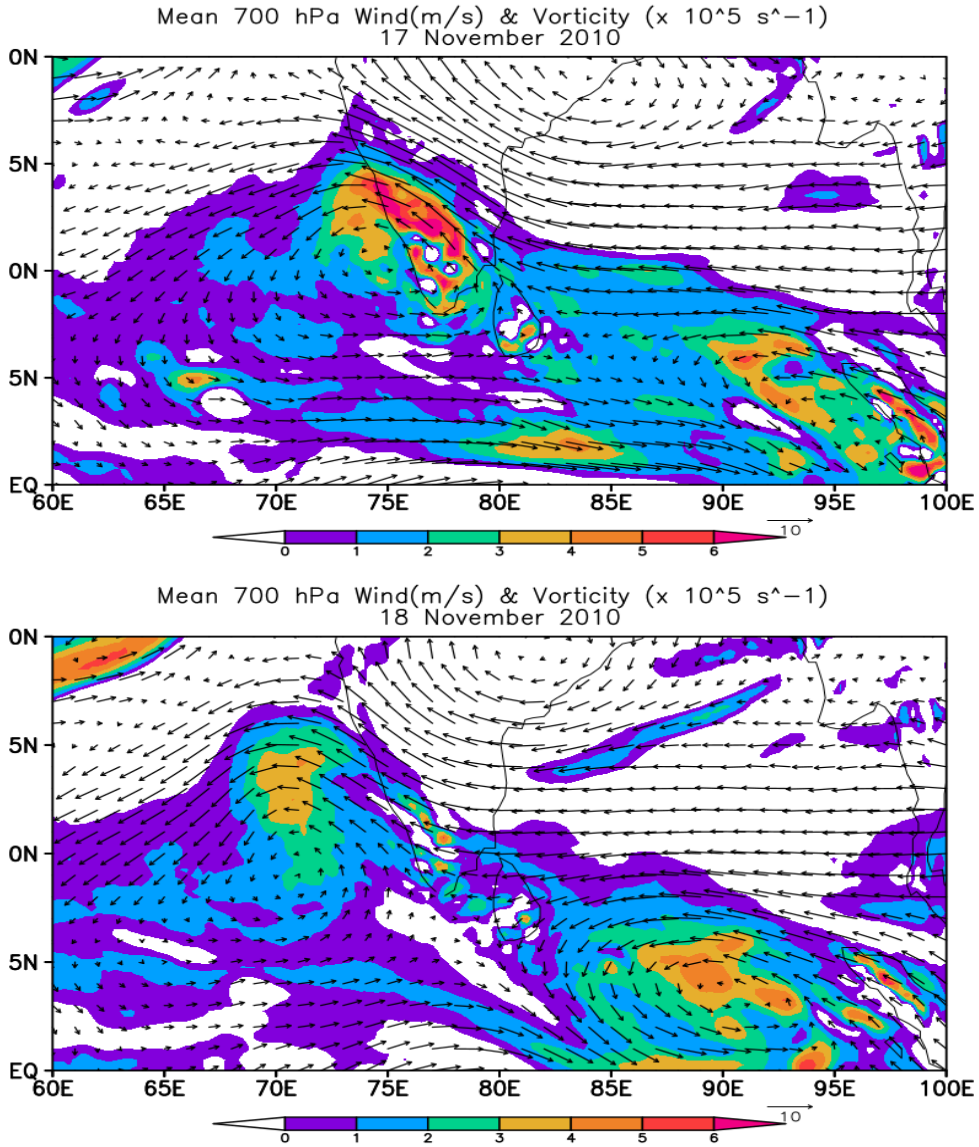

Fig. 4.24. Spatial distribution of 700 hPa winds and vorticity from 13 -18 November, 2010, showing westward movement of an easterly wave, which caused widespread rainfall activity over south Peninsula.

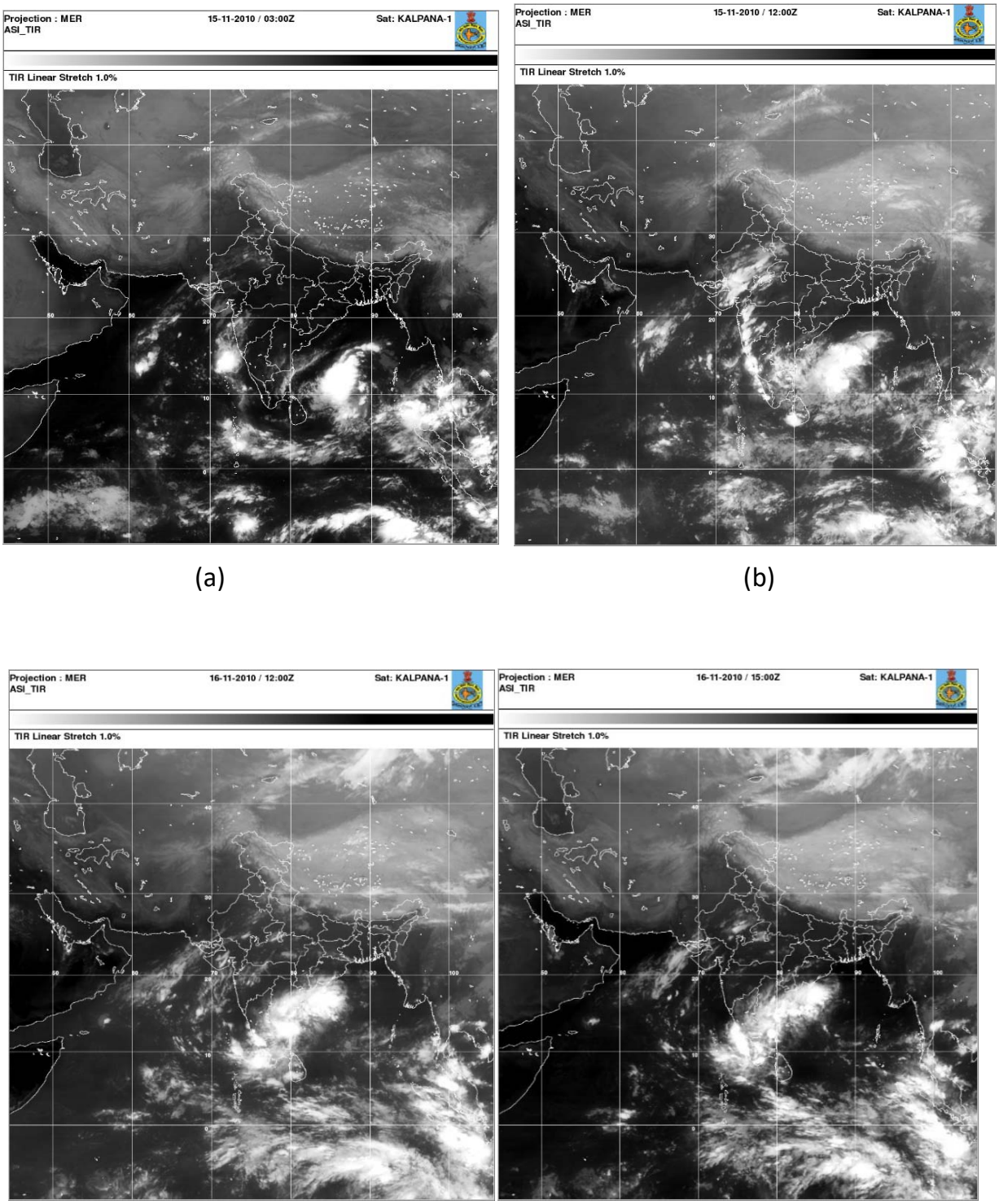

Fig 4.25. Kalpana IR Satellite Pictures showing the presence of easterly wave over the Bay of Bengal. a) 0300 UTC 15 November b) 1200 UTC 15 November, C) 1200 UTC 16 November and d) 1500 UTC 16 November. Source: IMD Satellite Directorate.

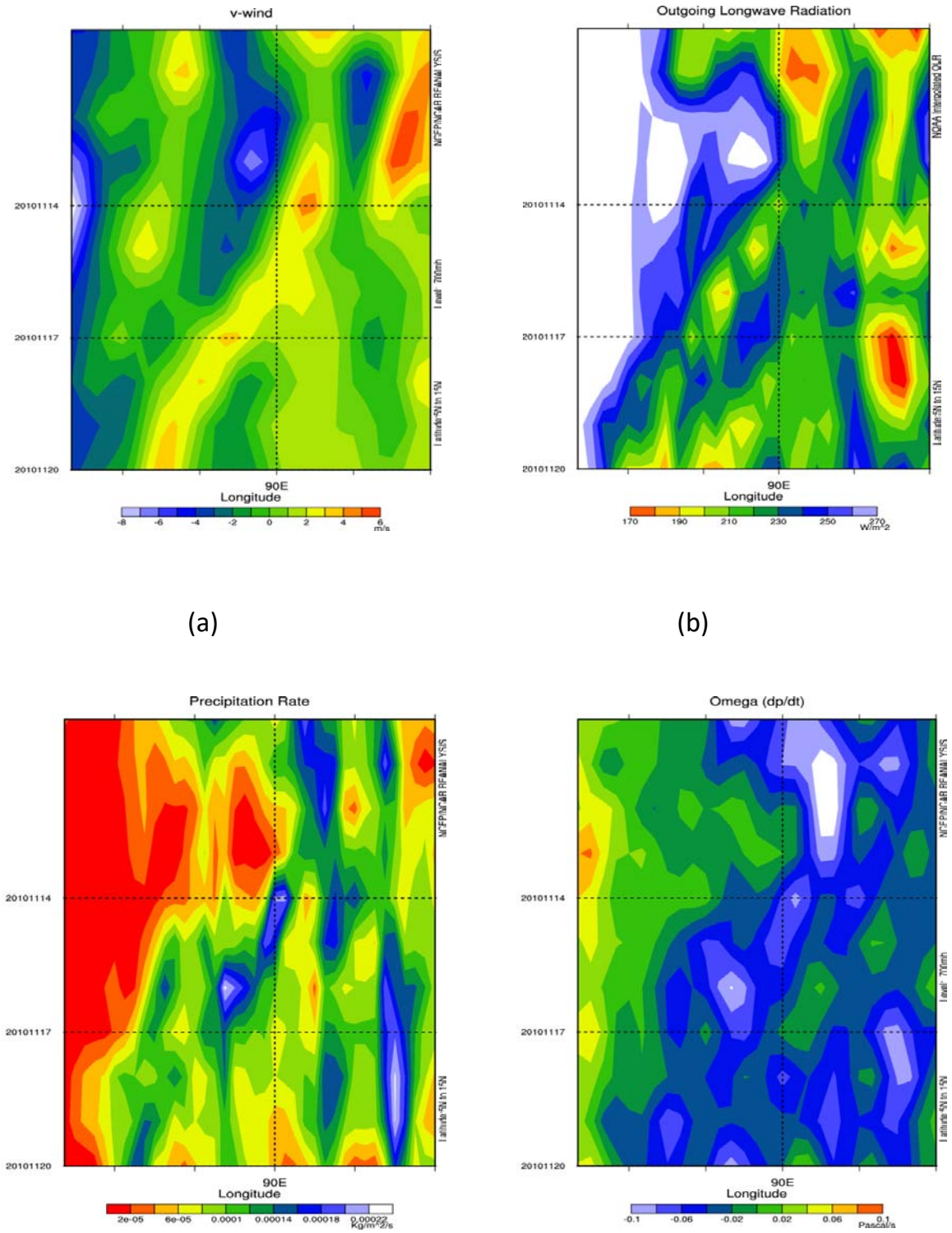

Fig 4.26. Longitude-Time cross section of a) Meridional wind at 700 hPa b) Outgoing Longwave Radiation (OLR) c) precipitation rate and d) vertical velocity, Omega averaged between 5-15^{0}N during the period 10-20 November 2010

Chapter-5

Onset and Withdrawal

NE monsoon advances into the south Peninsula in October/November after the Southwest monsoon completely withdraws from the country. India Meteorological Department (IMD) made the following criteria in August 1988 for declaring NE monsoon onset, which was further amended in August 2006 (IMD, 2008).

The criteria are:

1) Withdrawal of Southwest monsoon up to Latitude 15^0N
2) Onset of persistent surface easterlies over Tamil Nadu Coast
3) Depth of easterlies up to 850 hPa over Tamil Nadu Coast
4) Fairly widespread rainfall over coastal Tamil Nadu, South Coastal Andhra Pradesh and adjoining areas.

The withdrawal criteria of SW monsoon up to 15^0N becomes a constraint in some years. If due to operational constraints, the SW monsoon is not withdrawn, NEM could not be declared on real time basis even if conditions 2 to 4 above are satisfied (Raj, 2012).

IMD started announcing withdrawal dates of NEM only from the year 1993 and prior to that no such declaration appears to have been made. IMD has declared cessation of NEM rainfall by considering rainfall and may be a few other parameters such as depth of moisture, temperature etc. in a subjective way but no objective criteria or guidelines to determine NEM have so far been published (Raj 2012).

The IMD dates of NE monsoon onset and withdrawal are given in Table-5.1. The climatological NE monsoon onset date is 22 October with a standard deviation of about 7 days. The earliest onset date from 1977-2020 is 5 October in 1984. The most delayed onset date is 02 November which occurred in 1988, 1992 and 2000. The climatological withdrawal date is 04 January with a standard deviation of about 11 days. The earliest withdrawal date was 14 December 1994, and the most delayed withdrawal is 19 January

2021. The mean duration of the NE monsoon season is about 75 days. The smallest duration of 51 days occurred in 1992 and the highest duration of 98 days occurred in 2005. However, there is no statistical correlation of NE monsoon seasonal rainfall with either monsoon onset date, withdrawal date or duration. The highest correlation is between the monsoon onset and NE monsoon seasonal rainfall, which is -0.305, statistically significant only at the 90% significance level.

Raj (1992, 2003) and Geetha and Raj (2011) extensively studied the onset and withdrawal of NE monsoon. Geetha and Raj (2011) re-determined the onset and withdrawal dates of NE monsoon for the 100- years of 1901-2000 based on the daily rainfall data of 25 rain-gauge stations. Stations of south Coastal Andhra Pradesh and coastal Tamil Nadu which were located within a distance of 100 Kms from the coast were considered. The comparison of the dates thus identified are compared with the IMD dates. There is a negligible difference in respect of onset dates. However, the difference in respect of withdrawal dates is quite substantial over several years. The onset and withdrawal dates determined by Geetha and Raj (2011) and Raj (2012) are also given in Table-5 for comparison with the IMD onset and withdrawal dates. As per the data of Raj (2012), the mean onset date is 20 October with a standard deviation of about 8 days and mean withdrawal date is 29 December with a standard deviation of about 14 days. Mean duration of the NE monsoon season is about 70 days.

We follow the onset and withdrawal dates as determined by IMD for further analysis and discussions. In the following sections, more analysis with respect to NE monsoon onset and withdrawal dates is discussed.

Table 5.1

NE monsoon onset and withdrawal dates as determined by

IMD and Raj (2012)

Year	Onset Date (IMD)	Onset Date (Raj, 2012)	Withdrawal Date (IMD)	Withdrawal Date (Raj, 2012)
1977-78	14-Oct	10-Oct		
1978-79	23-Oct	21-Oct		
1979-80	22-Oct	22-Oct		
1980-81	11-Oct	10-Oct		
1981-82	23-Oct	23-Oct		
1982-83	19-Oct	18-Oct		
1983-84	24-Oct	24-Oct		
1984-85	05-Oct	03-Nov		
1985-86	25-Oct	25-Oct		
1986-87	27-Oct	26-Oct		
1987-88	30-Oct	20-Oct		
1988-89	02-Nov	03-Nov		
1989-90	27-Oct	29-Oct		
1990-91	19-Oct	18-Oct	10-Jan	27-Dec
1991-92	20-Oct	19-Oct	24-Dec	23-Dec
1992-93	02-Nov	02-Nov	22-Dec	09-Dec
1993-94	20-Oct	13-Oct	11-Jan	01-Jan
1994-95	18-Oct	18-Oct	14-Dec	24-Dec
1995-96	23-Oct	23-Oct	22-Dec	13-Dec
1996-97	11-Oct	10-Oct	23-Dec	19-Dec
1997-98	13-Oct	13-Oct	31-Dec	23-Dec

1998-99	28-Oct	28-Oct	22-Dec	04-Jan
1999-00	21-Oct	04-Oct	28-Dec	12-Jan
2000-01	02-Nov	05-Nov	06-Jan	02-Jan
2001-02	16-Oct		11-Jan	
2002-03	25-Oct		27-Dec	
2003-04	19-Oct		08-Jan	
2004-05	18-Oct		25-Jan	
2005-06	12-Oct		18-Jan	
2006-07	19-Oct		28-Dec	
2007-08	22-Oct		10-Jan	
2008-09	15-Oct		31-Dec	
2009-10	29-Oct		18-Jan	
2010-11	29-Oct		17-Jan	
2011-12	24-Oct		10-Jan	
2012-13	19-Oct		11-Jan	
2013-14	21-Oct		18-Jan	
2014-15	18-Oct		04-Jan	
2015-16	28-Oct		07-Jan	
2016-17	30-Oct		04-Jan	
2017-18	27-Oct		15-Jan	
2018-19	01-Nov		02-Jan	
2019-20	16-Oct		10-Jan	
2020-21	28-Oct		19-Jan	

Fig 5.1 shows the super-epoch analysis of rainfall with respect to IMD NE monsoon onset date. Super epoch analysis is a composite analysis (averaging over many years) in which the origin is taken as the monsoon onset date and 50 days before and

after the onset date are considered. Rainfall data in the box 79-81^0 E, 10-14^0 N have been used for this analysis for the period 1977-2020. The analysis shows a very sharp rise of rainfall on the monsoon onset date over the coastal areas of Tamil Nadu and coastal Andhra Pradesh. Before the onset date up to 50 days, the mean daily rainfall over this region is around 6 mm/day. Just after the monsoon onset, mean rainfall over this region sharply increases to around 14 mm/day, which persists almost for two weeks. We can observe strong intra-seasonal activity even in this super-epoch analysis. For example, after about 20 days after the onset rainfall activity is reduced and it picks up again around 40 days after the monsoon onset.

Fig 5.2 shows super epoch analysis of rainfall with respect to IMD NE monsoon withdrawal date. Rainfall data in the box 79-81^0 E, 10-14^0 N have been used for this analysis for the period 1977-2020. This super epoch analysis shows a reduction (not very sharply as we see with respect to monsoon onset) of rainfall activity just after the monsoon withdrawal. Raj (2012) suggested that the monsoon withdrawal date decided by IMD is done subjectively and no official objective definition exists. However, there is a sharp decline in rainfall activity associated with the withdrawal date of Raj (2012), as these dates are determined in hindcast mode using only rainfall criteria.

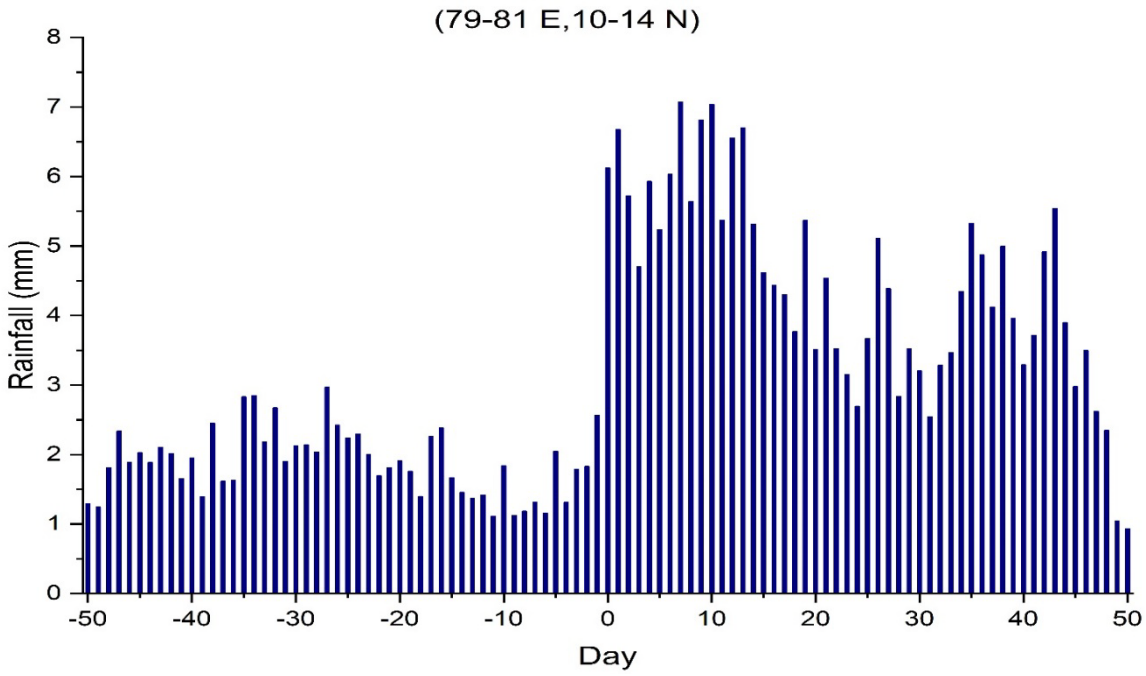

Fig 5.1. Super epoch analysis of rainfall with respect to IMD NE monsoon onset date. Rainfall data in the box 79.5-80.5^0 E, 10-14^0 N have been used for this analysis. Period of analysis: 1977-2020.

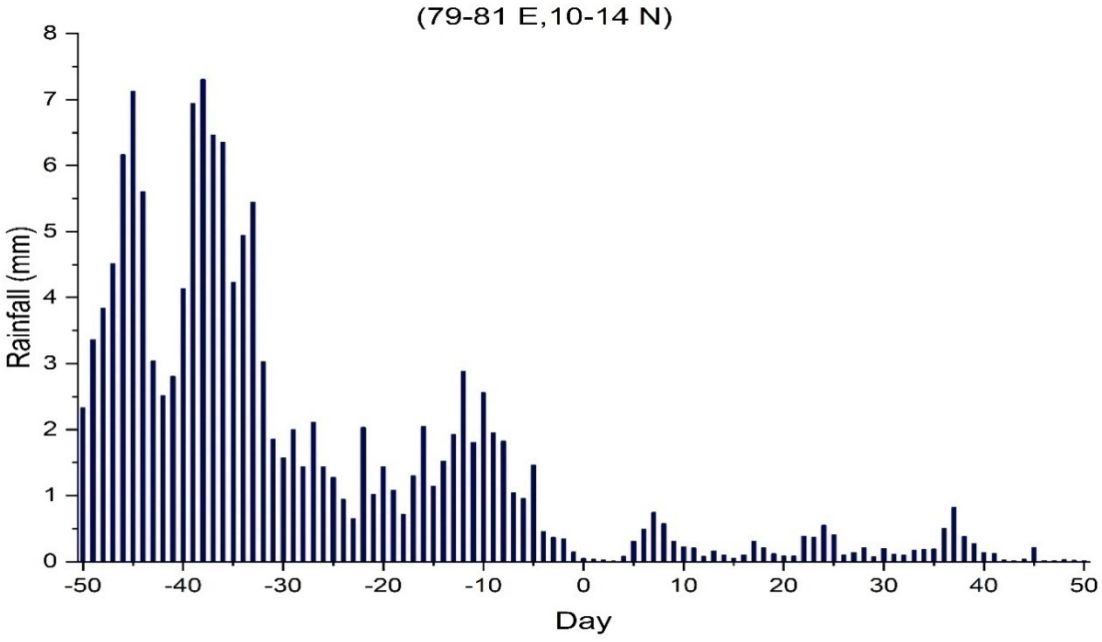

Fig 5.2. Super epoch analysis of rainfall with respect to IMD NE monsoon withdrawal date. Rainfall data in the box 79.5-80.5^0 E, 10-14^0 N have been used for this analysis. Period of analysis: 1977-2020.

5.1. **Composite meteorological features associated with the monsoon onset**

To understand the changes in dynamical and thermodynamical parameters occurring associated with the NE monsoon onset, a composite analysis was made with Mean Sea Level Pressure (MSLP), winds at 1000, 850 and 700 hPa level, Outgoing Longwave Radiation (OLR), and precipitable water content. The analysis was made as a pentad (5 days) composite with the onset date as the central date. The other dates in the pentad are two days before the onset and two days after the onset date. Such composites will provide useful information on the dynamical and thermodynamical changes occurring in the region associated with the monsoon onset. Also, they will provide clues for some important parameters to be considered for developing criteria to declare the monsoon onset.

Fig 5.3 shows the composite MSLP pattern associated with the NE monsoon onset. It clearly shows the presence of a low-pressure area over the southwest Bay of Bengal, off the Tamil Nadu coast, suggesting an area of convergence and associated rainfall activity. However, the surface pressure gradient over the South Bay of Bengal is not strongly associated with the monsoon onset. Instead, a trough of low pressure at the surface extends from the northwest Arabian sea across the southern part of the peninsula to the southeast Bay of Bengal.

Fig 5.4, 5.5 and 5.6 show the composite mean wind flow at 1000, 850 and 700 hPa levels associated with the monsoon onset. These maps clearly show the presence of east-west trough (ITCZ), from south-west Arabian sea to south-east Bay of Bengal across south Peninsula right from 1000 hPa to 700 hPa. At 1000 hPa, there is a cyclonic circulation over southwest Bay of Bengal associated with the low-pressure area observed at the mean sea level (Fig 5.3). At 850 hPa and 700 hPa levels, the east-west trough across south peninsula is very prominent. At 850 hPa and 700 hPa levels, the east-west trough passes across south peninsula around 9^0N. It may be also noted that the strong easterlies north of the trough line, between 12^0N and 20^0N and strong

westerlies south of the trough line, between the equator and 5^0N. Therefore, the east-west trough zone is an area of strong horizontal wind shear and associated convergence.

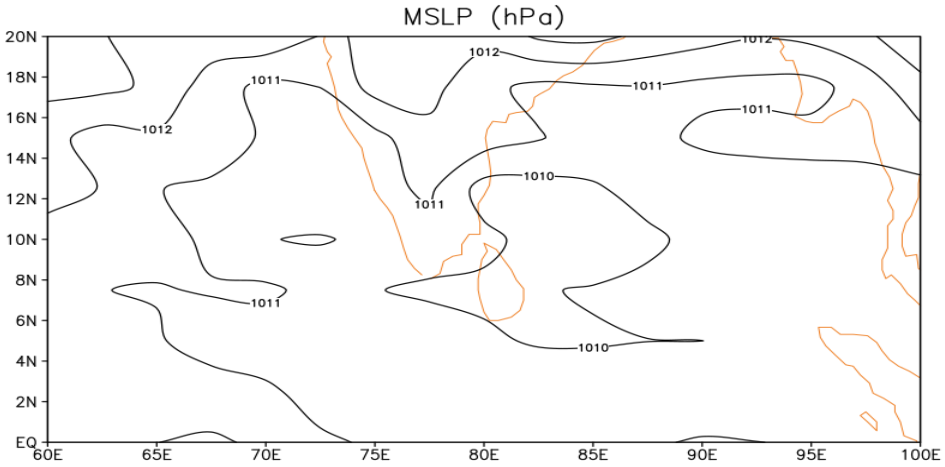

Fig 5.3. Composite Mean Sea Level Pressure (MSLP) during the pentad of monsoon onset date. The onset date is the central date of the pentad. Onset dates of 1977-2020 were considered for the analysis. Data source: NCEP/NCAR reanalysis.

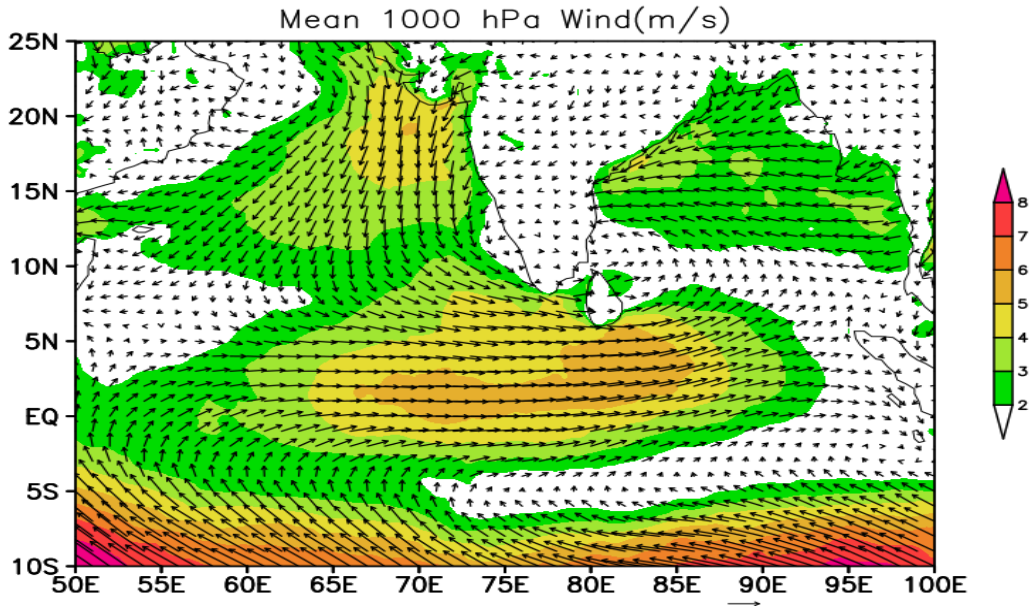

Fig 5.4. Composite wind flow at 1000 hPa during the pentad of monsoon onset date. The onset date is the central date of the pentad. Onset dates of 1977-2020 were considered for the analysis. Data source: NCEP/NCAR reanalysis.

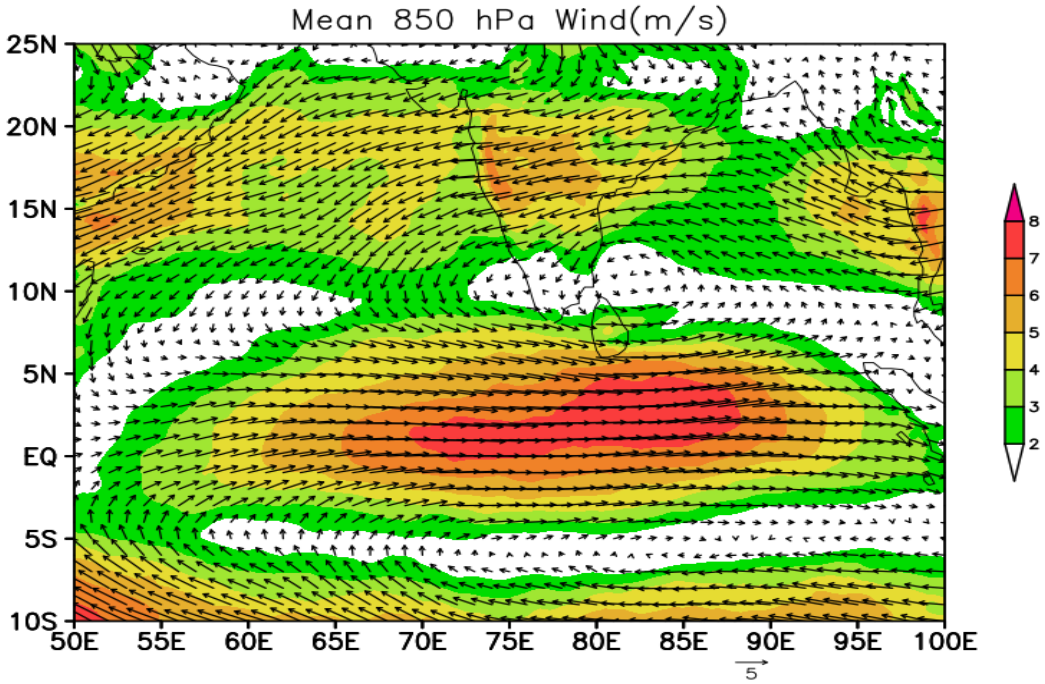

Fig 5.5. Same as Fig 5.4, but for 850 hPa winds.

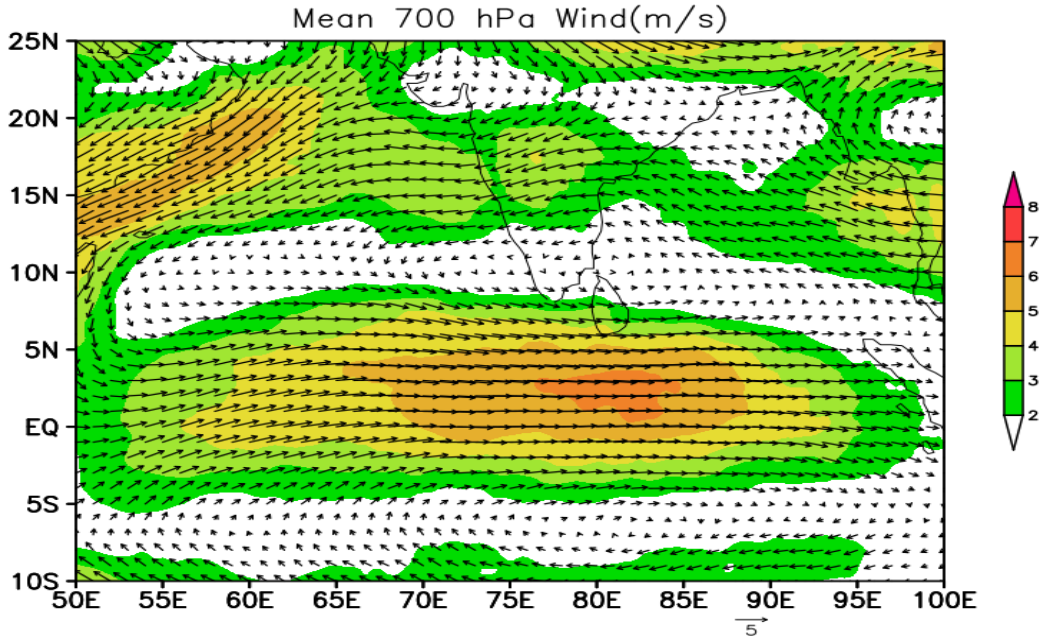

Fig 5.6. Same as Fig 5.4, but for 700 hPa winds.

Fig 5.7 shows composite latitude-height distribution of zonal winds averaged between 80^0E-90^0E. There is an easterly wind maximum from 975 hPa to 700 hPa between 13^0-17^0E. At the surface the zero zonal wind line is close to 10^0N, which suggests the presence of the east-west trough line. Between the equator and 5^0N, there is a maximum of westerly zonal winds. The zonal wind pattern clearly shows a small southward tilt with height.

Fig 5.8 shows the pentad composite OLR pattern associated with the NE monsoon onset. This plot was made using observed OLR data derived from National Oceanographic and Atmospheric Administration (NOAA) satellites (http://psl.noaa.gov). The plot shows the southern part of Peninsula, especially the eastern coast is covered with large scale convection with OLR values less than 220 Wm^{-2}.

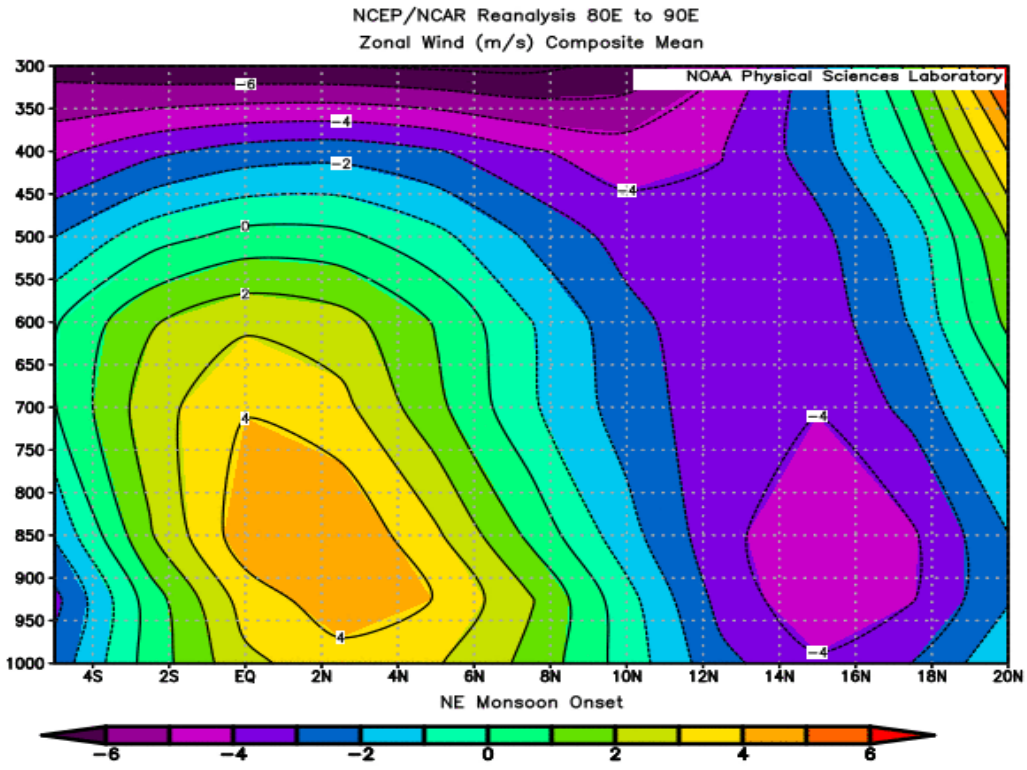

Fig 5.7. Composite Latitude-Height distribution of zonal winds averaged between 80-90E during the pentad of monsoon onset date. The onset date is the central date of the pentad. Data source: NCEP/NCAR reanalysis.

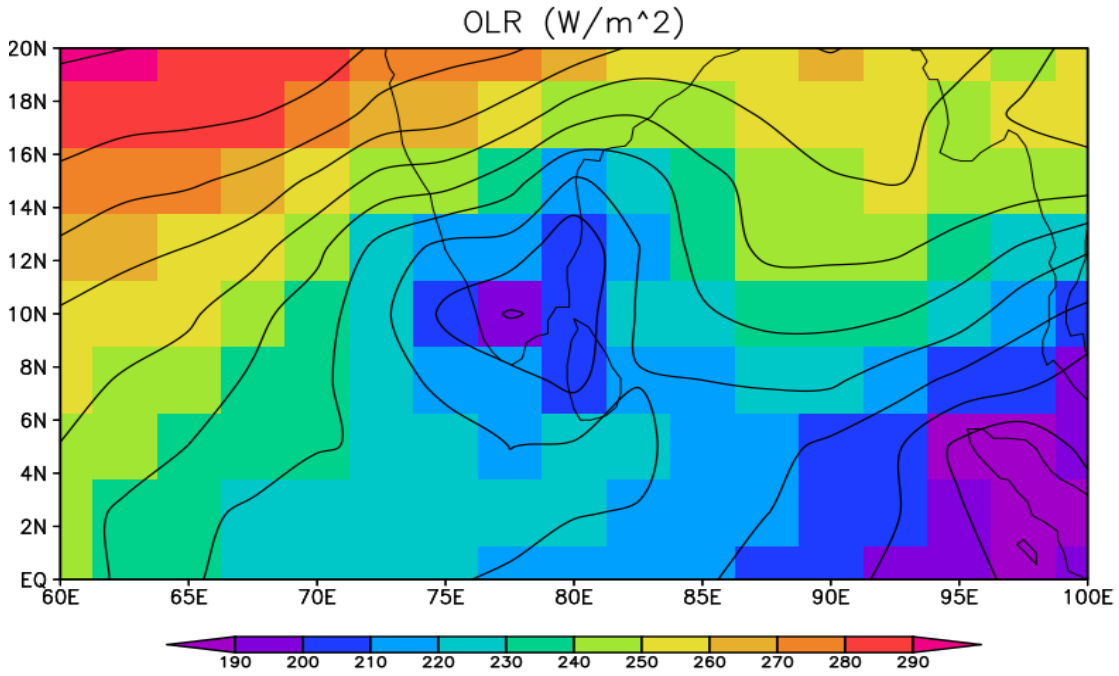

Fig 5.8. Composite Outgoing Long Wave Radiation (OLR) during the pentad of monsoon onset date. The onset date is the central date of the pentad. Onset dates of 1977-2020 were considered for the analysis. Data source: NOAA OLR Data.

Over the eastern coast of Tamil Nadu (up to 14^0N) the composite OLR value is less than 210 Wm^{-2} suggesting severe convection over the region. Therefore, the NE monsoon onset is associated with large scale convection (with low OLR) over southern part of peninsula covering up to 16^0N or so. The monsoon onset is also associated with the presence of large amount of precipitable water content (moisture content) over the region (Fig 5.9). Over the extreme southern parts of peninsula and east coast of Tamil Nadu, high amount of PWC values (exceeding 42 kg/m^2) is observed. Fig 5.10 shows the spatial distribution of vertically integrated moisture convergence over the region associated with the NE monsoon onset. This plot also shows abundance of moisture flux off- east coast of south peninsula. Therefore, the monsoon onset is associated with the presence of large amount of moisture flux and large-scale convection over the region.

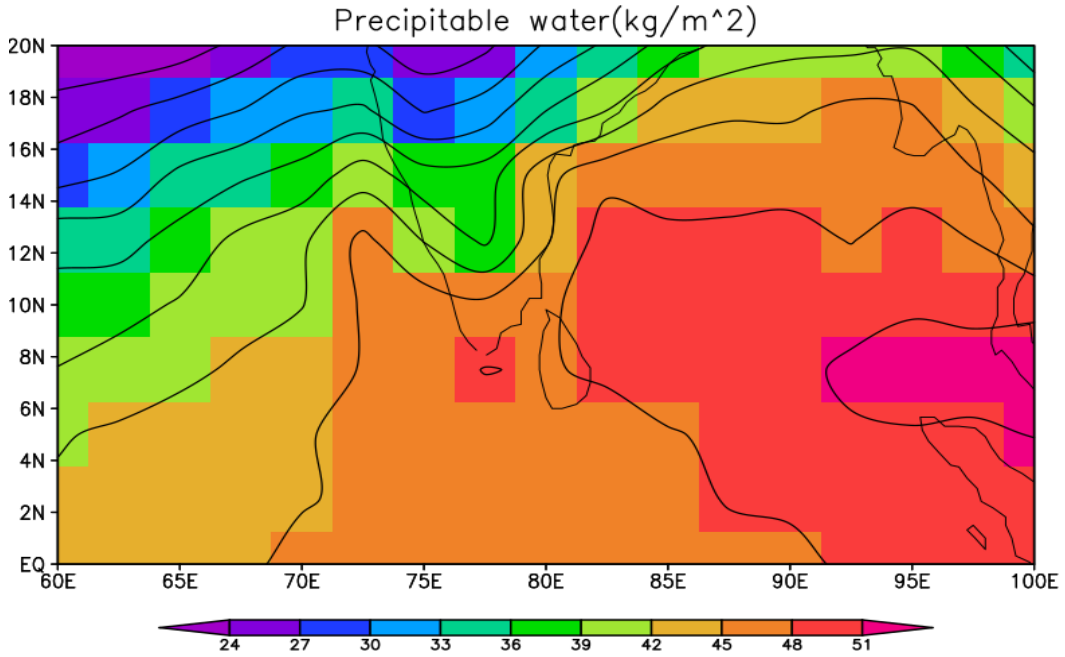

Fig 5.9. Composite precipitable water content (PWC) (in Kg/m^2) during the pentad of monsoon onset date. The onset date is the central date of the pentad. Onset dates of 1977-2020 were considered for the analysis. Data source: NCEP/NCAR reanalysis.

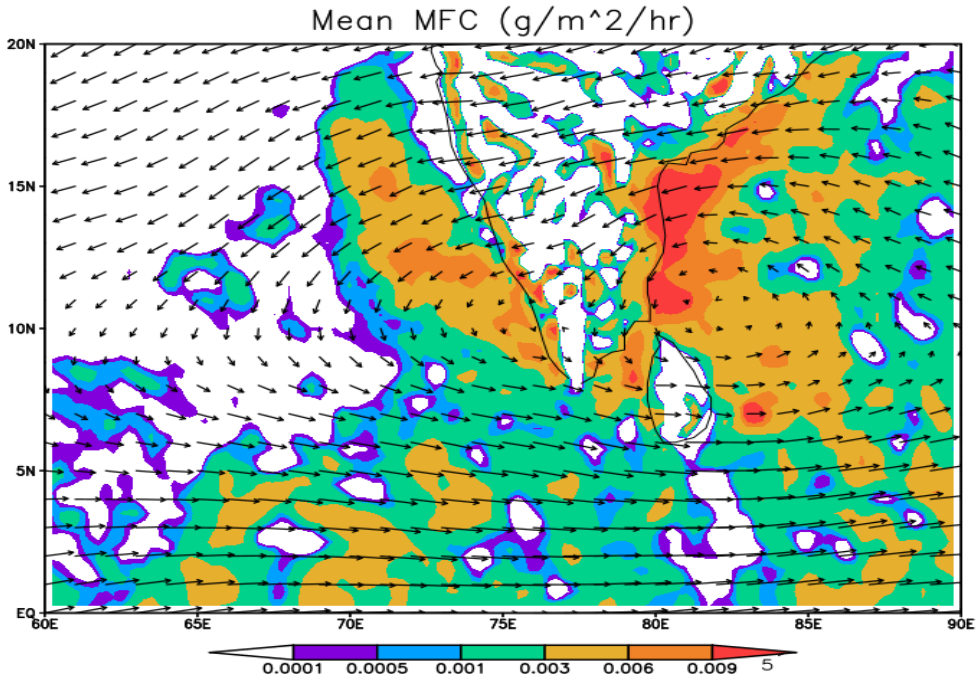

Fig 5.10. Mean moisture flux convergence (shaded) along with 850 hPa vector winds associated with NE Monsoon Onset.

5.2. A new method for declaring NE Monsoon Onset

In this section, a new method is proposed for objective declaring the NE monsoon onset. In this objective method, in addition to information on spatial distribution of rainfall, information of large-scale convection and wind patterns are also considered.

In the previous section, we have noted that the monsoon onset is associated with the presence of ITCZ as an east-west trough in the lower levels across south peninsula (Fig 25 b-d) along 10^0N. Large scale easterly wind flow is observed north of the trough. The emergence of this trough and easterlies are primary indications of the NE monsoon onset over south Peninsula. The monsoon onset is also associated with large scale convection over the region (Fig 26 a), in which OLR values over the east coast of Tamil Nadu are less than 220 Wm^{-2}. Therefore, in the new method of declaration of the NE monsoon onset, information about easterly zonal winds, OLR and spatial distribution of rainfall are considered.

For deriving information about these parameters, the following methodology is adopted. For calculating zonal wind, an area of 12-16^{0}N, 85-90^{0}E is considered to calculate zonal winds at 850 hPa. For calculating OLR, an area of 09-14^{0}N, 79-82^{0}E is considered. For spatial distribution of rainfall, following 25 rain-gauge stations of IMD are considered:

1) Adiramapatnam 2) Chengalpattu 3) Chidambaram 4) Cuddalore 5) Kodavasal 6) Madurabthagam 7) Minambakkam 8) Muthupet 9) Nagapattinam 10) Needamangalam 11) Nungambakkam 12) Pamban 13) Ponneri 14) Ramanathapuram 15) Srimushnam 16) Sriperumudur 17) Thiruvallur 18) Thirvararur 19) Thondi 20) Thoothukudi 21) Thiruchendur 22) Vanur 23) Vedaranniyam 24) Sulurpet and 25) Nellore

After analyzing the data for all the years from 1981-2020, the following objective criteria are proposed as a new method for identifying/declaring the monsoon onset.

1) The NE monsoon Onset is declared on any date after 10 October, provided the Southwest monsoon is completely withdrawn from the country.

2) Easterly trade winds should prevail north of 12^0N up to 20^0N (approx) and extending from surface up to at least 700 hPa level. The zonal wind at 850 hPa, averaged over the box (12-16^0N, 85-90^0E) should be moderately negative at least for three consecutive days. Due to its large variability, a quantitative measure of the strength of easterlies could not be identified.

3) There is large scale convection over the south eastern peninsula region as seen in satellite pictures, with OLR value less than 210 Wm^{-2}, averaged over the box (09-14^0N, 79-82^0E).

4) At least 50 per cent of the above mentioned 25 IMD rain-gauge stations should report rainfall of 2.5 mm or more. This is equivalent to at least fairly widespread rainfall activity over the region.

5) The first day is taken as the monsoon onset date, provided conditions (1) to (4) are satisfied.

With these objective criteria, a new onset date has been fixed for each year and the new onset dates thus estimated are given in Table-6 below.

The mean onset date of IMD is 22 October with a standard deviation of 6.6 days and the mean onset date from this new method is 24 October with a standard deviation of 8.5 days. The correlation coefficient between the IMD onset date and the new onset date is 0.60, which is statistically significant at the 99% significance level.

Table 5.2

New Onset Dates along with the IMD Onset Date and

Onset Dates identified by Raj (2012).

Year	IMD Onset Date	Onset Date by Raj (2012)	New Onset Date	Difference between the IMD date and new date
1981	23-Oct	23-Oct	23-Oct	0
1982	19-Oct	18-Oct	18-Oct	1
1983	24-Oct	24-Oct	25-Oct	-1
1984	05-Oct	03-Nov	06-Nov	-32
1985	25-Oct	25-Oct	25-Oct	0
1986	27-Oct	26-Oct	26-Oct	1
1987	30-Oct	20-Oct	20-Oct	10
1988	02-Nov	03-Nov	03-Nov	-1
1989	27-Oct	29-Oct	29-Oct	-2
1990	19-Oct	18-Oct	19-Oct	0
1991	20-Oct	19-Oct	27-Oct	-7
1992	02-Nov	02-Nov	03-Nov	-1
1993	20-Oct	13-Oct	12-Oct	8
1994	18-Oct	18-Oct	18-Oct	0
1995	23-Oct	23-Oct	28-Oct	-5
1996	11-Oct	10-Oct	10-Oct	1
1997	13-Oct	13-Oct	13-Oct	0
1998	28-Oct	28-Oct	28-Oct	0
1999	21-Oct	04-Oct	15-Oct	6
2000	02-Nov	05-Nov	19-Nov	-17
2001	16-Oct		26-Oct	-10

2002	25-Oct		30-Oct	-5
2003	19-Oct		19-Oct	0
2004	18-Oct		26-Oct	-8
2005	12-Oct		11-Oct	1
2006	19-Oct		19-Oct	0
2007	22-Oct		20-Oct	2
2008	15-Oct		12-Oct	3
2009	29-Oct		29-Oct	0
2010	29-Oct		29-Oct	0
2011	24-Oct		25-Oct	-1
2012	19-Oct		19-Oct	0
2013	21-Oct		21-Oct	0
2014	18-Oct		18-Oct	0
2015	28-Oct		28-Oct	0
2016	30-Oct		01-Nov	-2
2017	27-Oct		30-Oct	-3
2018	01-Nov		02-Nov	-1
2019	16-Oct		20-Oct	-4
2020	28-Oct		13-Nov	-16
			Difference	-2.0 days
			Correlation	0.607
Mean	22-Oct	21-Oct	24-Oct	
Std. Dev	6.65	8.57	8.65	

In general, the new onset dates and IMD onset dates are closer in most of the years. Both the onset dates are exactly the same in 14 years. However, there are

differences too. The largest difference for 10 days or more is found in years like 1984, 1987, 2000, 2001, and 2020. The mean difference between IMD onset date and New Onset date is about 2 days.

The new method of fixing the onset date is further discussed using a case study of the 1986 monsoon onset. Fig 5.11 shows the time series of percent of stations reporting 2.5 mm or more, Outgoing longwave radiation (OLR) in Wm^{-2} and the zonal wind at 850 hPa. As per the new method, the onset date in 1986 is 26 Oct. On this day, 63 percent stations reported 2.5mm or more rainfall, thus indicating fairly widespread rainfall activity. Enhanced rainfall activity continued for almost 10 days. OLR, which is a proxy for convection, started reducing a couple of days before the onset date. This suggests starting of large-scale convection over South peninsula associated with the monsoon onset. OLR values near the onset were less than 200 Wm^{-2}, which persisted for almost one week. By 16th itself, easterlies were set in and strong easterly zonal winds were prevailing during the onset date and subsequent 10 days. But the zonal wind component has shown large day to day variations.

The NE monsoon onset of 2020 is now discussed with a similar time series plot. Fig 5.12 shows the similar variation of parameters (as in 1986) from 24 Oct to 20 Nov. The IMD onset date in 2020 was 28 Oct and the new onset date as per the revised criteria was 13 Nov. On 28th October, only 14% of IMD stations reported rainfall and OLR values were more than 240 Wm^{-2}, suggesting not enough convection over the region. Weaker easterly winds had just set in. Thereafter, there was not much rainfall activity over the region. Rainfall activity again picked up on 12 November. Easterly winds started strengthening and OLR values started dipping below 210 Wm^{-2}. The new criteria with the inputs on easterly winds and OLR values were completely satisfied on 13 Nov, which is the new monsoon onset date. Therefore, the new objective criteria could identify the real onset date which is associated with large scale convective activity over the region.

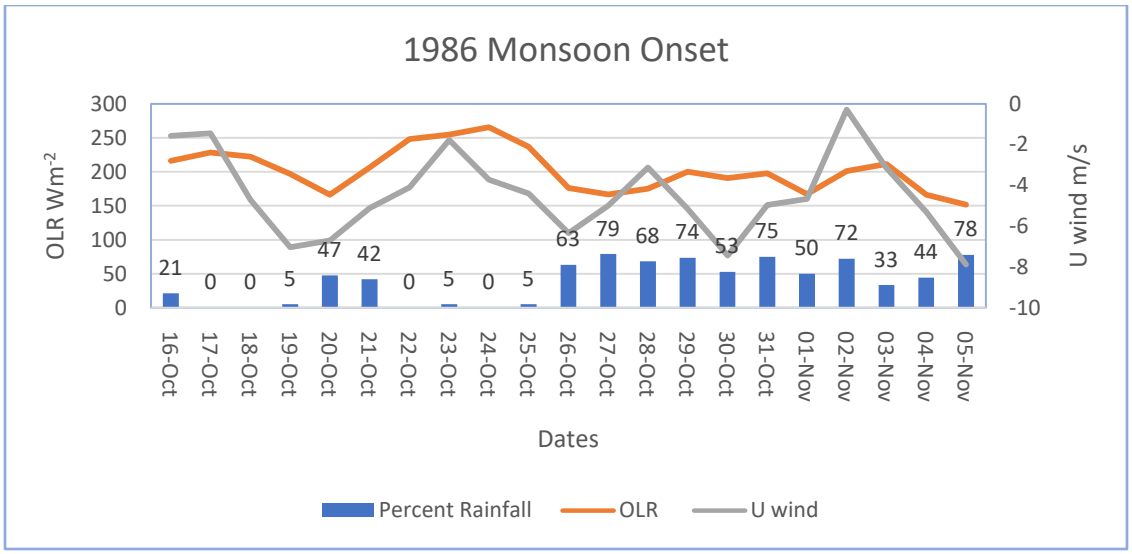

Fig 5.11. Monsoon Onset in 1986. Time series of percent of stations reporting rainfall of 2.5 mm or more (Vertical bars in blue), OLR value (Orange colour) and zonal wind at 850 hPa during 16 Oct to 05 Nov, 1986.

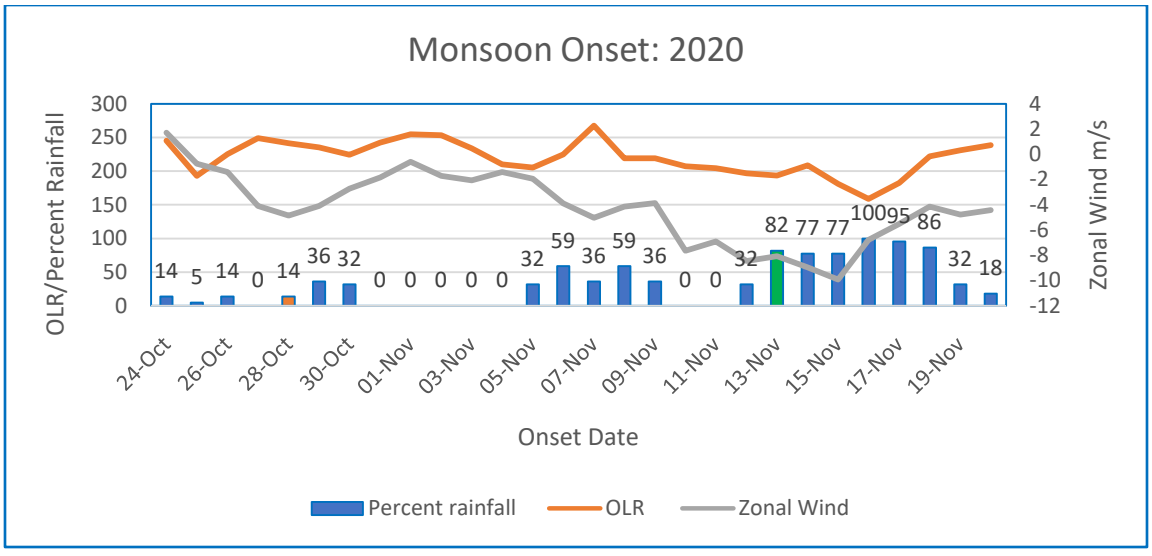

Fig 5.12. Monsoon Onset in 2020. Time series of percent of stations reporting rainfall of 2.5 mm or more (Vertical bars in blue), OLR value (Orange colour) and zonal wind at 850 hPa during 24 Oct to 20 Nov 2020. The IMD Onset date, 28 Oct is shown as red vertical bar and the new Onset date is shown as green vertical bar.

Chapter-6

Variability of NE Monsoon Rainfall

NE monsoon exhibits variability in all time scales, from diurnal, synoptic to intra-seasonal, inter-annual and decadal time scales. In this chapter, the NE Monsoon variability in all time scales is discussed.

6.1. Diurnal Cycle of NE Monsoon Rainfall

The diurnal cycle is one of the most important modes of precipitation variability over the Indian monsoon region (Rajeevan et al. 2012, Bhate et al. 2019, Raj and Amudha 2022). It is a manifestation of the atmosphere-ocean-land-cryosphere response to incoming solar radiation. A detailed analysis and discussions on diurnal variation during the southwest monsoon season are given in Sahany et al. (2010).

This section discusses the results from a detailed analysis of 3-hourly rainfall derived from TRMM satellite data. Harmonic analysis was made to understand the phase and amplitude of diurnal variations. More details of the analysis of diurnal variation are available in Bhate et al. (2019) and Rajeevan et al. (2012).

Fig 6.1 shows the 3 hourly variation of climatological rainfall over the Indian region during the northeast monsoon season as estimated using TRMM satellite data for the period 1998-2019. It shows distinct types of variations over the Oceans and land. Over the east coast of India, maximum rainfall is observed in the early morning hours, but over the interior parts, rainfall peaks in the late evening and early night.

The spatial map of the phase (hours with maximum rainfall) revealed by the Harmonic Analysis explained is shown in Fig 6.2. The phase diagram clearly shows the distinct difference in the rainfall peak over the oceans and land. Over the oceans and off the east coast of India, rainfall during the NE monsoon season peaks in the morning. On the other hand, rainfall peaks over the interior parts and the west coast, during the late evening/early night (between 1830 and 2130 IST). Thus, the northeast Monsoon over south peninsular India exhibits significant diurnal variations with large spatial variations.

Along the east coast of India, an early morning peak is observed and over the inland regions and the west coast, an afternoon/evening peaking is observed.

Fig. 6.3 shows hourly average rainfall during the NE monsoon season (Oct-Dec) showing the diurnal variation of observed rainfall over different stations over the south Peninsula. These plots are made using hourly station rainfall data, taken from the IMD archives. These plots clearly suggest that the stations over the east coast experience maximum rainfall during the morning hours. Over the interior parts and the west coast, maximum rainfall occurs during the evening and early night hours. Different physical mechanisms could be responsible for the observed rainfall diurnal variations over land and oceans. The observed rainfall peak in the late afternoon over the land could be due to intense surface solar heating and resultant convective instability. Over the east coast, the presence of a strong sea-land breeze is also noted to be responsible for diurnal variations (Bhate et al., 2019, Ramesh Reddy et al., 2021).

It is important to make a detailed analysis using Numerical Weather Prediction (NWP) model results, whether the NWP models are capable of predicting these observed diurnal variations. An analysis of diurnal variations for the southwest monsoon revealed that NWP model (WRF model) has constraints in predicting diurnal variations accurately (Bhat et al., 2019). The model was found successful in simulating the pattern of diurnal variation of rainfall, but underestimates its amplitude compared to the observed one especially over the western Himalayas, northeast India, central India, and the north Bay of Bengal (BoB). It is important to carry out an extensive analysis to examine how the NWP models are capable of predicting the diurnal variations of NE monsoon rainfall accurately.

6.2. Intra-seasonal variation of NE monsoon rainfall

Several studies have shown that during the southwest monsoon season (June to September) a substantial component of the variability of convection and rainfall over the Indian region arises from the fluctuations on the intra-seasonal scale between active

and weak or break spells (Ramamurthy, 1969; Goswami, 2005; Rajeevan et al., 2010). Long intense breaks are known to have an impact on the seasonal monsoon rainfall over the country (Webster et al., 1998; Gadgil and Joseph, 2003, Rajeevan et al., 2010). The dry and wet spells of the active and break conditions represent the sub-seasonal or intra-seasonal variations of the monsoon with timescales longer than synoptic activity (1–10 days) but shorter than a season.

Recent research results also provided new insights regarding the origin of the monsoon intra-seasonal variations. The ISOs of summer monsoon essentially have timescales between 10 and 90 days. Within the broad range of 10–90 day periods, two period ranges with periodicities between 10 and 20 days and 30 and 60 days respectively are particularly prominent (Goswami, 2005). Active and break spells and intra-seasonal variations of the Indian summer monsoon have been extensively studied. As far as the northeast monsoon is concerned, not much knowledge is available on the intra-seasonal activity during the NE monsoon season. Therefore, the results of the intra-seasonal activity during the northeast monsoon season are discussed in this section.

Fig 6.4 shows daily rainfall (averaged over the NE monsoon region) from 15 September to 15 January during two sessions, 2008-2009 and 2011-2012. These plots clearly show that rainfall activity over the region is confined to only a few days during the season, which is interspaced between dry or weak monsoon spells. For example, during 2008-2009, heavier rainfall activity was observed around 20-30 October. The next rainfall activity was observed almost after one month, from 20 Nov onwards. Between 30 October to 20 November, rainfall activity over the region was generally subdued. Similar intra-seasonal variability of rainfall with enhanced (suppressed) activity was observed during 2011-12 also.

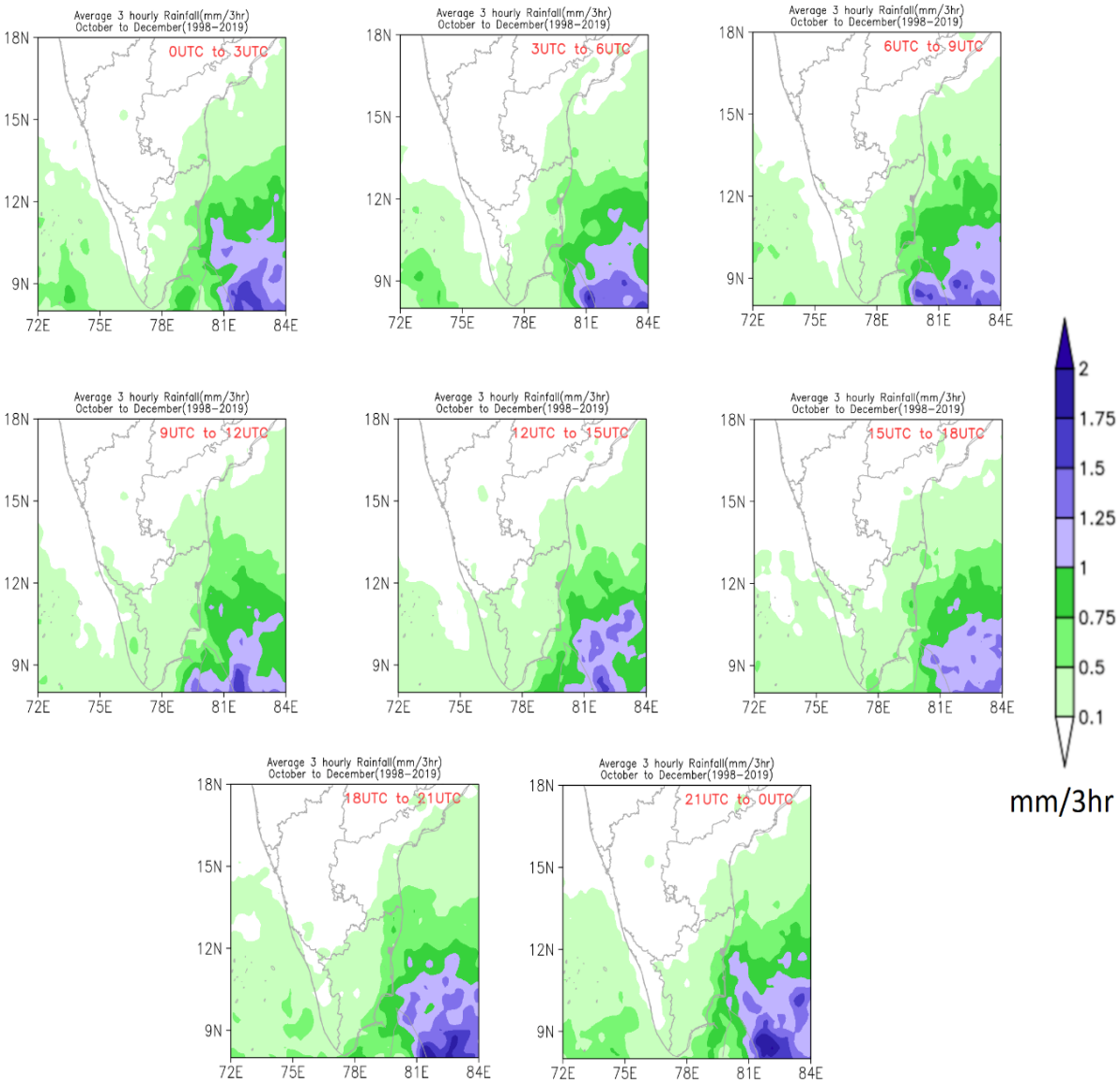

Fig. 6.1. Average 3-hourly seasonal (October to December) rainfall (mm/3h) over the Indian region averaged over the years 1998-2019 derived from the TRMM 3G68 data.

Fig 6.5 a shows the Hovmuller diagram showing Outgoing Longwave Radiation (OLR) anomalies averaged over 70^0 -90^0E plotted with latitude versus time (15 Sept 1998 to 15 January 1999). Fig 6.5 b shows the similar plot but for the period 15 Sept 2000 to 15 January 2001. OLR is a proxy for atmospheric convection. Low OLR suggests more convection. These two plots clearly show strong intra-seasonal activity during the NE

monsoon season. Fig 6.5 a shows clear northward propagation of OLR anomalies from the equator around 16 October and the next one around 15 November Another northward propagation is observed around 18 December. However, all the northward propagation of convections are limited to 15^0N only. During the southwest monsoon season, this northward propagation moves to even the foothills of the Himalaya. Fig 6.5 b shows a similar plot, but for zonal wind anomalies at 925 hPa. This plot clearly shows the strengthening of the shear zone (between westerlies in the south and easterlies in the north) at particular intervals. This plot also shows the slow southward movement of the horizontal wind shear zone by December, which represents the southward movement of ITCZ.

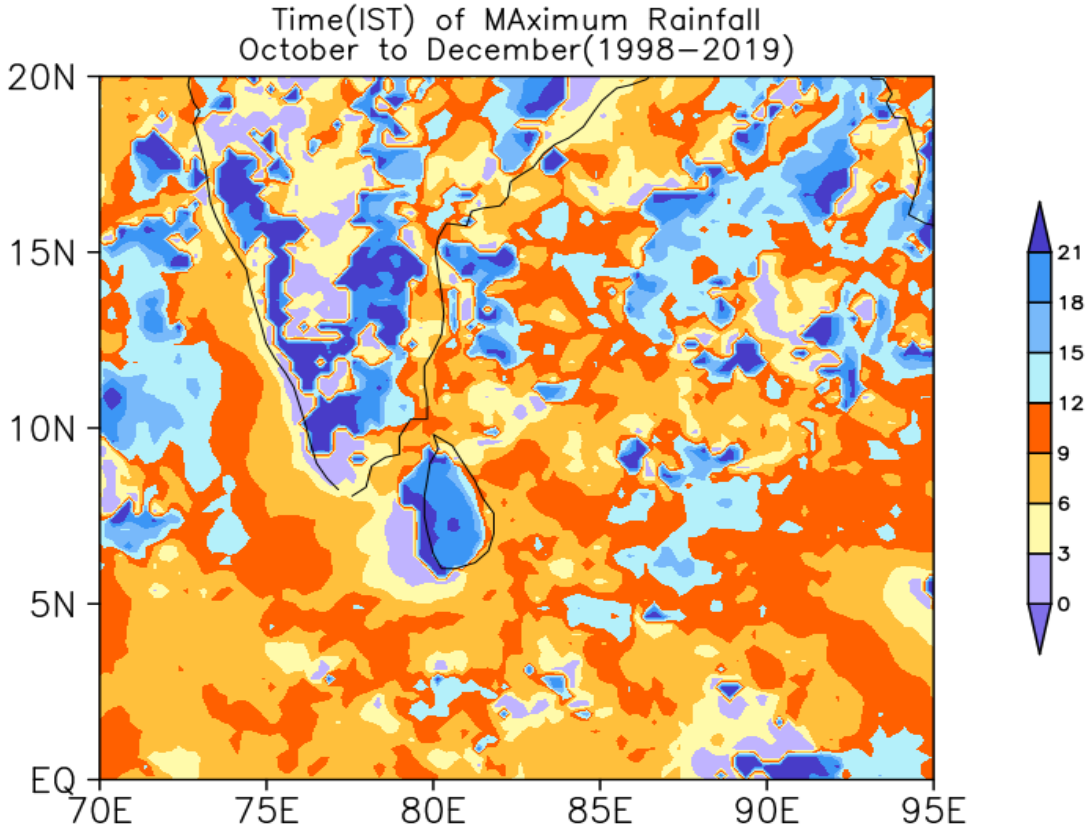

Fig. 6.2. Phase angle (time of maximum rainfall peak) in Indian Standard Time (IST) based on satellite data for the period using the Harmonic Analysis (1998-2019).

East Coast stations

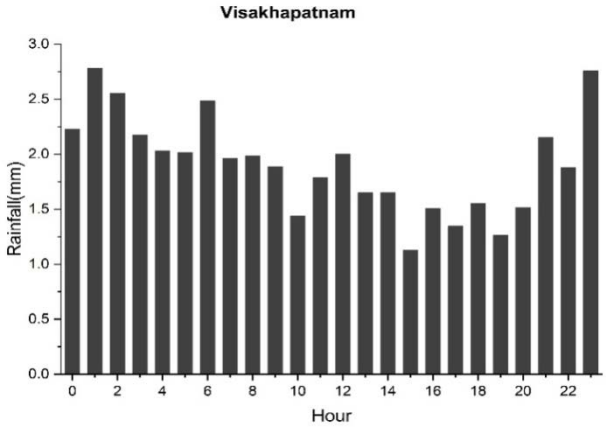

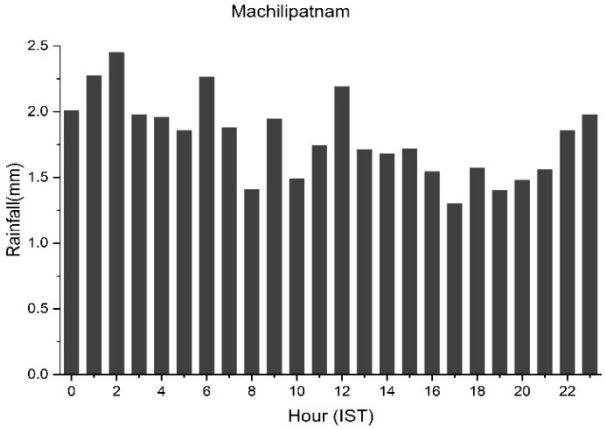

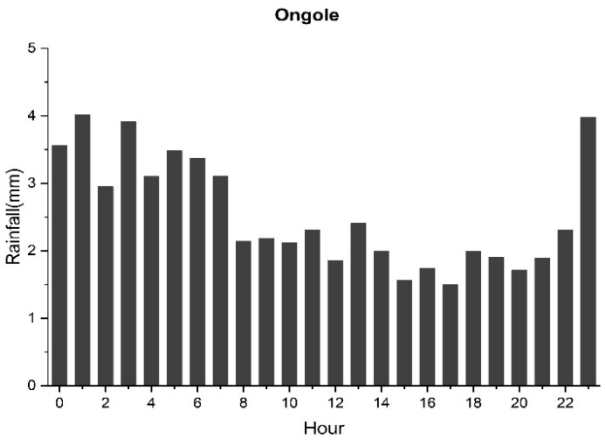

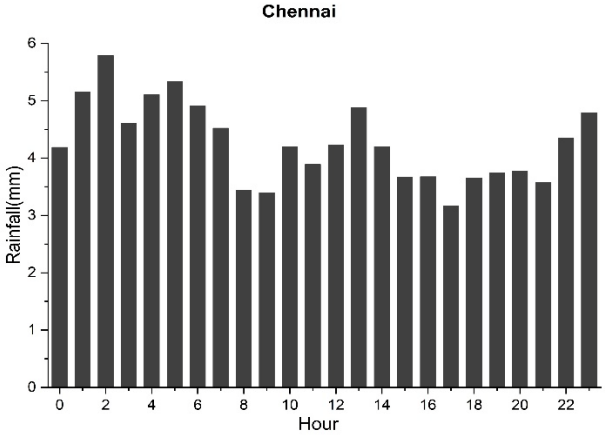

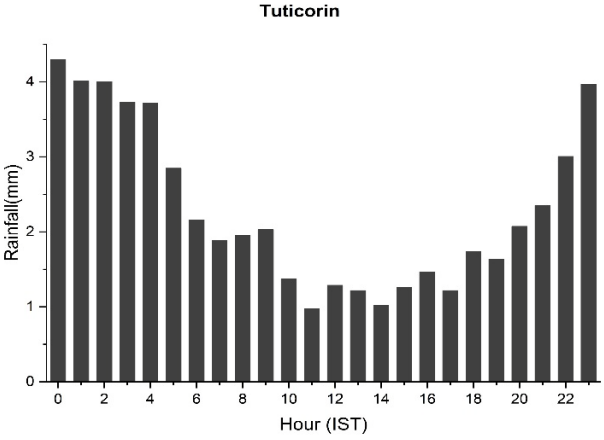

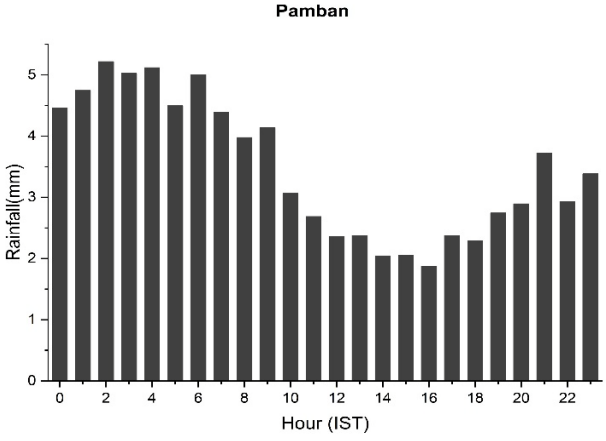

Central Region Stations

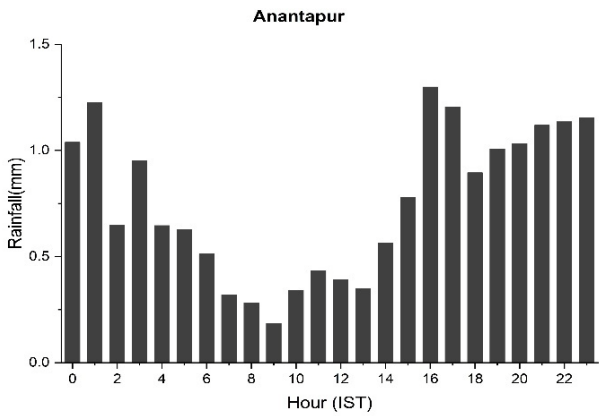

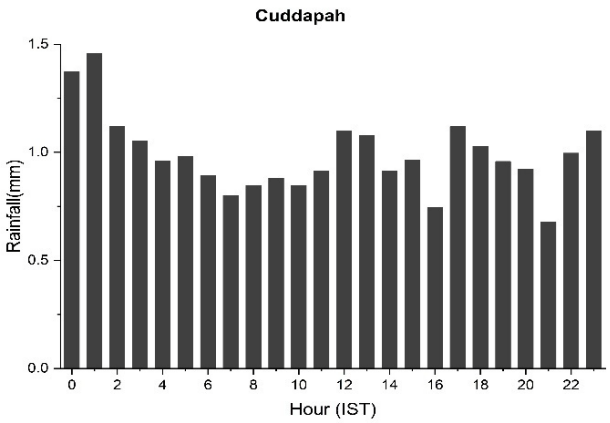

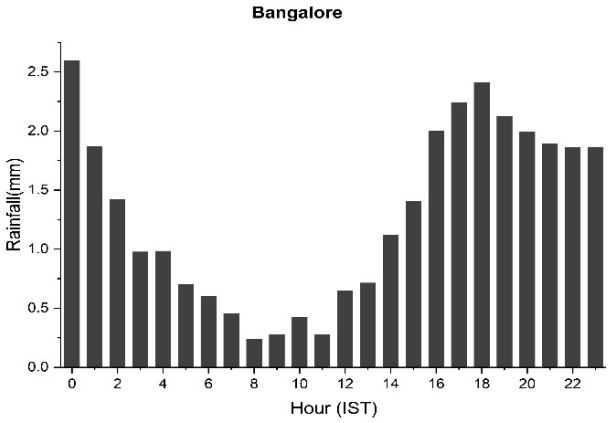

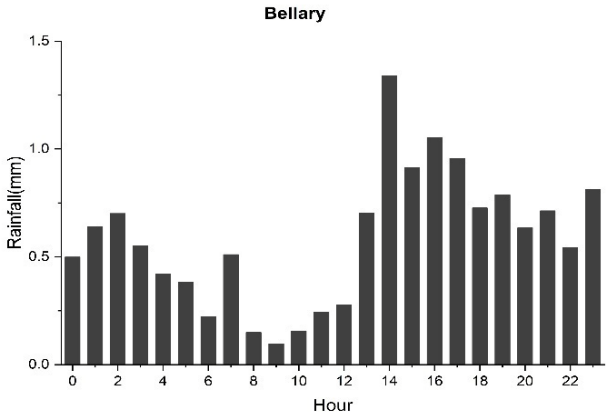

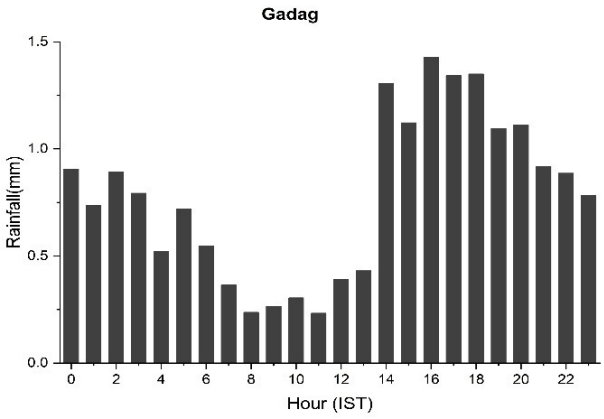

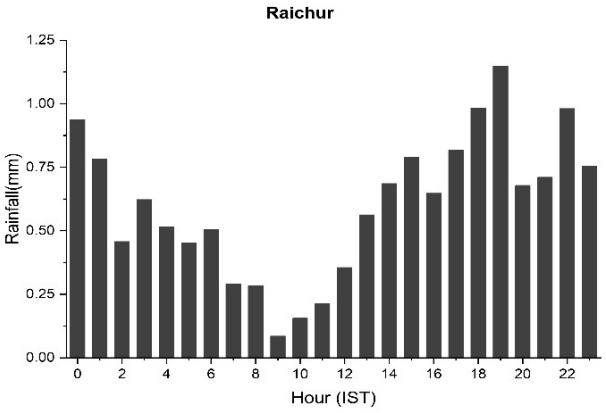

Central Region Stations

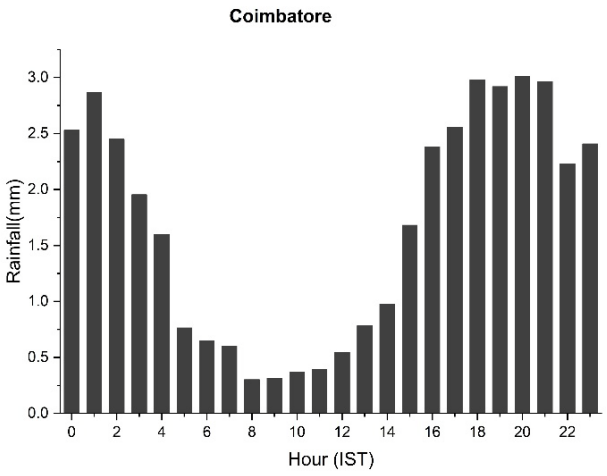

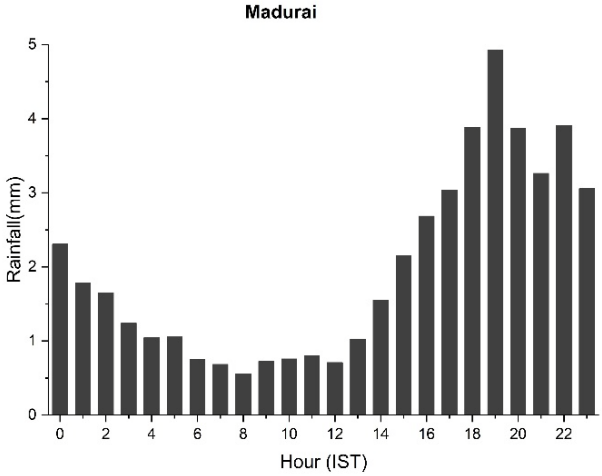

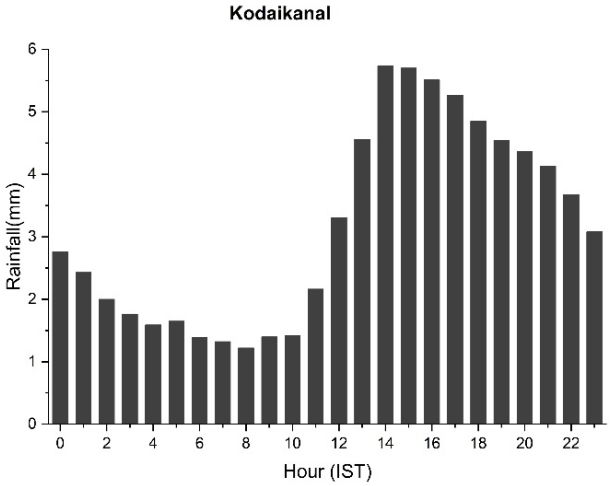

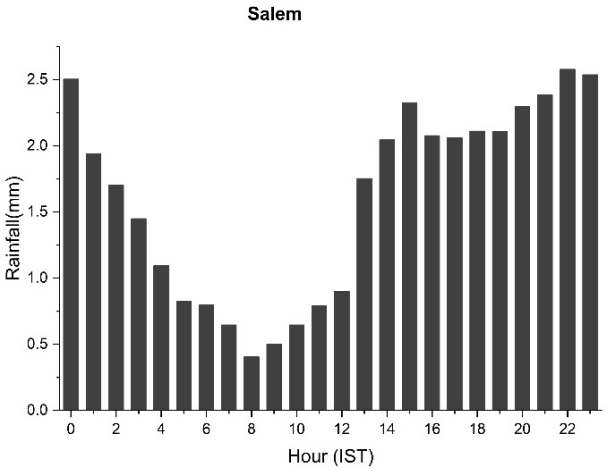

West Coast Stations

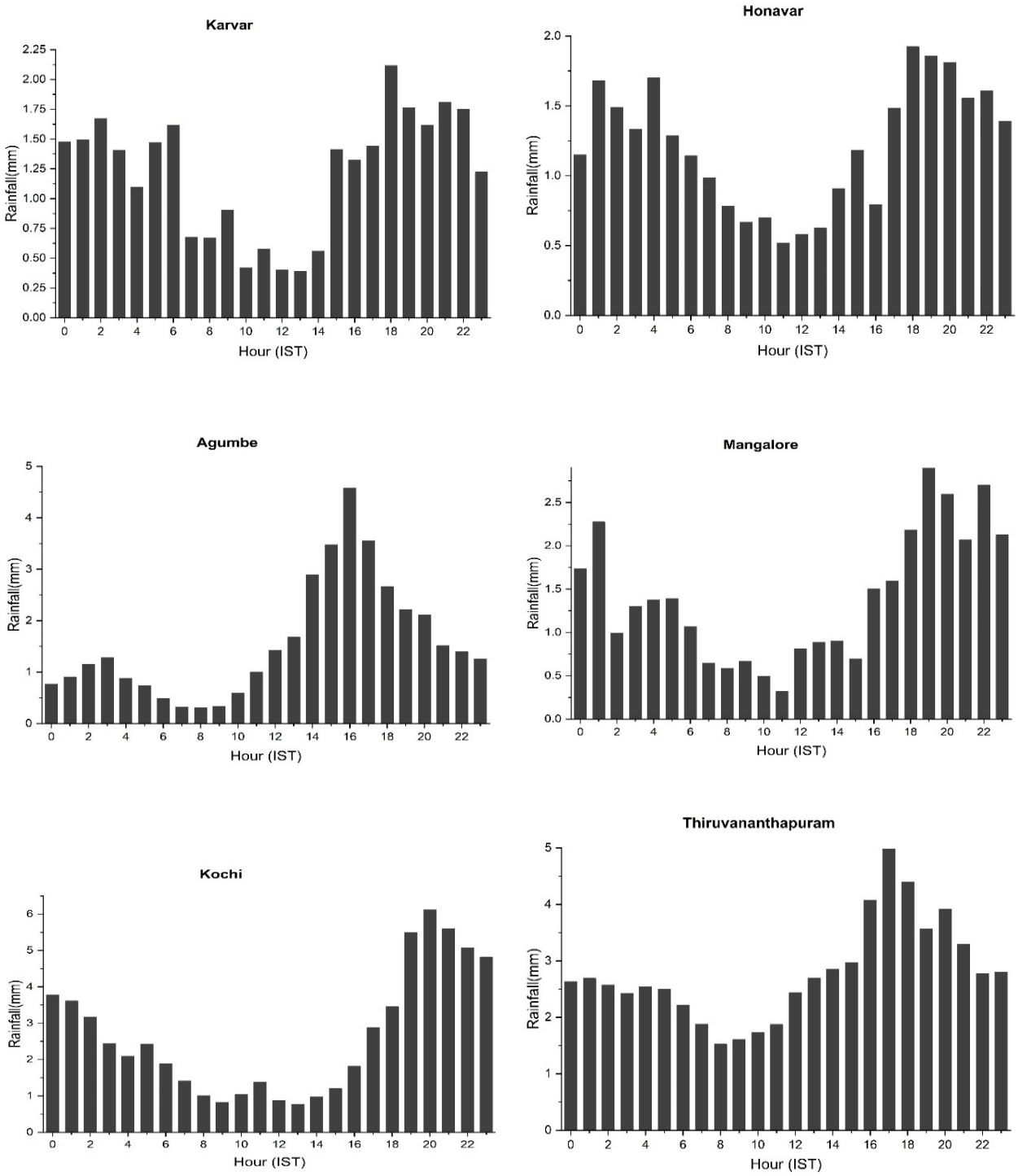

Fig 6.3. Hourly average rainfall (in mm) during the NE monsoon season (Oct-Dec) showing diurnal variation of rainfall at different stations over south Peninsula. Period: 1969-2021.

Using daily rainfall data from 15 September, 1998 to 15 January 1999, a spectral analysis was made to see the periodicities of rainfall during the NE monsoon season. The results are shown in Fig. 6.6. The spectral analysis shows a strong periodicity of rainfall activity with 30-40 days, which is also statistically significant. Another weaker periodicity is observed around 20 days. Fig 6.6 c shows the wavelet spectrum which also suggests the periodicity around 30-40 days. It may be interesting to note that these two periodicities are predominantly observed during the southwest monsoon season. More studies are required to understand the physical mechanisms of these oscillations during the NE monsoon season. What are the physical mechanisms for these oscillations and what is the predictability of this oscillation?

Sreekala et al., (2018) analyzed intra-seasonal rainfall activity during the NE monsoon season and the combined effect of Madden Julian Oscillation (MJO), NSO and IOD. The study has revealed that the intra-seasonal variation of daily rainfall over the south peninsula during the NEM season is associated with various phases of the eastward propagating MJO life cycle.

A similar study was made using more years of updated data to understand the ISO activity during the NE monsoon season in terms of different phases of MJO. ERA5 (Hersbach et al., 2020) daily precipitation datasets have been used for analyzing the intra-seasonal variation of NE Monsoon rainfall over the Oceanic region. Total hourly precipitation data are used in this study. In addition, zonal and meridional winds at 850 hPa from ERA5 data and Outgoing Long-wave Radiation (OLR) data (Liebmann and Smith 1996) from NCEP/NCAR during 1979-2021 are also used in the current study.

The Real-time Multivariate MJO indices (RMM1 and RMM2) from http://www.bom.gov.au/ bmrc/clfor/cfstaff/matw/maproom/RMM/ were used for defining the various Phases of MJO (Wheeler and Hendon 2004). MJO indices were calculated as the principal component (PC) time series of the two leading empirical

orthogonal functions (EOFs) of combined daily mean fields for 850 and 200 hPa zonal winds and OLR averaged over the tropics (15°S–15°N).

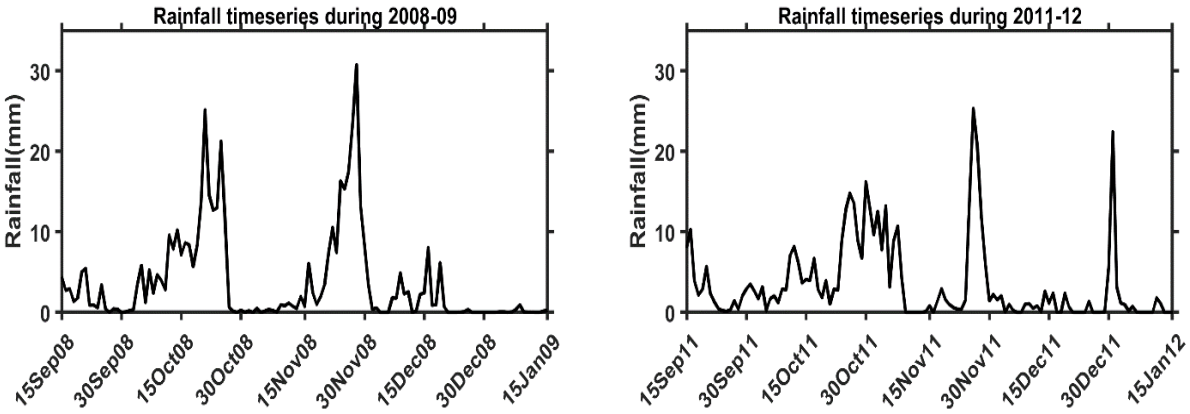

Fig. 6.4. Time series of daily rainfall averaged over NE Monsoon region during 15 September to 15 January a) 2008-2009 b) 2011-2012.

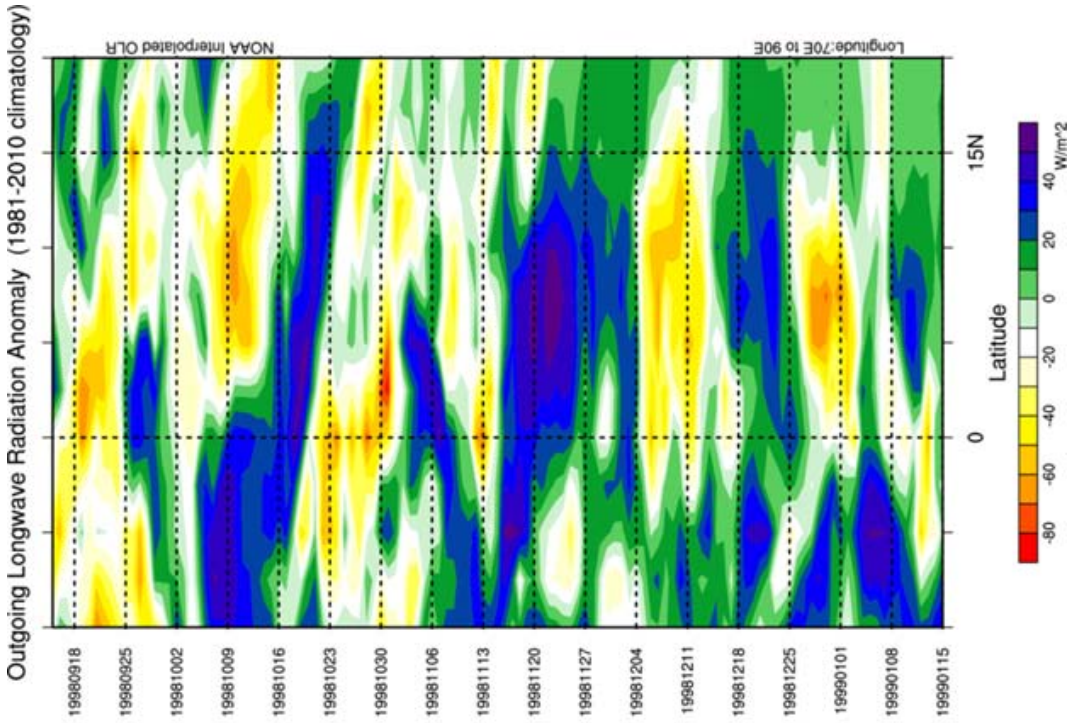

Fig. 6.5 a. Hovmuller diagram (Time vs Latitude) showing northward propagation of convection (OLR anomalies) during 15 Sept 1998 to 15 January 1999, averaged over 70^0-90^0E.

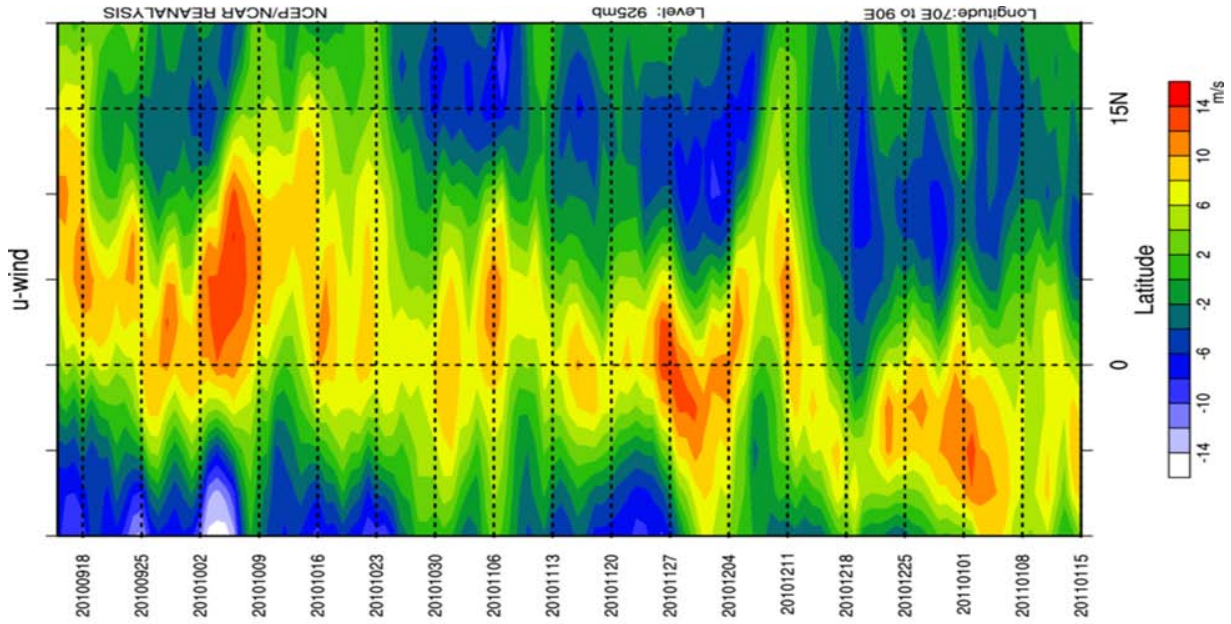

Fig 6.5 b. Hovmuller diagram (Time vs Latitude) of zonal wind (m/sec) at 925 hPa from 15 September 2010 to 15 January 2011.

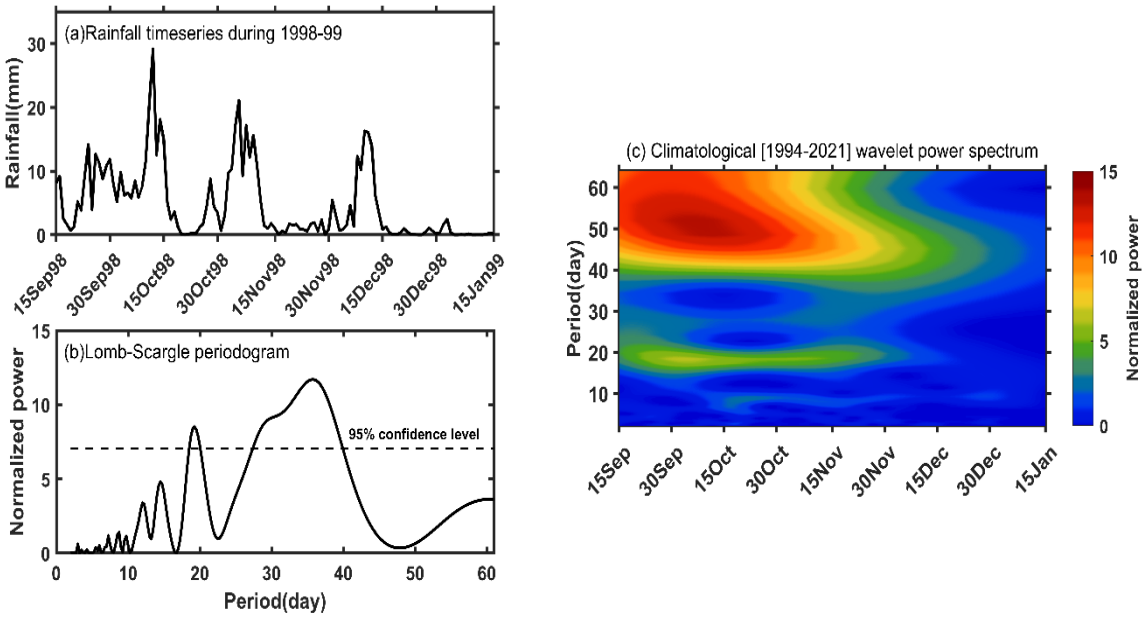

Fig 6.6. Daily rainfall (in mm) averaged over south Peninsular India from 15 September 1998 to 15 January 1999, b) Lomb-Scargle periodogram of daily rainfall over south Peninsular India from 15 September 1998 to 15 January 1999 and c) wavelet power spectrum of climatological daily rainfall averaged over south peninsular India (1994-2004).

Maps of composite rainfall anomaly (mm) in respect of eight strong phases of MJO superimposed with composite daily OLR anomalies (W/m^{-2}) and composite surface wind vector in the eight strong MJO phases were prepared using the data for the period 1979–2021. The results are shown in Fig. 6.7. Positive rainfall anomaly over south peninsular India and the surrounding Indian Ocean (IO) is observed during the strong MJO phases 2, 3 and 4; and negative rainfall anomaly during the strong MJO phases 6,7 and 8. Therefore, an understanding of the phase of MJO (which is available on real time at http://www.bom.gov.au/) is useful for assessing the prospects of NE monsoon rainfall over the south Peninsula. From Fig 6.7, it is very clearly seen the northeastward movement of positive rainfall anomalies from the equatorial Indian Ocean to the west Pacific and neighborhood.

Shanmugasundaram et al. (2017) employed hidden Markov model to characterize the spatio-temporal variations of NE monsoon rainfall at pentad time step and its probability of occurrence during 1982–2014. The results indicated the dominant presence of three rainfall states during the season, which were the wet (State-1), coastal wet (State-2), and dry (State-3) states. Seasonal total NEIMR was significantly and positively correlated with the frequency of State-1, whereas it was negatively correlated with that of State-3, indicating a crucial role of the rainfall states in determining water requirements in the southeastern peninsular India. Wet conditions were characterized by enhanced cyclonic activities and increased moisture convergence at 850 hPa over the southeastern peninsular India and its neighbouring oceanic regions (Bay of Bengal and Indian Ocean).

In contrast, dry conditions were associated with anticyclonic circulation and reduced moisture convergence at 850 hPa. The study by Somenath Dutta et al. (2016) revealed that the transition from weak phase to strong phase of north-east monsoon is associated with an enhancement in conversion of zonal potential energy to zonal kinetic

energy, implying a strengthening of Hadley circulation, favouring the above transition. It is also observed that the transition from weak phase to strong phase is associated with enhanced baroclinic energy conversion.

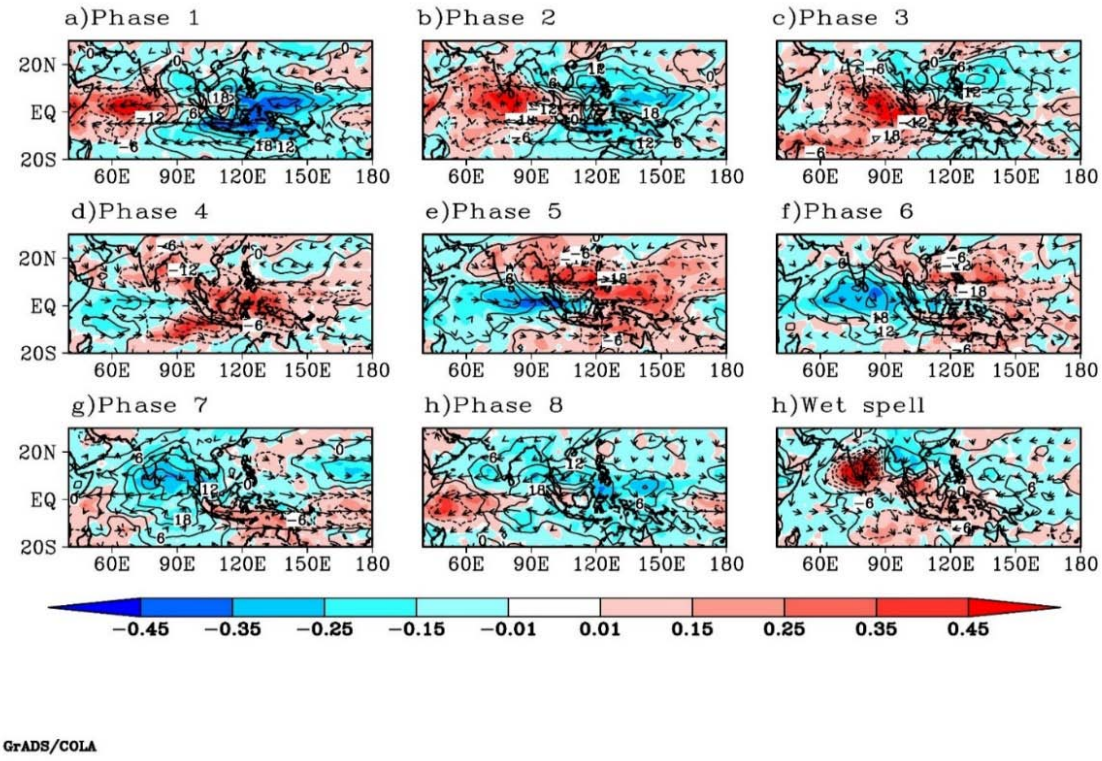

Fig 6.7. Maps of composite rainfall anomaly (mm) (shaded) in respect of eight strong phases of MJO superimposed with composite daily OLR anomalies (W/m^2) (lines) and composite surface wind vectors in the eight strong MJO phases and during wet spell using the data for the period 1979–2021.

6.2.1. **Active and Weak Spells of NE Monsoon**

Understanding of the intra-seasonal aspects of the NE monsoon is very important for prediction of rainfall. It is well known that the southwest monsoon season exhibits strong active and break spells during the season, and extensive analyses of monsoon active and break spells have been made. During southwest monsoon season, there are active and break spells, with specific characteristics (Ramaswamy 1969, Gadgil and Joseph, 2003 and Rajeevan et al. 2010). It was shown that the total number of active

and break spells during the season is statistically well correlated with the monsoon seasonal rainfall (Rajeevan et al. 2010). Larger number of break spells during the season could lead to a deficient monsoon. However, similar studies of active and break spells during the NE monsoon are unavailable. Since the earlier discussions suggest that there is strong intra-seasonal activity during the NE monsoon season, it is important to understand the active and break spells during the NE monsoon season. A similar analysis of active and weak spells during the NE monsoon season was carried out and the results are discussed below.

Using the IMD gridded daily rainfall data, an area averaged (8-14^0 N, 80-85^0 E) daily rainfall time series is prepared from 01 Oct to 31 Dec. Using the daily rainfall data, standardized rainfall is calculated for all these days from 1981-2021. An Active (wet) Spell is considered when the area averaged standardized rainfall is more than 1.0 for consecutively three days. Similarly, the weak (dry) spell is considered when the area averaged standardized rainfall is less than -0.8. The asymmetry in the threshold of standardized rainfall anomaly was made to ensure active and weak spell days are similar on a long-term climatological data. Using these criteria, active and weak spells during Oct-Dec are identified for the period 1981-2021. These criteria are similar to the criteria for the active and break events adopted for the southwest monsoon season (Rajeevan et al. 2010).

Table 6.1 shows the active and weak spell days during the period 1981-2021, identified using the above criteria.

The time series of total number of active and weak days during the season, year-wise is given in Fig. 6.8. The mean number of active (weak) days during the season is 7.07 (6.56) with a standard deviation of 5.89 and 6.08 respectively. The standard deviation of active and weak spells is very large. There are few years in which there is neither active nor weak spells. In 2003, maximum number of active days (24) was observed. In 1988 and 2016, maximum number of weak days (20) was observed. As

observed during the southwest monsoon season, total number of active and weak spells during the season influence the NE Monsoon seasonal rainfall. The correlation coefficient between the active and weak days during the season with the seasonal rainfall is 0.447 and -0.603 respectively, which are statistically significant at 95% significance level. Total number of weak days is more correlated with the seasonal rainfall, compared to the total number of active days.

Table 6.1

Active and Weak Spells during the NE Monsoon Season (Oct-Dec).

Period 1981-2021

Year	Active Days	Weak Days
1981	25-28 Oct, 02-04 Nov	11-17 Oct, 21-23 Nov
1982	26-28 Oct, 03-05 Nov	01-13Oct
1983	21-27 Dec	11-13Nov
1984	NIL	16-20 Oct, 31 Oct-4Nov
1985	01-03 Oct, 05-11 Oct	19-23 Oct
1986	05-07Nov,12-14Dec	20-25 Oct
1987	16-20 Oct	
1988	22-25Dec	11-18 Oct, 20-23 Oct, 27-31 Oct, 21-23Nov
1989	NIL	03-05 Oct, 14-16 Oct
1990	25-28Oct, 31Oct-2Nov,15-17Dec, 28-31Dec	7-9 Nov
1991	29-31Oct,15-18Nov,24-26Dec	NIL
1992	13-18 Nov,	20-31 Oct
1993	8-12Nov, 4-7 Dec	NIL
1994	04-06 Oct,7-9 Dec ,27-29 Nov	NIL
1995	NIL	NIL
1996	02-05 Oct,18-20 Oct,9-11 Dec, 13-17Dec	2-6 Nov
1997	8-10Nov, 24-30 Nov, 4-10 Dec	07-9 Oct
1998	11-18Oct, 7-10 Nov,8-12 Dec	NIL
1999	5-8Oct, 21-23 Nov	1-3Nov
2000	NIL	25-27 Oct,30Oct-9Nov
2001	NIL	NIL

2002	13-16 Oct	1-8 Oct,21-25 Oct
2003	6-8 Oct,21-24 Oct,1-17 Dec	11-13 Oct,15-17oct,2-6Nov
2004	3-5 Oct	3-5 Nov
2005	12-15 Oct,22-25 Nov	6-8 Oct
2006	26-30oct,4-6dec	12-14 Oct
2007	19-21 Dec	9-13 Oct
2008	24-30 Nov,19-21 Dec	1-3 Oct, 29 Oct-7 Nov
2009	1-5 Oct, 5-12 Nov, 14-16 Nov	10-12 Oct ,14-28 Oct
2010	31Oct-2 Nov ,17-19 Nov,21-23 Nov, 7-9 Dec	11-14 Oct
2011	NIL	1-3 Oct, 5-9 Oct,18-21 Oct, 21-23 Nov
2012	1-3 Nov	8-10 Oct,26-28 Oct
2013	22-26 Oct	9-11 Nov
2014	26-28 Oct	2-5 Oct
2015	30 Nov-3 Dec	16-18 Oct,21-24 Oct
2016	NIL	15-20 Oct,22-29 Oct, 6-8 Nov,11-13Nov
2017	NIL	17-19 Oct,23-26 Oct
2018	NIL	26-31 Oct,6-8Nov
2019	19-22 Oct, 24-26 Oct, 30Nov-3Dec, 13-15 Dec	NIL
2020	11-15 Oct,16-18 Nov, 3-5 Dec,7-9 Dec,	30 Oct-2 Nov
2021	17-19 Oct,12-15 Nov,18-21 Nov	NIL

To understand better the active and weak spells during the NE monsoon season, an analysis is made to make the composites of circulation and SST anomalies for the active and weak spells using the days of active and weak spells mentioned in Table 6.1. The results are discussed below.

Fig 6.9 shows the composite rainfall anomalies during the active and weak spell days, calculated using the rainfall data of ERA5. Fig 6.9 shows large positive (negative) anomalies over the south peninsula during the active (weak) spell days. Over the equatorial south Indian Ocean and the west Pacific, there are sharp differences between the active and weak spell days. An active (weak) spell is also associated with suppressed (enhanced) rainfall activity over the west Pacific and the equatorial Indian Ocean.

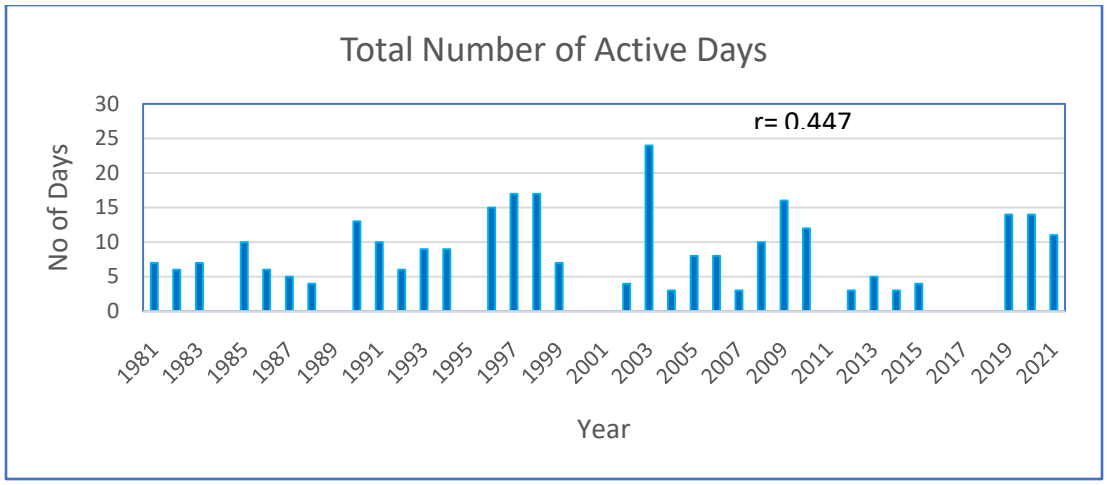

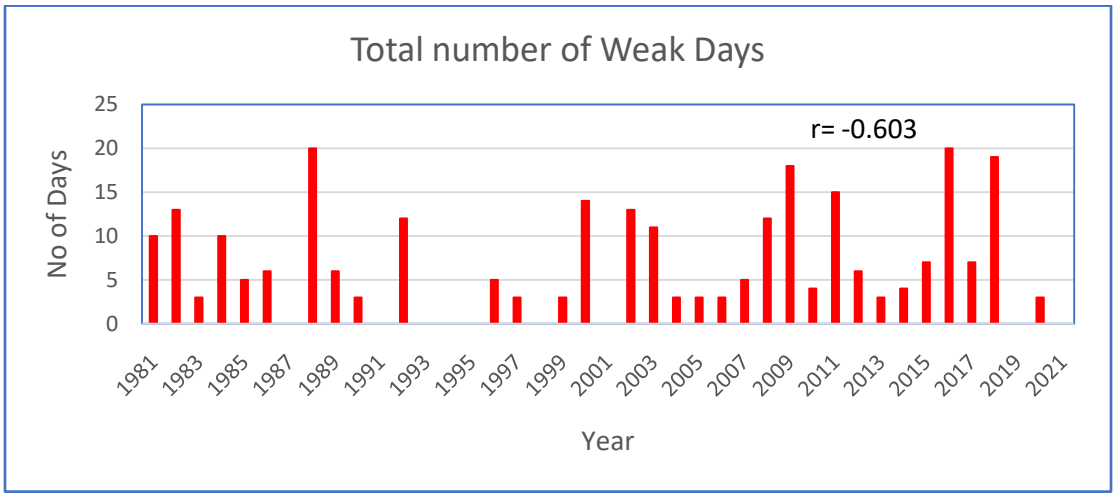

Fig 6.8. Total number of active (above) and weak (below) days during the OND season for different years, 1981-2021. The correlation coefficient between the total number of active and weak days with the seasonal rainfall is shown in the plots.

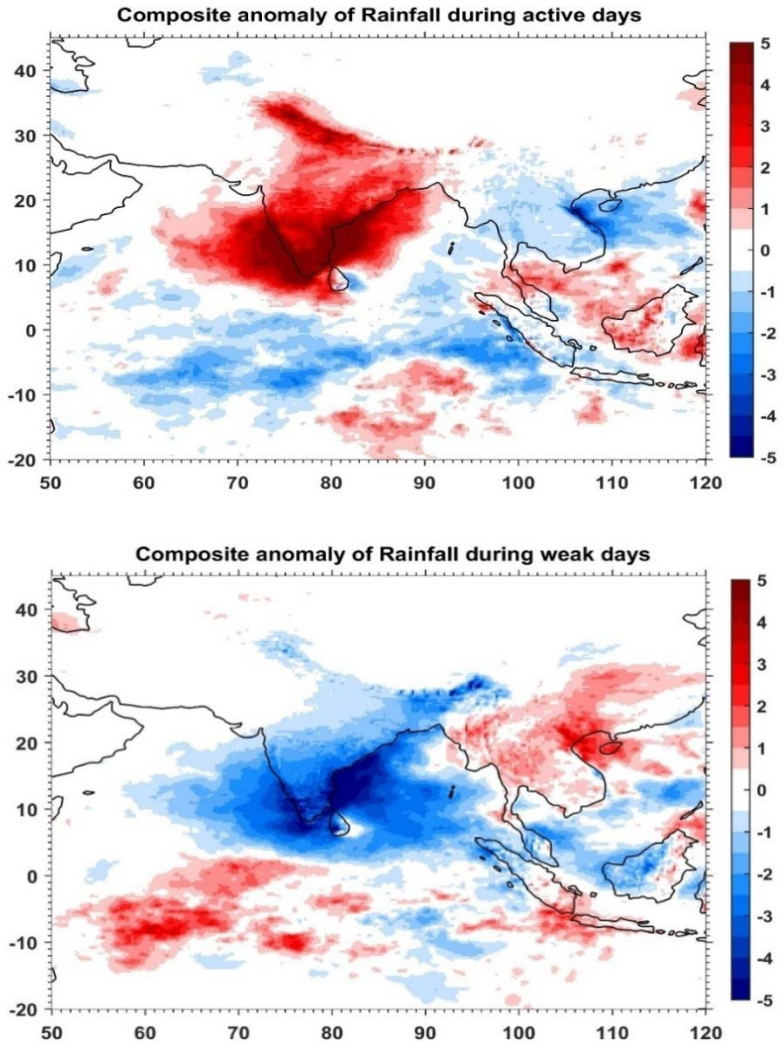

Fig 6.9. Composite rainfall anomalies (mm) during the active spell days (above) and weak spell days (below) for the period 1981-2021.

Fig 6.10 shows the composite SST anomalies during the active and weak spell days. The largest differences between the active and weak spells are observed over the equatorial Pacific and the north Indian Ocean. Over the equatorial Pacific Ocean, the SST anomalies are positive (negative) during the active (weak) spells. This indicates that enhanced rainfall activity (more active days) is observed during the El Nino years. Similarly, during the La Nina years, the weak spell days are more. During the active (weak) spell days, SST anomalies over the equatorial Bay of Bengal and Arabian Sea are

large negative (positive). However, over the north Bay of Bengal, positive (negative) anomalies are observed during the active (weak) spell days.

Fig 6.11 shows the similar composite plots, but for the OLR anomalies. The results are consistent with the rainfall anomaly plots. During the active (weak) spell days, OLR anomalies are large negative (positive) over the Indian sub-continent suggesting enhanced (suppressed) rainfall activity. The drastic difference between these two cases is observd over the west Pacific Ocean and China and adjoining area. During the active (weak) phase of the monsoon, convection over the west pacific is suppressed (enmhanced). The enhanced convection over the west Pacific could cause anomalous descending motion over the Indian region and thus reduce the NE monsoon activity.

Fig 6.12 shows the 850 hPa wind anomalies during the active and weak spells of NE monsoon. The most striking feature of the wind anomalies is observed over the Indian region. The active (weak) phase of the NE monsoon is associated with cyclonic (anti-cyclonic) circulation anomalies over the Indian region, which is consistent with the observed rainfall anomalies. The other significant anomalies are observed over the west Pacific and adjoining eastern parts of China. During the active (weak) phase, an anomalous anticyclonic (cyclonic) circulation is observed over the region, suggesting below (above) normal convection over the region. This is consistent with the OLR anomalies discussed above.

6.3. **Interannual variation of NE monsoon rainfall (NEMR)**

In this section, the inter-annual variability of NE monsoon rainfall is discussed. There are not adequate studies examining the inter-annual variability of NE monsoon rainfall except the studies by De and Mukhopadhyay, 1999; Kripalani and Kumar, 2004; Raj and Geetha, 2008; Zubair and Ropelewski, 2006; Kumar et al., 2007; Sreekala et al., 2012, Rajeevan et al., 2012.

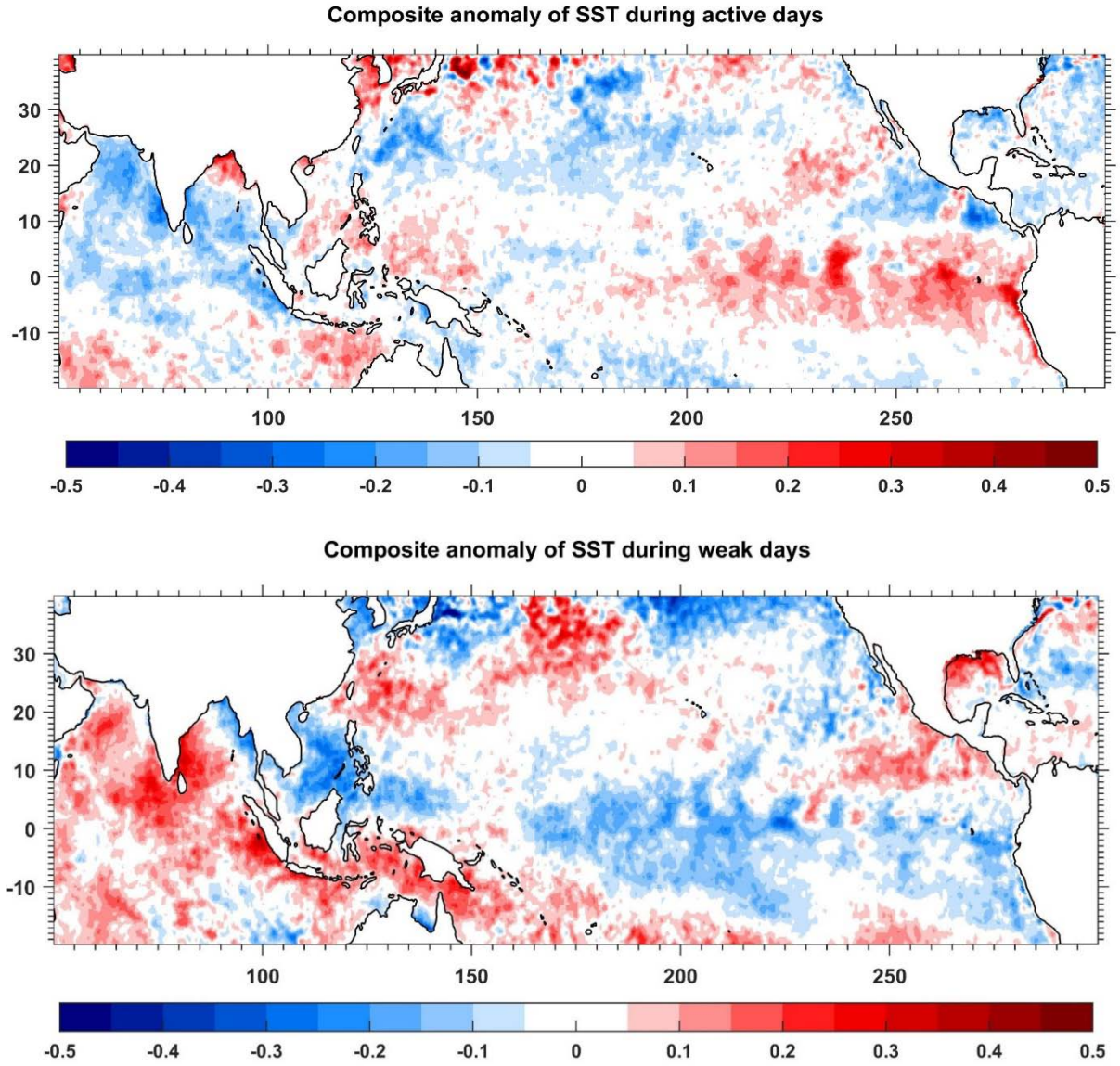

Fig 6.10. Composite Sea Surface Temperature (SST) (^{0}C) anomalies during the active spell days (above) and weak spell days (below) for the period 1981-2021.

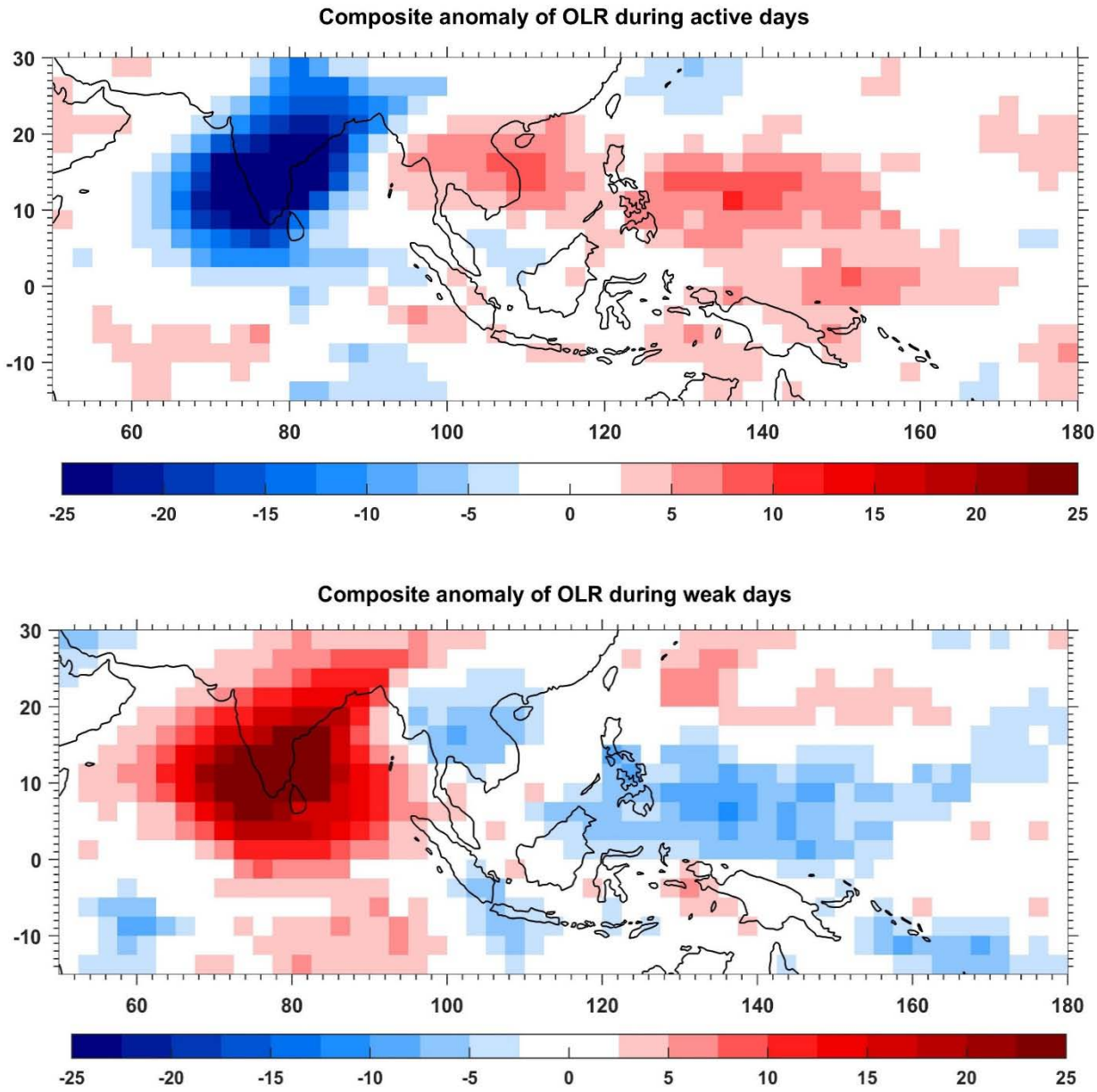

Fig 6.11. Composite OLR anomalies (Wm^{-2}) during the active spell days (above) and weak spell days (below) during the period 1981-2021.

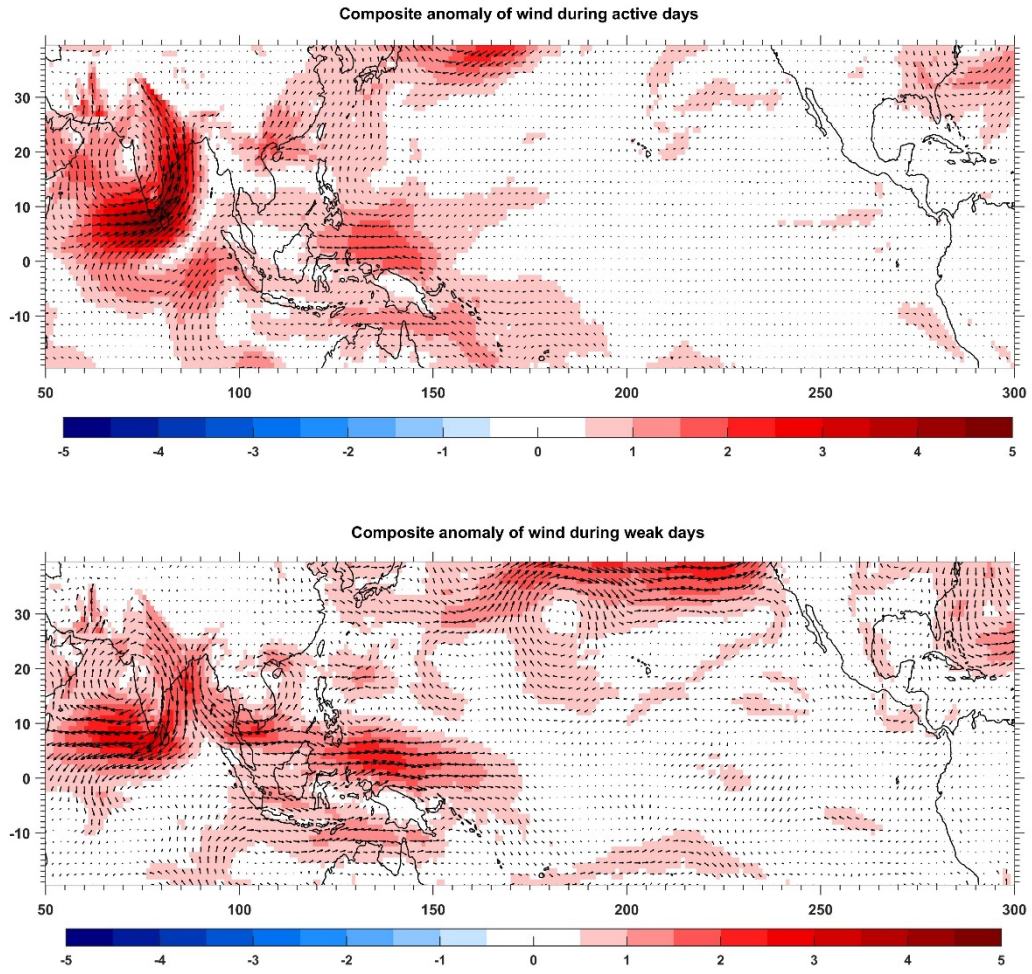

Fig 6.12. Composite OLR anomalies (Wm^{-2}) during the active spell days (above) and weak spell days (below) during the period 1981-2021.

The inter-annual variability of the NEMR is calculated using the sub-divisional rainfall data for the period 1901–2021. During the northeast monsoon season, south peninsular India receives a mean rainfall of 338.4 mm with a coefficient of variation of about 25%. It may be noted that the coefficient of variation during the NE monsoon season is much more than that of SW monsoon rainfall (June to September) for the whole country which is around 10%.

Fig. 6.13 a shows the interannual variation of the NEMR as expressed as percent departure of the seasonal rainfall. No long-term trend in the NEMR is noticed, but there

are years with large rainfall departures, even exceeding 40%. The years with more (less) than 1 Standard Deviation (25%) are termed as excess (deficient) years. If the departure is more than -25% but less than 25%, then those years are termed as normal years. Out of 121 years (1901-2021), there were 78 normal years, 23 excess years and 20 deficient years. Among these years, the 2021 monsoon season has the highest positive departure (73%). The year 2016 was the worst deficient year with a deficiency of 65%. The other two notable excess years are 2010 and 2015. The other two notable deficient years are 1938 and 1988. Recently, three consecutive years 2016-2018 experienced below normal rainfall with large negative rainfall departures. However, the subsequent three years witnessed above normal monsoon rainfall with positive departures. Fig. 6.13 b shows the 21-year moving average of the NEMR during the period 1901–2021. It clearly shows the multi-decadal variations of the NEMR with epochs of above normal and below normal rainfall. An increasing trend in the NEMR during the recent years is observed.

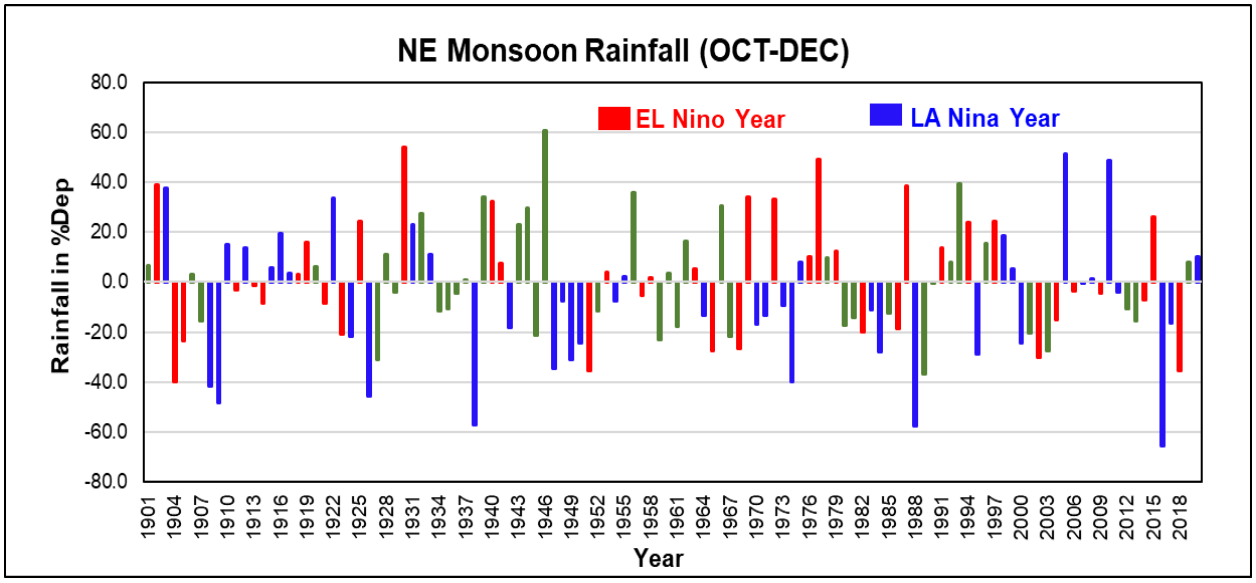

Fig 6.13 a: Time series of NE monsoon seasonal rainfall as % Departure from 1901-2020. El Nino year is shown as red and La Nina year is shown as blue lines.

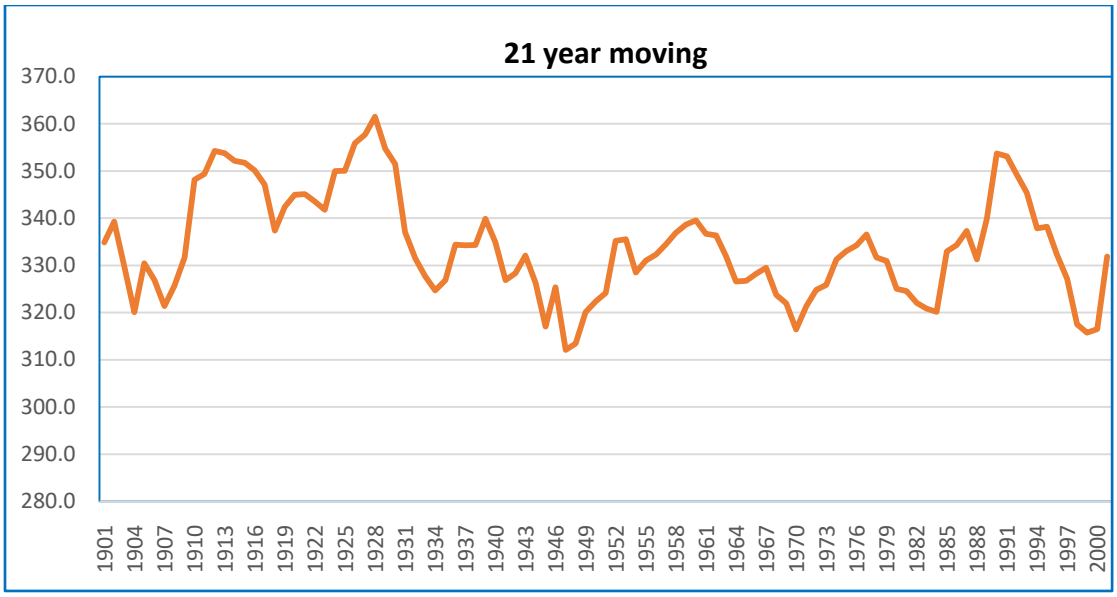

Fig 6.13 b. The 21 year moving mean of NE monsoon seasonal rainfall (Oct-Dec) in mm, showing multi-decadal variations of NE monsoon rainfall.

Fig 6.14 a shows the periodogram of NE Monsoon seasonal rainfall for the period 1901-2021. Even though many periodicities of shorter duration are seen, the periodicity of about 16 years is close to the significant (90% significance) level. Fig 6.14 b shows the wavelet spectrum of NE monsoon seasonal rainfall for the same period 1901-2021. It clearly shows the periodicity of about 16 years, which is statistically significant. This periodicity, however, was not uniformly active during the whole period. It was active till about 1950. Then, it became active from 1980s till date. Raj (2012) also suggested the periodicity of similar periods for NE monsoon rainfall. This periodicity is also apparent in the 21-year running mean shown in Fig 6.13 b. The periodicity of 2-3 years (quasi biennial) is observed during 1920s to 1970s. Kripalani and Kumar (2004) also suggested the NE monsoon rainfall undergoes different epochs of above and below normal rainfall. These epochs last about a decade or two. More studies are required to understand the decadal variations of NE monsoon rainfall using long term data.

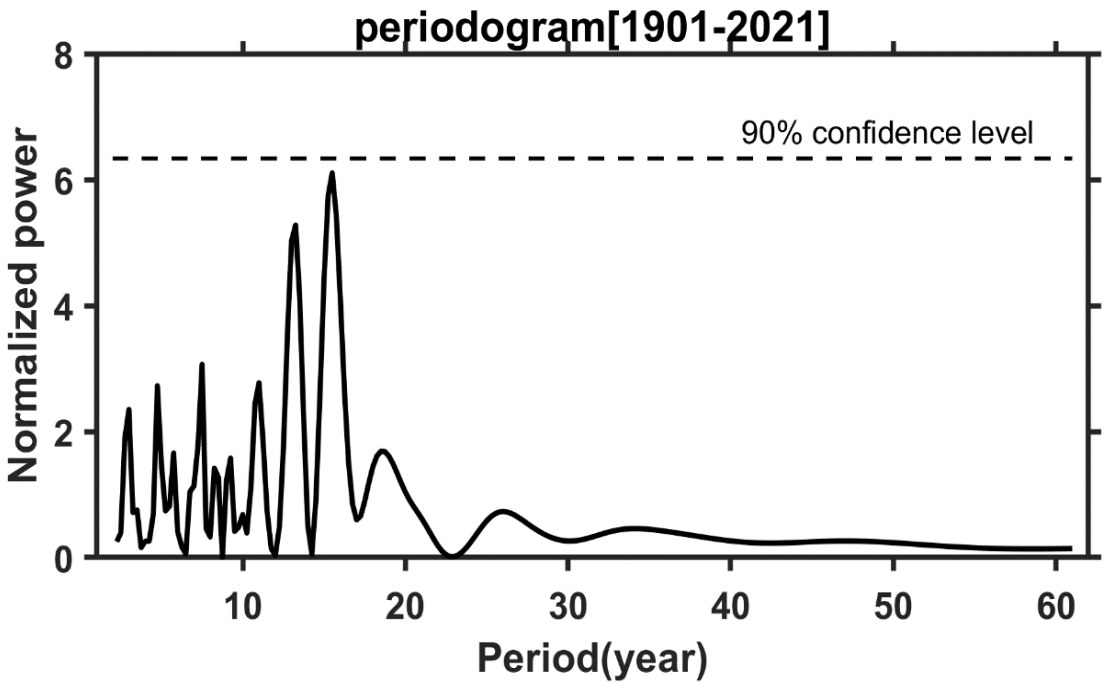

Fig 6.14 a. Periodogram of NE Monsoon seasonal rainfall (1901-2021). The peak around 16 years is close to significance level at 90%.

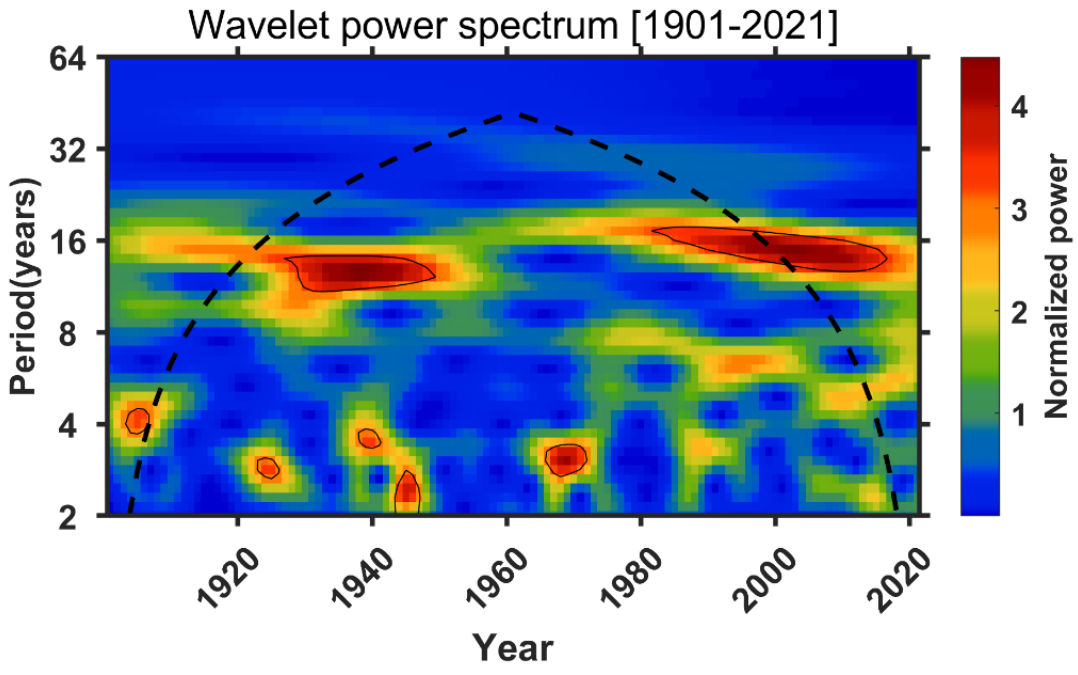

Fig.6.14 b. Wavelet power spectrum (1901-2021) of NE monsoon seasonal rainfall. The periodicity close to 16 years is statistically significant.

The inter-annual variability of the NEMR is linked to the El Nino/Southern Oscillation (ENSO), the Indian Ocean Dipole and the EQUINOO (De and Mukhopadhyay, 1999; Kripalani and Kumar, 2004; Raj and Geetha, 2008; Jayanthi and Govindachari 1999; Zubair and Ropelewski, 2006; Kumar et al. 2007; Sreekala et al. 2012, Rajeevan et al. 2012). ENSO is an irregular periodic variation in Sea surface temperatures and winds over the equatorial Pacific Ocean. ENSO influences the climate of much of the tropics and subtropics. ENSO is a coupled process in which the equatorial Pacific and atmosphere interact. The warming phase of the sea surface temperature is known as El Nino and the cooling phase as La Nina. The Southern Oscillation is the accompanying atmospheric component, coupled with the changes in SST.

The Indian Ocean Dipole (IOD) is defined by the difference in sea surface temperature between two areas – a western pole in the Arabian Sea (western Indian Ocean) and an eastern pole in the eastern Indian Ocean south of Indonesia. The IOD affects the climate of Australia and other countries surrounding the Indian Ocean Basin, and is a significant contributor to rainfall variability in this region. Positive Dipole events are characterized by positive (negative) SST anomalies over the west (east) equatorial Indian Ocean. Conversely, the negative phase is characterized by negative (positive) SST anomalies over the west (east) equatorial Indian Ocean.

Fig. 6.15 a shows the spatial pattern of correlations between Oct-Dec SST and NE monsoon rainfall during two 30-year periods, 1961-1990 and 1991-2020. The plot for the period 1961-1990 clearly shows that positive SST anomalies over the equatorial Pacific Ocean (El Nino) are associated with normal or above normal rainfall. However, during the recent 30-year period, the positive correlations over the equatorial Pacific have weakened. Another interesting area of strong correlation is over the North Atlantic. During the period 1961-1990, strong positive correlations are observed, which are replaced by weak negative correlations during the period 1991-2020.

Raj and Geetha (2008) analyzed the relationship between Southern Oscillation Index (SOI) and NE monsoon rainfall in antecedent and concurrent mode and found there is a negative relationship. The relationship in antecedent mode is stronger. Sengupta and Nigam (2019) studied the aspects of ENSO impact on NE monsoon rainfall. Their study suggested stronger NE monsoon rainfall over south peninsula and Sri Lanka during El Nino events. The impact varies sub-seasonally, being weak in October and strong in November. The positive anomalies over the south peninsula are generated by anomalous anticyclonic flow centered over the Bay of Bengal, which is forced by an El Nino-related reduction in deep convection over the Maritime continent.

In fact, the correlation between NE monsoon rainfall and Nino 3.4 changes its sign by middle of October. Till middle of October, the correlation is negative and it changes to positive correlation by November. Fig 6.15 b clearly suggests this shift in the sign of correlation between Nino 3.4 and NE monsoon rainfall by October end.

However, the relationship between NE monsoon and ENSO is not very stable. It was weakened during the recent epoch (1991-2020) (Fig.6.15 c). Another interesting aspect to be noticed is the positive correlation of SSTs over the north Bay of Bengal with the NE monsoon rainfall, suggesting a warmer Bay of Bengal could be related to better performance of NE monsoon rainfall. It may be interesting to examine long term data to understand why the relationship between ENSO and NE Monsoon rainfall undergoes secular variations.

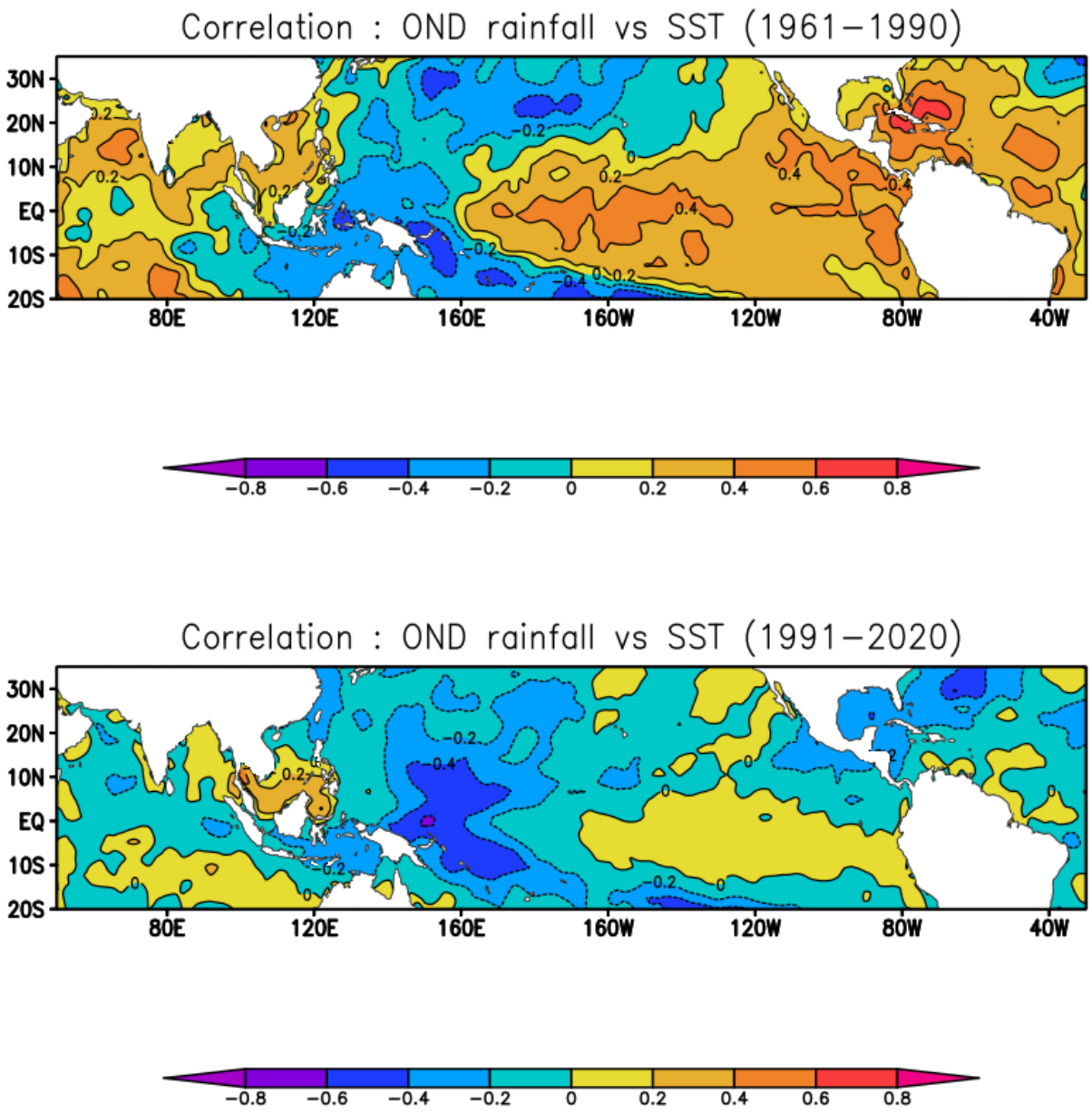

Fig 6.15 a. Spatial Pattern pf correlation between Sea Surface Temperature (SST) and NE Monsoon seasonal rainfall during the period 1961-1990 (above) and 1991-2020 (below).

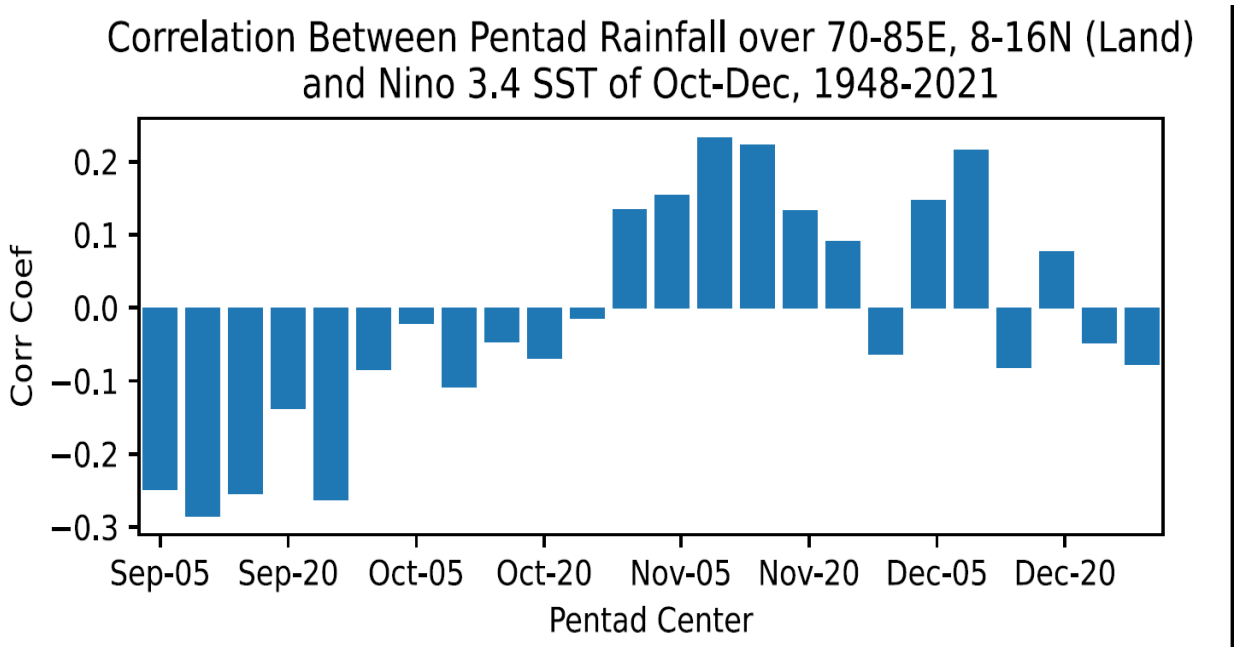

Fig 6.15 b. Correlation between pentad rainfall averaged over south peninsula and Nino 3.4 SST index. The period 1948-2021 is considered for the analysis.

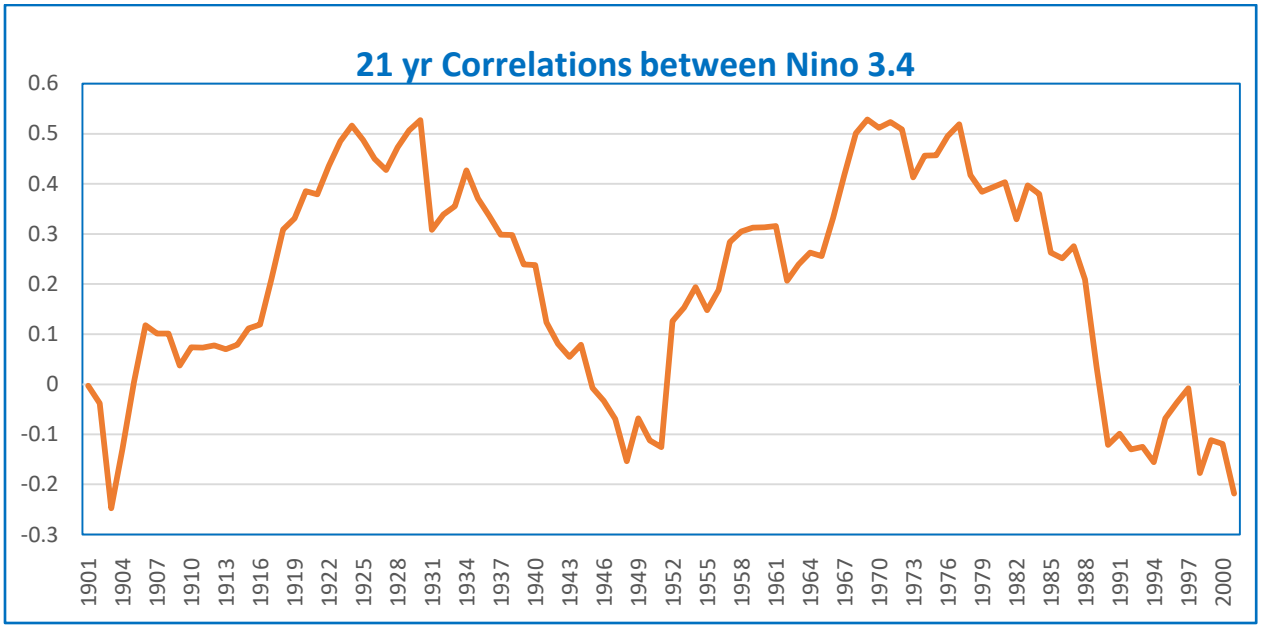

Fig 6.15 c. The 21 year moving correlations between Nino 3.4 index during OND and NE Monsoon seasonal rainfall (OND) suggesting multi-decadal variation of relationship between NE monsoon rainfall and El Nino.

Table-6.2 below shows El Nino/La Nina's relationship with NE monsoon rainfall.

Table 6.2.
Relationship between ENSO and NE Monsoon Rainfall
Period: 1940-2021

El Nino Years (39)			La Nina Year (42)		
Excess >25%	Normal -25% to 25%	Deficient < -25%	Excess >25%	Normal -25% to 25%	Deficient < -25%
11	22	6	6	23	13
28%	57%	15%	14%	55%	31%

The analysis shows that the probability of an El Nino year being an excess NEMR year is higher (28%) compared to the year being a deficient (15%) monsoon year. However, the probability of a La Nina year being an excess monsoon year (14%) is smaller compared to an excess (31%) monsoon year. Therefore, more confidence in excess or deficient monsoons may be obtained with the additional information on IOD. However, compared to the Southwest monsoon, the NE monsoon is not very strongly related to ENSO or IOD.

An analysis was carried out by Prasanna et al. (2019) of two successive La Niña years, referred to as the first and second year during the period 1900–2010 to see the impact on NE monsoon rainfall. Observations show that despite noticeable weakening in the equatorial Pacific cooling from the first year to the second year, strong La Niña teleconnections and the rainfall deficiency over the region remains the same in most of the multiyear-La Niña events (70%).

Even though, there is a high probability for NE monsoon to be on lower side of the normal during the La Nina years, there have been three major exceptions to be examined in detail. These years occurred recently, 2010 and 2021, when the ENSO-NE

monsoon rainfall relationship was weaker. The NE monsoon rainfall percent departure during these three seasons was 49% and 73% respectively. The year 2021 was truly an exception.

Kripalani and Kumar (2004) documented the NEMR and IOD relationship. They suggested that the NEMR variability is enhanced during the decades when the IOD exhibits its active phase, and is suppressed during the decades when the IOD is inactive. This relationship suggests that the positive (negative) phase enhances (suppresses) the northeast monsoon activity. During the positive phase, the anomalous flow pattern shows winds converging and suggesting moisture transport from the southeast Indian Ocean and the Bay of Bengal towards south peninsular India. In contrast, the negative phase reveals winds diverging and transporting moisture away from the south Indian region. These results show the direct influence of the IOD phenomenon on the interannual NE monsoon rainfall variability over south India.

Balachandran et al. (2006) examined the local and teleconnective association between Northeast Monsoon Rainfall over Tamil Nadu and global surface temperature anomalies (STA) using the monthly gridded STA data for the period 1901–2004. It is observed that the meridional gradient in surface air temperature anomalies between Europe and north Africa, in the month of September is directed from the subtropics (higher latitudes) to higher latitudes (subtropics). It is also observed that North Atlantic Oscillation (NAO) during September influences the surface air temperature distribution over north Africa and Europe. Also, the NAO index in January shows significant inverse relationship with the NE monsoon rainfall since recent times. The central and eastern equatorial Pacific oceanic regions have significant and consistent positive correlation with NE monsoon rainfall while the western equatorial region has significant negative correlation with Northeast monsoon rainfall. A zonal temperature anomaly gradient index (ZTAGI) defined between eastern equatorial Pacific and western equatorial Pacific shows stable significant inverse relationship with Northeast monsoon rainfall.

The unusual excess year of the 2021 NE monsoon season is discussed below.

6.4. **The unusual NE monsoon during the year 2021**

During the year 2021, the southwest monsoon withdrew from the Indian region on 25th October. Simultaneously, the Northeast monsoon (NEM) of 2021 commenced over the southeastern parts of peninsular India on 25th October against the normal date of 20th October. Excepting Coastal Andhra Pradesh (CAP), which received normal rainfall during the season, the other four sub-divisions [Tamil Nadu (TN (including Puducherry & Karaikal), Kerala (KER), Rayalaseema (RYS) and South Interior Karnataka (SIK)] benefitted from the NE monsoon. These sub-divisions received excess to large excess rainfall during the NEM season (October-December) with KER, SIK, RYS recording more than 100% excess (large excess) rainfall. During the season, there were 30 days of active to vigorous monsoon conditions over Tamil Nadu and Kerala. There were 65 days of isolated heavy rainfall activity with 33 days of isolated very heavy rain, including 09 days of isolated extremely heavy rainfall activity over Tamil Nadu. Two Depressions formed over the North Indian Ocean during November contributed significantly to NEM rainfall over the peninsular India. Cyclonic Storm (CS) Jawad over the Bay of Bengal (BOB) during 02-06 December tracked northwards towards West Bengal- Bangladesh coasts and did not contribute towards NEM seasonal rainfall. However, two days of extremely heavy rainfall occurred over Chennai (i) 06th November night & (ii) 30th December 2021. Recurrent heavy rainfall over the coastal and adjoining districts from the last week of October to November led to the filling up of water bodies, and inland and riverine flooding occurred over several areas of Tamil Nadu and Rayalaseema. As a result, NE monsoon 2021 was extended into January 2022 and cessation of NEM 2021 rainfall over peninsular India was declared on 22nd January 2022 (Geetha et al., 2022). A more detailed report on 2021 NE monsoon is available for reference (Geetha et al., 2022).

The Table-6.3 presents the frequency of active and vigorous monsoon days and heavy rainfall days during the 2021 NE monsoon season (after Geetha et al., 2022).

Table 6.3

Subdivision	Number of Days				
	Activity		Heavy Rainfall		
	Vigorous	Active	Extremely Heavy	Very Heavy	Heavy
Tamil Nadu	8	22	9	33	65
Coastal Andhra Pradesh	2	7	0	8	28
Rayalaseema	8	12	1	4	22
Kerala	11	19	2	18	40
South Interior Karnataka	5	10	0	9	28

Note: Heavy Rainfall > 6.5 cm/day Very Heavy rainfall> 12 cm/day and Extremely Heavy rainfall >21 cm/day

Active: Failrly widespread to widespread sub-divisional rainfall with rainfall more than 1.5 to 4 times the normal with at least two stations reporting more than or equal 5 cm in coastal Tamil Nadu and south coastal Andhra Pradesh and 3 cm elsewhere in the NEM region.

Vigourous: Fairly widespread to widespread sub-divisional rainfall with rainfall more than 4 times the normal with at least two stations reporting more than or equal to 5 cm in the coastal Tamil Nadu and the south coastal Andhra Pradesh and 3 cm elsewhere in the NEM region.

Fig 6.16 a shows the seasonal (Oct-Dec) rainfall over the south peninsula and neighborhood (in mm/day) during the 2021 monsoon season. It shows widespread abundant rains over the south Peninsula and the adjoining southwest Bay, suggesting an excess monsoon year (73% above its long period average).

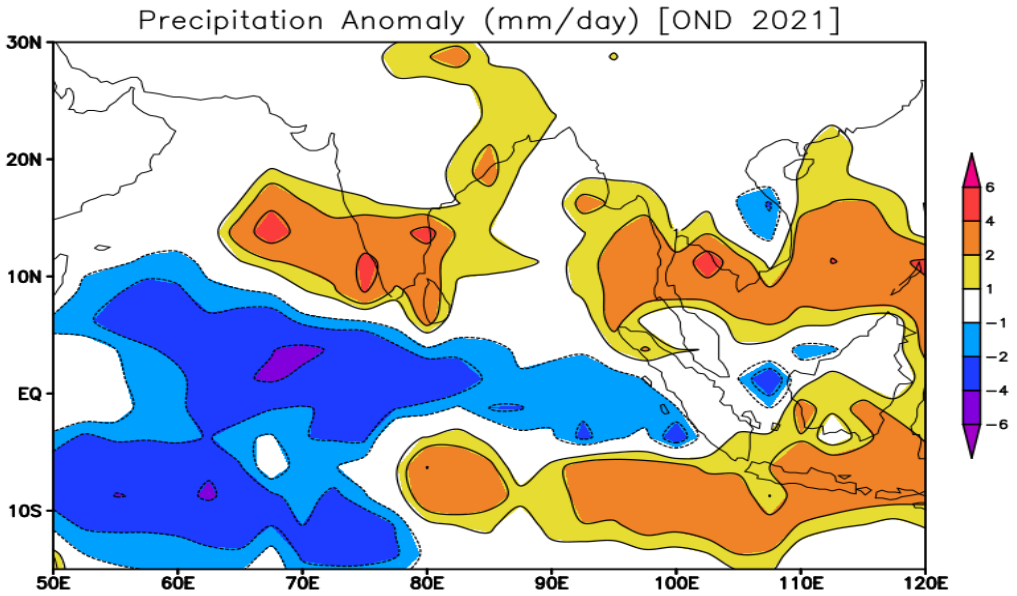

Fig 6.16 a Precipitation anomaly (mm/day) during OND 2021. Source: ERA5 reanalysis.

The 850 hPa wind pattern (Fig 6.16 b) shows an extended east-west trough extending from the east central Arabian sea to the west equatorial Pacific Ocean across the south peninsula and south Bay of Bengal. This suggests the presence of active ITCZ over the region during the NE monsoon season. This convergence zone must be the cause of the genesis of several weather systems over the south Bay of Bengal and their westward movement towards the south Peninsula. The SST anomaly during Oct-Dec 2021 (Fig 6.16 c) shows the presence of cold SST anomalies over the equatorial Pacific, suggesting La Nina conditions. It may be interesting to note the presence of above normal SSTs over the Bay of Bengal. Some recent studies like Singh et al. (2017) suggested that local air-sea interaction plays a crucial role in modulating or driving extremes over South Peninsula associated with ENSO. More studies are required to understand the physical mechanisms of relationship of Bay of Bengal SSTs and the NE monsoon rainfall.

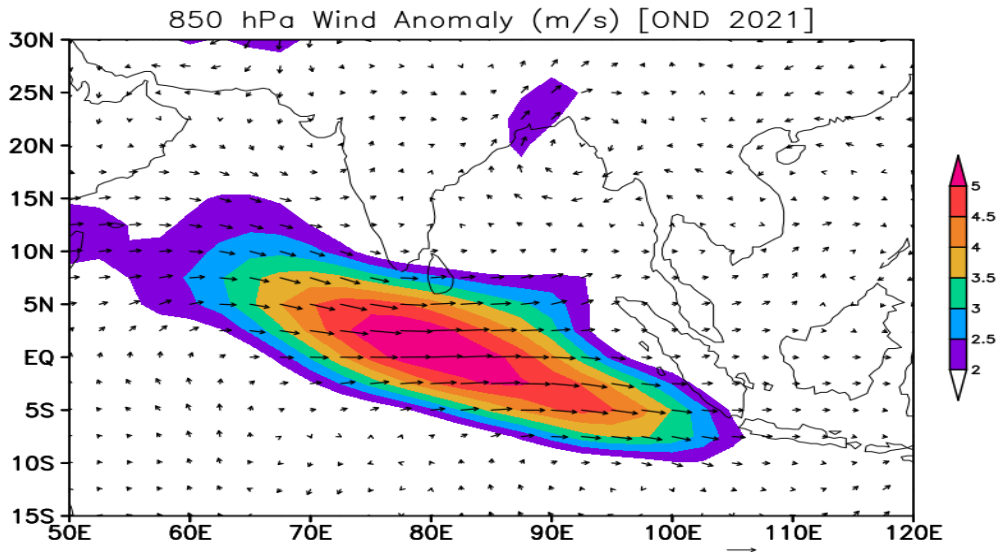

Fig 6.16 b. 850 hPa wind anomalies during OND 2021. Source: ERA5 reanalysis.

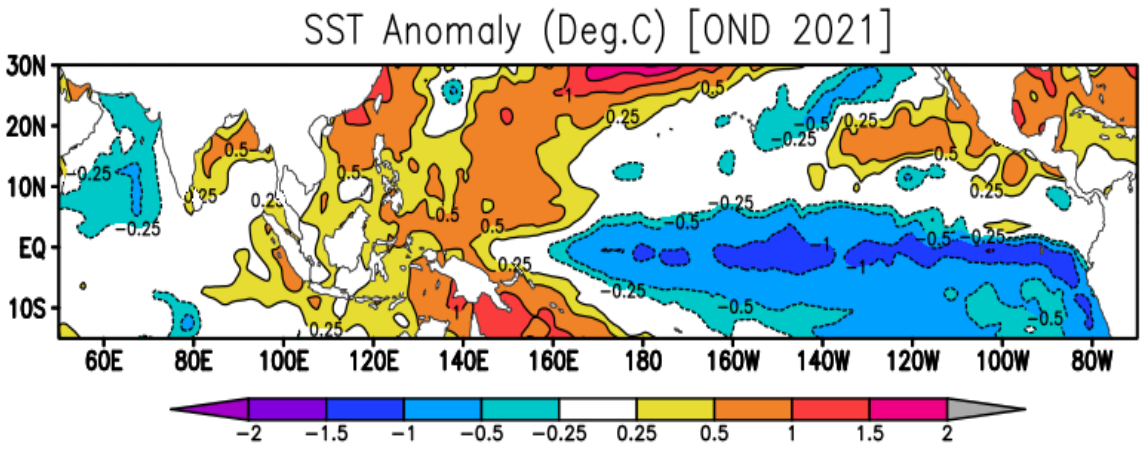

Fig 6.16 c. SST anomalies during OND 2021. Source: NOAA OI SST data.

6.5. **Seasonal Forecasting of NE Monsoon**

India Meteorological Department (IMD) has been attempting to prepare long-range forecasting of NE Monsoon rainfall (Oct-Dec) using indigenously developed statistical models based on principal component analysis (PCA). The parameters used for the statistical models are shown in Fig.6.17. Overall, five predictors are used for long range prediction of NE monsoon rainfall. Out of these five predictors, four predictors are

derived from the Indian and West Pacific regions, while the fifth parameter is derived from the Atlantic Ocean. Since the inter-annual variability of NE monsoon rainfall is quite large (25%), developing a skillful statistical prediction scheme could be challenging. IMD, however, shares the long-range forecasts confidentially with the concerned state governments every year. Therefore, more research studies are required to understand the inter-annual variability of NE monsoon rainfall better and develop skillful long-range forecast models.

Rajeevan et al. (2012) suggested that present-day dynamical models have serious problems in properly simulating mean monsoon rainfall and its teleconnections. Coupled climate models do not correctly simulate the sign of the ENSO-NE Monsoon rainfall relationship. Furthermore, there is absolutely no skill with the present dynamical models in predicting inter-annual variability of NE monsoon.

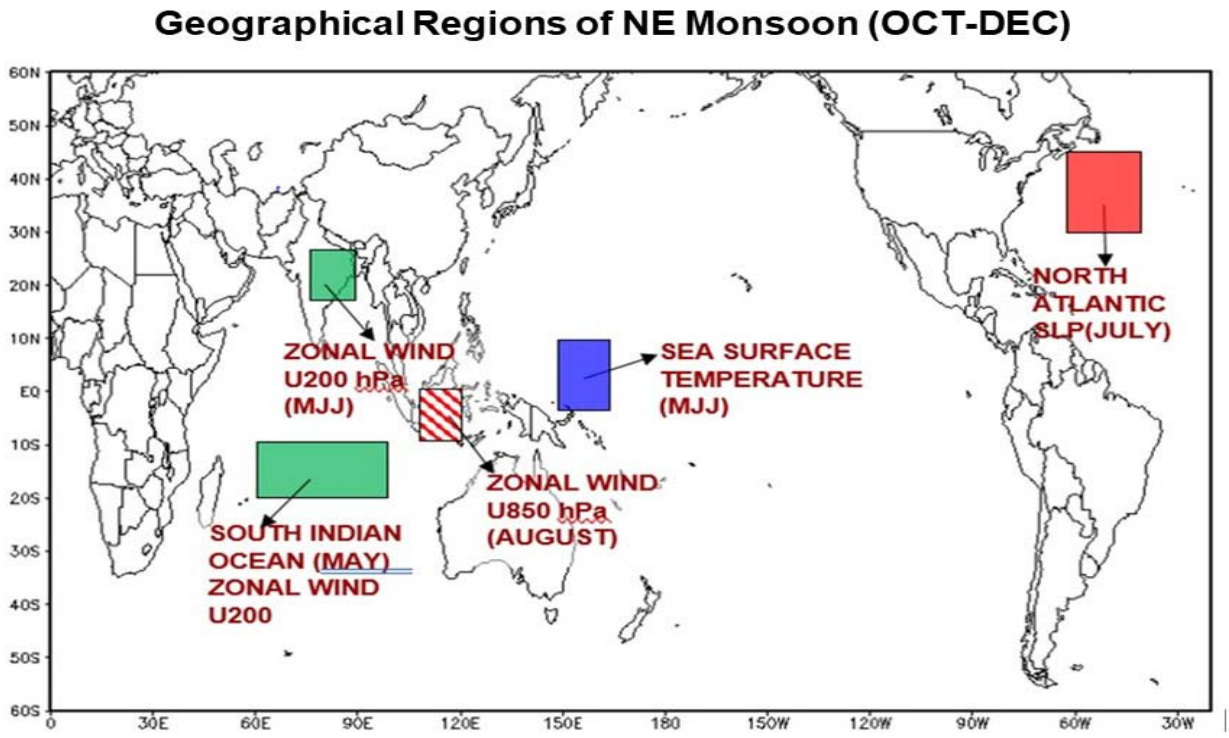

Fig 6.17. The parameters used in the statistical model for the long-range forecasting of NE Monsoon rainfall by the India Meteorological Department.

The study by Acharya et al. (2011) suggested that the general circulation models considered in the study are not able to simulate the observed interannual variability of rainfall. They attributed this to inaccurate response of the models to sea surface temperatures. They found that the multi-model ensemble scheme improved the accuracy of simulations. The study by Sengupta and Nigam (2019) revealed that the historical twentieth-century climate simulations informing the Intergovernmental Panel on Climate Change's Fifth Assessment (IPCC-AR5) showed varied deficiencies in the NEM rainfall distribution and a markedly weaker (and often unrealistic) ENSO–NEM rainfall relationship.

Prasanna et al. (2021) examined the fidelity of the eight Asia-Pacific Economic Cooperation (APEC) Climate Center (APCC) models in representing the inter-annual variability and decadal shift in the northeast monsoon (NEM; October–December) rainfall over Southern Peninsular India (SPI). The observations showed a clear inter-annual and inter-decadal variability of NE monsoon rainfall. The analysis suggested that most of the models exhibited poor skill in representing the inter-annual variability. Only APCC model rainfall is in phase with observed SPI rainfall variations on the inter-annual time scale. More research work is required to improve both the statistical and dynamical models in making reliable long-range forecasts of NE Monsoon rainfall in the coming years.

.

Chapter-7

NE monsoon over Sri Lanka

Sri Lanka lies within the tropics between 5° 55' to 9° 51' North latitude and between 79° 42' to 81° 53' East longitude, with a tropical climate. The central part of the southern half of the island is mountainous with heights more than 2.5 Km. The remainder of the island is practically flat except for several small hills that rise abruptly in the lowlands. These topographical features strongly affect the spatial patterns of winds, seasonal rainfall, temperature, relative humidity and other climatic elements, particularly during the monsoon season.

7.1. **Mean Rainfall**

Sri Lanka received rainfall due to southwest and northeast monsoons, local convective storms (thunderstorms) and low-pressure systems like lows/depressions moving across the region. The mean annual rainfall varies from 900 mm in the driest parts (southeastern and northwestern) to over 5000 mm in the wettest parts (western slopes of the central highlands). Fig 7.1 shows the spatial distribution of annual rainfall over Sri Lanka taken from the Sri Lanka Met Department.

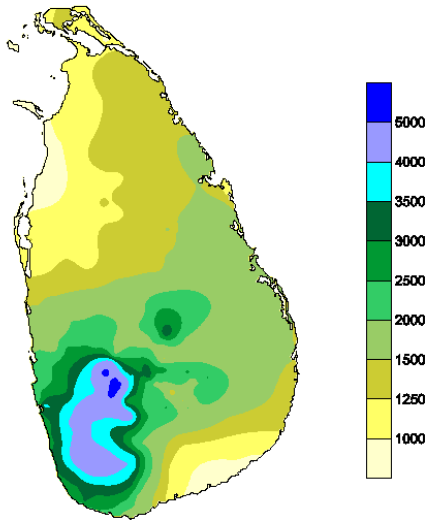

Fig 7.1 Annual rainfall over Sri Lanka in mm. (Source: Sri Lanka Met Department).

As per the Sri Lanka Met Department, the seasons in Sri Lanka are classified into 1) First inter-monsoon season (March-April) 2) Southwest monsoon (May- September) 3) Second Inter-monsoon season (October-November) and 4) Northeast monsoon (December-February). The spatial distribution of mean rainfall during these four seasons are shown in Fig 7.2.

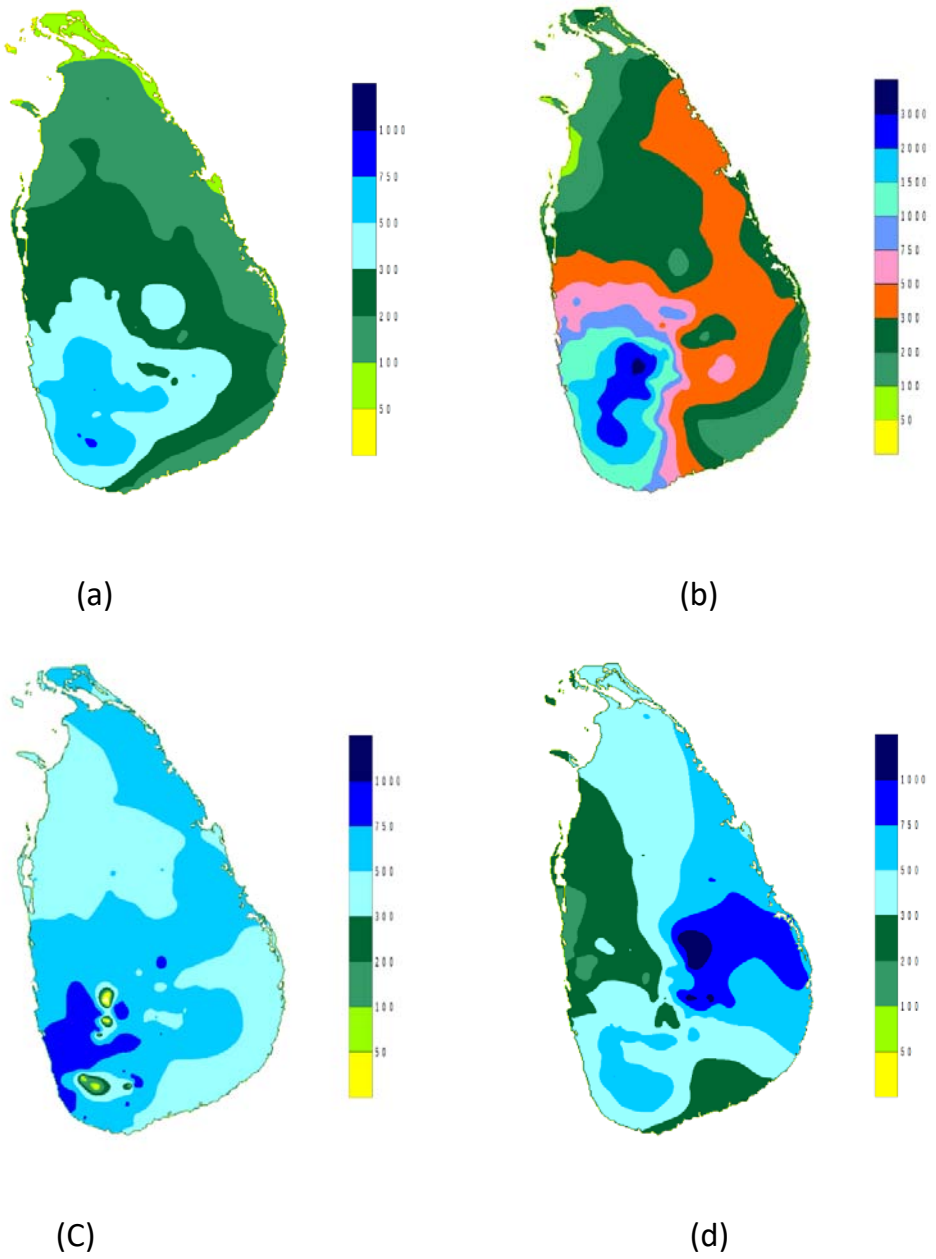

(a) (b)

(C) (d)

Fig. 7.2. Mean rainfall in mm during a) March-April b) May-Sept c) Oct-Nov and d) Dec-Feb. Source: Sri Lanka Meteorological Department.

The months October-November contributes maximum rainfall with the whole country experiencing rainfall more than 300 mm. Except during December-February, maximum rainfall is observed over the western coast, especially the southwest coast. During the December-February season, maximum rainfall is observed over the east coast.

The monthly mean rainfall averaged over the whole Sri Lanka is shown in Fig.7.3. This time series was prepared using the merged rainfall data of CHIRPS (https://www.chc.ucsb.edu/data/chirps). The Climate Hazards Group InfraRed Precipitation with Station Data (CHIRPS) is a 35+ year quasi-global rainfall data set ranging from 1981 to near present. This data set incorporates o.05^0 resolution satellite imagery and in-situ station data.

This plot of monthly rainfall clearly suggests that October-December months contribute to maximum rainfall over Sri Lanka. Another smaller peak is observed in April and May. This peak could be associated with the northward movement of ITCZ from the equator and associated convective activity, before the southwest monsoon sets in. During the month of April and May, the ITCZ starts moving northwards and there could be large scale convective activity associated with this movement due to low-level convergence and abundant moisture content.

For the rest of this chapter, we refer to October to December as the northeast monsoon (NEM) season, consistent with the designation of the India Meteorological Department (IMD).

Domroes and Ranatunge (1992) have identified three types of orthogonal structure of the monsoon regime in Sri Lanka using long-term mean monthly rainfall data. Their analysis revealed that a large amount of rainfall occurs from March to October in the southwestern parts of Sri Lanka, from December to February in the eastern parts, and in November in the northern and mid-western parts. Orthogonal factor scores for the first three factors account for 93.6% of the total variance of mean monthly rainfall. Seasonal

changes in the monsoon wind system, ITCZ weather phenomena, and topography are the main factors which influence the spatial structure of monsoon rainfall over Sri Lanka.

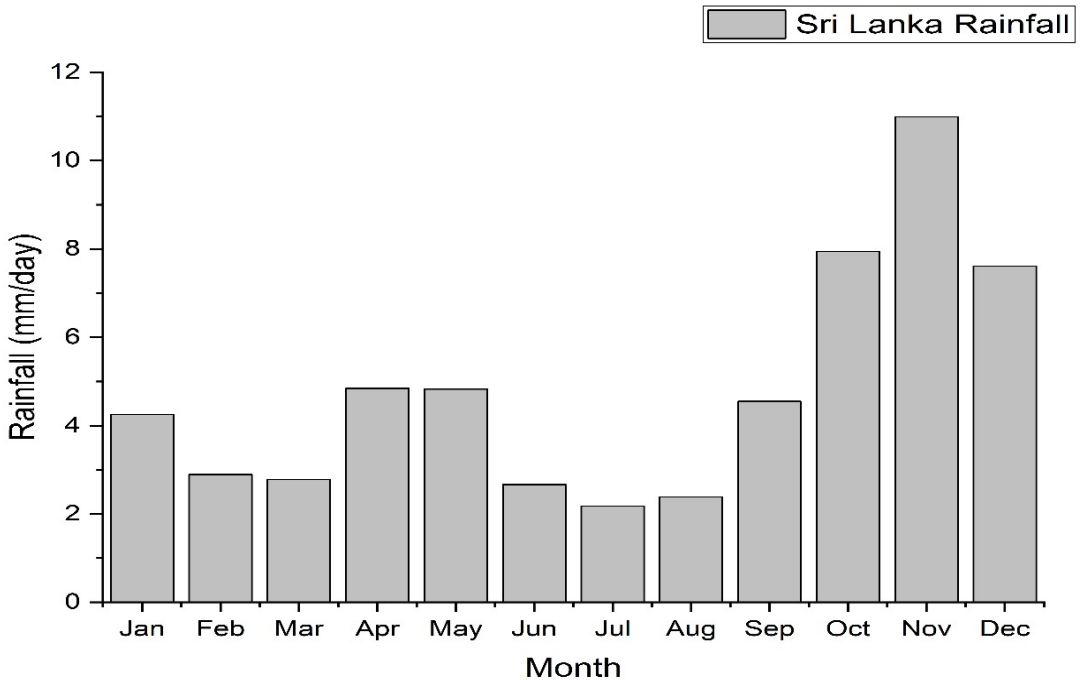

Fig. 7.3 Mean Monthly rainfall (mm/day) averaged over Sri Lanka using CHIRPS data.

Nisansala et al. (2019) analyzed Sri Lanka rainfall using the data during the period 1987-2017. They found increasing trends in annual rainfall at 24 stations with five stations showing significant increasing trend. Annual rainfall at 13 locations (35%) showed decreasing trend, but these trends were not significant ($p < .05$). There is an increasing trend at 76, 51, 32, and 86% of stations during the First Inter-Monsoon (FIM), Second Inter-Monsoon (SIM), South West Monsoon (SWM), and North East Monsoon (NEM) seasons, respectively. In general, the eastern, south eastern, north and north central regions of the country showed increasing rainfall trend over the last 31 years (1987–2017) while western, part of north western and central part of the country indicated a decreasing rainfall trend during the same period. The annual trend in rainfall is shown in Fig. 7.4 below.

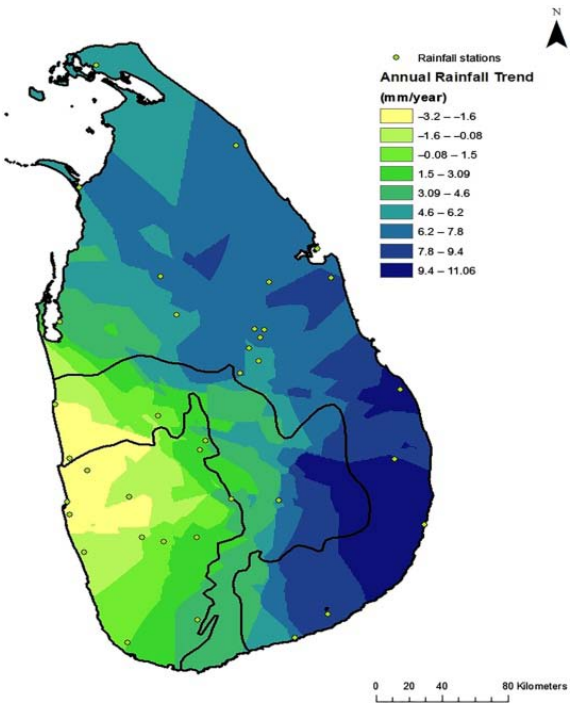

Fig 7.4. Spatial distribution of linear trends of annual rainfall for the period 1987-2017. This plot is taken from Nisansala et al. (2020).

In Sri Lanka, convective activity with lightning contributes abundant quantity of rainfall. Jayawardhana et al. (2014) studied the lightning activities over Sri Lanka using data Lightning Imaging Sensor of TRMM Satellite. The period 1998-2012 was used for the analysis. The highest occurrence of lighting activities is confined to the highly populated western part of the island while the south eastern and mountain areas have low occurrences. There is a clear spatial polarization of lightning activities during the south-west and north-east monsoon seasons. There is an increasing trend in lightning activities, they appear to be increasing by 50 flashes per year. It has a seasonal dependency with the south-west and first inter-monsoon seasons having the higher increase. The percentage of lightning per month is highest (46%) during the Inter-monsoon-1 period and the lowest (7%) during the Northeast monsoon season. Second highest percentage of lightning per month (25%) can be observed during the inter-monsoon-2 period followed by the Southwest monsoon (22%) period.

During the Oct-Dec season, Sri Lanka receives rainfall, often heavy rainfall due to westward moving depressions and tropical cyclones over the south Bay of Bengal. Fig 7.5 shows the tracks of depressions and tropical cyclones which crossed the coasts of Sri Lanka during the October-December season for the period, 1971-2021.

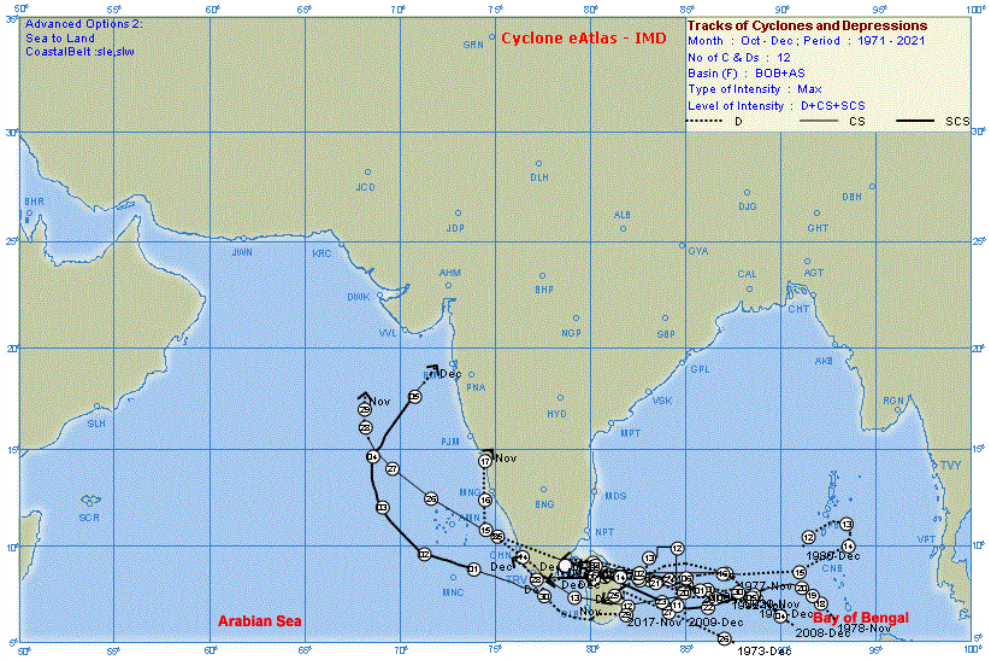

Fig. 7.5 Tracks of Depressions and tropical cyclones crossing the coasts of Sri Lanka during the period Oct-Dec, 1971-2021.

7.1. **Diurnal Variations.**

An analysis of diurnal variations over Sri Lanka was made using sub-daily TRMM data set for the period 1998-2019. Similar results for the NE monsoon season over the south peninsula are discussed in Chapter-6 (section 6.1). The same methodology was followed for this analysis also.

Fig 7. 6 shows the three hourly mean rainfall over Sri Lanka and adjoining region, averaged during the period 1998-2019. The plot clearly shows that there is significant diurnal variation of rainfall over Sri Lanka and neighborhood during the NE monsoon season. The changes are more evident over the western parts of Sri Lanka, where

rainfall peaks during the evening time (09-12 UTC). Over the eastern parts and adjoining oceanic area, there is hardly any diurnal variation, but a major peak during the early hours (00-03 UTC).

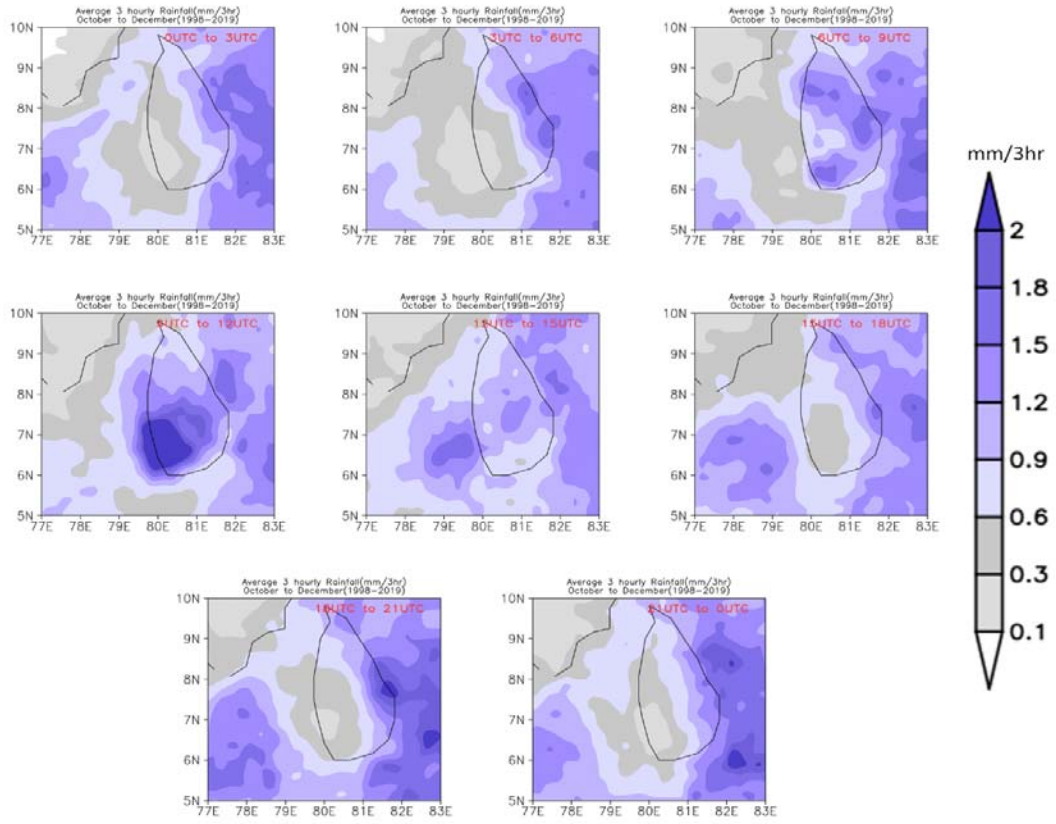

Fig. 7.6. Three hourly mean rainfall over Sri Lanka and neighborhood, averaged using the TRMM satellite data of 1998-2019.

The similar results are revealed in the Phase diagram obtained from the Harmonic analysis as shown in Fig 7.7. The phase diagram shows clear peaking of rainfall during evening and early night hours, which is consistent with Fig 7.6. This peaking could be associated with the solar heating during day time and initiation of convection. More studies are required to establish the physical mechanisms for this observed diurnal pattern. Also, it is important to understand whether the NWP model is capable of predicting this observed diurnal pattern over Sri Lanka.

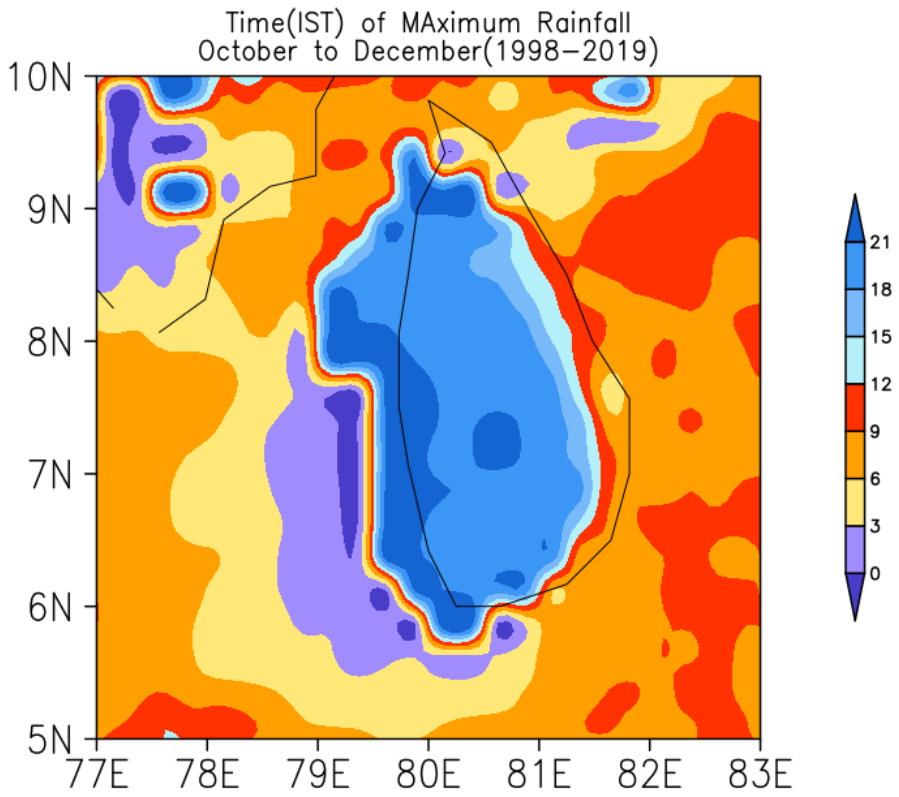

Fig.7.7. The phase diagram of the harmonic analysis of hourly rainfall using the satellite data of 1998-2019. The phase diagram shows the time (IST) of maximum rainfall.

7.2. **Intra-seasonal variations**

There are not many studies addressing the intra-seasonal variability of the NE monsoon rainfall over Sri Lanka, which is an important component of rainfall variability. Therefore, a preliminary analysis on the intra-seasonal variability of rainfall over Sri Lanka is done and the results are discussed below.

Fig 7.8 shows the daily rainfall averaged over Sri Lanka during the period 1 Oct 2018- 31 Jan 2019 (above) and 1 Oct 2019- 31 Jan 2020 (below). These two years are selected just as examples to show the rainfall variations within the season. The plot suggests that there is significant rainfall variability within the season, with specific periods of more rainfall, interspaced with little or no rains.

To examine whether daily rainfall has particular periodicity, a spectral analysis of daily rainfall was made for both the years, 2018-2019 and 2019-2020. The results are shown in Fig 7.9.

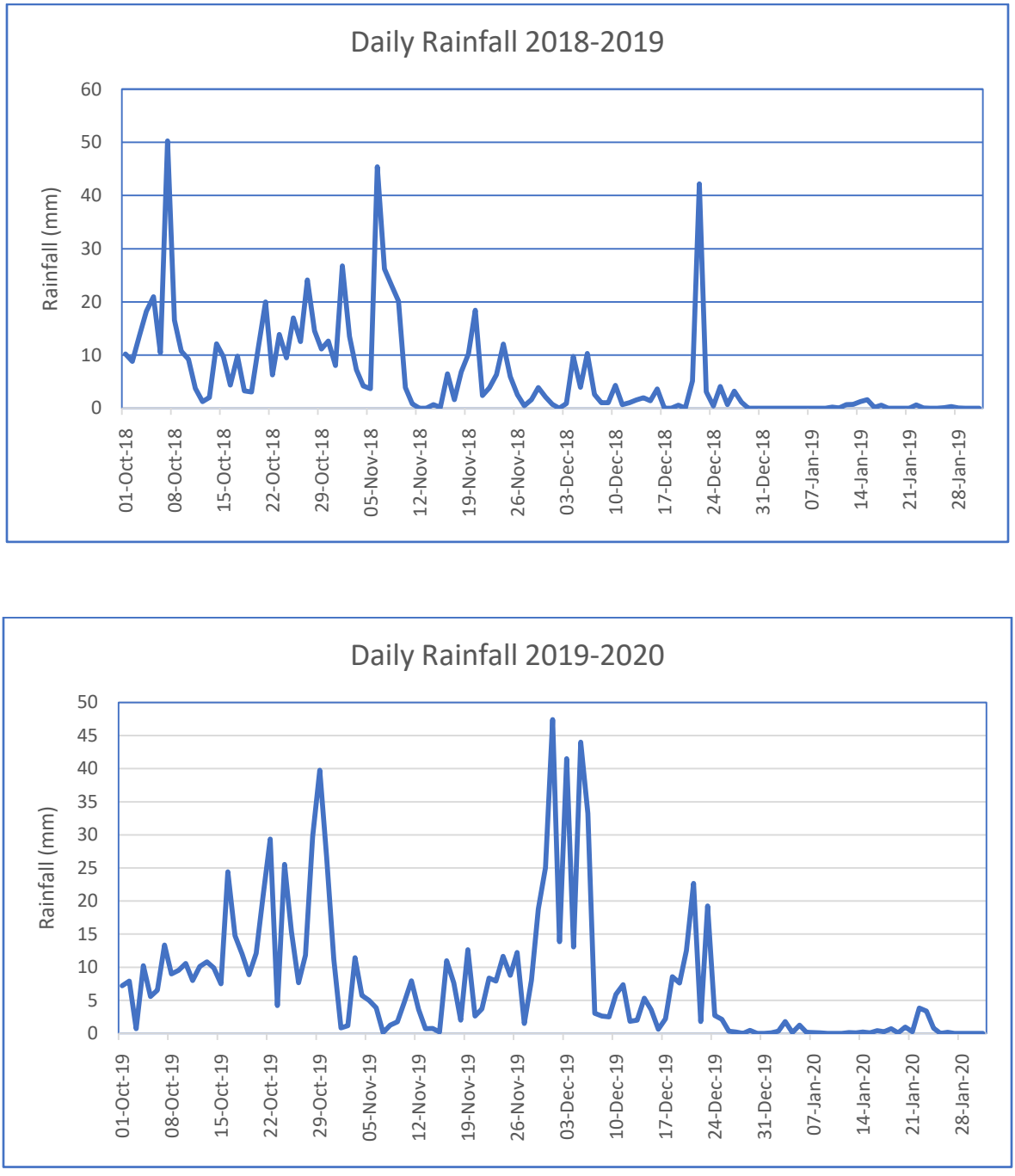

Fig 7.8. Daily rainfall (in mm) averaged over Sri Lanka during the period 1 Oct 2018- 31 Jan 2019 (above) and 1 Oct 2019- 31 Jan 2020 (below).

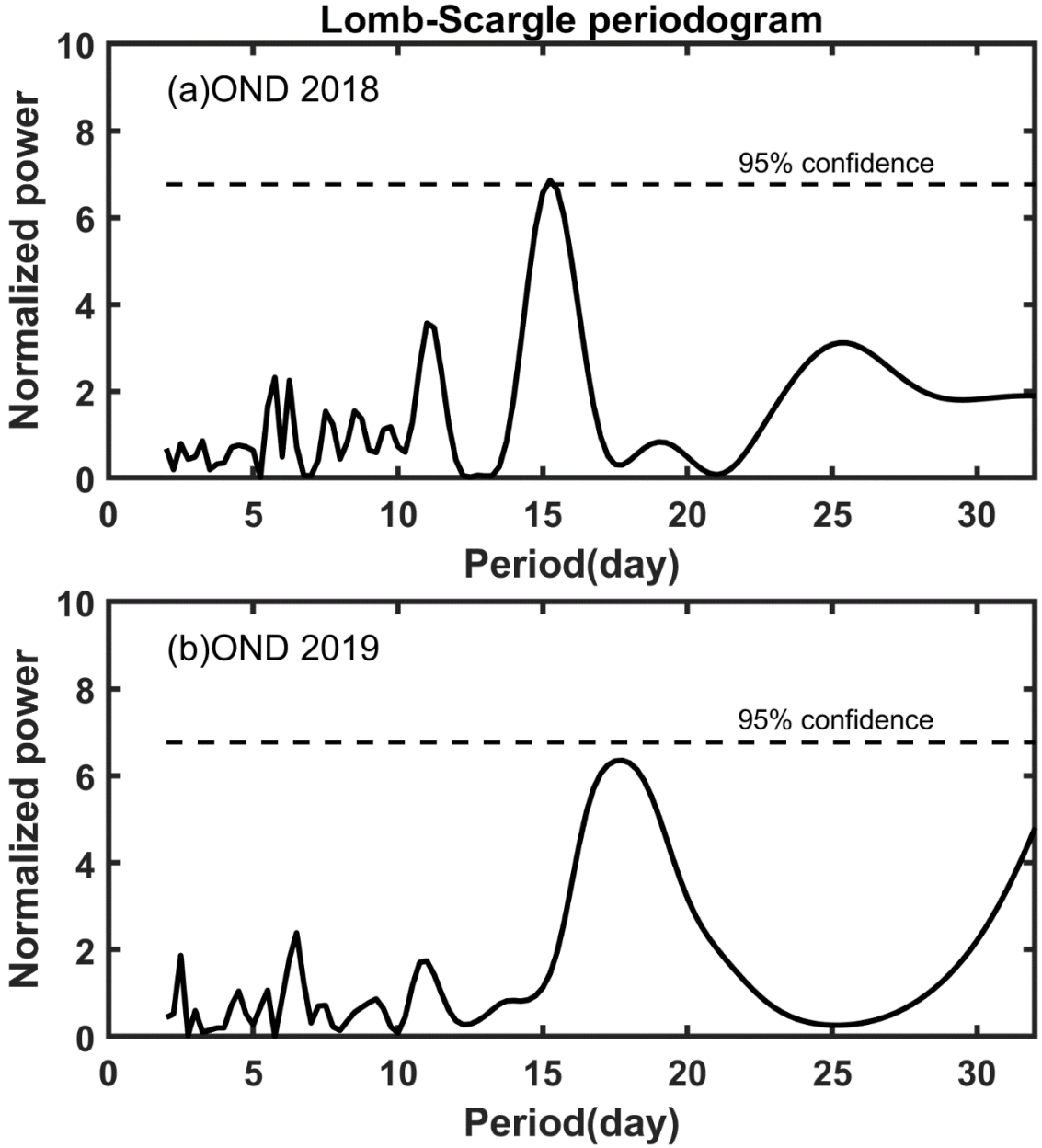

Fig 7.9. The spectral analysis (Lomb-Scargle periodogram) of daily rainfall for the two seasons. 2018-2019 (above) and 2019-2020 (below). The 95% significance level is shown as horizontal line in both the plots.

The results indicate that there is a strong periodicity of about 15-20 days, which is statistically significant. The physical mechanisms of such periodicity are immediately

not known. More studies are required to understand the intra-seasonal variability of rainfall over Sri Lanka and to examine the skill of its predictions using NWP models.

7.3. **Inter-annual variations**

A detailed analysis of year to year variations of NE monsoon over Sri Lanka is discussed in this section. There are only a few studies on the inter-annual variability of NE monsoon rainfall over Sri Lanka.

Suppiah (1996) studied the spatial and temporal variations in the relationships between the Southern Oscillation Index (SOI) and rainfall over Sri Lanka. Major changes in spatial patterns of correlations between seasonal rainfall and the SOI have occurred in Sri Lanka during the Southwest monsoon (SWM) and Second inter-monsoon (SIM) seasons. The periods of strong positive (negative) correlations during the SWM season coincide with weak (strong) negative correlations during the SIM season. This contrasting pattern is clear when the Indian and Sri Lankan summer monsoon rainfalls were out of phase between 1900 and 1960, but not before 1900, or after 1960. The sudden change in correlations around 1960 suggests a change in the coupled ocean–atmosphere system that dominates the climate of these regions.

Suppiah (1997) studied the extremes of the Southern Oscillation (SO) Phenomenon over the equatorial Pacific and Sri Lanka rainfall. There were 27 El Niño and 22 La Niña events, during the period from 1881 to 1990. Positive and negative rainfall anomalies during the south-west monsoon (SWM) season are associated with La Niña and El Niño events, but negative and positive rainfall anomalies are linked to La Niña and El Niño events during the second intermonsoon (SIM) season. These contrasting patterns are dominant in the dry zone of Sri Lanka.

Zubair and Ropelewski (2006) reported that the relationship between ENSO and the northeast monsoon (NEM) in south peninsular India and Sri Lanka from October to December has not weakened. The mean circulation associated with ENSO over this region during October to December does not show the weakening evident in the

summer and indeed is modestly intensified so as to augment convection. The intensification of the ENSO–NEM rainfall relationship is modest and within the historical record but stands in contrast to the weakening relationship in summer. There is modestly intensified convection over the Indian Ocean, strengthening of the circulation associated with ENSO (Walker circulation), and enhanced rainfall during El Niño episodes in a manner consistent with an augmented ENSO–NEM relationship.

Zubair et al. (2009) studied the predictability of Sri Lankan rainfall based on ENSO. The El Niño-Southern Oscillation (ENSO) is a primary mode of climate variability of this area. They found that the rainfall is modestly predictable based on ENSO during January–March, July–August and October–December. El Niño typically leads to wetter conditions during October to December and drier conditions during January to March and July to August on average. The correlations of ENSO indices with rainfall are statistically significant for October to December, January to March and July to August and an analysis based on contingency tables shows modest predictability. The use of ENSO indices derived from the central Pacific Ocean improves the predictability from January to June. The predictability based on ENSO for October to December rainfall is robust on a decadal scale.

Abeysekera et al. (2019) studied the relationship between ENSO and rainfall over Sri Lanka. The results clearly revealed a significant reduction of rainfall during both First Inter Monsoon (FIM) and North East Monsoon (NEM) seasons during the El Niño years. The Second Inter Monsoon (SIM) season showed a positive anomaly of rainfall during the El Niño years. However, the effect of El Niño condition on the Southwest Monsoon season (SWM) was not consistent. During La Niña conditions, an above normal rainfall was observed in the FIM, SWM and NEM seasons where the strongest correlation was evident during the NEM season. The SIM season has shown a below normal rainfall during the La Niña period.

Using the seasonal (OND) rainfall over Sri Lanka, a detailed analysis on the inter-annual variability and its teleconnections with ENSO and IOD has been carried out. Fig 7.10 shows the year to year variations of NE monsoon rainfall over Sri Lanka, expressed as percent deviations. The OND mean monsoon rainfall (1971-2021) is 822 mm with 23% as coefficient of variation. Therefore, Sri Lanka receives much more rainfall during the NE monsoon season, compared to the south peninsula and even comparable with the southwest monsoon rainfall over India for four months (June to Sept), which is 870mm.

The green (red) lines suggest excess (deficient) monsoon years. During the period, 1961-2021, there were 12 deficient monsoon years and 10 excess monsoon years. In 1980s and 1990s, Sri Lanka experienced more deficient years. During the recent decade there were four excess years and two deficient years.

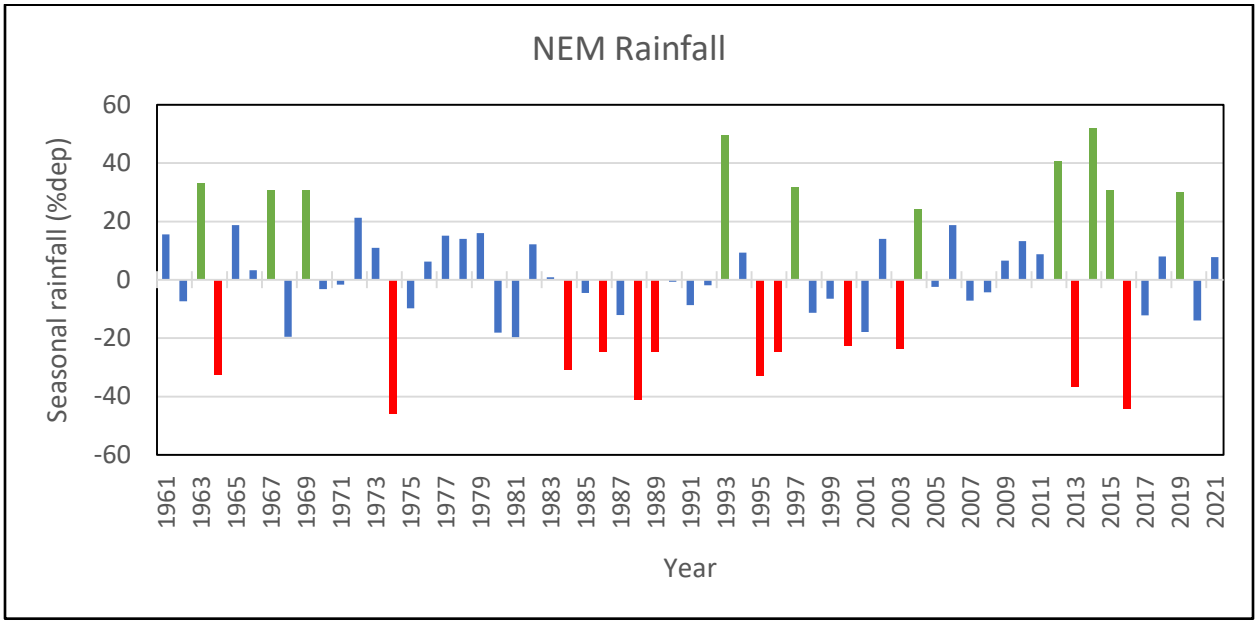

Fig 7.10. The inter-annual variation of NE monsoon rainfall (OND) over Sri Lanka, expressed as percent departures.

A spectral analysis of seasonal rainfall is made and the results are given below. Fig 7.11 a shows the spectral normalized power (Lomb-Scargle periodogram) using the data of 1961-2021. It suggests a peak around 2-3 years, but this periodicity is statistically not significant. The wavelet analysis shows the periodicity of 2-4 years during 1990-2000 and in the recent years, 2010-2020 as shown in Fig 7.11 b.

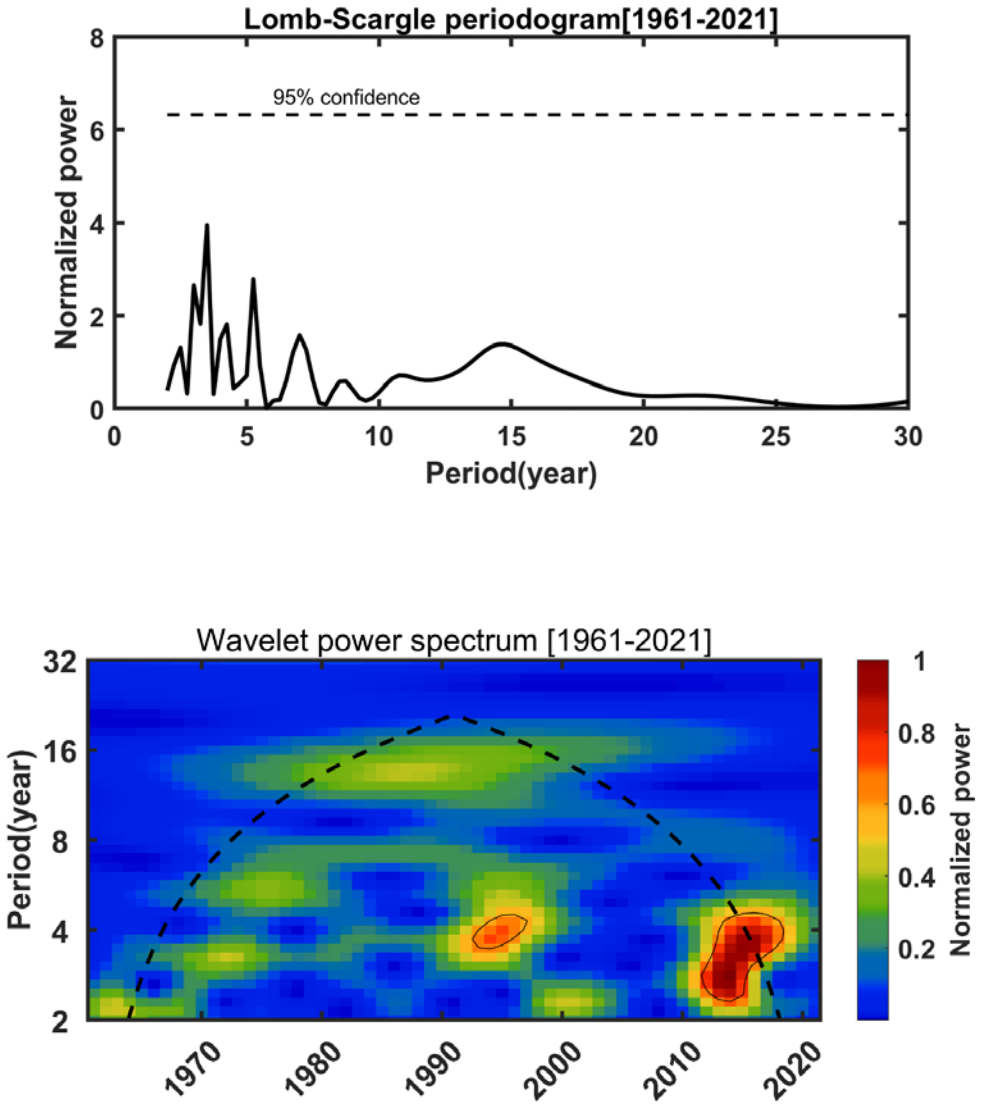

Fig 7.11. Spectral analysis of NE monsoon seasonal rainfall (1961-2021). a) the normalized power using the Lomb-Scargle periodogram and b) wavelet power spectrum. The 95% significance cone is also shown in Fig 7.11 b.

Further, to explore the teleconnections with global forcings like ENSO, IOD etc, a spatial analysis of correlations between the NE monsoon rainfall and SST, OLR and 850 hPa zonal winds was done and the results are shown in Fig 7.12. There is significant correlation between NE monsoon rainfall and SST over the equatorial Pacific (Fig 7.12 a) and the equatorial Indian Ocean (Fig 7.12 b), representing the influence of ENSO and IOD events. Please note the dipole like correlation patterns over the equatorial Indian Ocean with negative (positive) correlation over the east equatorial Indian Ocean. Thus, the NE monsoon rainfall is positively correlated to ENSO and IOD. An El Nino event and positive IOD event are likely to enhance seasonal rainfall over Sri Lanka. This relationship is further seen in Fig 7.12 c and d. The NE monsoon rainfall over Sri Lanka is positively correlated with the zonal winds over the equatorial east Pacific, but negatively correlated with the zonal winds over the equatorial west Pacific Ocean. The same kind of relationship exists with OLR also, suggesting the strong influence of ENSO and IOD events.

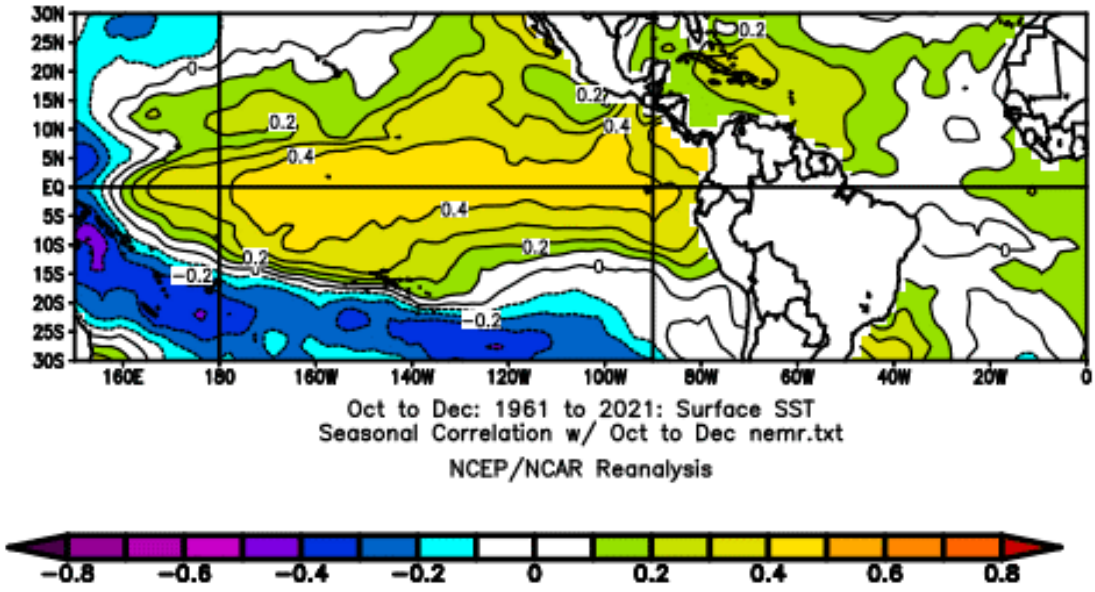

Fig 7.12 a Spatial distribution of correlations between OND NE monsoon rainfall and Sea Surface Temperatures (SST) during the period 1961-2021.

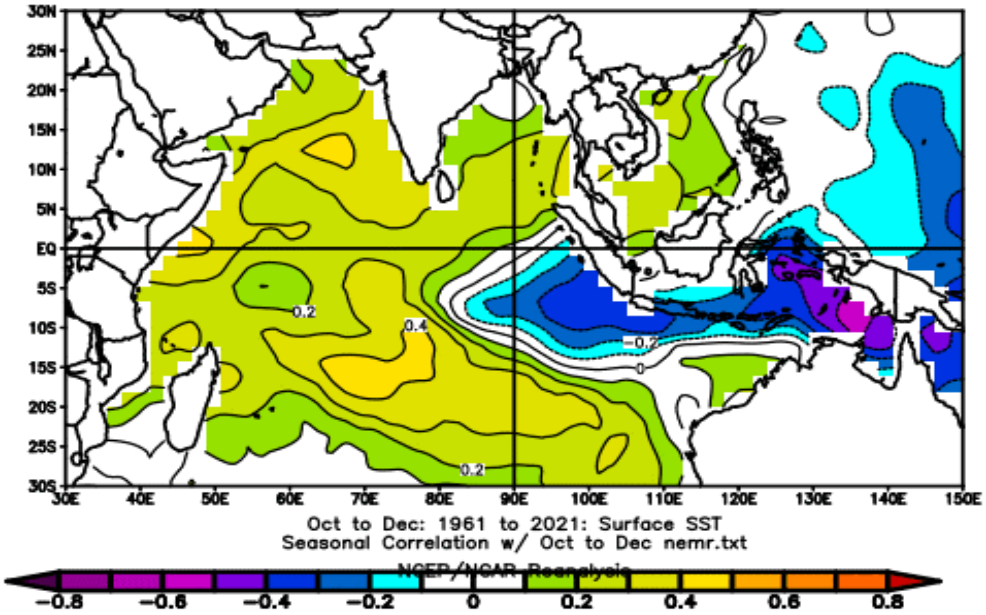

Fig 7.12 b Spatial distribution of correlations between OND NE monsoon rainfall and Sea Surface Temperatures (SST) during the period 1961-2021.

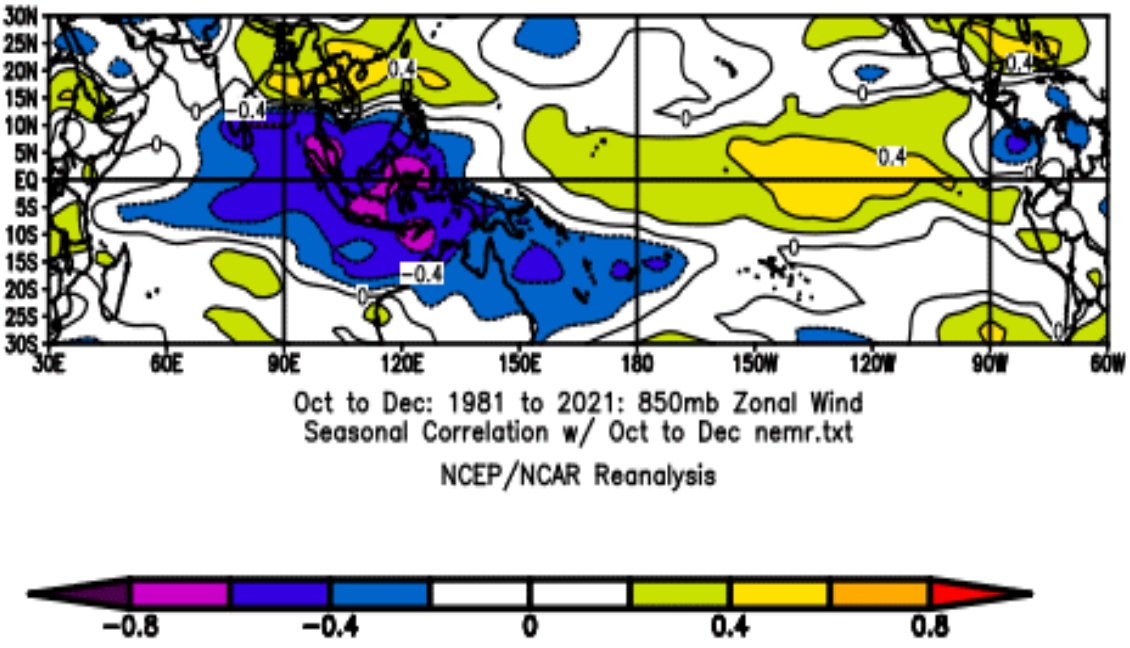

Fig 7.12 c Spatial distribution of correlations between OND NE monsoon rainfall and 850 hPa zonal wind during the period 1961-2021.

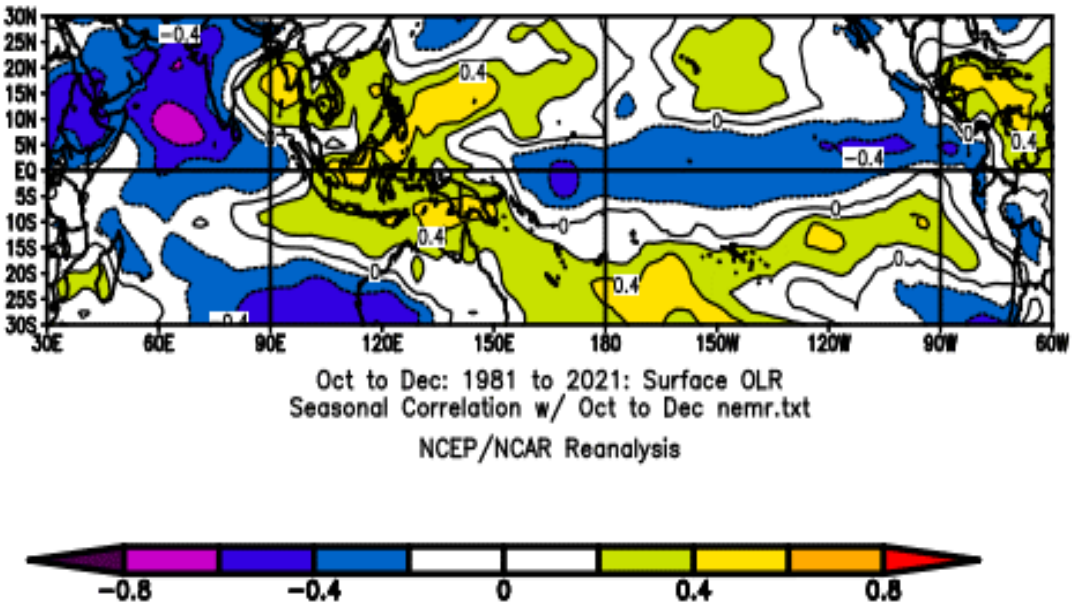

Fig 7.12 d Spatial distribution of correlations between OND NE monsoon rainfall and OLR during the period 1961-2021.

Fig 7.13 a shows the monthly variations of correlations between monthly Nino 3.4 and IOD index with OND NE monsoon rainfall over Sri Lanka. The plot shows the concurrent and strong correlations between Nino 3.4 and IOD Index with monsoon rainfall. Comparatively, IOD index has stronger correlation with NE monsoon rainfall over Sri Lanka compared to the Nino 3.4 during the OND season. But what is more important is that statistically significant correlations are observed even before the NE monsoon season, especially with the Nino 3.4. For example, the Nino 3.4 is significantly correlated right from May onwards with the NE monsoon rainfall over Sri Lanka. Similarly, the IOD index during August and September months is significantly correlated with NE monsoon rainfall. These inferences suggest scope for long range predictability of NE Monsoon rainfall over Sri Lanka. More work is required to explore these relationships and to develop useful long-range prediction methods.

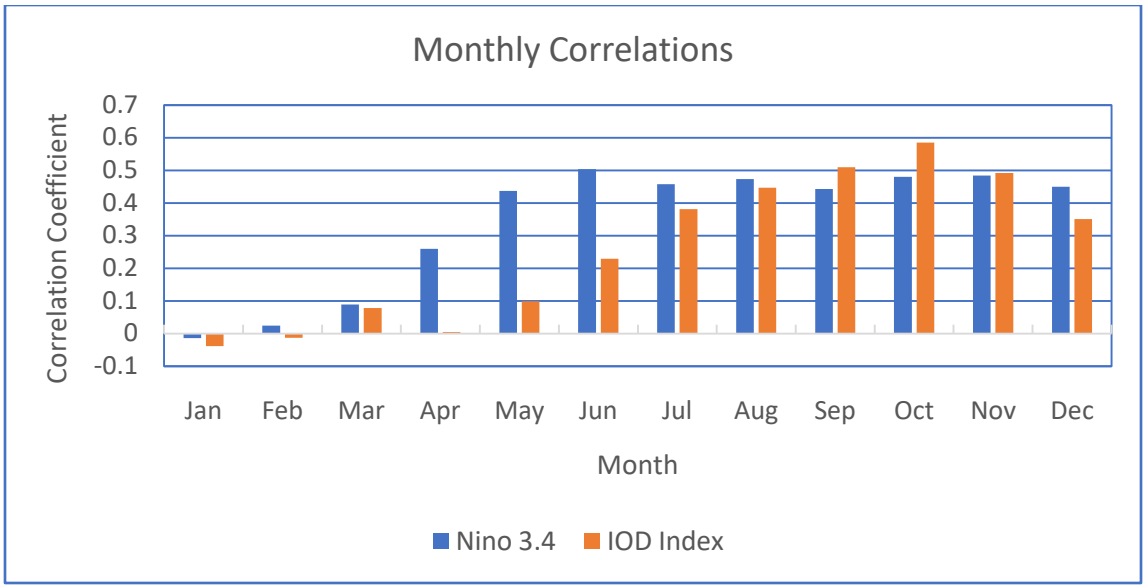

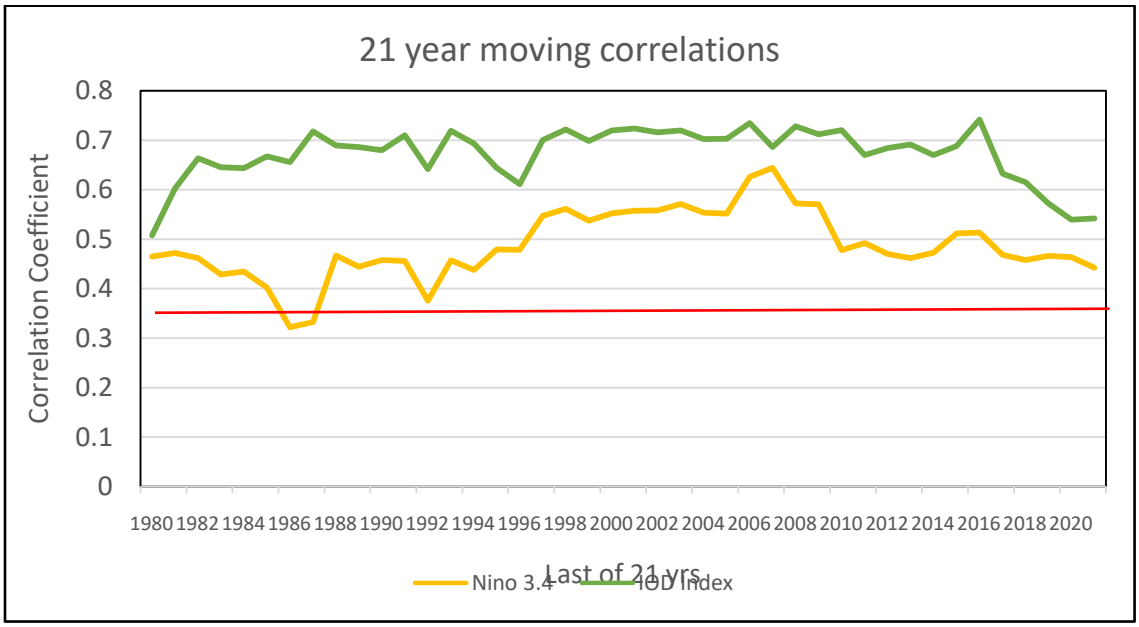

Fig 7.13 a) Monthly correlations between Nino 3.4 (Blue) and IOD index (red) with OND NE monsoon rainfall. Data of 1961-2021 was used. b) the 21 year moving correlations between OND Nino 3.4 (Orange colour) and OND IOD index with the OND NE monsoon rainfall showing secular variations.

.

Fig 7.13 b shows the 21-year running correlations between the NE monsoon rainfall and the Nino 3.4 and IOD index, showing the secular variations of the relationships. It shows the relationship has been more or less very robust throughout the analysis period (1981-2021). However, during the recent years, the correlation strength is shown as decreasing, especially the IOD Index. More work is required to understand the physical reasons for this observed weakening of the relationships.

Chapter-8

Numerical Weather Prediction Guidance

Numerical Weather Prediction (NWP) Models are extensively used to prepare forecasts for short to medium range forecasts (up to 10 days) and extended range forecasts (up to one month). Over the years, the skill of NWP systems has improved substantially due to a) better assimilation methods of more quantity of data including non-conventional data b) higher resolution NWP models c) improved model Physics and d) better methods of post-processing of model output data. At the Ministry of Earth Sciences (MOES), there are two global forecasting systems which are now operational. The first system is based on the NCEP Global Forecasting System (GFS) model, which IMD uses to prepare the forecasts, four times a day (0000, 0600, 1200 and 1800 UTC). These are deterministic forecasts up to 10 days. The GFS model is a global model with 12 km horizontal resolution. Using the same model, an ensemble prediction system was also developed by IITM scientists and put on operational work by IMD. This system operational since 2017, provides probability forecasts of different parameters. All these IMD forecast products are available at the IMD website https://nwp.imd.gov.in/gfsproducts_cycle00_mausam.php.

Another operational system is used by NCMRWF, Noida for generating forecasts (both deterministic and ensemble) twice a day. The NCMRWF Unified Model (NCUM) was implemented in 2012 with a grid resolution of 25km (NCUMG:V1) which was upgraded to 17km (NCUM-G:V3) in 2015, 12km (NCUM-G:V5) in 2018. The present version (NCUM-G:V6) of NCUM-G has a horizontal grid resolution of ~12 km with 70 levels in the vertical reaching 80 km height. An advanced data assimilation method of Hybrid 4-Dimensional Variational (4D-Var) is used for the creation of NCUM global analysis. The NCMRWF forecast products are available at https://www.ncmrwf.gov.in/

There are not enough studies on systematic verification of weather forecasts for the NE monsoon season, except the two reports brought out by NCMRWF for 2020 and 2021 seasons.

Salient aspects of verification of forecasts during November 2021 using the NCMRWF model are given below.

November 2021 witnessed unprecedented rainfall activity over south peninsula during the NE monsoon season. Fig 8.1 shows the monthly accumulated rainfall during November 2021 and its anomalies. This shows above normal rainfall activity over South Peninsula with more than 100 mm excess rainfall over parts of Tamil Nadu and Rayalaseema.

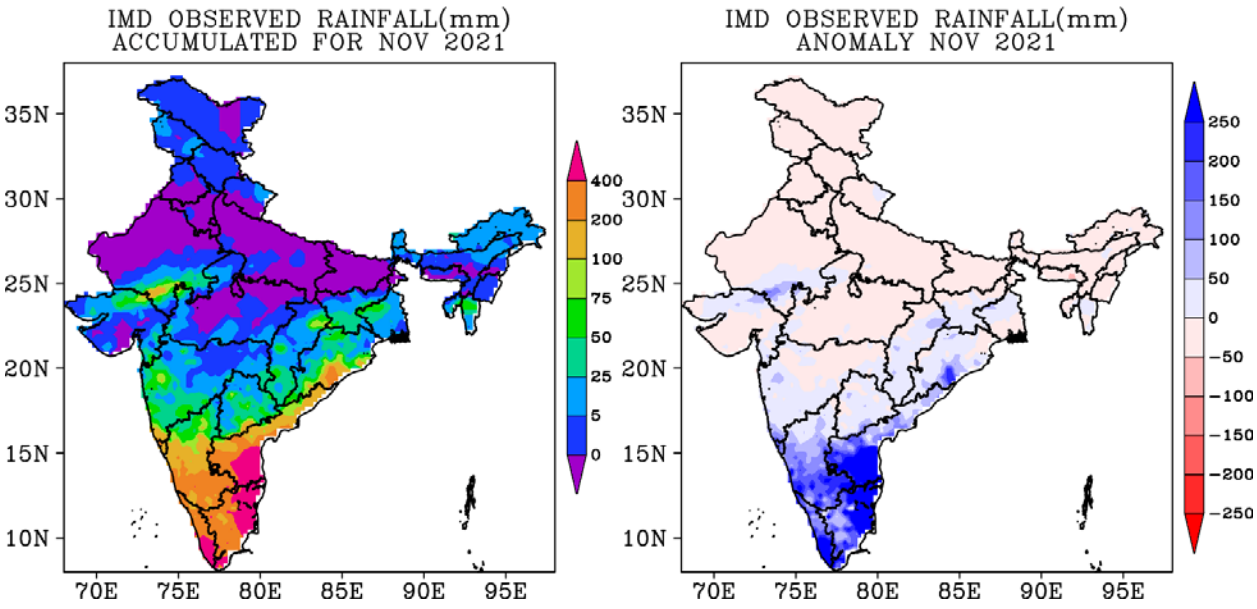

Fig 8.1. Observed monthly rainfall (IMD) during November 2021 (left) and its anomaly (right). Unit: in mm.

Fig 8.2 shows the vertically integrated moisture transport (VIMT) integrated up to 300 hPa level. The NCUM analysis shows strong easterlies bringing abundant moisture towards south Peninsula. However, the NCUM model predictions underestimated this large-scale moisture transport towards South Peninsula. The anomalies are much bigger

in Day-5 forecast. The moisture transport was much weaker than observed. This has resulted in negative bias in rainfall over south Peninsula (Fig 8.3). Rainfall predicted by the model was less than that observed, even though the model predicted the spatial distribution of rainfall very well. The underestimation of rainfall could be related to under-estimation of moisture transport to the region in the lower tropospheric levels.

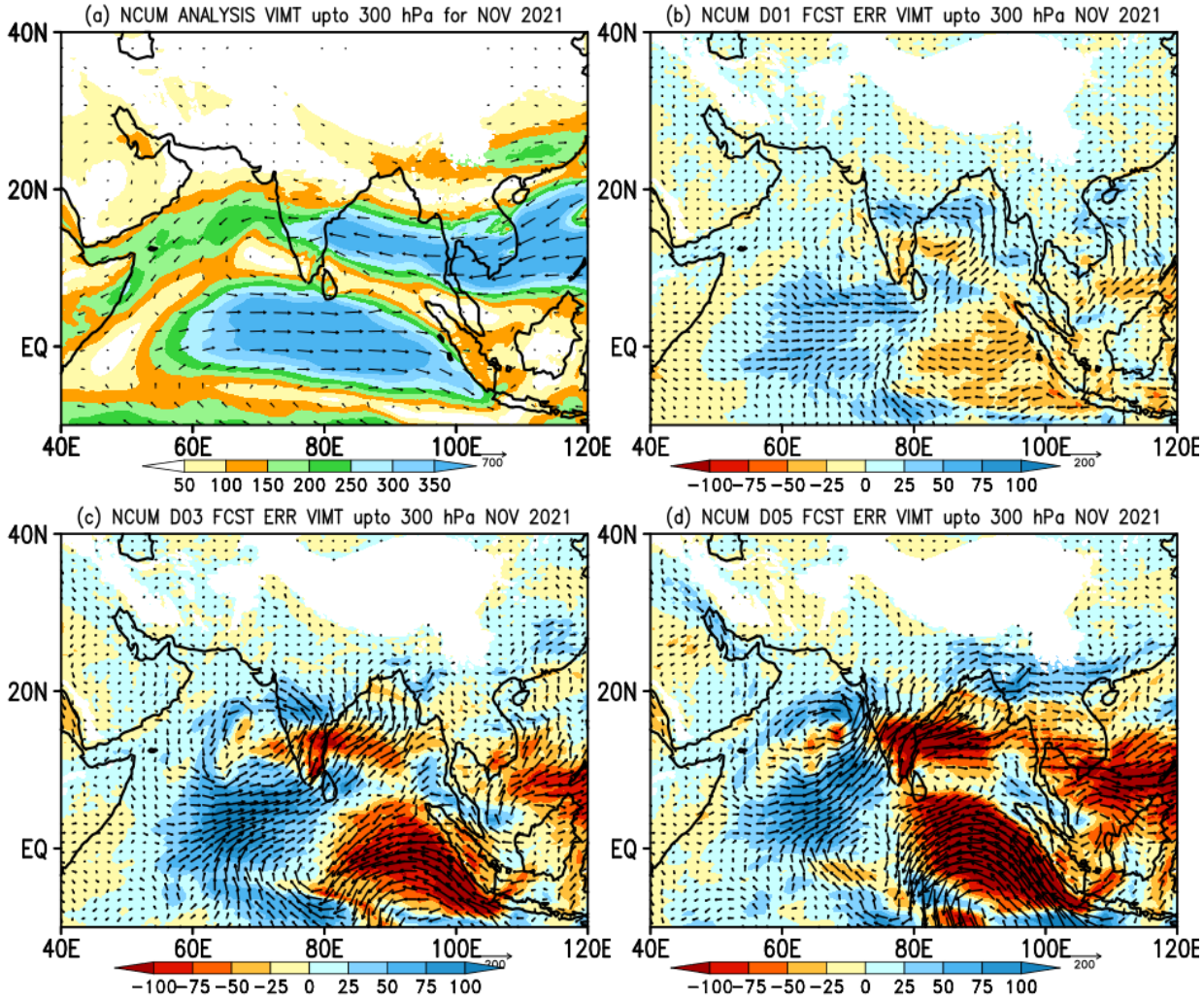

Fig 8.2. a) The NCUM model analysis of vertically integrated (up to 300 hPa) moisture transport (VMT) during Nov 2021. The forecast error in VMT for day-1 (b), day-2(c) and day-3(d).

The Skill scores of forecast categories with the NCUM model are given in Fig 8.4.

The Skill Scores are defined as follows:

1) Probability of Detection (POD): hits/(hits+misses)
2) False Alarm Rate (FAR)= False alarms/ (Hits+false alarms)
3) Critical Success Index (CSI)= Hits/ (hits+false alarms+misses)
4) BIAS= (hits+false alarms)/(total number of observed events)
5) Pierce's Skill Score (PSS)= hits/(hits+misses) – false alarms/(false alarms+correct negatives)
6) Symmetric Extreme Dependency Index (SEDI) is defined as

SEDI = (log F-log H-log (1-F)+log (1-H))/ (log F+ Log H+ log(1-F)+log (1-H)

Where, H is Hit rate and F is false alarm rate.

Probability of Detection (POD) is larger for lower rainfall thresholds, but it drastically reduces for larger amount of rainfall. POD for 2 cm rainfall at Day-1 forecast is close to 0.30, but it is around 0.1 for Dady-5 forecast. False Alarm Rate (FAR) is larger for higher amount of rainfall thresholds. FAR is more than 0.7 for larger amount of rainfall. Therefore, the model has tendency of over predicting frequency of higher amount of rainfall. The other skill scores (like CSI, BIAS, PSS and SEDI) are better for Day-1 and Day-3 forecasts but reduces sharply for Day-5 forecasts.

Next, a discussion is made on the fidelity of the NCUM model in predicting two weather systems which developed in November 2021 and affected South Peninsula. The first weather system was a low-pressure system that formed over the Bay of Bengal and moved northwestwards. It crossed the border of Tamil Nadu and Andhra Pradesh on 12 November 2021.

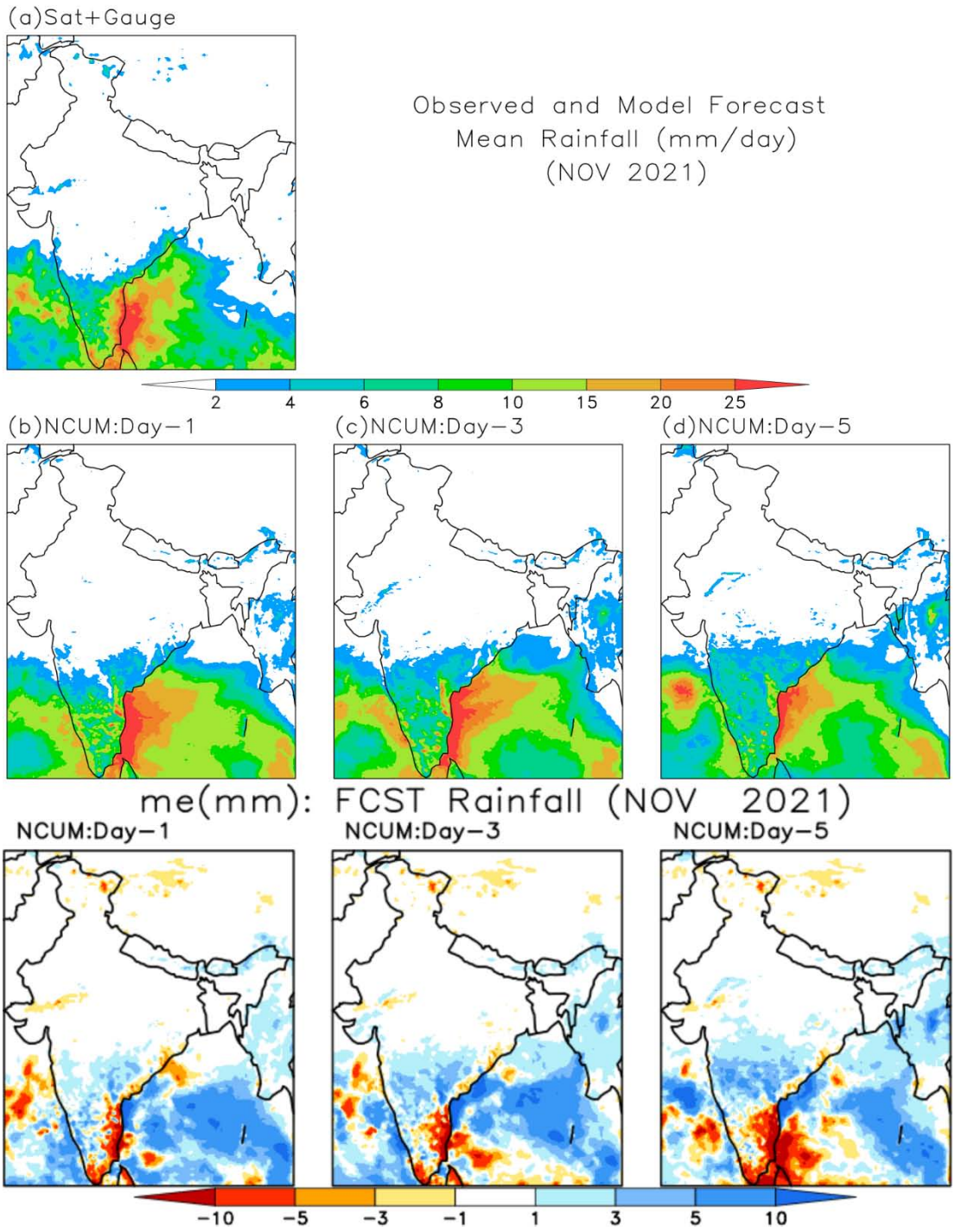

Fig 8.3. Observed and Model Forecast Mean rainfall (mm/day) during November 2021. a) Observed merged rainfall in mm/day. b) to d) represent model forecasts for day-1 to day-3. Bottom three plots show model forecast errors for day-1 to day-3 forecasts.

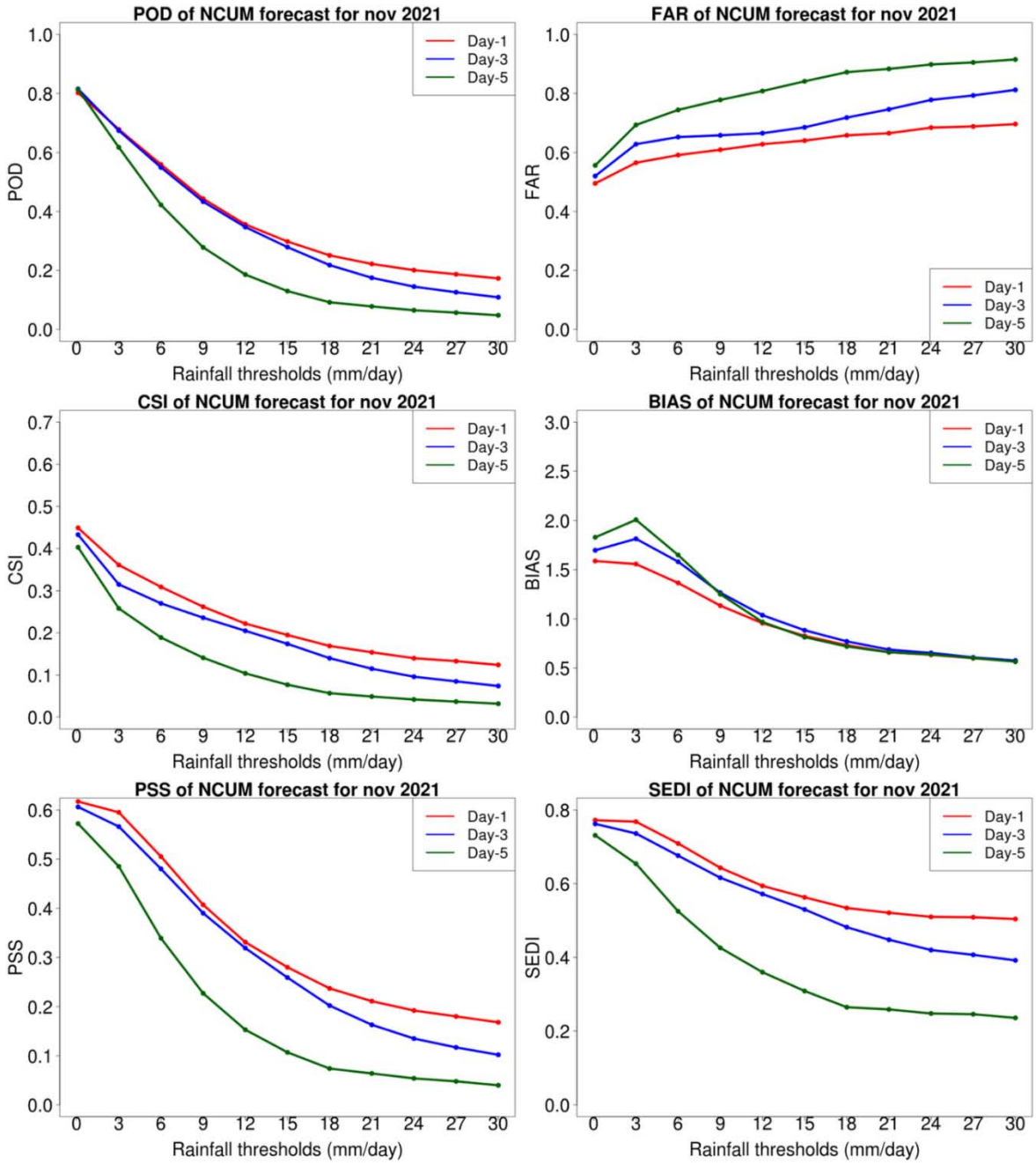

Fig. 8.4. Statistical Skill Scores for the NCUM forecasts of rainfall during November 2021, a) POD b) FAR c) CSI d) BIAS e) PSS and f) SEDI for day-1 to day-3 forecasts.

Fig 8.5 shows the 850 hPa wind analysis of 11 Nov 2021 and NCUM forecasts up to 120 hrs in advance. The low pressure system with cyclonic circulation was clearly seen in the analysis off Tamil Nadu coast on 11 November. It is interesting to see the

NCUM model is able to predict the presence of cyclonic circulation off the Tamil Nadu coast with similar intensity up to 72 hours in advance. However, beyond 72 hours, model could not predict the cyclonic circulation correctly. Accordingly, the rainfall activity is also well predicted by the model up to 72 hours in advance (Fig 8.6). Beyond 72 hours, the model under-predicted the intensity of rainfall and the model forecasts have shown large biases.

Fig 8.7 and Fig 8.8 show the same details but for another weather system which crossed the land near north Andhra Pradesh on 19 Nov 2021. As in the previous case, the model could predict the presence of cyclonic circulation off Andhra coast up to 72 hours in advance. Rainfall was also well predicted by the model up to 72 hours in advance.

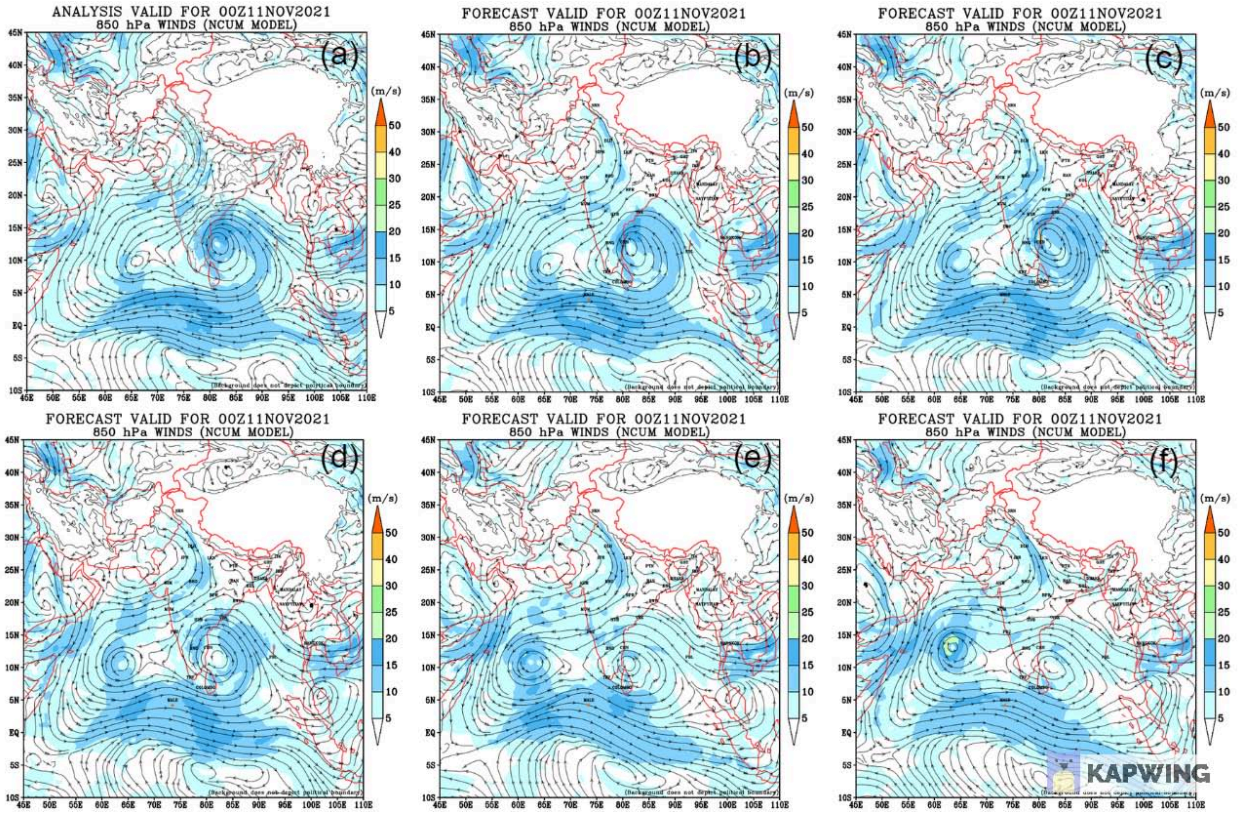

Fig 8.5. NCUM model analysis of 850 hPa winds at 0000 UTC, 11 November 2021 (a) and model forecast for day-1 (b), day-2 (c), day-3 (d), day-4 (e) and day-5 (f).

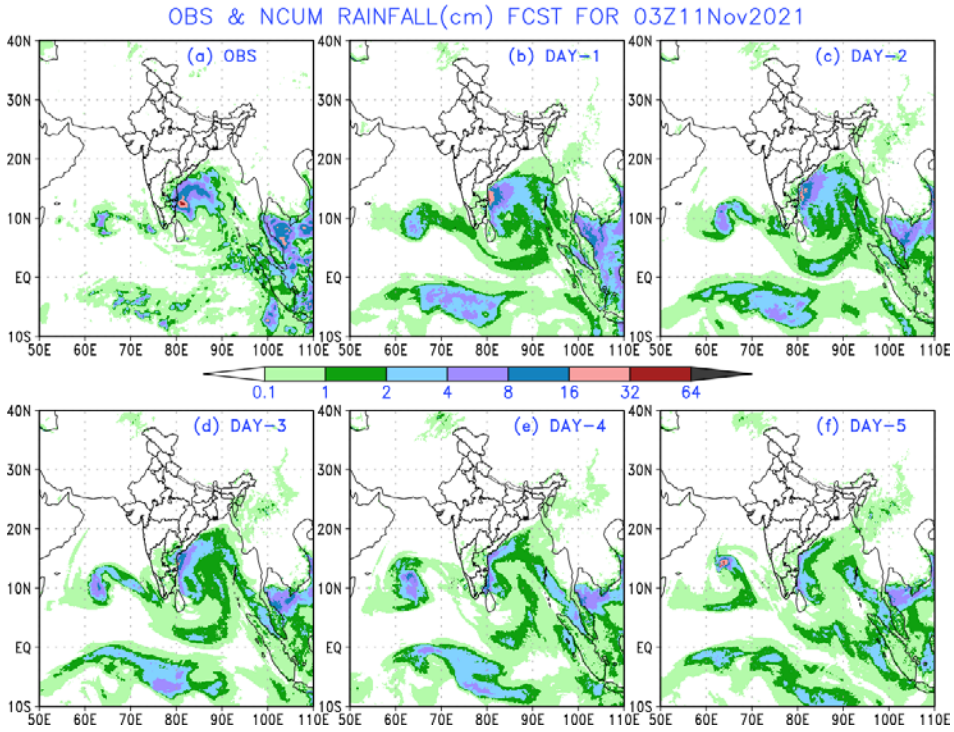

Fig 8.6. Observed and NCUM model predictions of rainfall (cm) for 03 UTC 11 November 2021. a) observed, b) to f) represent forecasts of day-1 to day-5.

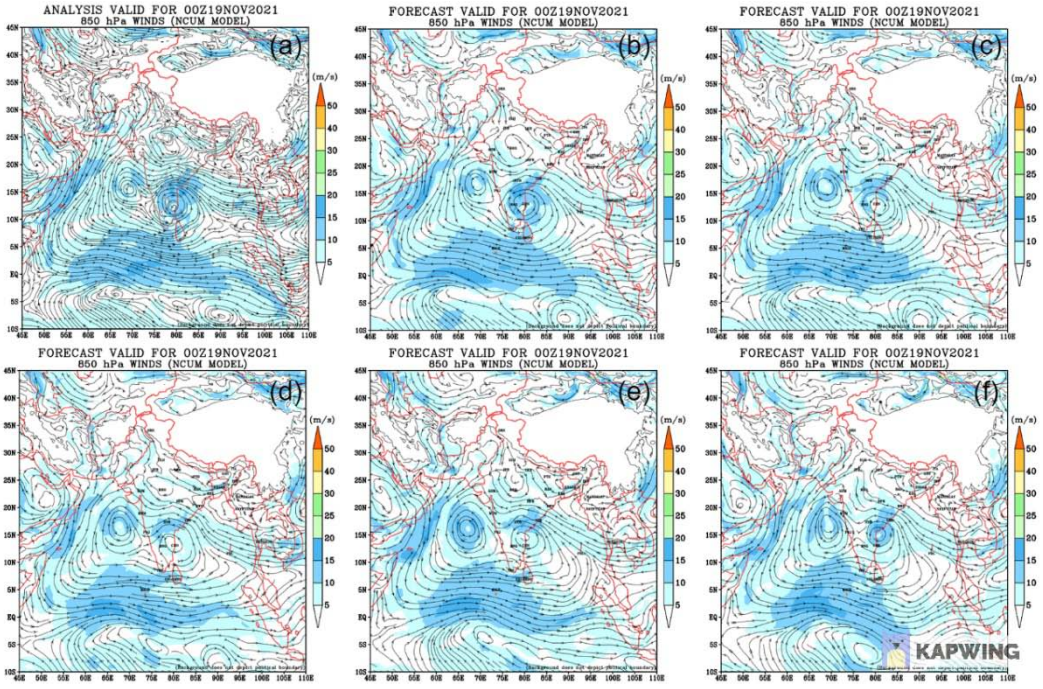

Fig 8.7. NCUM model analysis of 850 hPa winds at 0000 UTC, 19 November 2021 (a) and model forecast for day-1 (b), day-2 (c), day-3 (d), day-4 (e) and day-5 (f).

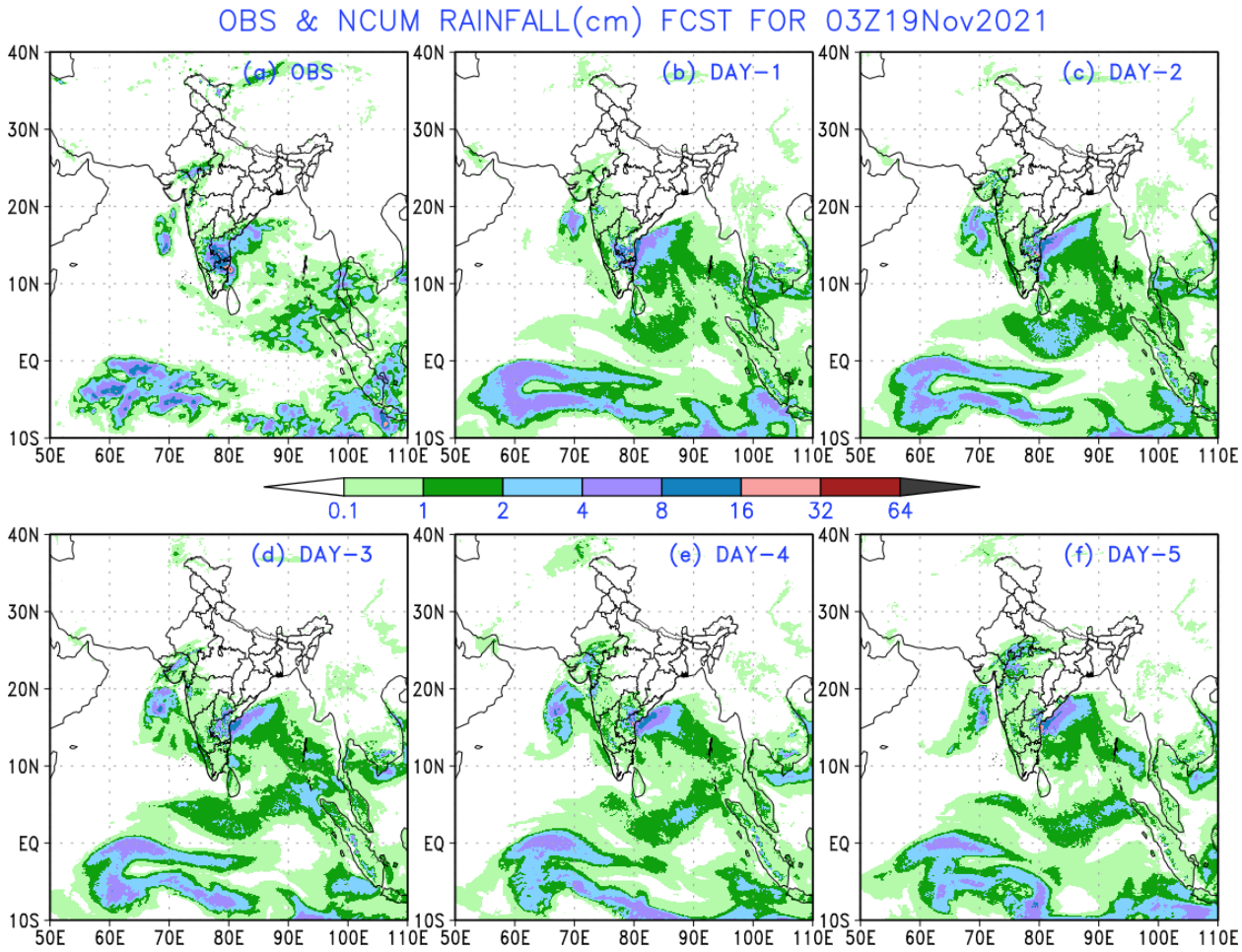

Fig 8.8. Observed and NCUM model predictions of rainfall (cm) for 03 UTC 19 November 2021. a) observed, b) to f) represent forecasts of day-1 to day-5.

Thus, the NCUM models have shown some useful skill in predicting large scale circulation and rainfall patterns associated with weather systems during the NE Monsoon season, at least up to 72 hours in advance.

In the next section, analysis of forecast verification using IMD/IITM GFS and GEFS models is presented.

The categorical statistical scores for verification of precipitation forecasts based on GFS T1534 for south peninsula are shown in Fig 8.9 for Day-1, Day-3 and Day-5 forecasts. This verification is made for three NE monsoon seasons, 2019-2021.

Probability of Detection (POD) is larger for lower rainfall thresholds, but it drastically reduces for larger amount of rainfall. POD for 2 cm rainfall at Day-1 forecast is close to 0.35, but it is around 0.2 for Dady-5 forecast. False Alarm Rate (FAR) is larger for higher amount of rainfall thresholds. FAR is more than 0.7 for larger amount of rainfall. Therefore, the model has tendency of over predicting frequency of higher amount of rainfall. The other skill scores (like CSI, BIAS, PSS and SEDI) are better for Day-1 and Day-3 forecasts but reduces sharply for Day-5 forecasts.

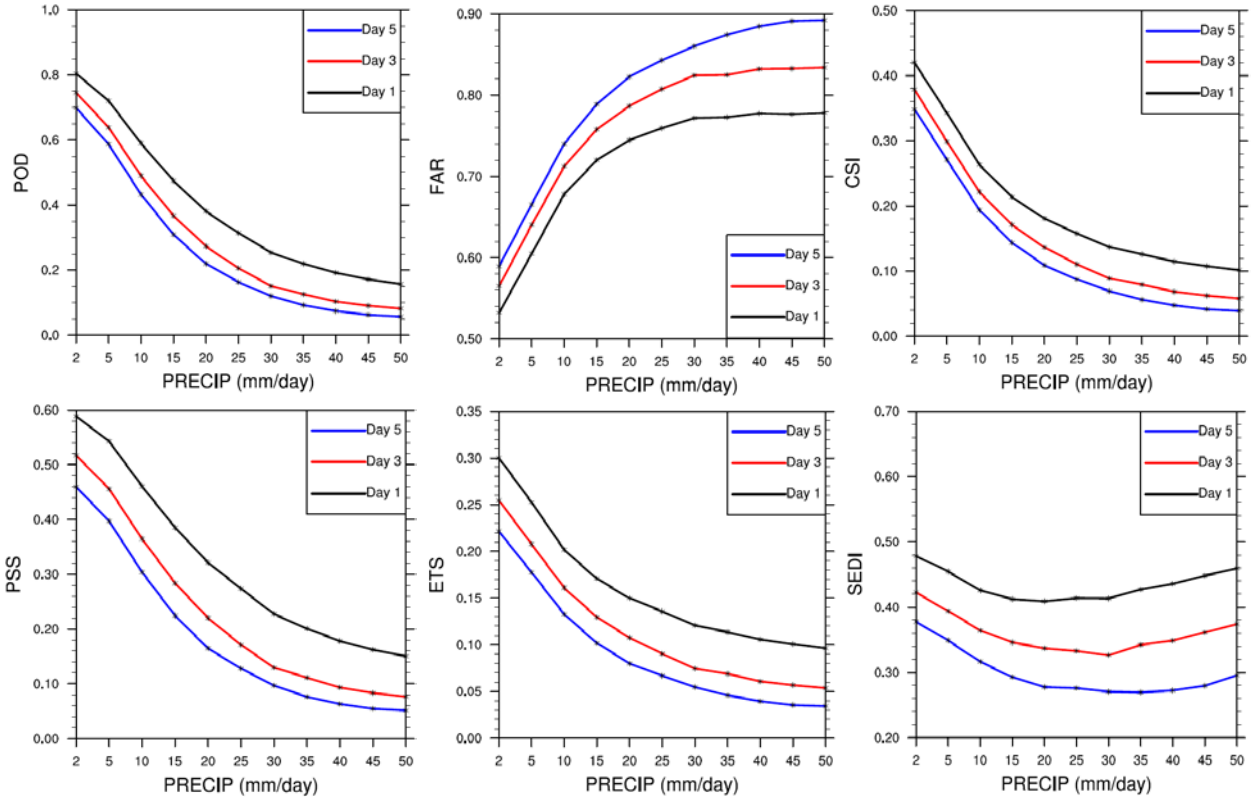

Fig.8.9. Categorical skill scores for rainfall forecast of OND 2019-2021 from GFS T1534 for the Southern Peninsula region (8°-20°N, 68°-97.5°E, land only)

Fig 8.10 shows the Reliability Diagram of prediction of rainfall during the NE monsoon season (OND) (2019-2021) from the model GEFS T1534 for the southern Peninsula region (8°-20°N, 68°-97.5°E, land only). The observed merged (satellite-rain-gauge) rainfall data are taken from Mitra et al. (2009). The columns are for Day 1, 2, and 3, respectively, and the rows are for rainfall thresholds of 2.5 mm/day, 15.6 mm/day, and 65.5 mm/day, respectively. A reliability diagram is a graph where the conditional distribution of the observations, given the forecast probability, is plotted against the forecast probability. The distributions of perfectly reliable forecasts are plotted along the 45- degree diagonal. If the curve falls in the grey-shaded region, it indicates a skilful forecast. The curve obtained below the diagonal indicates over-forecasting and vice-versa. Fig 46 shows that the model can display a skilful forecast which decreases with increasing thresholds. For a threshold of 2.5 mm/day rainfall, the forecast shows a consistent skill through Day 1 to 3 as the curve is in the grey shaded region of the graph. For the threshold of 15.6 mm/day of rainfall, the curve falls just below the grey region for higher forecast probability categories for all lead times. For the threshold of 65.5 mm/day, the Day 1 curve shows a comparatively reliable forecast. However, the type of curve obtained for Day 2 and 3 forecasts indicates under-sampling. As all the curves are below the diagonal, we can say that the model forecast is over-confident or under-spread.

Fig 8.11 shows the Relative Operating Characteristic (ROC) for the rainfall forecast of OND 2019-2021 from the model GEFS T1534 for the Southern Peninsula region (8°-20°N, 68°-97.5°E, land only). The columns are for Day 1, 2, and 3, respectively, and the rows are for rainfall thresholds of 2.5 mm/day, 15.6 mm/day, and 65.5 mm/day, respectively. The ROC is conditioned on the observations and gives a measure of the resolution of the forecast. Here resolution of the model forecast means the distinguishing capacity between events and non-events. The ROC shows the forecast in terms of Hit Rate and False Alarm Rate. The perfect forecast displays the curve along the

bottom left to the top left and then to the top right corner. A curve along the diagonal indicates no skill, and a curve below the diagonal shows negative skill. Fig. 8.11 shows a near-perfect ROC for the 2.5 mm/day threshold and at all lead times. The skill decreases for the 15.6 mm/day rainfall threshold, but there is a considerable dip in skill for the 65.5 mm/day threshold, but it still shows a positive skill of the forecast. Hence the ROC gives a measure of the potential skill of the forecast.

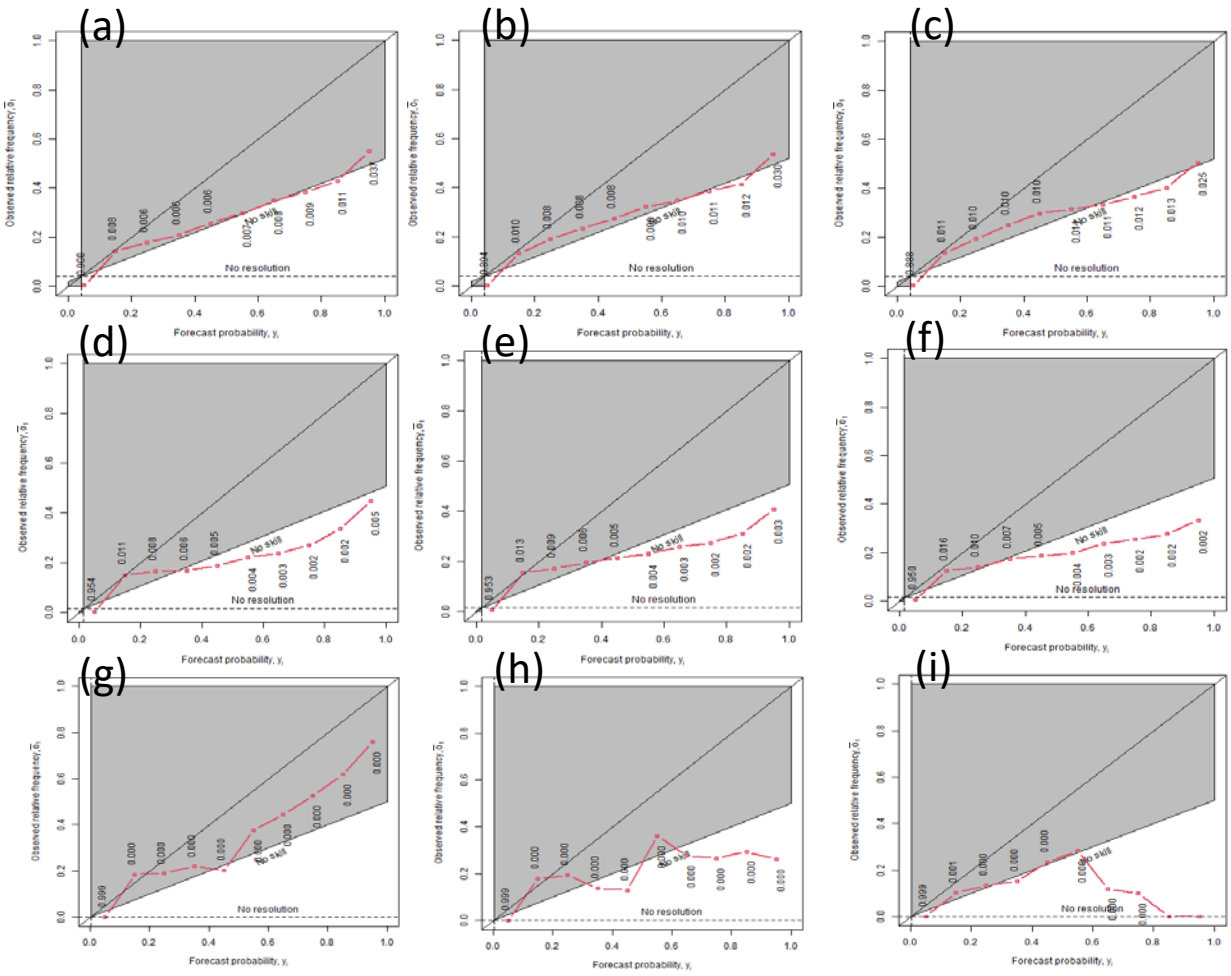

Fig.8.10. Reliability Diagram for rainfall forecast of OND 2019-2021 from GEFS T1534 for the Southern Peninsula region (8°-20°N, 68°-97.5°E, land only). The columns are for Day 1, 2 and 3 respectively and the rows are for rainfall thresholds of 2.5 mm/day, 15.6 mm/day and 65.5 mm/day respectively.

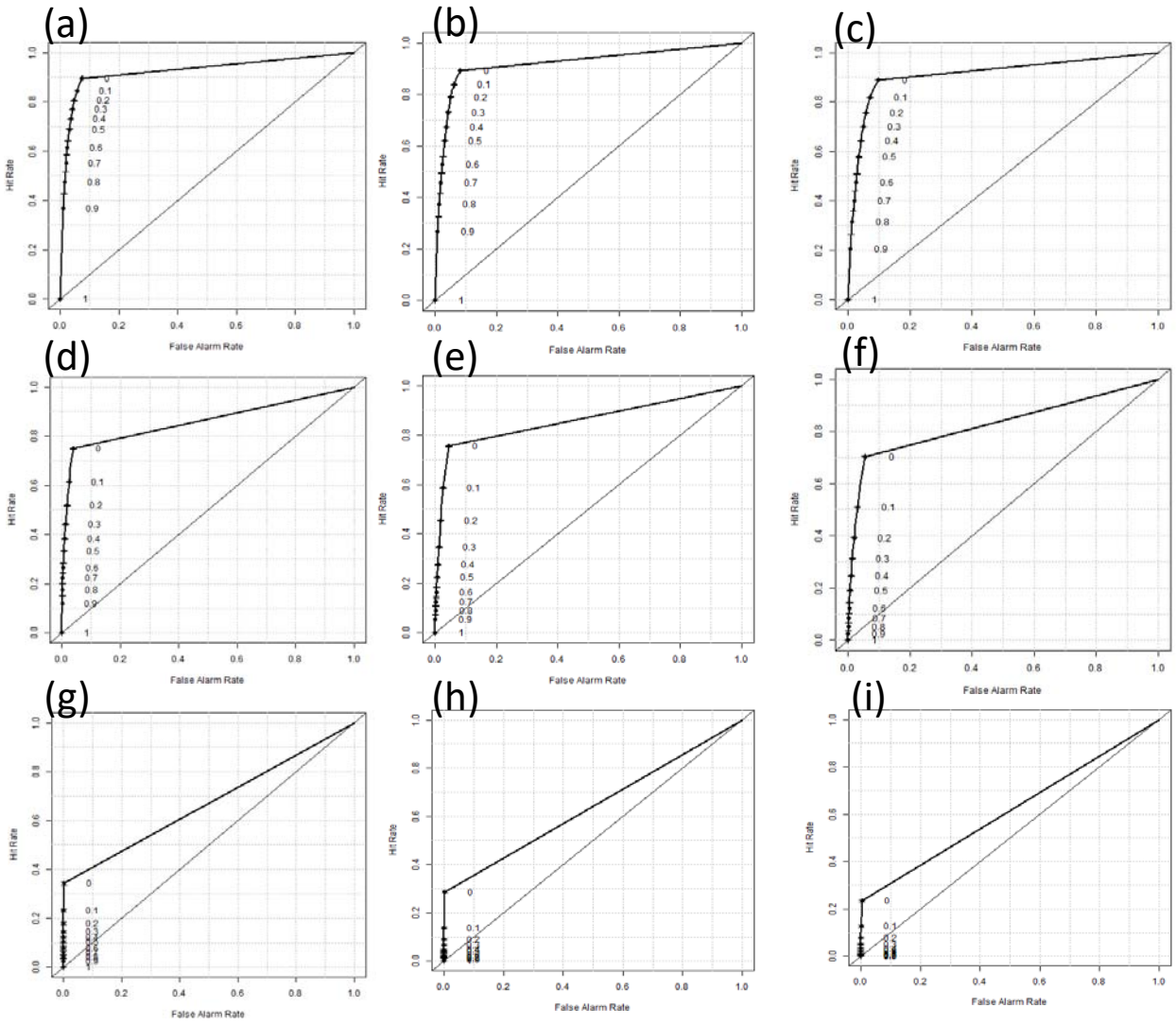

Fig.8.11. Relative Operating Characteristic (ROC) for rainfall forecast of OND 2019-2021 from GEFS T1534 for the Southern Peninsula region (8°-20°N, 68°-97.5°E, land only). The columns are for Day 1, 2 and 3 respectively and the rows are for rainfall thresholds of 2.5 mm/day, 15.6 mm/day and 65.5 mm/day respectively.

In the earlier section, it was shown that the deterministic forecast skill is reduced for rainfall of larger thresholds. Since we need to predict heavy rainfall events, depending upon the deterministic forecasts alone will not be fruitful. We need to refer to Ensemble forecasts to understand the uncertainties involved in the forecasts and thus to prepare probabilistic forecasts.

An ensemble weather forecast is a set of forecasts that present the range of future weather possibilities. Multiple simulations are run, each with slight variation of its initial conditions and with slightly perturbed weather models. These variations represent the inevitable uncertainty in the initial conditions and approximations in the models. They produce a range of possible weather conditions. The uncertainty associated with every forecast means that different scenarios are possible and the forecast should reflect that. Single “deterministic” forecasts can be misleading as they fail to provide this information.

Under the Monsoon Mission project of the MoES, two ensemble forecasting systems have been developed and put on operational use. One system is based on UK Met office weather prediction model and the second one is based on the NCEP Global Forecasting System (GFS) weather prediction model. The details of these weather prediction models are available in the papers by Sarkar et al. (2016), Chakraborty et al. (2020), Deshpande et al. (2020, and Mukhopadhyay et al. (2022).

Here, a case study is discussed to demonstrate the utility of ensemble weather forecasts during the NE monsoon season. The case study pertains to a heavy rainfall event (exceeding 10 cm) which occurred over Tamil Nadu-South Andhra coast on 7 Nov 2021. Fig 8.12 a, b and c show rainfall forecast from Global Ensemble Forecasting System (GEFS) T1534 model of IMD/IITM valid for 7 Nov 2021 for Day-1, Day-3 and Day-5 forecasts. The IMD-GPM observed rainfall is shown in Fig 8.12 a, which shows heavy rainfall over the east coast of Tamil Nadu/Andhra coast. The forecasts show higher probabilities of rainfall of even 15.6 mm/day. It is interesting to note the GEFS model indicated a chance of heavy rainfall exceeding 65 mm/day even at Day-3 and Day-5 forecasts. This ensemble forecast product thus provides an additional tool for forecasters on the possibility of extreme events like heavy rainfall and therefore such ensemble forecast products should be extensively used.

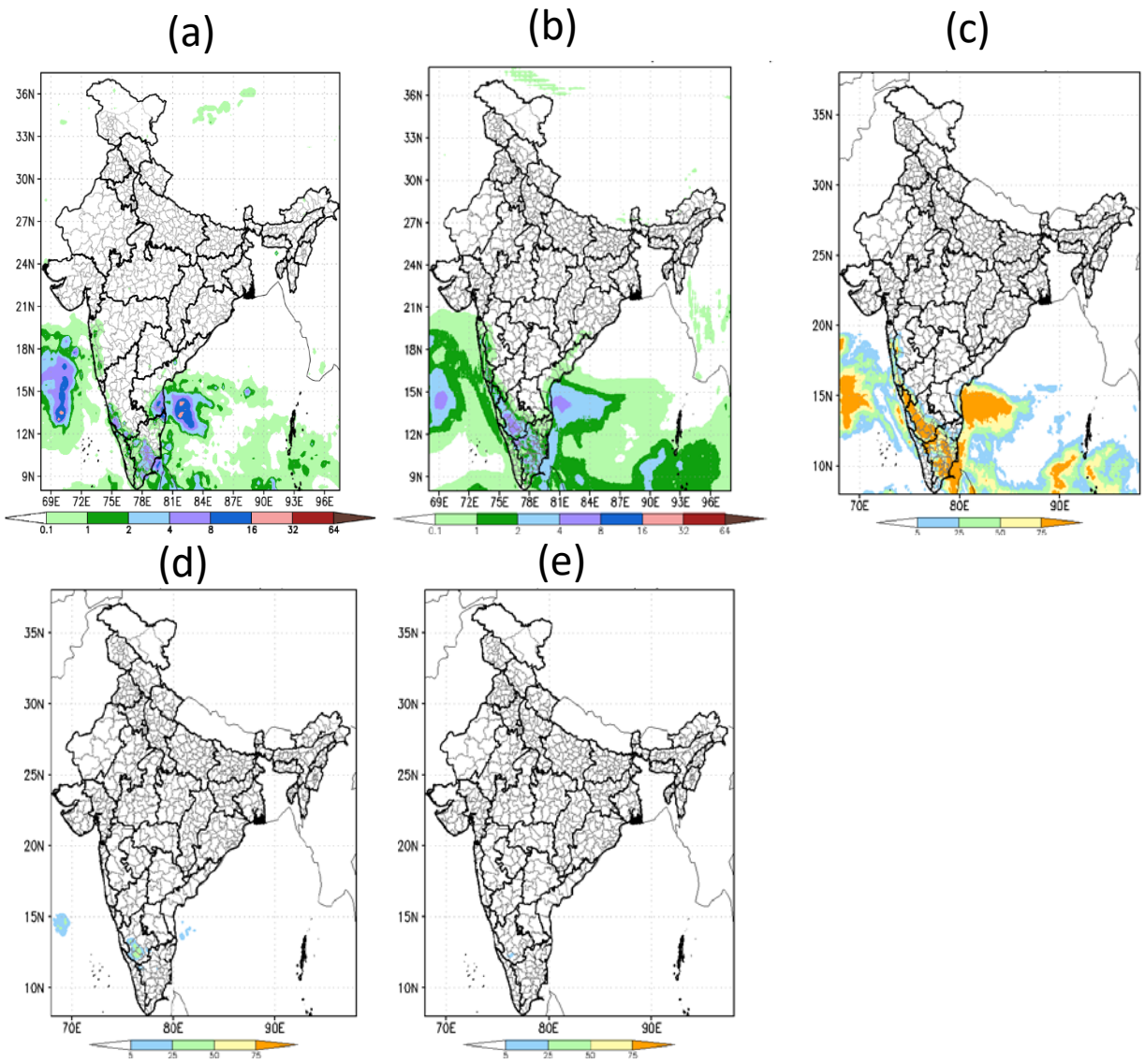

Fig. 8.12 a Day 1 rainfall forecast from GEFS T1534 valid for 7 November 2021 with (a) IMD-GPM (b) Ensemble mean and forecast showing probability of exceedance from (c) 15.6 mm/day (d) 65.5 mm/day (e) 115 mm/day rainfall threshold.

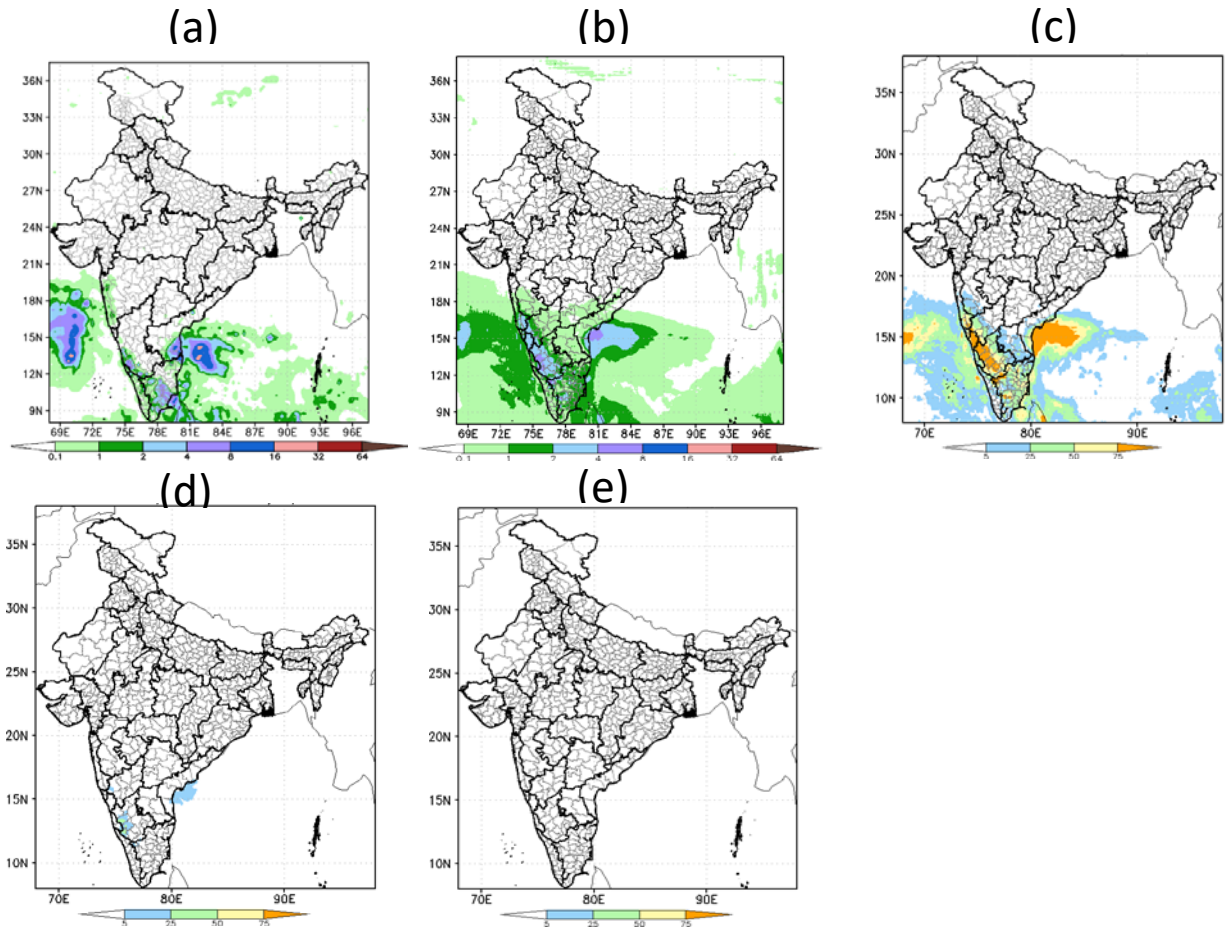

Fig. 8.12 b. Day 3 rainfall forecast from GEFS T1534 valid for 7 November 2021 with (a) IMD-GPM (b) Ensemble mean and forecast showing probability of exceedance from (c) 15.6 mm/day (d) 65.5 mm/day (e) 115 mm/day rainfall threshold.

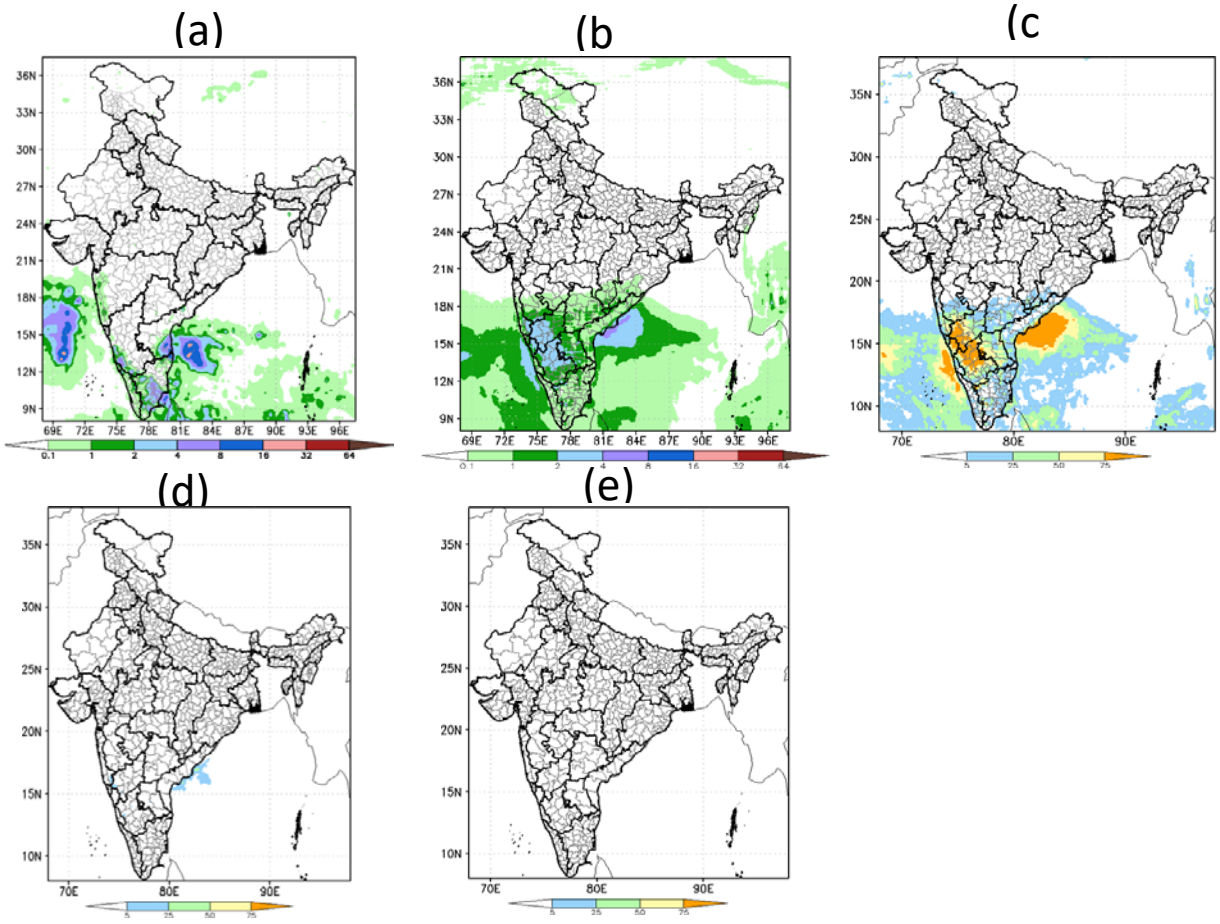

Fig. 8.12 c. Day 5 rainfall forecast from GEFS T1534 valid for 7 November 2021 with (a) IMD-GPM (b) Ensemble mean and forecast showing probability of exceedance from (c) 15.6 mm/day (d) 65.5 mm/day (e) 115 mm/day rainfall threshold.

Thus, from the above discussions, we can conclude that the present-day NWP model forecasts have some useful skill in predicting various aspects of the NE Monsoon season. Forecasters should make use of the NWP model forecasts along with other forecasting tools like satellite pictures, radar data etc for preparing more skillful forecasts during the NE monsoon season. The ensemble forecasts are very useful for preparing probability forecasts to account uncertainties involved in the forecasts.

References

1. Abeysekera, A.B., Punyawardena, B.V.R., Marambe, B., Jayawardena, I.M., Wickremasinghe, V.N., Senarathna, S.D. and Wijerathna, W.M., 2019. Effect of El Niño Southern Oscillation (ENSO) events on inter-seasonal variability of rainfall in wet and intermediate zones of Sri Lanka. *Trop Agric*, *167*, pp.14-27.
2. Acharya, N., Kar, S.C., Kulkarni, M.A., Mohanty, U.C. and Sahoo, L.N., 2011. Multi-model ensemble schemes for predicting northeast monsoon rainfall over peninsular India. *Journal of earth system science*, *120*(5), pp.795-805.
3. Achyuthan, H., 2021. Middle to late Holocene alluvial history of the northeast monsoon dominated coastal tropical rivers of south India. *Quaternary International*, https://doi.org/10.1016/j.quaint.2021.09.012.
4. Amudha, B., 2016, CHARACTERISTICS OF INDIAN NORTHEAST MONSOON AND CYCLONIC STORMS OF NORTH INDIAN OCEAN OBSERVED THROUGH MODERN METEOROLOGICAL OBSERVING SYSTEMS, Ph.D Thesis, University of Madras. PP 245.
5. Amudha, B., Raj, Y.E.A., Asokan, R. and Thampi, S.B., 2016 a. Spatial rainfall patterns associated with Indian northeast monsoon derived from high resolution rainfall estimates of Chennai DWR. *MAUSAM*, *67*(4), 767-788.
6. Amudha, B., Raj, Y.E.A. and Asokan, R., 2016 b. Spatial variation of clouding/rainfall over southeast Indian peninsula and adjoining Bay of Bengal associated with active and dry spells of northeast monsoon as derived from INSAT OLR data. *MAUSAM*, *67*(3), 559-570.
7. Balachandran, S., Pai, D.S. and Prasad, S.K., 1998. Some features of an inverted V-type easterly wave over Indian seas. *Mausam*, *49*(2), 266-268.
8. Balachandran S, Asokan A, Sridharan S. 2006. Global surface temperature in relation to northeast monsoon rainfall over Tamil Nadu. J. Earth Syst. Sci. 115: 349–362.

9. Berry, G.J. and Thorncroft, C., 2005. Case study of an intense African easterly wave. *Monthly Weather Review*, *133*(4), 752-766.
10. Bhate, Jyoti, A. Kesarkar, V.P.M. Rajasree, 2019. Simulation of the diurnal cycle of rainfall during Indian summer monsoon season using mesoscale model, Theor. App. Climat., 138, 185-200.
11. Burpee, R.W., 1974. Characteristics of North African easterly waves during the summers of 1968 and 1969. *Journal of Atmospheric Sciences*, *31*(6), 1556-1570.
12. Cangialosi, J.P., Blake, E., DeMaria, M., Penny, A., Latto, A., Rappaport, E. and Tallapragada, V., 2020. Recent progress in tropical cyclone intensity forecasting at the National Hurricane Center. *Weather and Forecasting*, *35*(5), 1913-1922.
13. Chakraborty, A., 2016. A synoptic-scale perspective of heavy rainfall over Chennai in November 2015, Current Science, 111, 201-207.
14. Chakraborty, P., Sarkar, A., Kumar, S., George, J.P., Rajagopal, E.N. and Bhatla, R., 2020. Assessment of NCMRWF Global Ensemble System with differing ensemble populations for Tropical cyclone prediction. *Atmospheric research*, *244*, p.105077.
15. Dash, Y., Mishra, S.K. and Panigrahi, B.K., 2019. Predictability assessment of northeast monsoon rainfall in India using sea surface temperature anomaly through statistical and machine learning techniques. *Environmetrics*, *30*(4), p.e2533.
16. De, U.S. and Mukhopadhyay, R.K., 1999. The effect of ENSO/Anti ENSO on northeast monsoon rainfall. *Mausam*, *50*(4), 343-354.
17. Deshpande, M., Johny, C. J., Kanase, R., Tirkey, S., Sarkar, S. Goswami, T., Roy, K., Ganai, M., Krishna, R. P. M., Prasad, V. S., Mukhopadhyay, P., Durai, V. R., Nanjundiah, R. S. and Rajeevan, M., 2020, “Implementation of Global Ensemble Forecast System (GEFS) at 12 km Resolution”, ISSN 0252-1075, IITM Technical Report No.TR-06, ESSO/IITM/MM/ TR/02(2020)/200.

18. Dhar ON, Rakhecha PR. 1983. Forecasting northeast monsoon rainfall over Tamil Nadu, India. Mon. Weather Rev. 111, 109–112.
19. Domroes, M. and Ranatunge, E., 1992. The orthogonal structure of Monsoon rainfall variation over Sri Lanka. *Theoretical and applied climatology*, *46*(2), pp.109-114.
20. Dunn, G.E., 1940. Cyclogenesis in the tropical Atlantic. *Bulletin of the American Meteorological Society*, *21*(6), 215-229.
21. Gadgil, S., Joseph PV, Joshi NV, 1984. Ocean-atmosphere coupling over monsoon regions. *Nature* **312**: 141– 143.
22. Gadgil, S., and Joseph PV. 2003. On breaks of the Indian monsoon, Proceedings of the Indian Academy of Sciences–Earth and Planetary Sciences, 112(4): 529–558.
23. Geetha, B., 2011. Indian northeast monsoon as a component of Asian winter monsoon and its relationship with large scale global and regional circulation features, Ph.D Thesis of Geetha B, University of Madras.
24. Geetha, B and S. Balachandran, 2014 a. An analytical study of easterly waves over Southern Peninsular India during the Northeast monsoon of 2010, Mausam, 65, 4, 591-602.
25. Geetha, B. and Raj, Y.E.A., 2014 b. Spatial patterns of Northeast Monsoon rainfall over sub-regions of Southern Peninsular India and Sri Lanka as revealed through Empirical Orthogonal Function analysis. *Mausam*, *65*(2), 185-204.
26. Geetha, B and S. Balachandran, 2020. Development and Rapid Intensification of Tropical Cyclone OCKHI (2017) over the North Indian Ocean, Journal of Atmospheric Science Research, DOI: https://doi.org/10.30564/jasr.v3i3.2177.
27. Geetha, B. and Balachandran, S., 2021. Diagnostic analysis of two dos-à-dos extreme northeast monsoon seasons with dipolar rainfall performance. *Theoretical and Applied Climatology*, *144*, 675-690.

28. Geetha, B., K.Ramesh, R.V.Deepa, Y.P.Mourya, S.Balachandran, K. Santosh, S.Stella, Geeta Agnihotri and K. Nagaratna, 2022. Report on Northeast Monsoon – 2021, IMD Chennai Scientific Report No. IMDC-SR/12, 62pp.
29. Goswami BN., 2005. Intraseasonal variability (ISV) of south Asian summer monsoon. In Intraseasonal Variability of the Atmosphere – Ocean Climate System, Lau K, Waliser D (eds). pp. 19–61, DOI: 10.1007/3-540-27250-X 2. Springer – Praxis: Chichester, UK.
30. Hersbach, H., Bell, B., Berrisford, P., Hirahara, S., Horányi, A., Muñoz-Sabater, J., Nicolas, J., Peubey, C., Radu, R., Schepers, D. and Simmons, A., 2020. The ERA5 global reanalysis. *Quarterly Journal of the Royal Meteorological Society*, *146*(730), 1999-2049.
31. Hess, S.L., 1959. *Introduction to Theoretical Meteorology*, New York, NY: Holt Rinehart and Winston.
32. India Meteorological Department, Srinivasan, V., and K. Ramamurthy, 1973. Northeast monsoon. Comprehensive articles on selected topics, India Meteorological Department Forecasting Manual Rep. 18.4, Vol. 4.
33. India Met. Dep (IMD), 2008. Forecaster's Guide, 86-88.
34. Jangir, B., Swain, D. and Ghose, S.K., 2021. Influence of eddies and tropical cyclone heat potential on intensity changes of tropical cyclones in the North Indian Ocean. *Advances in Space Research*, *68*(2), 773-786.
35. Jayanthi, N. and Govindachari, S., 1999. El Nino and northeast monsoon rainfall over Tamil Nadu, Mausam,50,2,217-218.
36. Jayawardena, W., M. Fernando, and DUJ Sonnadara, 2014. Satellite observations of Lightning Activities over Sri Lanka, Proceedings of the Technical Sessions, 30 (2014) 61-66 Institute of Physics – Sri Lanka.

37. Jyothi, L., Joseph Sudheer, and P. Suneetha., 2020. Role of Environmental Factors in Rapid Intensification and Weakening of Cyclone Ockhi (2017), *Earth and Space Science Open Archive ESSOAr*.
38. Jury, M.R., Pathack, B., Campbell, G., Wang, B. and Landman, W., 1991. Transient convective waves in the tropical SW Indian Ocean. *Meteorology and Atmospheric Physics*, *47*(1), 27-36.
39. Koteswara Rao, K, Ashwini Kulkarni, Savita Patwardhan, B. Vinodh Kumar, T. V. Lakshmi Kumar., 2020. Future changes in precipitation extremes during northeast monsoon over south peninsular India, Theor. Appl Climatology, **142**, 205–217.
40. Kripalani, R.H. and Kumar, P., 2004. Northeast monsoon rainfall variability over south peninsular India vis-à-vis the Indian Ocean dipole mode. *International Journal of Climatology: A Journal of the Royal Meteorological Society*, *24*(10), 1267-1282.
41. Krishna Kumar, K., K. Rupa Kumar, R. G. Ashrit, N. R. Deshpande, and J. W. Hansen, 2004. Climate impacts on Indian agriculture. Int. J. Climatol., 24, 1375–1393, https://doi.org/10.1002/joc.1081.
42. Kumar P, Rupa Kumar K, Rajeevan M, Sahai AK., 2007. On the recent strengthening of the relationship between ENSO and northeast monsoon rainfall over South Asia. Clim. Dyn. 8: 649–660.
43. Lau, K.M., Wu, H.T. and Bony, S., 1997. The role of large-scale atmospheric circulation in the relationship between tropical convection and sea surface temperature. *Journal of Climate*, *10*(3), 381-392.
44. Liebmann, B. and Smith, C.A., 1996. Description of a complete (interpolated) outgoing longwave radiation dataset. *Bulletin of the American Meteorological Society*, *77*(6), 1275-1277.

45. Maharana, P., Kumar, D., Rai, P., Tiwari, P.R. and Dimri, A.P., 2022. Simulation of Northeast Monsoon in a coupled regional model framework. *Atmospheric Research*, *266*, p.105960.
46. Manas Roshan, 2019. Cyclone Ockhi Disaster risk management and sea safety in the Indian marine fisheries sector, FAO, United Nations. FAO ISBN 978-92-5-131225-4.
47. Mishra, V and Amit Bharadwaj, 2019, Defining the Northeast Monsoon of India, Mon Wea Review, Vol, 147, 791-808, https://doi.org/ 10.1175/MWR-D-18-0287.1
48. Mitra, A. K., A. K. Bohra, M. Rajeevan and T. N. Krishnamurti, 2009. Daily Indian precipitation analyses formed from a merged of rain-gauge with TRMM TMPA satellite derived rainfall estimates, J of Met Soc of Japan, 87A, 265-279.
49. Mohapatra, M. and Adhikary, S., 2011. Modulation of cyclonic disturbances over the north Indian Ocean by Madden-Julian oscillation. *Mausam*, *62*(3), 375-390.
50. Mohapatra, M., Nayak, D.P., Sharma, R.P. and Bandyopadhyay, B.K., 2013. Evaluation of official tropical cyclone track forecast over north Indian Ocean issued by India Meteorological Department. *Journal of Earth System Science*, *122*(3), 589-601.
51. Mohapatra, M., Nayak, D.P., Sharma, M., Sharma, R.P. and Bandyopadhyay, B.K., 2015. Evaluation of official tropical cyclone landfall forecast issued by India Meteorological Department. *Journal of Earth System Science*, *124*(4), 861-874.
52. Mondal, P. and Chaudhuri, S., 2022. Temporal variability in the withdrawal phase of southwest monsoon over India and related consequences in northeast monsoon: a climatological perspective. *Theoretical and Applied Climatology*, *148*(3), 1021-1034.
53. Mukhopadhyay, P., Bechtold, P., Zhu, Y., Murali Krishna, R.P., Kumar, S., Ganai, M., Tirkey, S., Goswami, T., Mahakur, M., Deshpande, M. and Prasad, V.S., 2021. Unraveling the mechanism of extreme (More than 30 sigma) precipitation during

august 2018 and 2019 over Kerala, India. *Weather and Forecasting*, *36*(4), pp.1253-1273.

54. Nageswara Rao, M.M., M.C. Sannan and U.C. Mohanty, 2019. Characteristics of various rainfall events over South Peninsular India during northeast monsoon using high-resolution gridded dataset (1901–2016), Theor Appl. Climatology, **137**, 2573–2593.
55. Nisansala, W.D.S., Abeysingha, N.S., Islam, A. and Bandara, A.M.K.R., 2020. Recent rainfall trend over Sri Lanka (1987–2017). *International Journal of Climatology*, *40*(7), pp.3417-3435.
56. Naidu, C.V., Satyanarayana, G.C., Durgalakshmi, K., Rao, L.M., Mounika, G.J. and Raju, A.D., 2012. Changes in the frequencies of northeast monsoon rainy days in the global warming. *Global and Planetary Change*, *92*, 40-47.
57. Nair, A., Acharya, N., Singh, A., Mohanty, U.C. and Panda, T.C., 2013. On the predictability of northeast monsoon rainfall over south peninsular India in general circulation models. *Pure and Applied Geophysics*, *170*(11), 1945-1967.
58. Omvir Singh and Pankaj Bhardwaj, 2017. Spatial and temporal variations in the frequency of thunderstorm days over India, Weather, https://doi.org/10.1002/wea.3080
59. Pai, D.S., M. Rajeevan, O.P.Sreejith, B. Mukhopadhyay, N.S. Sathbai, 2014. Development of a new high spatial resolution (0.25 X 0.25) long period (1901-2010) daily gridded rainfall data set over India and its comparison with existing data sets over the region, Mausam, vol. 65, no. 1, pp. 1–18.
60. Parvathi, V., I. Suresh, M. Lengaigne, T. Izumo, and J. Vialard, 2017. Robust projected weakening of winter monsoon winds over the Arabian Sea under climate change. Geophys. Res. Lett., 44, 9833–9843.

61. Pattanaik, D.R. and Mohapatra, M., 2017. Active northeast monsoon over India during 2015–an assessment of real-time extended range forecast. *Current Science*, 2253-2262.
62. Prakash, S. and Gairola, R.M., 2013. Relationship between northeast monsoon rainfall and near-surface atmospheric wind convergence over the North Indian Ocean using multisatellite data. *Natural hazards*, *68*(2), 763-774.
63. Prasanna, K., Singh, P., Chowdary, J.S., Naidu, C.V., Parekh, A., Gnanaseelan, C. and Dandi, R., 2019. Northeast monsoon rainfall variability over the southern Peninsular India associated with multiyear La Niña events. *Climate Dynamics*, *53*(9), 6265-6291.
64. Prasanna, K., Vinay Kumar, P. and Naidu, C.V., 2020. Precursors of northeast monsoon rainfall variability during extreme epochs of the global warming era. *Meteorological Applications*, *27*(2), p.e1894.
65. Prasanna, K., Chowdary, J.S., Singh, P., Chiranjeevi, D., Naidu, C.V., Parekh, A. and Gnanaseelan, C., 2021. Assessment of APCC models fidelity in simulating the Northeast monsoon rainfall variability over Southern Peninsular India. *Theoretical and Applied Climatology*, *144*(3), 931-948.
66. Raj, YEA, 1992. Objective determination of northeast monsoon onset dates over coastal Tamil Nadu for the period 1901-90, Mausam, 43, 273-282.
67. Raj, Y.E.A., 2003. Onset, withdrawal and intra-seasonal variation of northeast monsoon over coastal Tamil Nadu, 1901-2000, Mausam, 3, 605-614.
68. Raj, Y.E.A., and Geetha, B., 2008. Relationship between Southern Oscillation Index and Indian northeast monsoon as revealed in antecedent and concurrent modes, Mausam, 59, 15-34.
69. Raj, Y.E.A., 2012. INDIAN NORTHEAST MONSOON, In *Monsoon Monograph*, Vol. 1, Edited by Ajit Tyagi, G.C. Asnani, U.S.De, H.R.Hatwar and A.B.Mazumdar, 606-670.

70. Raj Y.E.A. and Amudha B, 2022. Extent of diurnal cycle of rainfall and its intraseasonal variation over coastal Tamil Nadu during northeast monsoon season, Mausam, 73, 1, https://doi.org/10.54302/mausam.v73i1.4984.
71. Rajeevan M, Gadgil S, Bhate J. 2010. Active and break spells of the Indian summer monsoon. J. Earth Syst. Sci. 119: 229–247.
72. Rajeevan, M., C. K. Unnikrishnan, Jyoti Bhate, K. Niranjan Kumar and P. P. Sreekala, 2012. Northeast monsoon over India: variability and prediction, Meteorol. Appl. 19: 226–236, DOI: 10.1002/met.1322.
73. Ramamurthy, K., 1969. Monsoon of India: Some aspects of the 'break' in the Indian southwest monsoon during July and August; Forecasting Manual 1–57 No. IV 18.3, India Met. Dept., Pune, India.
74. Ramesh Reddy, T.V., Mehta, S.K., Ananthavel, A., Saleem Ali, V. Annamalai, D. Narayana Rao, 2021. Seasonal Characteristics of Sea breeze and thermal internal boundary layer over Indian east coast region, Met and Atmospheric Physics, 133, 217-232.
75. Ranalkar, M.R. and Chaudhari, H.S., 2009. Seasonal variation of lightning activity over the Indian subcontinent. *Meteorology and atmospheric physics*, *104*(1), 125-134.
76. Rao, T.N., B. Radhakrishna, K. Nakamura and N. Prabhakara Rao, 2009. Differences in raindrop size distribution from Southwest monsoon to northeast monsoon at Gadanki, Quart Roy Met Society, 1630-1637, https://doi.org/10.1002/qj.432.
77. Riehl, H., 1968, Tropical Meteorology, McGraw-Hill Book Co., Inc., New York, 392 pp.
78. Rao, K.V, 1961. A study of the Indian Northeast Monsoon season, Ind.J. Meteor. Geophysics, 143-155.

79. Reba, RM, D.R. Pattanaik, and PVS Raju, 2022. Easterly waves and ocean–atmospheric oscillations associated with contrasting northeast monsoon seasons over India, J. Earth Syst. Sci. 131:52, https://doi.org/10.1007/s12040-021-01807-8.
80. Ross, R.S. and Krishnamurti, T.N., 2007. Low-level African easterly wave activity and its relation to Atlantic tropical cyclogenesis in 2001. *Monthly Weather Review*, *135*(12), 3950-3964.
81. Rossow, W.B. and Schiffer, R.A., 1991. ISCCP cloud data products. *Bulletin of the American Meteorological Society*, *72*(1), 2-20.
82. Sabin, T.P., C.A.Babu and P.V. Joseph., 2012. SST-Convection relation over Tropical Oceans, Int J Climatology, 1424-1435, https://doi.org/10.1002/joc.3522.
83. Saha, K., Sanders, F. and Shukla, J., 1981. Westward propagating predecessors of monsoon depressions. *Monthly Weather Review*, *109*(2), 330-343.
84. Sahany, S., Venugopal, V. and Nanjundiah, R.S., 2010. Diurnal scale signatures of monsoon rainfall over the Indian region from TRMM satellite observations. *Journal of Geophysical Research: Atmospheres*, *115*(D2).
85. Sanap, S.D., P. Priya, G. K. Sawaisarje and K. S. Hosalikar, 2018. Heavy Rainfall Events over South-East Peninsular India during North-East Monsoon: Role of El-Niño and Easterly Wave Activity, Int J Climatology, DOI: 10.1002/joc.5926.
86. Sanap, S.D., Mohapatra, M., Ali, M.M., Priya, P. and Varaprasad, D., 2020. On the dynamics of cyclogenesis, rapid intensification and recurvature of the very severe cyclonic storm, Ockhi. *Journal of Earth System Science*, *129*(1), 1-13.
87. Sarkar, A., P.Chakraborty, John.P.George and E.N. Rajagopal, 2016. Implementation of Unified Model based Ensemble Prediction System at NCMRWF (NEPS), NCMRWF Report NMRF/TR/02/2016, https://www.ncmrwf.gov.in/Reports-eng/NMRF_TR2_2016.pdf.

88. Satyanarayana, G.C., Naidu, C.V., Rao, D.V.B., Umakanth, N., and Naveena, N., 2020. Onset and northeast monsoon over south peninsular India, Mausam, 71, 3, https://doi.org/10.54302/mausam.v71i3.51 .
89. Sengupta, A. and Nigam, S., 2019. The northeast winter monsoon over the Indian subcontinent and Southeast Asia: Evolution, interannual variability, and model simulations. *Journal of Climate*, *32*(1), 231-249.
90. Shanmugasundaram, J., Lee, E. and Srinivasan, G., 2018. Characterizing pentad rainfall variations during the North East Indian monsoon season over the southeastern peninsular India. Int Journal of Climatology, *38*, 1044-1060.
91. Singh, P., Gnanaseelan, C. and Chowdary, J.S., 2017. North-East monsoon rainfall extremes over the southern peninsular India and their association with El Niño. *Dynamics of Atmospheres and Oceans*, *80*, 1-11.
92. Singh Vineet Kumar, M.K.Roxy and Medha Deshpande, 2020. The unusual long track and rapid intensification of very severe cyclone Ockhi, CURRENT SCIENCE, VOL. 119, NO. 5, 10 SEPTEMBER, 771-779.
93. Somenath Dutta, D.M.Rase, and Sunitha Devi., 2016. A diagnostic study on the energetic aspects of weak/strong spell of northeast monsoon, Mausam, 67, 2, 493-498.
94. Sreekala, P.P., Rao, S. and Rajeevan, M., 2012. Northeast monsoon rainfall variability over south peninsular India and its teleconnections. *Theoretical and applied climatology*, *108*(1), 73-83.
95. Sreekala, P.P., S. Vijaya Bhaskara Rao, K. Rajeevan, M. S. Arunachalam, 2018. Combined effect of MJO, ENSO and IOD on the intraseasonal variability of northeast monsoon rainfall over south peninsular India, Climate Dynamics, https://doi.org/10.1007/s00382-018-4117-3.

96. Srivastava, A. K., M. Rajeevan, and S. R. Kshirsagar, 2009. Development of a high resolution daily gridded temperature data set (1969–2005) for the Indian region. Atmos. Sci. Lett., 10, 249–254, https://doi.org/10.1002/asl.232.
97. Subbaramayya, I., 1976. The North-east monsoon and the caused of the winter rains of South-east India, Meteorological Magazine, 106, P 153.
98. Suneetha, P., Latha, P., Ramalingeswara Rao, S. and Bhanu Kumar, O.S.R.U., 2018. Influence of moisture source and sink regions on northeast monsoon rainfall. *Meteorological Applications*, *25*(3), 376-383.
99. Suppiah, R., 1996. Spatial and temporal variations in the relationships between the Southern Oscillation phenomenon and the rainfall of Sri Lanka. *International Journal of Climatology: A Journal of the Royal Meteorological Society*, *16*(12), pp.1391-1407.
100. Suppiah, R., 1997. Extremes of the southern oscillation phenomenon and the rainfall of Sri Lanka. *International Journal of Climatology: A Journal of the Royal Meteorological Society*, *17*(1), pp.87-101.
101. Tai, K.S. and Ogura, Y., 1987. An observational study of easterly waves over the eastern Pacific in the northern summer using FGGE data. *Journal of the atmospheric sciences*, *44*(2), 339-361.
102. Webster, P.J., V.O Magana, T.N. Palmer, J. Shukla, R.A. Tomas, M. Yanai and T. Yasunari, 1998. Monsoons: Processes, predictability and the prospects for prediction, J. Geophys. Res (Oceans), https://doi.org/10.1029/97JC02719
103. Wheeler, M.C. and Hendon, H.H., 2004. An all-season real-time multivariate MJO index: Development of an index for monitoring and prediction. *Monthly weather review*, *132*(8), 1917-1932.
104. Zubair, L. and Ropelewski, C.F., 2006. The strengthening relationship between ENSO and northeast monsoon rainfall over Sri Lanka and southern India. *Journal of Climate*, *19*(8), 1567-1575.

105. Zubair, L., Siriwardhana, M., Chandimala, J. and Yahiya, Z., 2008. Predictability of Sri Lankan rainfall based on ENSO. *International Journal of Climatology: A Journal of the Royal Meteorological Society*, *28*(1), pp.91-101.

BIBLIOGRAGHY

1. Abeysekera, A.B., Punyawardena, B.V.R., Marambe, B., Jayawardena, I.M., Wickremasinghe, V.N., Senarathna, S.D. and Wijerathna, W.M., 2019. Effect of El Niño Southern Oscillation (ENSO) events on inter-seasonal variability of rainfall in wet and intermediate zones of Sri Lanka. *Trop Agric*, *167*, pp.14-27.
2. Acharya, N., Kar, S.C., Kulkarni, M.A., Mohanty, U.C. and Sahoo, L.N., 2011. Multi-model ensemble schemes for predicting northeast monsoon rainfall over peninsular India. *Journal of earth system science*, *120*(5), pp.795-805.
3. Achyuthan, H., 2021. Middle to late Holocene alluvial history of the northeast monsoon dominated coastal tropical rivers of south India. *Quaternary International*, https://doi.org/10.1016/j.quaint.2021.09.012
4. Amudha, B., 2016, CHARACTERISTICS OF INDIAN NORTHEAST MONSOON AND CYCLONIC STORMS OF NORTH INDIAN OCEAN OBSERVED THROUGH MODERN METEOROLOGICAL OBSERVING SYSTEMS, Ph.D Thesis, University of Madras. PP 245.
5. Amudha, B., Raj, Y.E.A., Asokan, R. and Thampi, S.B., 2016 a. Spatial rainfall patterns associated with Indian northeast monsoon derived from high resolution rainfall estimates of Chennai DWR. *MAUSAM*, *67*(4), 767-788.
6. Amudha, B., Raj, Y.E.A. and Asokan, R., 2016 b. Spatial variation of clouding/rainfall over southeast Indian peninsula and adjoining Bay of Bengal

associated with active and dry spells of northeast monsoon as derived from INSAT OLR data. *MAUSAM*, *67*(3), 559-570.

7. Asokan, R and Balachandran, S., 2008, "A pre-monsoon precursor for foreshadowing of northeast monsoon rainfall over Tamilnadu", Mausam, 59, 4, 445-452.
8. Balachandran, S., Pai, D.S. and Prasad, S.K., 1998. Some features of an inverted V-type easterly wave over Indian seas. *Mausam*, *49*(2), 266-268.
9. Balachandran S, Asokan A, Sridharan S. 2006. Global surface temperature in relation to northeast monsoon rainfall over Tamil Nadu. J. Earth Syst. Sci. 115: 349–362
10. Berry, G.J. and Thorncroft, C., 2005. Case study of an intense African easterly wave. *Monthly Weather Review*, *133*(4), 752-766.
11. Bhate, Jyoti, A. Kesarkar, V.P.M. Rajasree, 2019. Simulation of the diurnal cycle of rainfall during Indian summer monsoon season using mesoscale model, Theor. App. Climat., 138, 185-200.
12. Burpee, R.W., 1974. Characteristics of North African easterly waves during the summers of 1968 and 1969. *Journal of Atmospheric Sciences*, *31*(6), 1556-1570.
13. Cangialosi, J.P., Blake, E., DeMaria, M., Penny, A., Latto, A., Rappaport, E. and Tallapragada, V., 2020. Recent progress in tropical cyclone intensity forecasting at the National Hurricane Center. *Weather and Forecasting*, *35*(5), 1913-1922.
14. Chakraborty, A., 2016. A synoptic-scale perspective of heavy rainfall over Chennai in November 2015, Current Science, 111, 201-207.
15. Chakraborty, P., Sarkar, A., Kumar, S., George, J.P., Rajagopal, E.N. and Bhatla, R., 2020. Assessment of NCMRWF Global Ensemble System with differing ensemble populations for Tropical cyclone prediction. *Atmospheric research*, *244*, p.105077.

16. Dash, Y., Mishra, S.K. and Panigrahi, B.K., 2019. Predictability assessment of northeast monsoon rainfall in India using sea surface temperature anomaly through statistical and machine learning techniques. *Environmetrics*, *30*(4), p.e2533.

17. De, U.S. and Mukhopadhyay, R.K., 1999. The effect of ENSO/Anti ENSO on northeast monsoon rainfall. *Mausam*, *50*(4), 343-354.

18. Deshpande, M., Johny, C. J., Kanase, R., Tirkey, S., Sarkar, S. Goswami, T., Roy, K., Ganai, M., Krishna, R. P. M., Prasad, V. S., Mukhopadhyay, P., Durai, V. R., Nanjundiah, R. S. and Rajeevan, M., 2020, "Implementation of Global Ensemble Forecast System (GEFS) at 12 km Resolution", ISSN 0252-1075, IITM Technical Report No.TR-06, ESSO/IITM/MM/ TR/02(2020)/200

19. Dhar ON, Rakhecha PR. 1983. Forecasting northeast monsoon rainfall over Tamil Nadu, India. Mon. Weather Rev. 111, 109–112.

20. Domroes, M. and Ranatunge, E., 1992. The orthogonal structure of Monsoon rainfall variation over Sri Lanka. *Theoretical and applied climatology*, *46*(2), pp.109-114.

21. Doraiswamy, Iyer V., 1941, "Forecasting of northeast monsoon rainfall of south Chennai", India Met. Dep., Sci.Notes, 8, 98.

22. Dunn, G.E., 1940. Cyclogenesis in the tropical Atlantic. *Bulletin of the American Meteorological Society*, *21*(6), 215-229.

23. Gadgil S, Joseph PV, Joshi NV, 1984. Ocean-atmosphere coupling over monsoon regions. *Nature* **312**: 141– 143.

24. Gadgil S, Joseph PV. 2003. On breaks of the Indian monsoon, Proceedings of the Indian Academy of Sciences–Earth and Planetary Sciences, 112(4): 529–558.

25. Gasper, S. 1962: On the intensity and area' coverage of the northeast monsoon rains in the districts of Madras State. IJMG Vol.13 No.2, pp.183-194. 16.

26. George, C.J. 1962: Rainfall peaks over West coast and East coast of Peninsular India. IJMG Vol.13 No.l, pp.1-14. 17.
27. George, C.J. and Vasudevan, V.K. 1963: Some Features of the rainfall over a belt in the Madras State. IJMG Vol.14 No.2 pp.190-195.
28. Geetha, B. and Raj, Y.E.A., 2011. Indian northeast monsoon as a component of Asian winter monsoon and its relationship with large scale global and regional circulation features, Ph.D Thesis of Geetha B, University of Madras.
29. Geetha, B and S. Balachandran, 2014 a. An analytical study of easterly waves over Southern Peninsular India during the Northeast monsoon of 2010, Mausam, 65, 4, 591-602.
30. Geetha, B. and Raj, Y.E.A., 2014 b. Spatial patterns of Northeast Monsoon rainfall over sub-regions of Southern Peninsular India and Sri Lanka as revealed through Empirical Orthogonal Function analysis. *Mausam*, *65*(2), 185-204.
31. Geetha, B and S. Balachandran, 2020. Development and Rapid Intensification of Tropical Cyclone OCKHI (2017) over the North Indian Ocean, Journal of Atmospheric Science Research, DOI: https://doi.org/10.30564/jasr.v3i3.2177
32. Geetha, B. and Balachandran, S., 2021. Diagnostic analysis of two dos-à-dos extreme northeast monsoon seasons with dipolar rainfall performance. *Theoretical and Applied Climatology*, *144*, 675-690.
33. Geetha, B., K.Ramesh, R.V.Deepa, Y.P.Mourya, S.Balachandran, K. Santosh, S.Stella, Geeta Agnihotri and K. Nagaratna, 2022. Report on Northeast Monsoon – 2021, IMD Chennai Scientific Report No. IMDC-SR/12, 62pp.
34. Goswami BN. 2005. Intraseasonal variability (ISV) of south Asian summer monsoon. In Intraseasonal Variability of the Atmosphere – Ocean Climate System, Lau K, Waliser D (eds). pp. 19–61, DOI: 10.1007/3-540-27250-X 2. Springer – Praxis: Chichester, UK.

35. Hersbach, H., Bell, B., Berrisford, P., Hirahara, S., Horányi, A., Muñoz‐Sabater, J., Nicolas, J., Peubey, C., Radu, R., Schepers, D. and Simmons, A., 2020. The ERA5 global reanalysis. *Quarterly Journal of the Royal Meteorological Society*, *146*(730), 1999-2049.

36. Hess, S.L. *Introduction to Theoretical Meteorology*. 1959. New York, NY: Holt Rinehart and Winston

37. India Meteorological Department, Srinivasan, V., and K. Ramamurthy, 1973. Northeast monsoon. Comprehensive articles on selected topics, India Meteorological Department Forecasting Manual Rep. 18.4, Vol. 4.

38. India Met. Dep (IMD), 2008. Forecaster's Guide, 86-88.

39. India Met. Dep., 1987, Report of 10th conference of forecasting officers, pp.43-46.

40. India Met. Dep., 2006, Report of Annual Monsoon Review meeting, pp 137-139.

41. Jangir, B., Swain, D. and Ghose, S.K., 2021. Influence of eddies and tropical cyclone heat potential on intensity changes of tropical cyclones in the North Indian Ocean. *Advances in Space Research*, *68*(2), 773-786.

42. Jayanthi, N. and Govindachari, S., 1999,"El Nino and northeast monsoon rainfall over Tamil Nadu" Mausam,50,2,217-218.

43. Jayawardena, W., M. Fernando, and DUJ Sonnadara, 2014. Satellite observations of Lightning Activities over Sri Lanka, Proceedings of the Technical Sessions, 30 (2014) 61-66 Institute of Physics – Sri Lanka.

44. Jyothi, L., Joseph Sudheer, and P. Suneetha. 2020. Role of Environmental Factors in Rapid Intensification and Weakening of Cyclone Ockhi (2017), *Earth and Space Science Open Archive ESSOAr*.

45. Jury, M.R., Pathack, B., Campbell, G., Wang, B. and Landman, W., 1991. Transient convective waves in the tropical SW Indian Ocean. *Meteorology and Atmospheric Physics*, *47*(1), 27-36.

46. Khole, M. and De, U.S., 2003, “A study on northeast monsoon rainfall over India” Mausam,54,2,419-426.

47. Koteswara Rao, K, Ashwini Kulkarni, Savita Patwardhan, B. Vinodh Kumar, T. V. Lakshmi Kumar. 2020. Future changes in precipitation extremes during northeast monsoon over south peninsular India, Theor. Appl Climatology, **142**, 205–217.

48. Kripalani, R.H. and Kumar, P., 2004. Northeast monsoon rainfall variability over south peninsular India vis-à-vis the Indian Ocean dipole mode. *International Journal of Climatology: A Journal of the Royal Meteorological Society*, *24*(10), 1267-1282.

49. Krishna Kumar, K., K. Rupa Kumar, R. G. Ashrit, N. R. Deshpande, and J. W. Hansen, 2004. Climate impacts on Indian agriculture. Int. J. Climatol., 24, 1375–1393, https://doi.org/10.1002/joc.1081.

50. Krishna Rao, P.R. 1953: Rainfall of Madras State with special reference to Tamil Nadu and Rayalaseema. Memoirs of the IMD Vol.XXX Part I.

51. Krishna Rao, P.R. and Jagannathan, P. 1953: A study of the northeast monsoon rainfall of Tamil Nadu. IJMG Vol.4, No.1, pp.22-44.

52. Krishna Rao, P.R. 1958: The Indian Northeast monsoon in relation to the general circulation - Symposium on "Monsoons of the World", New Delhi, p. 89.

53. Kumar P, Rupa Kumar K, Rajeevan M, Sahai AK. 2007. On the recent strengthening of the relationship between ENSO and northeast monsoon rainfall over South Asia. Clim. Dyn. 8: 649–660.

54. Lau, K.M., Wu, H.T. and Bony, S., 1997. The role of large-scale atmospheric circulation in the relationship between tropical convection and sea surface temperature. *Journal of Climate*, *10*(3), 381-392.

55. Liebmann, B. and Smith, C.A., 1996. Description of a complete (interpolated) outgoing longwave radiation dataset. *Bulletin of the American Meteorological Society*, *77*(6), 1275-1277.

56. Maharana, P., Kumar, D., Rai, P., Tiwari, P.R. and Dimri, A.P., 2022. Simulation of Northeast Monsoon in a coupled regional model framework. *Atmospheric Research*, *266*, p.105960.

57. Malurkar, S.L. 1932s On the extreme dryness observed at Kodaikanal during the winter months. I.Met.D. Sc. Note Vol.IV No. 43.

58. Malurkar, S.L. and Desai, B.N. 1943: Notes on forecasting weather in India. IMD Tech. Note No.l.

59. Manas Roshan, 2019. Cyclone Ockhi Disaster risk management and sea safety in the Indian marine fisheries sector, FAO, United Nations. FAO ISBN 978-92-5-131225-4.

60. Mishra, V and Amit Bharadwaj, 2019, Defining the Northeast Monsoon of India, Mon Wea Review, Vol, 147, 791-808, https://doi.org/ 10.1175/MWR-D-18-0287.1.

61. Mitra, A. K., A. K. Bohra, M. Rajeevan and T. N. Krishnamurti, 2009. Daily Indian precipitation analyses formed from a merged of rain-gauge with TRMM TMPA satellite derived rainfall estimates, J of Met Soc of Japan, 87A, 265-279.

62. Mohapatra, M. and Adhikary, S., 2011. Modulation of cyclonic disturbances over the north Indian Ocean by Madden-Julian oscillation. *Mausam*, *62*(3), 375-390.

63. Mohapatra, M., Nayak, D.P., Sharma, R.P. and Bandyopadhyay, B.K., 2013. Evaluation of official tropical cyclone track forecast over north Indian Ocean

issued by India Meteorological Department. *Journal of Earth System Science*, *122*(3), 589-601.

64. Mohapatra, M., Nayak, D.P., Sharma, M., Sharma, R.P. and Bandyopadhyay, B.K., 2015. Evaluation of official tropical cyclone landfall forecast issued by India Meteorological Department. *Journal of Earth System Science*, *124*(4), 861-874.

65. Mondal, P. and Chaudhuri, S., 2022. Temporal variability in the withdrawal phase of southwest monsoon over India and related consequences in northeast monsoon: a climatological perspective. *Theoretical and Applied Climatology*, *148*(3), 1021-1034.

66. Mukhopadhyay, P., Bechtold, P., Zhu, Y., Murali Krishna, R.P., Kumar, S., Ganai, M., Tirkey, S., Goswami, T., Mahakur, M., Deshpande, M. and Prasad, V.S., 2021. Unraveling the mechanism of extreme (More than 30 sigma) precipitation during august 2018 and 2019 over Kerala, India. *Weather and Forecasting*, *36*(4), pp.1253-1273.

67. Nageswara Rao, M.M., M.C. Sannan and U.C. Mohanty, 2019. Characteristics of various rainfall events over South Peninsular India during northeast monsoon using high-resolution gridded dataset (1901–2016), Theor Appl. Climatology, **137**, 2573–2593.

68. Naidu, C.V., Satyanarayana, G.C., Durgalakshmi, K., Rao, L.M., Mounika, G.J. and Raju, A.D., 2012. Changes in the frequencies of northeast monsoon rainy days in the global warming. *Global and Planetary Change*, *92*, 40-47.

69. Nair, A., Acharya, N., Singh, A., Mohanty, U.C. and Panda, T.C., 2013. On the predictability of northeast monsoon rainfall over south peninsular India in general circulation models. *Pure and Applied Geophysics*, *170*(11), 1945-1967.

70. Nisansala, W.D.S., Abeysingha, N.S., Islam, A. and Bandara, A.M.K.R., 2020. Recent rainfall trend over Sri Lanka (1987–2017). *International Journal of Climatology*, *40*(7), pp.3417-3435.

71. Omvir Singh and Pankaj Bhardwaj, 2017. Spatial and temporal variations in the frequency of thunderstorm days over India, Weather, https://doi.org/10.1002/wea.3080.

72. Pai, D.S., M. Rajeevan, O.P.Sreejith, B. Mukhopadhyay, N.S. Sathbai, 2014. Development of a new high spatial resolution (0.25 X 0.25) long period (1901-2010) daily gridded rainfall data set over India and its comparison with existing data sets over the region, Mausam, vol. 65, no. 1, pp. 1–18.

73. Parvathi, V., I. Suresh, M. Lengaigne, T. Izumo, and J. Vialard, 2017. Robust projected weakening of winter monsoon winds over the Arabian Sea under climate change. Geophys. Res. Lett., 44, 9833–9843.

74. Pattanaik, D.R. and Mohapatra, M., 2017. Active northeast monsoon over India during 2015–an assessment of real-time extended range forecast. *Current Science*, 2253-2262.

75. Prakash, S. and Gairola, R.M., 2013. Relationship between northeast monsoon rainfall and near-surface atmospheric wind convergence over the North Indian Ocean using multisatellite data. *Natural hazards*, *68*(2), 763-774.

76. Prasanna, K., Singh, P., Chowdary, J.S., Naidu, C.V., Parekh, A., Gnanaseelan, C. and Dandi, R., 2019. Northeast monsoon rainfall variability over the southern Peninsular India associated with multiyear La Niña events. *Climate Dynamics*, *53*(9), 6265-6291.

77. Prasanna, K., Vinay Kumar, P. and Naidu, C.V., 2020. Precursors of northeast monsoon rainfall variability during extreme epochs of the global warming era. *Meteorological Applications*, *27*(2), p.e1894.

78. Prasanna, K., Chowdary, J.S., Singh, P., Chiranjeevi, D., Naidu, C.V., Parekh, A. and Gnanaseelan, C., 2021. Assessment of APCC models fidelity in simulating the Northeast monsoon rainfall variability over Southern Peninsular India. *Theoretical and Applied Climatology*, *144*(3), 931-948.

79. Rai Sarcar, N.C., Jayaraman, S. and Srinivasan, T.R. 1968: A study of wind distribution and associate© dry or wet weather probability over Madras during Monsoon and post-monsoon months. IMD Pre-published Sc. Report No. 57.

80. Rai Sircar, N.C., Jayaraman, S. and Srinivasan, T.R. 1968: Isohyetal patterns over south India in relation to the locations of various storms/depressions of the Bay striking east peninsular coast during the post-monsoon season. IJMG Vol.19, No.3, pp.305-310.

81. Rai Sircar, N.C., Jayaraman. S. and Srinivasan, T.R. 1969: A study of wind distribution and associated dry or wet weather probability over Madras during monsoon and post-monsoon months. IJMG Vol.20, No.3, pp.267-270.

82. Raj, Y.E.A., 1989, “Statistical relations between winter monsoon rainfall and the preceeding summer monsoon”, Mausam, 40, 1, 51-56.

83. Raj, Y.E.A., 1996, “Inter and intra seasonal variation of thermodynamic parameters of the atmosphere over coastal Tamil Nadu during northeast monsoon season”, Mausam, 47, 3, 259-268.

84. Raj, Y.E.A., 1998a, “A scheme for advance prediction of northeast monsoon rainfall of Tamil Nadu”, Mausam, 49, 2, 247-254.

85. Raj, Y.E.A., 1998b, “A statistical technique for determination of withdrawal of northeast monsoon over coastal Tamilnadu”, Mausam, 49, 3, 309-320.

86. Raj, YEA, 1992. Objective determination of northeast monsoon onset dates over coastal Tamil Nadu for the period 1901-90, Mausam, 43, 273-282.

87. Raj, Y.E.A., 2003. Onset, withdrawal and intra-seasonal variation of northeast monsoon over coastal Tamil Nadu, 1901-2000, Mausam, 3, 605-614,

88. Raj, Y.E.A., Asokan, R. and Revikumar, P.V., 2007, "Contrasting movement of wind based equatorial trough and equatorial cloud zone over Indian southern peninsula and adjoining Bay of Bengal during the onset phase of northeast monsoon", Mausam, 58,1,33-48.

89. Raj, Y.E.A., and Geetha, B., 2008. Relationship between Southern Oscillation Index and Indian northeast monsoon as revealed in antecedent and concurrent modes, Mausam, 59, 15-34.

90. Raj, Y.E.A., 2012. INDIAN NORTHEAST MONSOON, In *Monsoon Monograph*, Vol. 1, Edited by Ajit Tyagi, G.C. Asnani, U.S.De, H.R.Hatwar and A.B.Mazumdar, 606-670.

91. Raj Y.E.A. and Amudha B, 2022. Extent of diurnal cycle of rainfall and its intraseasonal variation over coastal Tamil Nadu during northeast monsoon season, Mausam, 73, 1, https://doi.org/10.54302/mausam.v73i1.4984

92. Rajeevan M, Gadgil S, Bhate J. 2010. Active and break spells of the Indian summer monsoon. J. Earth Syst. Sci. 119: 229–247.

93. Rajeevan, M., C. K. Unnikrishnan, Jyoti Bhate, K. Niranjan Kumar and P. P. Sreekala, 2012. Northeast monsoon over India: variability and prediction, Meteorol. Appl. 19: 226–236, DOI: 10.1002/met.1322.

94. Ramakrishnan, K.P. 1940s The rainfall in the Indian Peninsula associated with cyclonic storms from the Bay of Bengal during the post-monsoon and early winter seasons. I.Met.D. Sc. Notes Vol.VII No. 74, 1940.

95. Ramakrishnan, K.P. and Narayanan, J. 1953: A study of fifty years rainfall over Visakhapatnam.. Memoirs of the India Meteorological Department Vol.XXX, Part IV.

96. Ramakrishnan, K.P. 1953: A study of fifty years' rainfall of Madras city. IJMG Vol.4 No.2, pp.123-144. 46. Ramakrishnan, K.P. and Narayanan, J. 1953: A study of fifty years' rainfall of Nagapattinam. IJMG Vol.4 No.4, pp. 310-338.

97. Ramakrishnan, K.P. and Ganapathiraman, G.V. 1953: Squalls in Madras. IJMG Vol.4 No.l, pp.103-105. 48. Ramakrishnan, K.P. and Modak, K.L. 1958: A study of fifty years' rainfall of Trivandrum. Memoirs of I.M.D.

98. Ramaswamy, C. 1972: The severe drought over Tamil Nadu during the retreating monsoon period of 1968 and its association with anamalies in the upper level flow patterns over the northern hemisphere. IJMG Vol.23 No.3, pp.303-316.

99. Ranalkar, M.R. and Chaudhari, H.S., 2009. Seasonal variation of lightning activity over the Indian subcontinent. *Meteorology and atmospheric physics*, *104*(1), 125-134.

100. Ranganathan C. and K. 1965. A study of a typical case of interaction of an easterly wave with a westerly trough during the post-monsoon period, IJMG, Vol. 16, No.4, 607-616.

101. Rao, T.N., B. Radhakrishna, K. Nakamura and N. Prabhakara Rao, 2009. Differences in raindrop size distribution from Southwest monsoon to northeast monsoon at Gadanki, Quart Roy Met Society, 1630-1637, https://doi.org/10.1002/qj.432.

102. Rao, K.V., 1963. A study of Indian Northeast Monsoon season. IJMG Vol.14 No.2, pp.143-155.

103. Riehl, H., 1968. Tropical Meteorology, McGraw-Hill Book Co., Inc., New York, 392 pp.

104. Ramamurthy, K., 1969. Monsoon of India: Some aspects of the 'break' in the Indian southwest monsoon during July and August; Forecasting Manual 1–57 No. IV 18.3, India Met. Dept., Pune, India.

105. Ramesh Reddy, T.V., Mehta, S.K., Ananthavel, A., Saleem Ali, V. Annamalai, D. Narayana Rao, 2021. Seasonal Characteristics of Sea breeze and thermal internal boundary layer over Indian east coast region, Met and Atmospheric Physics, 133, 217-232.

106. Rao, K.V, 1961. A study of the Indian Northeast Monsoon season, Ind.J. Meteor. Geophysics, 143-155.

107. Reba, RM, D.R. Pattanaik, and PVS Raju, 2022. Easterly waves and ocean–atmospheric oscillations associated with contrasting northeast monsoon seasons over India, J. Earth Syst. Sci. 131:52, https://doi.org/10.1007/s12040-021-01807-8.

108. Ross, R.S. and Krishnamurti, T.N., 2007. Low-level African easterly wave activity and its relation to Atlantic tropical cyclogenesis in 2001. *Monthly Weather Review*, *135*(12), 3950-3964.

109. Rossow, W.B. and Schiffer, R.A., 1991. ISCCP cloud data products. *Bulletin of the American Meteorological Society*, *72*(1), 2-20.

110. Sabin, T.P., C.A.Babu and P.V. Joseph., 2012. SST-Convection relation over Tropical Oceans, Int J Climatology, 1424-1435, https://doi.org/10.1002/joc.3522.

111. Saha, K., Sanders, F. and Shukla, J., 1981. Westward propagating predecessors of monsoon depressions. *Monthly Weather Review*, *109*(2), 330-343.

112. Sahany, S., Venugopal, V. and Nanjundiah, R.S., 2010. Diurnal scale signatures of monsoon rainfall over the Indian region from TRMM satellite observations. *Journal of Geophysical Research: Atmospheres*, *115*(D2).

113. Sanap, S.D., P. Priya, G. K. Sawaisarje and K. S. Hosalikar, 2018. Heavy Rainfall Events over South-East Peninsular India during North-East Monsoon: Role of El-Niño and Easterly Wave Activity, Int J Climatology, DOI: 10.1002/joc.5926.

114. Sanap, S.D., Mohapatra, M., Ali, M.M., Priya, P. and Varaprasad, D., 2020. On the dynamics of cyclogenesis, rapid intensification and recurvature of the very severe cyclonic storm, Ockhi. *Journal of Earth System Science*, *129*(1), 1-13.
115. Sarkar, A., P.Chakraborty, John.P.George and E.N. Rajagopal, 2016. Implementation of Unified Model based Ensemble Prediction System at NCMRWF (NEPS), NCMRWF Report NMRF/TR/02/2016, https://www.ncmrwf.gov.in/Reports-eng/NMRF_TR2_2016.pdf.
116. Satyanarayana, G.C., Naidu, C.V., Rao, D.V.B., Umakanth, N., and Naveena, N., 2020. Onset and northeast monsoon over south peninsular India, Mausam, 71, 3, https://doi.org/10.54302/mausam.v71i3.51.
117. Sengupta, A. and Nigam, S., 2019. The northeast winter monsoon over the Indian subcontinent and Southeast Asia: Evolution, interannual variability, and model simulations. *Journal of Climate*, *32*(1), 231-249.
118. Shanmugasundaram, J., Lee, E. and Srinivasan, G., 2018. Characterizing pentad rainfall variations during the North East Indian monsoon season over the southeastern peninsular India. Int Journal of Climatology, *38*, 1044-1060.
119. Singh, P., Gnanaseelan, C. and Chowdary, J.S., 2017. North-East monsoon rainfall extremes over the southern peninsular India and their association with El Niño. *Dynamics of Atmospheres and Oceans*, *80*, 1-11.
120. Singh, O.P., 1995, “Influence of Bay of Bengal on winter monsoon rainfall”, Mausam, 46, 3,307-312.
121. Singh Vineet Kumar, M.K.Roxy and Medha Deshpande, 2020. The unusual long track and rapid intensification of very severe cyclone Ockhi, CURRENT SCIENCE, VOL. 119, NO. 5, 10 SEPTEMBER, 771-779.
122. Somenath Dutta, D.M.Rase, and Sunitha Devi, 2016. A diagnostic study on the energetic aspects of weak/strong spell of northeast monsoon, Mausam, 67, 2, 493-498.

123. Sreekala, P.P., Rao, S. and Rajeevan, M., 2012. Northeast monsoon rainfall variability over south peninsular India and its teleconnections. *Theoretical and applied climatology*, *108*(1), 73-83.

124. Sreekala, P.P., S. Vijaya Bhaskara Rao, K. Rajeevan, M. S. Arunachalam, 2018. Combined effect of MJO, ENSO and IOD on the intraseasonal variability of northeast monsoon rainfall over south peninsular India, Climate Dynamics, https://doi.org/10.1007/s00382-018-4117-3.

125. Sridharan, S. and Muthuchami, A., 1990, Northeast monsoon rainfall in relation to El Nino, QBO and Atlantic hurricane frequency, Vayumandal, 20, 3-4, 1.08-1.11.

126. Srivastava, A. K., M. Rajeevan, and S. R. Kshirsagar, 2009. Development of a high resolution daily gridded temperature data set (1969–2005) for the Indian region. Atmos. Sci. Lett., 10, 249–254, https://doi.org/10.1002/asl.232.

127. Subbaramayya, I., 1976. The North-east monsoon and the causes of the winter rains of South-east India, Meteorological Magazine, 106, P 153.

128. Suneetha, P., Latha, P., Ramalingeswara Rao, S. and Bhanu Kumar, O.S.R.U., 2018. Influence of moisture source and sink regions on northeast monsoon rainfall. *Meteorological Applications*, *25*(3), 376-383.

129. Suppiah, R., 1996. Spatial and temporal variations in the relationships between the Southern Oscillation phenomenon and the rainfall of Sri Lanka. *International Journal of Climatology: A Journal of the Royal Meteorological Society*, *16*(12), pp.1391-1407.

130. Suppiah, R., 1997. Extremes of the southern oscillation phenomenon and the rainfall of Sri Lanka. *International Journal of Climatology: A Journal of the Royal Meteorological Society*, *17*(1), pp.87-101.

131. Tai, K.S. and Ogura, Y., 1987. An observational study of easterly waves over the eastern Pacific in the northern summer using FGGE data. *Journal of the atmospheric sciences*, *44*(2), 339-361.

132. Webster, P.J., V.O Magana, T.N. Palmer, J. Shukla, R.A. Tomas, M. Yanai and T. Yasunari, 1998. Monsoons: Processes, predictability and the prospects for prediction, J. Geophys. Res (Oceans), https://doi.org/10.1029/97JC02719.

133. Wheeler, M.C. and Hendon, H.H., 2004. An all-season real-time multivariate MJO index: Development of an index for monitoring and prediction. *Monthly weather review*, *132*(8), 1917-1932.

134. Zubair, L. and Ropelewski, C.F., 2006. The strengthening relationship between ENSO and northeast monsoon rainfall over Sri Lanka and southern India. *Journal of Climate*, *19*(8), 1567-1575.

135. Zubair, L., Siriwardhana, M., Chandimala, J. and Yahiya, Z., 2008. Predictability of Sri Lankan rainfall based on ENSO. *International Journal of Climatology: A Journal of the Royal Meteorological Society*, *28*(1), pp.91-101.